VASCULAR ENDOTHELIAL GROWTH FACTOR A COORDINATES PANCREATIC ISLET VASCULARIZATION, INNERVATION, AND FUNCTION

By

Rachel Byerley Reinert

Dissertation

Submitted to the Faculty of the

Graduate School of Vanderbilt University

in partial fulfillment of the requirements

for the degree of

DOCTOR OF PHILOSOPY

in

Molecular Physiology and Biophysics

December, 2012

Nashville, Tennessee

Approved:

Professor Maureen Gannon, Chair

Professor Masakazu Shiota

Professor Danny Winder

Professor Wenbiao Chen

Professor Patricia Labosky

To my grandmothers, who shared great love and support

and demonstrated personal strength.

I miss you both dearly.

ACKNOWLEDGMENTS

I must first thank the Vanderbilt Medical Scientist Training Program for giving me the initial opportunity to pursue this work, and for providing a wonderfully supportive environment in which I could strive to become the physician-scientist that I hope to be. Thanks especially to Terry Dermody, who gave me the final push to submit my first grant application, emphasizing early on that each opportunity must be taken in order to be successful. Additional thanks go out to the MSTP co-directors and administrative staff, past and present, who have made the last seven years an invaluable experience. This work was supported by the National Institutes of Health (T32 GM07347), multiple grants from the National Institute of Diabetes and Digestive and Kidney Diseases (including National Research Service Award F30 DK085932), JDRF International, and the U.S. Department of Veterans Affairs.

An enormous thank you is necessary for my mentor of the last five years, Al Powers. Thank you for being so passionate about our work on pancreatic islets, and so driven to care for people with diabetes—these are qualities that I hope to take with me. Thank you for providing me with many opportunities to present my research. I am grateful for the constant encouragement to become a better writer, speaker, and collaborator, all of which ultimately makes a great scientist. Finally, thank you for being one who truly cares about your lab members not only as part of your team, but also as individuals with lives and interests outside of lab.

I am so grateful to all of the present and former members of the Powers laboratory, each of whom has contributed to this work in some form or another and

provided special friendships along the way. To our excellent research technicians, Radhika Aramandla, Anastasia Coldren, Greg Poffenberger, Alena Shostak, and Courtney Thompson, thanks for all of your efforts in advancing these experiments, from laying the foundation for a productive lab environment to contributing "world-renowned" technical skills. To the past and present postdoctoral fellows, Priyanka Brahmachary, Danielle Dean, Joe Henske, Ji-Young Hong, Alexandra Martin, Lara Nyman, Ioannis Papagiannis, Neil Phillips, Ana Maria Robledo Reyes, and Jack Virostko, thank you all for being great sources of knowledge, advice, support, and friendship. To my fellow graduate students in the lab, Kristie Aamodt, Qing Cai, Jeannelle Kantz, Nora Kayton, thank you for being such great lab mates. I am so happy to have been able to take this journey through graduate school along with you, and to share our joys, disappointments, achievements, and struggles. And finally, to all those summer students, thank you for keeping us on our toes! Thanks to one student in particular, Nadia Ansari, who was especially helpful in some of this work. I am so thankful for everyone who has made the lab such a wonderful place to work. I can only hope to have the opportunity to work with such kind, helpful, and dedicated people in the future. I have truly enjoyed working with and learning from each of you and hope to stay in touch.

Over the past ten years, I have been privileged to meet and work with some fantastic women in science, and for that I am very grateful. My career in biomedical research would not have even begun without Tracy Anthony, who introduced me to "real" science as a young undergraduate student. Her motivation and passion for research was contagious, inspiring me to add a research focus to my intended career in medicine. To Marcela Brissova and Chunhua Dai, thank you for providing expertise, leadership,

and wisdom for the trainees in our laboratory, in addition to being always willing to lend a hand in experiments. Thanks to Maureen Gannon and Trish Labosky, who (along with their laboratories) were especially supportive in particular aspects of the work described in this Dissertation. Finally, thanks to Elizabeth Blackburn, who was enthusiastic about this research and provided a fresh perspective from someone far outside the islet biology field. These women have each demonstrated passion for scientific discovery and are inspiring in their success. I want to personally thank each of them for being supportive of me as both a young scientist and mother.

Many thanks to my thesis committee members, Maureen Gannon, Wenbiao Chen, Patricia Labosky, Masakazu Shiota, and Danny Winder. I have truly enjoyed getting your constructive feedback, which has made this work much stronger and more interesting. Thanks to Wenbiao Chen for introducing me to the zebrafish community. Thanks to Masa Shiota for providing helpful surgical skills for several of these experiments. Thanks to Danny Winder for being enthusiastic about this research and providing helpful advice, even as it turned out to be a little further from his own work than expected. Additional thanks go to Dr. Joyce Johnson, who provided very helpful analysis and discussions.

I must also send many thanks to the faculty, administration, and students of the Department of Molecular Physiology and Biophysics. Thanks to the faculty for maintaining a rigorous training environment and fostering the development of individual students. Thanks to Angie Pernell for coordinating departmental programming and taking on administrative issues for the students, allowing us to focus on our studies. Finally, thanks to the students for forming such a wonderfully collaborative community. I have made many friends along the way, and am thankful for their support as well.

At Vanderbilt, we are fortunate to have such strong communities in which to work and learn, and I especially benefitted from being part of the Diabetes Research and Training Center and the Beta Cell Interest Group. Thanks to the faculty and staff who organize these groups for fostering a learning environment in which trainees have many opportunities to meet and network with others in our field. Many additional thanks go to Terri Ray, who (among may other things) works hard to solve technical and logistical issues around the lab.

I am so blessed to have such a wonderfully supportive family and group of friends. To my parents, thank you for the many sacrifices it took to get me here. I appreciate the constant encouragement in the pursuit my goals, and the expectation of hard work that would lead to success. I would not be where I am today without you. To my brothers, Rocky, Aaron, and Travis, thank you for making our childhood so entertaining, and filled with lots of happy memories. I am excited to see where life takes you all. Thanks to my extended family, who have long provided love and support. A special thanks also goes to the Reinert family, who have been so welcoming.

Finally, to my dearest Drake and Liam: Words cannot express how fortunate I am to have you both. Drake, thank you so much for taking this journey with me. You have sacrificed so much for me to accomplish my goals, and I am honored to have such a kind, loving and supportive husband by my side. Liam, your dimpled smile warms my heart and brings me immeasurable joy. After a long day of work, I am so blessed to come home and share your passion for life and discovery. I cannot wait to see what the future holds for us.

TABLE OF CONTENTS

LIST OF TABLES

LIST OF FIGURES

LIST OF ABBREVIATIONS

ACh	acetylcholine
ANOVA	analysis of variance
β-gal	β-galactosidase
bp	base pairs
BSA	bovine serum albumin
cAMP	cyclic adenosine monophosphate
Cre	Cre recombinase
db	diabetes (leptin receptor gene) mutation
DM	diabetes mellitus
DMEM	Dulbecco's modified Eagle's medium
Dox	doxycycline
DT	diphtheria toxin
DTR	diphtheria toxin receptor
E	embryonic day
ECM	extracellular matrix
ELISA	enzyme-linked immunosorbent assay
ER	estrogen receptor
EYFP	enhanced yellow fluorescent protein
FBS	fetal bovine serum
fl	flox, flanked by loxP sites
GDNF	glial cell line-derived neurotrophic factor

GFAP	glial fibrillary acidic protein
GFP	green fluorescent protein
GTT	glucose tolerance test
HBSS	Hanks balanced salt solution
HFD	high fat diet
HGF	hepatocyte growth factor
IBMX	3-isobutyl-1-methylxanthine
IP	intraperitoneal
IPa	intrapancreatic
kb	kilobase
MGI	Mouse Genome Informatics
NGF	nerve growth factor
NOD	non-obese diabetic
NRP1	neuropilin 1
ob	obese (leptin gene) mutation
P	postnatal day
PBS	phosphate-buffered saline
PCR	polymerase chain reaction
PDX1	pancreatic-duodenal homeobox factor 1
Pdx^{PB}	Pst-Bst fragment of *Pdx1* promoter enhancer
PECAM1	platelet endothelial cell adhesion molecule 1
pSc	peri-islet Schwann cell
R26	*ROSA26*

RIA	radioimmunoassay
RIP	rat insulin promoter
RPKM	reads per kilobase of exon model per million mapped reads
RPM	rotations per minute
RPMI	Roswell Park Memorial Institute (medium)
rtTA	reverse tetracycline-controlled transactivator
SCID	severe combined immunodeficiency
TBE	Tris/borate/EDTA buffer
TEM	transmission electron microscopy
TetO	tetracycline operator
TH	tyrosine hydroxylase
Tm	tamoxifen
TUJ1	neuron-specific β-III tubulin
VAChT	vesicular acetylcholine transporter
VEGF-A	vascular endothelial growth factor A
VEGFR2	vascular endothelial growth factor receptor 2
Veh	vehicle
wt	wild-type

CHAPTER I

BACKGROUND AND SIGNIFICANCE

Diabetes Mellitus

Epidemiology

Diabetes mellitus (DM) refers to a collection of disorders in glucose metabolism, all of which are characterized by abnormally high blood glucose levels, or hyperglycemia. It is estimated that 25.8 million Americans have some form of DM, and 7 million are undiagnosed. Type 2 DM is the most common form, occurring in about 90-95% of patients with DM, while type 1 DM accounts for 5%. Gestational DM, rare monogenic forms of DM, and DM secondary to other medical conditions account for the rest (Centers for Disease Control and Prevention, 2011). Long-term consequences of DM (in particular, consequences of hyperglycemia) include macrovascular complications, such as heart disease and stroke, and microvascular complications, including retinopathy, glomerulopathy, and neuropathy (Defronzo and Abdul-Ghani, 2011). The estimated total cost of DM in the United States was $174 billion in 2007 alone (Centers for Disease Control and Prevention, 2011). The incidence of both type 1 and type 2 DM are increasing, and the average age of newly diagnosed patients is decreasing, so developing optimal strategies for prevention and treatment are of utmost importance (Wentworth et al., 2009).

Pathophysiology

There are many mechanisms involved in the pathogenesis of DM, but a key component is dysfunction of the pancreatic islets that results in a relative deficiency in insulin (Ashcroft and Rorsman, 2012). In type 1 DM, the autoimmune destruction of pancreatic β-cells leads to inadequate insulin production, and an inability to lower blood glucose levels (van Belle et al., 2011). In contrast, the hyperglycemia in type 2 DM results from β-cell dysfunction in the setting of insulin resistance, in which insulin signaling is disrupted in several target organs (Muoio and Newgard, 2008). In gestational DM, the onset of abnormalities in glucose metabolism occurs during pregnancy. Following parturition, gestational DM resolves, though patients have an increased risk of developing type 2 DM (Lain and Catalano, 2007). Several rare genetic mutations lead to other forms of diabetes, including mature onset diabetes of the young (MODY), which resembles type 2 DM clinically (Vaxillaire and Froguel, 2008), and neonatal DM, an early-onset disorder of insufficient insulin secretion (Aguilar-Bryan and Bryan, 2008).

Islet transplantation as a therapeutic goal

One promising therapeutic approach for type 1 DM is islet transplantation, in which the cellular source of insulin, the pancreatic β-cell, is replaced. First attempted as transplantation of minced sheep pancreata in the 19th century, islet transplantation has been refined over the past 30 years into a feasible treatment for DM (Robertson, 2004). In recent years, the success of clinical islet transplantation was improved by development of the Edmonton protocol, which utilized a glucocorticoid-free immunosuppressive regimen (Shapiro et al., 2000). Nevertheless, the majority of patients currently undergoing islet

transplantation still do not achieve long-term insulin independence, though many are cured of the recurrent dangerous hypoglycemic episodes they once experienced (Barton et al., 2012).

Even with the demonstrated successes of islet transplantation, many obstacles must be overcome before it can become a widely used approach for diabetes treatment (Harlan et al., 2009; Khan and Harlan, 2009; McCall and James Shapiro, 2012). Typically, multiple donor pancreata are required to achieve a sufficient islet mass for transplantation into one recipient (Shapiro et al., 2000), in part because a large proportion of islets are lost in the first few days after transplantation (Biarnés et al., 2002; Eich et al., 2007). Furthermore, the surviving islets do not function identically to endogenous islets, in part because of inadequate revascularization (Carlsson et al., 2001; Mattsson et al., 2002) and reinnervation (Korsgren et al., 1996). Currently, islets are infused into the portal vein, which provides sufficient oxygen tension but also exposes the islets to potentially damaging elements in the blood (Korsgren et al., 2008). Finally, immunologic barriers remain, from dampening the autoimmune reaction of type 1 DM to preventing alloimmune rejection of the graft (Harlan et al., 2009; Khan and Harlan, 2009). The immunosuppressive agents used in the Edmonton protocol may themselves be detrimental to long-term islet survival and function (Chatenoud, 2008; Froud et al., 2006; Nir et al., 2007). To address these issues, the islet biology field is striving to generate new sources of β-cells (Efrat and Russ, 2012), to improve upon islet delivery by revising the transplantation site and devising islet encapsulation methods (Harlan et al., 2009; McCall and James Shapiro, 2012), and to enhance engraftment itself by improving islet revascularization (Brissova and Powers, 2008).

The Pancreas

Anatomy and physiology

The pancreas is a mixed glandular organ located in the retroperitoneal cavity (Figure 1). Anatomically, the pancreas is divided into three portions: the head, which is cradled by the duodenum; the body, which travels alongside the inferior portion of the stomach; and the tail, which attaches to the spleen (Suda et al., 2006). It has both exocrine and endocrine functions.

The exocrine pancreas comprises about 95% of the total mass of the organ (Chen et al., 2011). It is composed of acinar cells, which produce a multitude of digestive enzymes such as pancreatic amylase, and ductal cells, which produce bicarbonate to neutralize stomach acid. Acinar cells line a highly branched system of ductules, which coalesce as the main pancreatic duct in the center of the pancreas. The main pancreatic duct joins the common bile duct within the head of the pancreas, and their combined secretions are released into the duodenum through the ampulla of Vater (Slack, 1995). Pancreatic exocrine secretion is extensively controlled by the autonomic nervous system and gut hormones (Konturek et al., 2003). Parasympathetic nerves integrate a variety of signals from the brain and digestive system to stimulate secretion of digestive enzymes during food consumption. In contrast, activation of the sympathetic nervous system inhibits pancreatic exocrine secretion by reducing pancreatic blood flow (Love et al., 2007).

The endocrine pancreas is composed of distinct islands of tissue, the islets of Langerhans, scattered throughout the pancreatic parenchyma (In't Veld and Marichal, 2010). Pancreatic islets contain five types of hormone-secreting cells: glucagon-

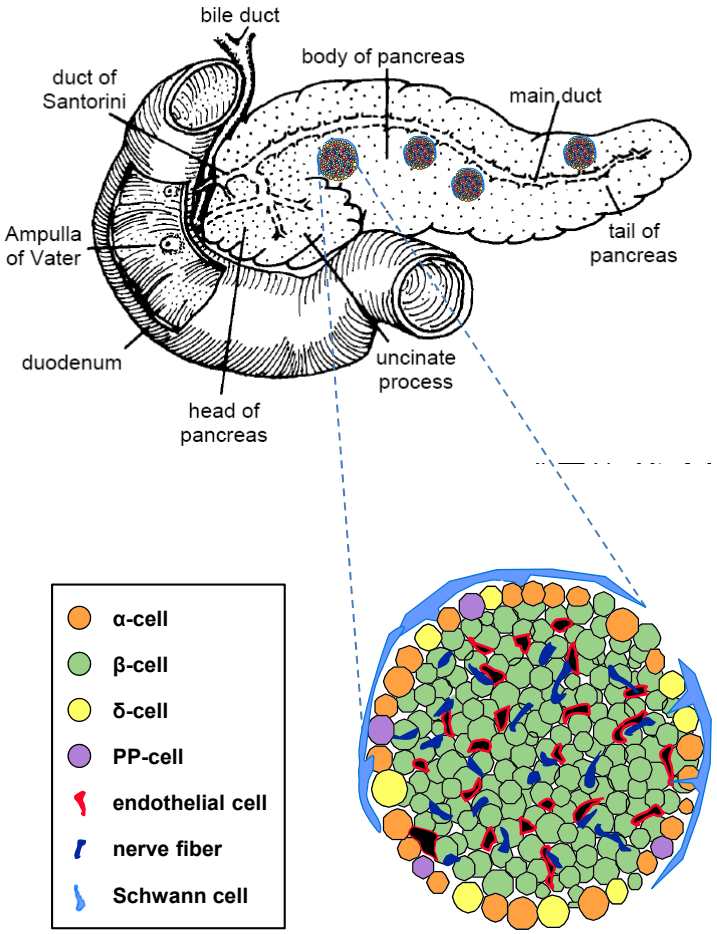

Figure 1. Anatomy of the pancreas and pancreatic islets. The pancreas is a mixed gland, containing an exocrine portion that secretes digestive fluid into the duodenum, and an endocrine portion composed of dispersed pancreatic islets that secrete hormones into the bloodstream. Adapted from Slack (1995). A schematic of the cellular composition of the mouse pancreatic islet is highlighted.

producing α-cells, insulin-producing β-cells, somatostatin-producing δ-cells, ghrelin-producing ε-cells, and PP cells, which secrete pancreatic polypeptide (Pan and Wright, 2011). In mice, β-cells comprise approximately 75% of the islet endocrine cells and occupy the islet core; the other four types of endocrine cells are located at the islet periphery. In contrast, human islets show more equal numbers of α-, β-, and δ-cells, which do not typically segregate into the typical β-cell core and non-β-cell mantle (Figure 2; Brissova et al., 2005; Cabrera et al., 2006). Instead, β-cells are much more likely to contact α-cells in human islets compared to mouse islets (Bosco et al., 2010). Finally, pancreatic islets are highly vascularized and richly innervated, and can be considered as miniature organs (Figures 3-4).

The pancreatic islets play an essential role in whole-body glucose homeostasis. Islet endocrine cells integrate a variety of signals before rapidly secreting the appropriate peptide hormones into the bloodstream. These signals include glucose and other nutrients, hormones, neurotransmitters, and neuropeptides (Ahrén, 2000; Kim and Egan, 2008; Nolan and Prentki, 2008). β-cells synthesize and secrete insulin, which promotes the uptake and utilization of glucose by insulin-sensitive tissues, including the liver, skeletal muscle, and fat (Samuel and Shulman, 2012). In contrast, α-cells synthesize and secrete glucagon, which increases hepatic glucose production to raise blood glucose levels (Gromada et al., 2007). In the multiple forms of diabetes, the combination of insulin deficiency (absolute or relative) and glucagon excess result in poorly controlled glycemia (Unger and Cherrington, 2012).

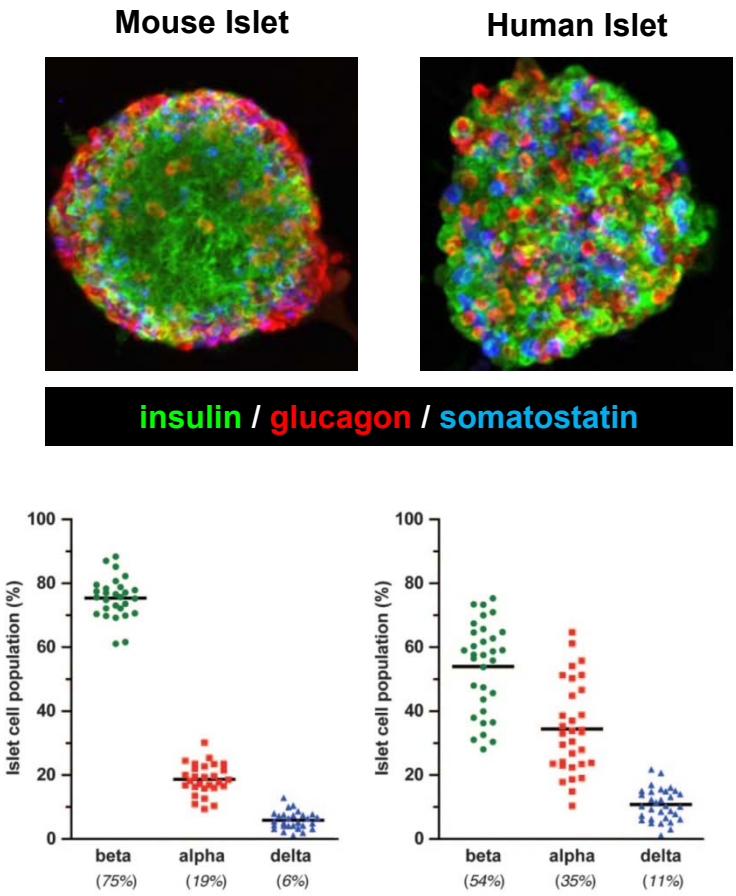

Figure 2. Pancreatic islet morphology varies between mouse and human. Top, Representative mouse islet and representative human islet, immunolabeled for insulin (green), glucagon (red), and somatostatin (blue). **Bottom**, "Optical sections of entire mouse (n = 28) and human (n = 32) islets were 3D reconstructed and analyzed for cellular composition. [Left] Mouse islets showed a high degree of homogeneity in abundance of three examined islet cell types: β cells (ranging from 61% to 88%), α cells (ranging from 9% to 31%), and δ cells (ranging from 1% to 13%). [Right] In contrast, human islets had a quite heterogeneous composition: β cells (ranging from 28% to 75%), α cells (ranging from 10% to 65%), and δ cells (ranging from 1.2% to 22%). The composition of human islets was statistically different across all three examined endocrine cell populations; $P < 0.0001$. Horizontal bar represents the mean of the islet cell population." From Brissova et al. (2005).

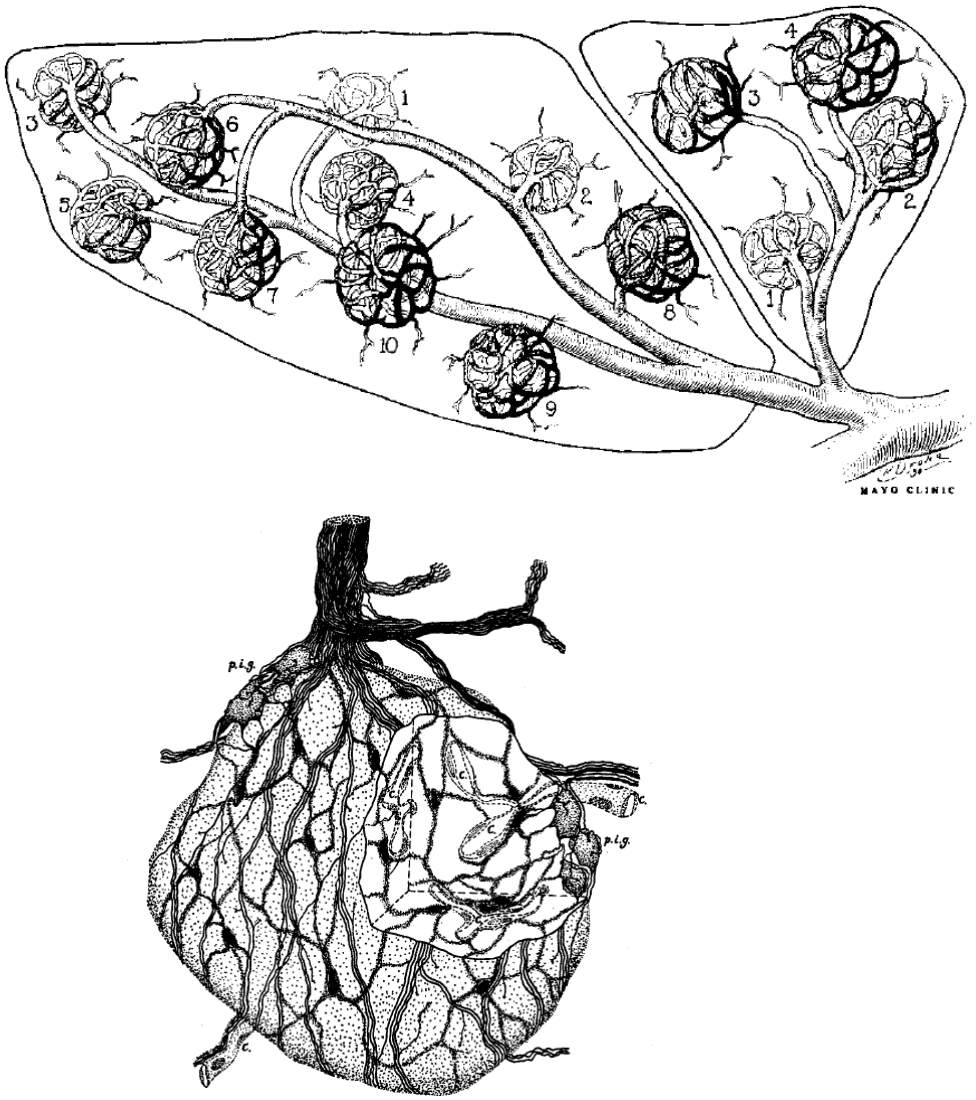

Figure 3. Pancreatic islets are highly vascularized and richly innervated. Top, Drawing of arterial supply to the pancreatic islets (Wharton, 1932). **Bottom,** Illustration of pancreatic islet innervation. Labels: c, capillary; p.i.g., peri-insular ganglion (Honjin, 1956).

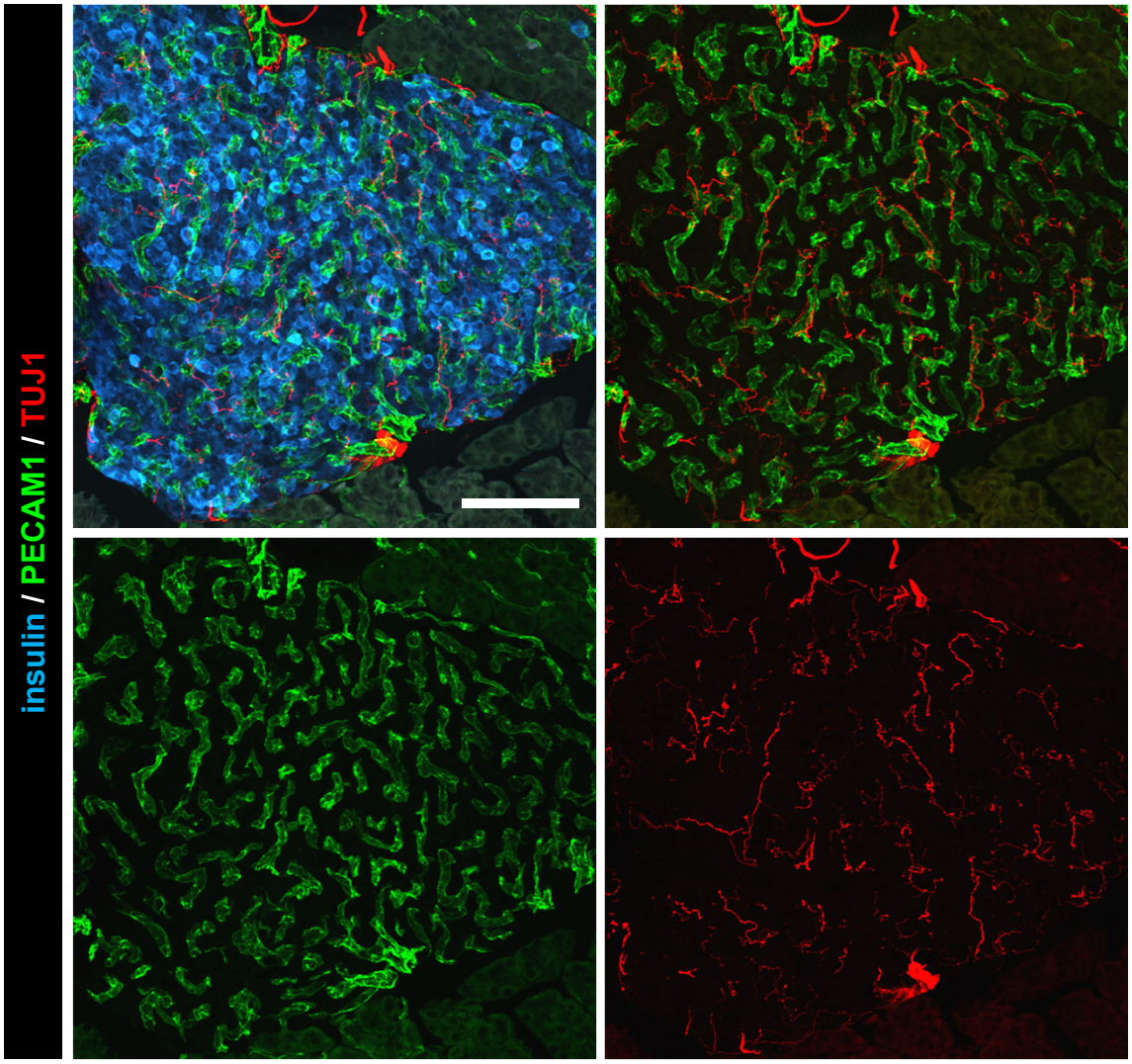

Figure 4. Pancreatic islets are highly vascularized and richly innervated. Representative islet from a 30 μm-thick mouse pancreatic cryosection, immuno-labeled for insulin (blue), the endothelial cell marker PECAM1 (green), and the neuron-specific tubulin marker TUJ1 (red). Scale bar is 100 μm and applies to all panels.

Development

While several recent studies have examined human pancreas development (Sarkar et al., 2007; Jeon et al., 2009; Riedel et al., 2011; Gregg et al., 2012; reviewed in Pan and Wright, 2011), many of the mechanisms controlling pancreas development have been revealed by studies in model organisms. Therefore, the data summarized here will focus on research performed in mice.

Pancreas development occurs with the progression of a complex cell specification pathway regulated by the sequential induction of transcription factors. Around embryonic day 8 (E8), expression of the transcription factor *Pdx1* is initiated in the posterior foregut endoderm, which gives rise to the entire pancreatic epithelium, caudal stomach, rostral duodenum, and common bile duct. Around E9, the pre-pancreatic endoderm evaginates from the foregut to form the ventral and dorsal pancreatic buds (Guz et al., 1995; Offield et al., 1996). Activation of the transcription factor *Ptf1a* (around E9.5) is required for growth of the pancreatic buds; its expression is later restricted to exocrine cells (Krapp et al., 1998). Mature endocrine cells are derived from endocrine progenitor cells that express the transcription factor neurogenin 3 (*Neurog3*), following the induction of transcription factors such as *Arx*, *Pax4*, *Pax6*, *Nkx2-2*, *Nkx6-1*, and *Neurod1* (Ackermann and Gannon, 2007).

The subsequent growth and differentiation of the embryonic pancreas occurs in two stages, termed the primary and secondary transitions (Pictet et al., 1972; reviewed in Pan and Wright, 2011). During the primary transition, from E9.5 to E13.5, multipotent pancreatic progenitor cells proliferate and compartmentalize into trunk and tip cells that will later differentiate into ductal and acinar cells, respectively (Gittes, 2009; Pan and

Wright, 2011). At this time, the first hormone-expressing cells also appear, but these cells are thought to be a transient population not well represented in the final islet structures (Gu et al., 2002; Herrera, 2000). By E12.5, gut rotation has allowed the ventral and dorsal buds to fuse and form a continuous gland (Ackermann and Gannon, 2007). During the secondary transition, from E13.5 to E16.5, pancreatic progenitor cells undergo branching morphogenesis and differentiation. Committed NEUROG3+ endocrine cell precursors within the trunk epithelium are allocated into individual endocrine cell types and begin to delaminate from the epithelial cord (Pan and Wright, 2011). Beginning in the secondary transition, PDX1 expression is downregulated in non-endocrine pancreatic cells but upregulated in β-cells, which continue to express high levels of PDX1 in postnatal life (Guz et al., 1995). β-cell expression of PDX1 is required during embryogenesis and adulthood to regulate islet endocrine cell proportions, maintain β-cell proliferation, and preserve islet function (Jonsson et al., 1994; Offield et al., 1996; Brissova et al., 2002; Holland et al., 2002; Gannon et al., 2008). In late embryogenesis (E16.5 to E18.5), large clusters of endocrine cells continue to delaminate, but most remain close to the ductal epithelium (Gittes, 2009; Pan and Wright, 2011).

Islet formation and maturation is still active neonatally and postnatally. At birth, long cords of highly proliferative endocrine cells are found at the core of the pancreas, near large blood vessels along the pancreatic duct. It is hypothesized that α-cells throughout this cord are distributed along sites of fission that form the individual islets found later in life (Miller et al., 2009). Distinct islets can be found within the first week after birth (Cai et al., 2012), a time when endocrine cell proliferation is high but starting to decline (Ackermann and Gannon, 2007). In normal mice, the formation of new islets

ceases around weaning (Jo et al., 2011). By adulthood, maintenance of the β-cell population is thought to occur primarily through replication (Dor et al., 2004; Georgia and Bhushan, 2004), which occurs very slowly (Ackermann and Gannon, 2007; Teta et al., 2005).

Islet Vascularization

Morphology and function of the islet vasculature

Blood flow to the pancreas is provided by the superior and inferior pancreaticoduodenal arteries and multiple branches of the splenic artery (Wharton, 1932). These larger arteries branch into interlobular and intralobular arteries that penetrate the pancreatic parenchyma and reach all of the islets in parallel. Each islet is supplied by one or more arterioles, which branch into capillaries to form a glomerulus-like structure (Bonner-Weir and Orci, 1982). Blood perfuses the islets in one of two patterns, core-to-mantle or side-to-side (Nyman et al., 2008), and is drained by either of the insulo-acinar or insulo-venous portal systems (Murakami et al., 1993). Venous blood containing islet products is carried to the liver by the portal vein, where islet hormones first act to modulate glucose homeostasis (Radziuk et al., 1993).

The islet vasculature is highly specialized (Figure 5), and distinct from the vasculature of the exocrine pancreas (Henderson and Moss, 1985). The intraislet capillary plexus has a higher vessel density and contains vessels that are thicker and more tortuous than capillaries of the exocrine pancreas (Brissova et al., 2006; Vetterlein et al., 1987). Ultrastructurally, islets have a fenestrated endothelium, in which the endothelial cells contain multiple pores that increase vessel permeability (Bearer and Orci, 1985; Brissova

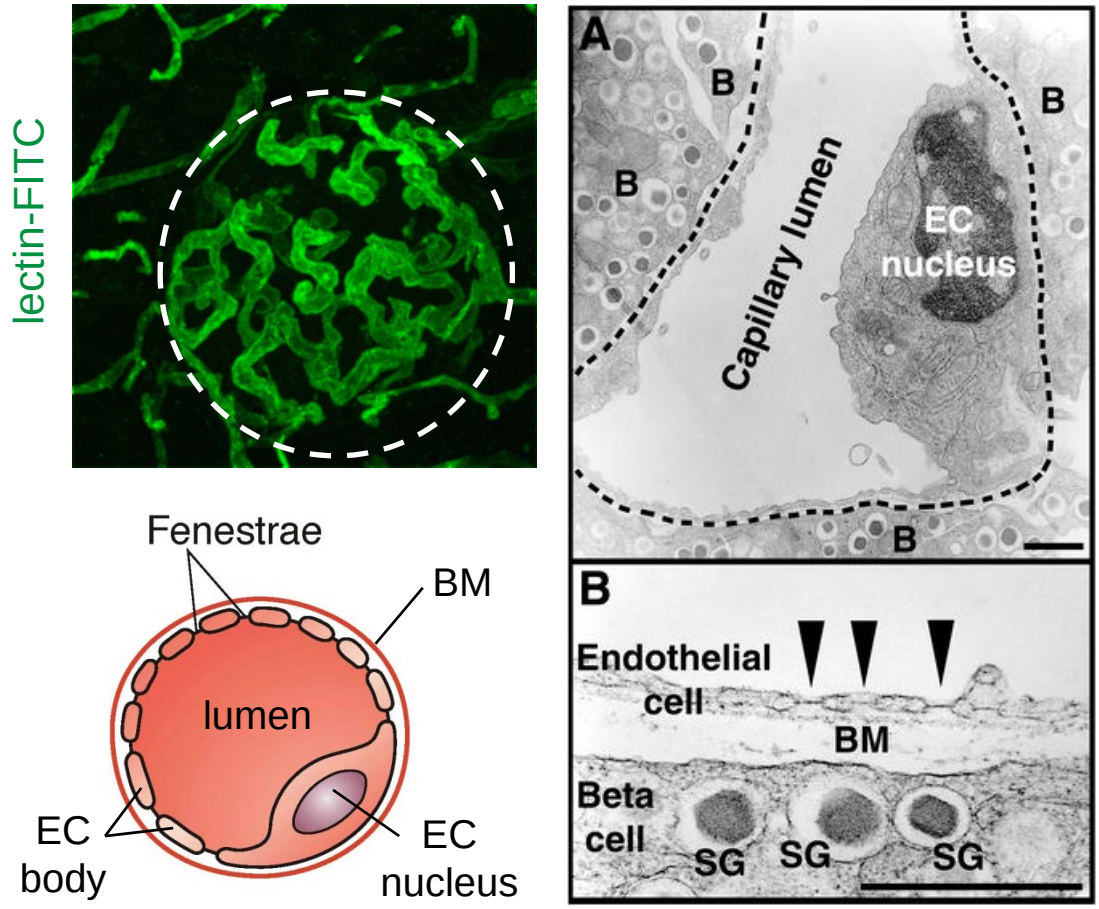

Figure 5. The pancreatic islet vasculature is highly specialized. Top left, Representative islet from a mouse infused with a FITC-conjugated tomato lectin to label the functional vasculature (green). Intraislet vessels (within dotted line) are thicker, denser, and more tortuous than vessels of the exocrine pancreas (outside of dotted line). Image courtesy of Marcela Brissova. **Bottom left**, Schematic of a cross-section of an intraislet capillary, demonstrating an endothelial cell (EC) body with its cellular processes and fenestrations, encircling the vascular lumen. A continuous basement membrane (BM) is produced by endothelial cells. Adapted from Cleaver and Melton (2003). **Right,** "Endothelial cell morphology in [mouse] pancreatic islets. **A.** A thin endothelial cell (EC, surrounded by a [dotted] black line) embraces the capillary lumen (see black line) and separates the blood from the pancreatic beta cells (B). **B.** A higher magnification shows that the fenestrated endothelium along with a thin BM separates the secretory granules (SG) from the blood. Crystalline insulin granules are visible in the secretory granules of the pancreatic beta cell. The fenestrae are cytoplasmic holes, in which a permeable diaphragm is located (arrowheads). Black bars 1 μm." From Nikolova and Lammert (2003).

et al., 2006; Kamba et al., 2006; Lammert et al., 2003b). The cellular architecture of the islet allows for each of the polyhedral β-cells to have multiple faces that contact blood vessels (Bonner-Weir, 1991). This specialized relationship between islet endocrine cells and blood vessels allows for the rapid exchange of nutrients and hormones between the islet and bloodstream.

While islets compose only 1-2% of the total pancreatic mass, they receive 6-20% of the total blood flow to the organ, and are therefore perfused by about five to ten times the amount of blood received by the exocrine pancreas (Lifson et al., 1980; Lifson et al., 1985). Furthermore, the oxygen tension within pancreatic islets is higher than that of the exocrine pancreas (Carlsson et al., 1998). Islet blood flow is dynamically regulated, and highly correlated with islet function. For example, experimentally induced increases or decreases in blood glucose levels can increase or decrease blood flow, respectively, without changing blood flow in the exocrine pancreas (Jansson, 1984; Jansson and Hellerström, 1983; Nyman et al., 2010). Interestingly, islet blood flow is also increased in hyperinsulinemic obese rodents, mediated primarily by signals from the parasympathetic nervous system (Atef et al., 1992; Carlsson et al., 1996; Jansson and Hellerström, 1986).

The precise structural mechanisms regulating islet blood flow remain unclear (Schaeffer et al., 2011). Capillaries within mouse islets are not directly associated with vascular smooth muscle cells (vSMCs), which are responsible for translating signals from the autonomic nervous system into changes in blood flow in resistance arteries (Storkebaum and Carmeliet, 2011). Instead, it has been proposed that intraislet endothelial cells may propagate signals to vSMCs located on arterioles just outside the islet (Jansson et al., 2010). Alternatively, islet blood flow could be regulated by intraislet

pericytes, which are contractile (Hamilton et al., 2010), and have been shown to regulate the diameter of capillaries in the central nervous system (Peppiatt et al., 2006). Nevertheless, the specific role of pericytes in islet function remains unclear (Richards et al., 2010).

Understanding islet vascularization is important for islet transplantation, because it has been proposed that inadequate revascularization is one major limitation for the success of islet grafts. Compared to endogenous pancreatic islets, a reduction in both graft vessel density (Mattsson et al., 2002) and oxygen tension (Carlsson et al., 2001) was observed in islets transplanted into the kidney cortex, liver, and spleen. Because islet grafts are revascularized with cells from both the donor and recipient (Brissova et al., 2004; Nyqvist et al., 2011), certain transplantation sites may provide advantages over others. For example, pancreatic islets transplanted into skeletal muscle show a vascular morphology and blood flow rate comparable to that of endogenous islets (Christoffersson et al., 2010), and intrapancreatic islet grafts also showed improved revascularization compared to grafts placed under the kidney capsule (Lau et al., 2009).

Role of the vasculature in islet development and function

The close relationship between islet endocrine and endothelial cells begins in early pancreas development. The dorsal and ventral pancreatic buds originate adjacent to the aorta and vitelline veins, respectively. The importance of endothelial cells in the induction of pancreas differentiation was first demonstrated in co-culture experiments, in which explants of the aortic endothelium were required for isolated foregut endoderm to initiate expression of *Pdx1* and *Ins2* (Lammert et al., 2001). Further studies expanded

upon this model by showing that aortal endothelial cells were responsible for specifically inducing the pancreatic transcription factor *Ptf1a*, which is required for outgrowth of the dorsal pancreatic bud. Additionally, endothelial cells were required for maintenance of *Pdx1* expression and for induction of *Ins2* and *Gcg* (encoding glucagon) in the early pancreas (Yoshitomi and Zaret, 2004). These data are supported by a clinical case report of an individual with aortic coarctation who also demonstrated agenesis of the dorsal pancreas (Kapa et al., 2007).

The relationship between islet endocrine cells and endothelial cells continues throughout life (Figure 6). Islet endocrine cell clusters are vascularized and exposed to blood flow as early as E13.5, the beginning of the secondary transition of islet endocrine cell formation (Brissova et al., 2006; Shah et al., 2011). During the normal expansion of β-cell mass in the first week of postnatal life, β-cell proliferation coincides with endothelial cell proliferation and an expansion of the intraislet vasculature to reach its final vessel density (Johansson et al., 2006a). Similarly, proliferation of intraislet endothelial cells precedes the proliferation and mass expansion of β-cells that occurs during pregnancy (Johansson et al., 2006b).

The delivery of oxygen and nutrients from the established vasculature is important for pancreatic development and growth, and endocrine differentiation (Fraker et al., 2009; Shah et al., 2011), but other bloodstream-derived molecules are also important. While dorsal pancreas agenesis was observed along with cardiac defects in N-cadherin-deficient mice (Esni et al., 2001), restoration of N-cadherin specifically in the heart rescued the cardiovascular defects and revealed that soluble factors from the bloodstream, including sphingosine-1-phosphate (S1P), promote pancreas bud formation

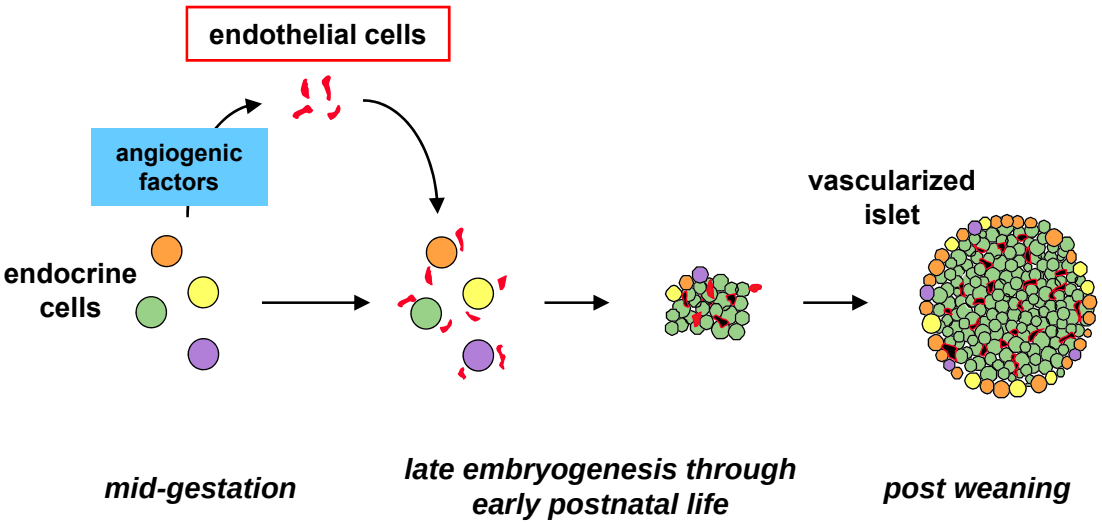

Figure 6. Model of islet vascularization during development. During embryogenesis and postnatal life, the development of islet vasculature occurs concomitantly with islet morphogenesis. As described in Brissova et al. (2006), "critical components of this islet vascularization model include: 1) production of angiogenic factors by early developing islet cells, 2) recruitment of endothelial cells and their association with developing islet cell clusters, 3) establishment of blood flow to small endocrine cell clusters before complete islet assembly, and 4) coordinated assembly of islet cell types and the islet vascular structures in late embryogenesis." Figure is adapted from Brissova et al. (2006).

(Edsbagge et al., 2005). Therefore, early tissue perfusion is crucial to supply oxygen, nutrients, and other signaling molecules for proper pancreas development.

In addition to providing the structural basis for islet blood flow, murine intraislet endothelial cells are also responsible for synthesis of the islet basement membrane. Indeed, the dramatic reduction in intraislet endothelial cells following pancreas-wide inactivation of *Vegfa* in *Pdx1-Cre;Vegfa*$^{fl/fl}$ mice results in a loss of islet basement membrane proteins, including laminin α4, laminin α5, collagen IV α1, collagen IV α2 and fibronectin (Nikolova et al., 2006). In addition to the vascular basement membrane, human islets also contain a second basement membrane that is continuous with the islet capsule, a feature present in both mice and humans (Virtanen et al., 2008). While the precise role of the islet basement membrane *in vivo* is unresolved, multiple *in vitro* studies indicate that extracellular matrix (ECM) components exert positive effects on β-cell proliferation, survival, and insulin secretion (Stendahl et al., 2009).

Endothelial cells also produce soluble factors that signal to islet endocrine cells. Experiments in which isolated islets are treated with medium previously conditioned with purified intraislet endothelial cells show that endothelial cells secrete factors that enhance glucose-stimulated insulin secretion and prevent insulin degradation in cultured islets. For example, isolated intraislet endothelial cells produce hepatocyte growth factor (HGF) to stimulate β-cell proliferation, but only in the presence of VEGF-A (Johansson et al., 2006b). Using a similar experimental design, endothelial cell-derived laminin β1 was found to enhance insulin content and glucose-stimulated insulin secretion by isolated islets (Johansson et al., 2009). Finally, connective tissue growth factor (CTGF), a protein expressed by pancreatic ductal cells, endocrine cells, and endothelial cells, promotes islet

endocrine cell differentiation and proliferation during development (Crawford et al., 2009). Genetic inactivation of *Ctgf* in any of these cell types impairs β-cell proliferation during embryogenesis, suggesting that this broad expression pattern is important for islet development. However, inactivation of *Ctgf* specifically in endothelial cells also decreases islet vascularization, so whether CTGF itself is the sole endothelial cell-derived signal responsible for enhancing β-cell proliferation remains to be determined (Guney et al., 2011).

Molecular mechanisms directing islet vascularization

To acquire their highly specialized vascular phenotype, islet endocrine cells produce several factors that target endothelial cells, including angiogenic factors from the vascular endothelial growth factor (VEGF), angiopoietin, and ephrin families, and basic fibroblast growth factor (Brissova et al., 2006). Normal islets also express angiostatic factors, including thrombospondin 1 (Olerud et al., 2008), which may counteract the abundant angiogenic factors within the islet but may also impair islet revascularization following transplantation. In particular, the potent angiogenic factor VEGF-A has been extensively studied as the major regulator of islet vascularization, revascularization, and function (see "Vascular Endothelial Growth Factor A," below)**.**

The angiopoietin family has been less well studied in the islet. Angiopoietin family members provide important cues for guiding blood vessel maturation and maintenance. For example, angiopoietin 1 (ANGPT1) promotes the stabilization of blood vessels, while angiopoietin 2 (ANGPT2) antagonizes ANGPT1 signaling (Gale and Yancopoulos, 1999). In the pancreatic islet, angiopoietins expressed by endocrine cells

bind to their receptors TIE1 and TIE2, which are expressed by intraislet endothelial cells (Brissova et al., 2006). In contrast to VEGF-A, angiopoietins play a lesser role in normal islet formation and function, as demonstrated with genetic mouse models. β-cell-specific overexpression of angiopoietins does not affect islet endocrine cell morphology or function, because isolated islets display normal glucose-stimulated insulin secretion *in vitro*. However, prolonged overexpression of either ANGPT1 or ANGPT2 during islet development reduces endothelial cell permeability and leads to glucose intolerance, without inducing major changes in islet vessel density and size (Cai et al., 2012). In the converse experiment, genetic inactivation of *Angpt1* after E13.5 does not affect islet vascularization or impair glucose tolerance (Cai, 2012). On the other hand, an experiment in which chick pancreata were transplanted into diabetic mice showed that disrupted angiopoietin signaling contributes to the formation of abnormal vessels during revascularization in the setting of hyperglycemia. In this model, hyperglycemia induced the specific overexpression of ANGPT2, thus impairing the proper revascularization of the graft (Calderari et al., 2012). Therefore, proper angiopoietin signaling may play a more significant role in islet adaptation to metabolic stress.

Finally, thrombospondin 1 (THBS1), a glycoprotein with antiangiogenic properties, has important roles in islet vascularization and function. Mice with global genetic deletion of *Thbs1* had hypervascularized and hyperplastic islets (Crawford et al., 1998), but were surprisingly hypoinsulinemic (Olerud et al., 2011). Further *in vitro* studies showed that both insulin production and glucose-stimulated insulin secretion were reduced in THBS1-deficient islets, likely as a result of decreased THBS1-mediated activation of TGFβ1, a protein that exerts positive effects on β-cells (Olerud et al., 2011).

However, experimental reduction of THBS1 expression in islet grafts, either through genetic deletion or siRNA-mediated inhibition, allowed for improved graft revascularization and function (Olerud et al., 2008).

Altered islet vascularization in mouse models of diabetes

Because the intraislet vasculature is critical for normal islet development and function, islet vascularization has been evaluated in several rodent models of obesity and diabetes. In some models, disruption of the intraislet vasculature appears to be a key component in the development of islet functional abnormalities, while other models demonstrate a progressive disruption in the integrity of the vasculature with prolonged hyperglycemia.

For example, the intraislet vasculature plays a critical role in the pathogenesis of islet dysfunction in the intrauterine growth-restricted (IUGR) rat model of diabetes. Following experimental ligation of the uterine artery, IUGR rat pups show early defects in insulin secretion, and hypovascularized islets that progressively lose β-cell mass. Interestingly, neonatal treatment of IUGR rats with exendin-4, an analog of the incretin hormone glucagon-like peptide 1, prevents the decline in β-cell mass (Stoffers et al., 2003), in part by rescuing islet VEGF-A production and normalizing islet vascularization (Ham et al., 2009). Similarly, disruption of the intraislet vasculature may be an important component of autoimmune diabetes, because intraislet endothelial cells are reduced in the non-obese diabetic (NOD) mouse before the onset of insulitis, islet destruction, and diabetes (Akirav et al., 2011).

In contrast to IUGR rats and NOD mice, in which impairments in the intraislet vasculature contribute to islet dysfunction, two rodent models of obesity demonstrate a capability of the intraislet vasculature to adapt to increased islet demand, at least in the initial stages of pathogenesis. The *ob/ob* and *db/db* mouse models contain spontaneous mutations in the genes for leptin and the leptin receptor, respectively, which lead to hyperphagia, morbid obesity, and several metabolic abnormalities. The two models are divergent in that *db/db* mice spontaneously develop diabetes, while *ob/ob* mice remain hyperinsulinemic and only slightly hyperglycemic (Coleman, 1978; Robinson et al., 2000). Surprisingly, the hyperplastic islets of both *ob/ob* and *db/db* mice have a decreased density of intraislet vessels (Nakamura et al., 1995; Dai et al., manuscript in preparation). However, these vessels are markedly dilated compared to islet vessels in controls, and, in *ob/ob* mice, demonstrate hyperperfusion by *in vivo* microscopy (Dai et al., manuscript in preparation). While the intraislet vessels in *ob/ob* mice remain structurally intact, and thus can cooperate with islet endocrine cells to maintain long-term normoglycemia, *db/db* islets eventually display pericapillary edema and fibrosis, suggesting that they may succumb to microangiopathy as a result of hyperglycemia (Nakamura et al., 1995).

In addition to *db/db* mice, two rat models have also shown that intraislet endothelial cells are susceptible to hyperglycemia-induced damage, leading to further islet dysfunction. The Zucker diabetic fatty (ZDF) rat, which also contains a mutation in the leptin receptor, is another model of obesity and type 2 diabetes. Young, normoglycemic male ZDF rats showed an initial increase in islet endothelial cell area that decompensated with the onset of hyperglycemia. Treatment with the anti-diabetic drug

pioglitazone prevented the vascular damage, suggesting that hyperglycemia is detrimental to the islet vascular remodeling necessary to maintain islet function (Li et al., 2006). Similarly, the altered islet vasculature in non-obese diabetic Goto-Kakizaki rats resembles microangiopathy associated with the early onset of metabolic abnormalities (Homo-Delarche et al., 2006). In this model, impaired islet angiogenesis and decreased islet vascularization early in life is accompanied by hypoinsulinemia, hypercholesterolemia, and altered pancreas development (Giroix et al., 2011).

Islet Innervation

Morphology of islet innervation

The pancreas receives neural input from the autonomic and enteric nervous systems, and sends information to the brain via sensory nerves (Ahrén et al., 2006; Lindsay et al., 2006; Sundler and Bottcher, 1991). Islet autonomic signals originate in a complex neural network within the lateral and ventromedial hypothalamus (Kiba, 2004). Preganglionic sympathetic nerves travel from the spinal cord to the celiac and superior mesenteric ganglia, where they synapse on postganglionic neurons that will enter the pancreas (Kiba, 2004). Preganglionic parasympathetic nerves travel within the vagus nerve and synapse in intrapancreatic ganglia, which contains cell bodies of intrinsic nerves that reach the exocrine and endocrine pancreas (Honjin, 1956; Ushiki and Watanabe, 1997). Additionally, the pancreas receives nerve fibers from the stomach and duodenal portions of the enteric nervous system, as shown by studies using *in vivo* retrograde tracing and *in vitro* co-culture of pancreas and gut explants (Kirchgessner and Gershon, 1990; Kirchgessner et al., 1992). Sensory nerves of the pancreas travel

alongside both pancreatic sympathetic and parasympathetic nerve pathways (Kiba, 2004). A schematic of pancreatic innervation is shown in Figure 7.

Anatomically, extrinsic nerves enter the pancreas alongside the splenic artery and the superior and inferior pancreaticoduodenal arteries (Honjin, 1956; Richins, 1945), and both extrinsic and intrinsic nerves penetrate the pancreatic islet alongside capillaries (Ahrén, 2000; Sunami et al., 2001). Within the islet, unmyelinated nerve bundles give rise to free nerve endings that intermingle with islet endocrine cells (Honjin, 1956; Ushiki and Watanabe, 1997; Woods and Porte, 1974), without forming a true synapse (Kobayashi and Fujita, 1969; Serizawa et al., 1979). Additionally, some islets are closely associated with nerve cell bodies in a formation termed a neuroinsular complex (Persson-Sjögren et al., 2001b; Serizawa et al., 1979).

Islet endocrine cells share several properties with neurons, including similarities in gene and protein expression (Atouf et al., 1997; Scharfmann, 1997) and function (Arntfield and van der Kooy, 2011; Maechler and Wollheim, 1999; Ohta et al., 2011; Reetz et al., 1991). Pancreatic islets were termed "paraneurons" because of their neuron-like secretory function (Fujita, 1989). Furthermore, several neurotrophic factors also have positive effects on islet endocrine cells, including nerve growth factor (NGF; Scharfmann, 1997). Interestingly, several autoantigens present in patients with type 1 diabetes are not specific to β-cells but are also expressed by neurons (Lieberman and DiLorenzo, 2003).

The morphology of human islet innervation has only recently been explored (Rodriguez-Diaz et al., 2011a; Rodriguez-Diaz et al., 2011b). In contrast to the dense nerve plexus found within rodent islets, human islets display fewer nerve fibers

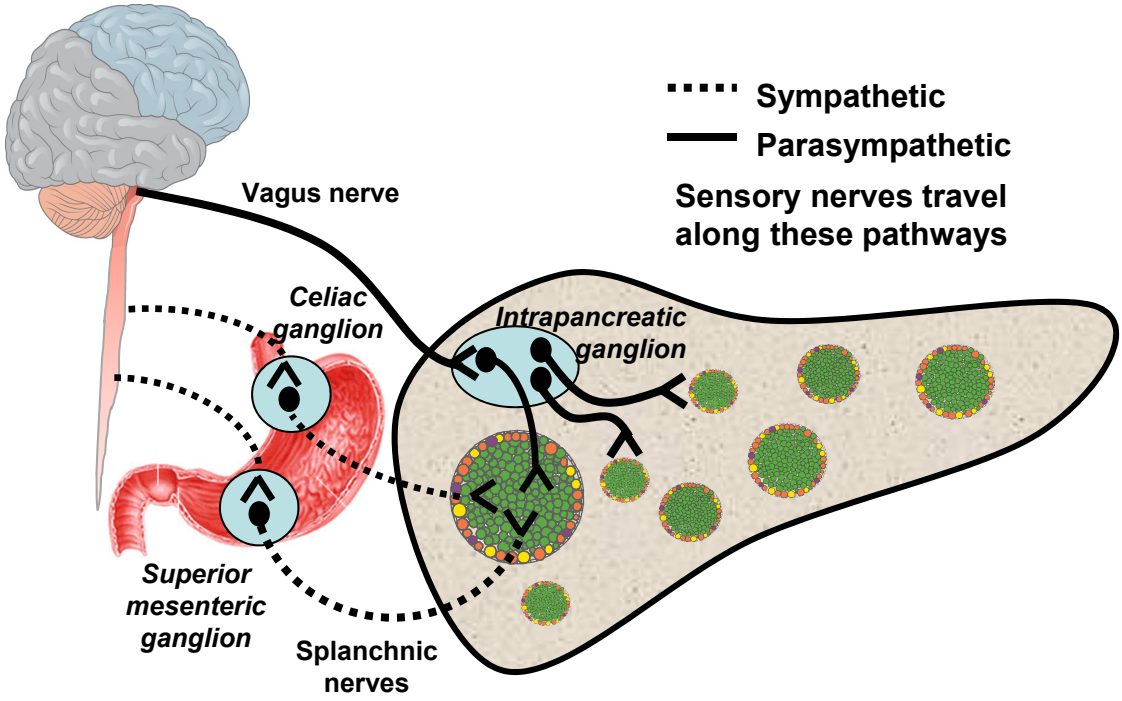

Figure 7. Pancreatic innervation. The pancreas receives parasympathetic innervation from the vagus nerve, whose branches synapse on intrapancreatic ganglia before innervating the pancreatic islets. Sympathetic neurons from the brain synapse in paravertebral ganglia on splanchnic nerves that travel to the pancreatic parenchyma. The pancreas also receives input from the enteric nervous system, whose branches travel along splanchnic nerves. Afferent sensory nerve fibers travel alongside efferent autonomic fibers.

(Rodriguez-Diaz et al., 2011a), suggesting that signals from autonomic nerves may not act directly upon human islet endocrine cells, as in the case of rodent islets (reviewed in Ahrén, 2000 and Taborsky, 2011). Instead, autonomic nerves in human islets are in close contact with vascular smooth muscle cells. Therefore, it was proposed that the autonomic nervous system indirectly affects human islet function by altering blood flow (Rodriguez-Diaz et al., 2011a).

Pancreatic islets also have a characteristic peri-islet sheath of non-myelinating Schwann cells, the glial cells of the peripheral nervous system. Peri-islet Schwann cells (pScs) localize to the endocrine-exocrine border on the islet periphery in multiple species, including mice, rats, sand rats, dogs, and humans (Donev, 1984; Smith, 1975; Sunami et al., 2001; Winer et al., 2003). Unlike myelinating Schwann cells elsewhere in the peripheral nervous system, which insulate axons to improve nerve conductance, pScs only partly envelop nerve fibers of the islet (Sunami et al., 2001; Woods and Porte, 1974). Mature pScs can be identified with antibodies to glial fibrillary acidic protein (GFAP) and/or S100β (Winer et al., 2003).

Role of innervation in islet development and function

Input from the autonomic nervous system is critical for the fine-tuning of islet function. While glucose is the primary stimulus for insulin secretion, islet nerves release neurotransmitters that regulate hormone secretion (Matthews and Clark, 1987). Activation of the sympathetic nervous system leads to the release of norepinephrine from islet nerves, which acts to inhibit insulin secretion and promote glucagon secretion, thereby increasing blood glucose levels (Ahrén, 2000). In contrast, activation of the

parasympathetic nervous system leads to the release of acetylcholine from islet nerves, which stimulates hormone secretion from all islet endocrine cell types and increases islet blood flow (Ahrén, 2000; Jansson and Hellerström, 1986). Centrally, the autonomic nervous system controls the cephalic phase of insulin secretion, in which the anticipation of food triggers insulin release from β-cells before a detectable rise in postabsorptive blood glucose levels (Ahrén and Holst, 2001; Berthoud et al., 1980). Islet innervation also plays major roles in triggering inter-islet Ca^{++} oscillations to coordinate hormone secretion throughout the pancreas (Fendler et al., 2009), and defining islet responses to metabolic stresses, including hypoglycemia (Taborsky and Mundinger, 2012) and neuroglycopenia (Thorens, 2011).

Sensory nerves of the pancreas are well known to mediate pain signals in pancreatitis and pancreatic cancer (Di Sebastiano et al., 1997; Lindsay et al., 2006), but also play an important role in islet physiology. In normal mice, islet sensory nerves expressing the capsaicin receptor TRPV1 dampen islet inflammation by releasing substance P and calcitonin gene-related peptide (CGRP) to reduce β-cell stress and protect against autoimmune attack. In contrast, NOD mice have a hypofunctional mutation in TRPV1, which reduces their ability to release protective neuropeptides into the islet microenvironment and increases their susceptibility to autoimmune diabetes (Razavi et al., 2006; Tsui et al., 2008b). In another study, destruction of sensory nerves by capsaicin treatment decreased the sensitivity of islets to the incretin hormone glucagon-like peptide 1 (GLP-1); these "sensory denervated" mice only showed augmented insulin secretion with a high dose of GLP-1 (Ahrén, 2004). Furthermore, mice lacking substance P show impaired glucose tolerance and insulin secretion, but improved

insulin sensitivity (Tsui et al., 2011). Because several models of sensory nerve inactivation also show improved insulin sensitivity (Koopmans et al., 1998; Moesgaard et al., 2005; Tsui et al., 2011), modulating the function of sensory nerves has been proposed as a potential therapeutic approach for both type 1 and type 2 diabetes (Suri and Szallasi, 2008; Tsui et al., 2011; Tsui et al., 2007).

In addition to classical neurotransmitters, islet nerves also produce a variety of neuropeptides, including cocaine and amphetamine-regulated transcript (CART; Wierup and Sundler, 2006), gastrin releasing peptide (GRP; Ahrén, 2006), pituitary adenylate cyclase activating polypeptide (PACAP; Ahrén, 2008), vasoactive intestinal peptide (VIP; Winzell and Ahrén, 2007), galanin (Adeghate, 2002), and neuropeptide Y (NPY; Adeghate and Donáth, 1990; Imai et al., 2007). Typically, CART, GRP, PACAP, and VIP are expressed by parasympathetic nerves, galanin and NPY by sympathetic nerves, and CGRP and substance P by sensory nerves (Figure 8). The role of neuropeptides in islet biology is complex and incompletely understood (Ahrén et al., 2006; Sundler and Bottcher, 1991).

The ability of islet endocrine cells to express neurotransmitters typically expressed by the nervous system is termed neuro-islet plasticity. For example, islets in diabetic rodents begin to express the neuropeptides VIP and CART (Ahrén et al., 2006). In human islets, in which cholinergic innervation is sparse, α-cells demonstrate the ability to secrete acetylcholine (Rodriguez-Diaz et al., 2011b). Furthermore, mouse β-cells have the capacity to synthesize serotonin, which acts both intracellularly as a post-translational protein modifier important in insulin secretion (Paulmann et al., 2009) and as a paracrine signal to increase β-cell proliferation and mass during pregnancy (Kim et al., 2010).

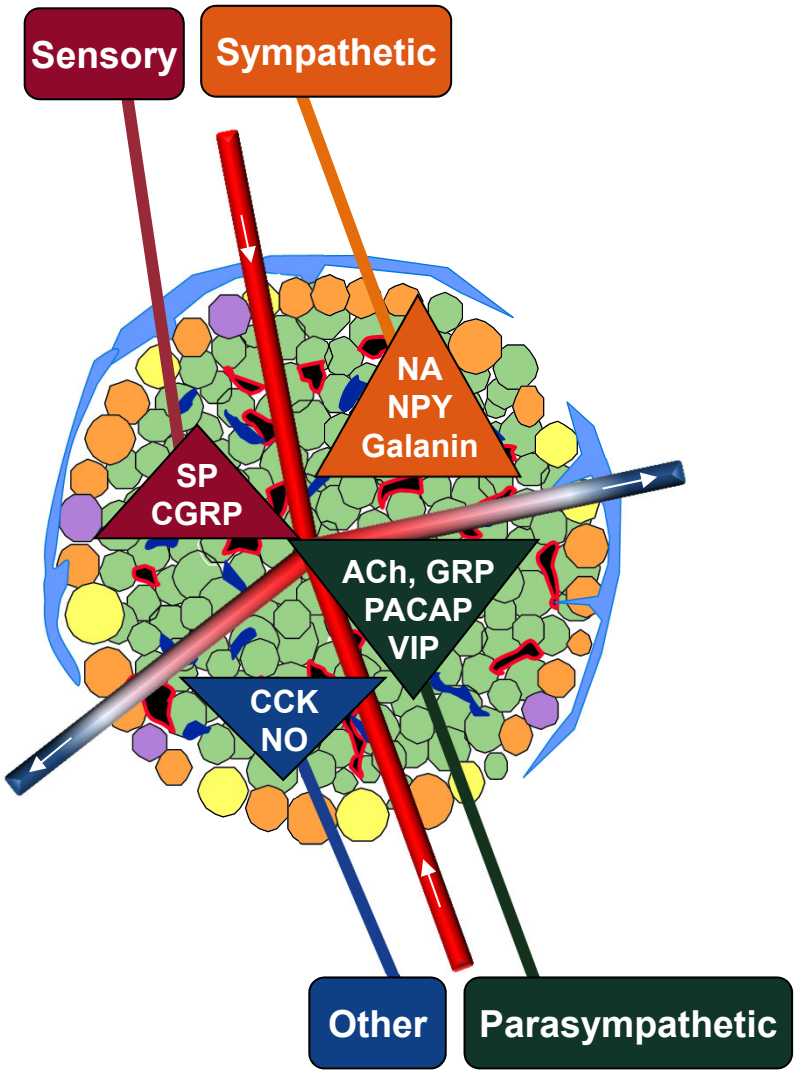

Figure 8. Schematic of islet nerve signals. Islet nerve endings penetrate the islet core alongside afferent capillaries and release several classical neurotransmitters, neuropeptides, and other signaling molecules into the islet microenvironment. Abbreviations are ACh, acetylcholine; CCK, cholecystokinin; CGRP, calcitonin gene-related peptide; GRP, gastrin releasing peptide; NA, noradrenaline; NO, nitric oxide; NPY, neuropeptide Y; PACAP, pituitary adenylate cyclase-activating peptide; SP, substance P; and VIP, vasoactive intestinal peptide. Adapted from Ahrén (2000).

In addition to the broad synthesis of serotonin or acetylcholine by murine β- and human α-cells, respectively, some endocrine cells in mouse islets also express tyrosine hydroxylase (TH), the enzyme mediating the rate-limiting step of catecholamine biosynthesis (Coker et al., 1990; Iturriza and Thibault, 1993; Karlsson et al., 1997; Korsgren et al., 1992; Lindsay et al., 2006; Persson-Sjögren et al., 1998; Persson-Sjögren et al., 2002). These observations were confirmed by crossing a knock-in mouse in which Cre recombinase was inserted in the endogenous TH locus with the *R26-lacZ* reporter mouse; in this model, scattered islet cells expressed the β-galactosidase reporter (Lindeberg et al., 2004). Islet TH expression has several proposed roles: (1) a marker of endocrine precursor cells during early pancreas development (Alpert et al., 1988; Teitelman and Lee, 1987; Teitelman et al., 1993); (2) a marker of post-proliferative, senescent β-cells (Teitelman et al., 1988); or (3) an indicator of endogenous islet catecholamine synthesis (Cegrell, 1968; Borelli and Gagliardino, 2001; Borelli et al., 2003). How TH expression is induced in selected cells is also unclear. One study found that vasoactive intestinal polypeptide enhanced the number of TH+ cells in cultured islets (Persson-Sjogren 2001), and another observed upregulation of TH in neuroblastoma cells treated with glial cell line derived neurotrophic factor (Xiao et al., 2002).

Recent studies have also demonstrated a role for the nervous system in islet development. Pancreatic nerves and glia are derived from the neural crest, which gives rise to cells of the peripheral and enteric nervous system, melanocytes, and cells forming cartilage, smooth muscle, and bone (Sauka-Spengler and Bronner-Fraser, 2008). Neural crest-derived cells can be identified by expression of the transcription factor *Wnt1* (Echelard et al., 1994). Using *Wnt1-Cre*-mediated labeling of neural crest cells with

genetic reporters, neural crest-derived cells were first found within the pancreatic mesenchyme around E10 (Plank et al., 2011), and adjacent to the pancreatic epithelium at E12.5 (Nekrep et al., 2008). At this time, the onset of the secondary transition of pancreas development, cell bodies expressing sympathetic (VMAT2) and sensory (CGRP) nerve markers were first found. While CGRP+ fibers were observed in the pancreas at E15.5 and found adjacent to islets at postnatal day 0 (P0), VMAT2+ fibers were not seen until P7, when they aligned with islets. In this study, GFAP+ glial cells were not detected until postnatal stages (Burris and Hebrok, 2007). However, the use of earlier markers of neurons (TUJ1) and glia (FABP7) demonstrated that these differentiated cell types could be found in contact with insulin+ cells as early as E15.5 (Figure 9; Plank et al., 2011).

Two genetic mouse models of neural crest cell ablation showed that pancreatic neural crest derivatives are important in regulating β-cell mass in the developing pancreas. Late-stage embryos lacking the transcription factor *Phox2b* failed to develop pancreatic nerves and glia but displayed increased β-cell mass. The authors proposed that a non-cell-autonomous inhibitory feedback loop exists between *Phox2b*-expressing neural crest cells and cells of the pancreatic epithelium, thus regulating the final populations of endocrine cells and neural crest derivatives in the pancreas (Nekrep et al., 2008). Similarly, neural crest cell ablation in *Wnt1-Cre;Foxd3*$^{fl/-}$ embryos also resulted in increased β-cell mass, but these β-cells also showed reduced expression of several markers of mature β-cells, including *Pdx1* and *Mafa* (Plank et al., 2011). Along with data showing that islet endocrine cell morphology is qualitatively normal in mice lacking the transcription factor *Sox10*, which is required for neural crest cell differentiation in the gut (Lioubinski et al., 2003), current evidence suggests that neural crest-derived cells in the embryonic pancreas

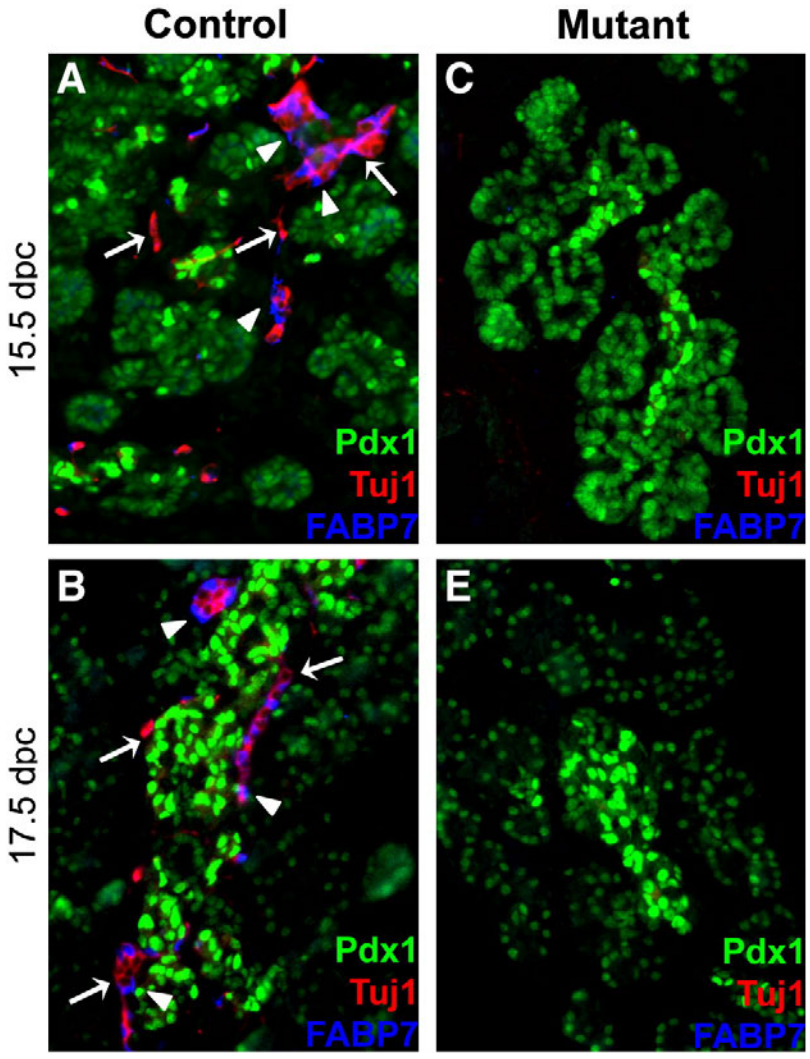

Figure 9. Islet nerves and Schwann cells are derived from the neural crest. In control mouse embryos, nerves (labeled by TUJ1, red) and Schwann cells (labeled by FABP7, blue) are found near PDX1+ islet cells (green) in late embryogenesis. In contrast, nerves and Schwann cells are absent in pancreata from *Wnt1-Cre;Foxd3*$^{fl/-}$ mutant mice, in which neural crest cells are genetically ablated. From Plank et al. (2011).

are not required for endocrine cell differentiation but instead are important in limiting β-cell proliferation and promoting β-cell maturation.

The nervous system also provides important signals for the regulation of β-cell mass in adult rodents. For example, *ob/ob* mice showed reduced β-cell proliferation two weeks after undergoing vagotomy, resulting in smaller islet volumes five months after the procedure (Edvell and Lindström, 1998). Similarly, Sprague-Dawley rats subjected to transection of the celiac branches of the vagus nerve show a 50% reduction in β-cell proliferation one week after surgery (Lausier et al., 2010). Finally, a neuronal relay from the liver, through the brain, to the pancreas can transmit the signal to increase β-cell mass in the setting of insulin resistance in the liver (Imai et al., 2008).

Peri-islet Schwann cells (pScs) are a type of peripheral glia, which are important in supporting peripheral nerves (Bhatheja and Field, 2006). Because pScs are non-myelinating, they may be most closely related to astrocytes of the central nervous system, which are also characterized by GFAP expression. One role of both astrocytes and Schwann cells is to respond to tissue damage (Pekny and Nilsson, 2005). Following nervous system injury, such as during hypoxia or following axotomy, astrocytes and Schwann cells hypertrophy, proliferate, and upregulate expression of GFAP in a process termed reactive gliosis (Buffo et al., 2008). Reactive gliosis allows tissue damage to be repaired in some cases (such as following peripheral nerve axotomy; Bhatheja and Field, 2006), but produces a scar in other cases (such as following a penetrating brain injury), hindering the repair process (Pekny and Nilsson, 2005).

The role of pScs in islet function is poorly understood. It has been proposed that pScs perhaps insulate electrical signals within the pancreatic islet, or may prevent

outward diffusion of neurotransmitters released into the islet core (Smith, 1975). Alternatively, they could provide a protective barrier for the endocrine cells, one that is disrupted in autoimmune diabetes (see "Altered islet innervation," below).

Peri-islet Schwann cells may also be important for islet endocrine cells, as glial cells are active participants in the neuroendocrine function of the hypothalamus (Garcia-Segura and McCarthy, 2004). A transgenic mouse model with global overexpression of glial cell line derived neurotrophic factor (GDNF) in GFAP+ cells showed increased β-cell mass, enhanced glucose stimulated insulin secretion, and resistance to streptozotocin-induced islet damage. These changes are thought to be the result of a direct effect of GDNF on β-cells, which express the GDNF receptor GFRα1 (Mwangi et al., 2008). Further studies with this model showed that the increased β-cell mass originated during pancreas development, as transgenic mice had a doubling of NEUROG3+ endocrine progenitor cells and increased β-cell proliferation perinatally (Mwangi et al., 2010). Nevertheless, the specific role of pScs in islet function remains unknown. One aim of this Dissertation is to improve our understanding of pScs.

Altered islet innervation in mouse models of diabetes

Islet innervation is structurally altered in several prediabetic and diabetic animal models, although it is unclear whether changes in islet innervation are contributory to or caused by the metabolic effects of the disease. For example, islet autonomic hyperinnervation was noted in prediabetic high fat diet (HFD)-fed rats. Following two to eight weeks on a HFD, islets showed an increase in the number of fibers expressing vasoactive intestinal peptide and neuropeptide Y, before any increase in islet mass

(Ahrén et al., 1999). Islet hyperinnervation was also noted in diabetic *db/db* mice and Goto-Kakizaki rats, although these models concomitantly displayed metabolic abnormalities (Ahrén et al., 2006).

In contrast, two models of autoimmune diabetes, the BioBreeder diabetic rat and the non-obese diabetic (NOD) mouse, showed reduced islet sympathetic innervation, as detected by expression of neuropeptide Y. This phenomenon was termed early sympathetic islet neuropathy (eSIN), because the change in innervation occurred early in the disease but resembled the peripheral nerve damage caused by long-term hyperglycemia in diabetic neuropathy. In these models, eSIN was correlated with the degree of infiltrating immune cells (insulitis) and the loss of the glucagon counterregulatory response to hypoglycemia (Mei et al., 2002; Mundinger et al., 2003; Taborsky et al., 2009). However, another group showed that while NOD islets lacked fibers expressing typical nerve markers, like PGP9.5 and acetylcholinesterase, they do contain fibers that express the neurotrophin receptors p75 and TrkA. From this data, the authors suggested that there is an active remodeling of islet innervation during the autoimmune process (Persson-Sjögren et al., 2005).

In addition to morphological changes in islet innervation, changes in the β-cell response to signals from the nervous system can also lead to metabolic abnormalities. Recently, the impaired insulin granule docking and reduced glucose-stimulated insulin secretion observed in a congenic strain of the Goto-Kakizaki rat was linked to overexpression of the α2A-adrenergic receptor, which binds adrenaline released from sympathetic nerves to inhibit insulin secretion (Rosengren et al., 2010). This phenotype matched that of transgenic mice with β-cell-specific overexpression of the receptor, in

which administration of an α2-agonist induced more pronounced hyperglycemia and hypoinsulinemia compared to controls (Devedjian et al., 2000). Further examination of human subjects with impaired insulin secretion revealed a single-nucleotide polymorphism in the human gene for the α2A-adrenergic receptor that imparts an increased risk for type 2 DM (Rosengren et al., 2010).

There is evidence that pScs are specifically targeted in the autoimmune destruction of islets in both non-obese diabetic (NOD) mice and humans with type 1 diabetes. During the early stages of autoimmune diabetes in NOD mice, autoreactive T-lymphocytes localize to the islet periphery, adjacent to pScs. Additionally, the GFAP and S100 antigens expressed by pScs trigger proliferative responses in T-lymphocytes from both NOD mice and humans with newly diagnosed type 1 diabetes (Winer et al., 2003). Further studies identified the target epitopes of GFAP that triggered T-cell responses, and showed that immunotherapy with one of these epitopes significantly delayed the development of type 1 diabetes in NOD mice (Tsui et al., 2008a). However, targeting of GFAP alone is not sufficient to induce autoimmune islet destruction, because diabetes does not develop in NOD-SCID mice receiving GFAP-specific T-lymphocytes alone (Winer et al., 2003). These data suggest that pScs are specifically targeted in autoimmune diabetes, and damage to the islet glial sheath may contribute to the pathogenesis of type 1 diabetes (Tsui et al., 2008b).

Finally, studies in two different models of β-cell ablation have shown that pScs dynamically respond to changes in β-cell mass, though with differing outcomes. In islets injured by the glucose analog streptozotocin, β-cell mass initially declines, while pScs hypertrophy and show an increase in cellular extensions, characteristic of reactive gliosis.

As β-cell mass returns, pScs resume their normal morphology at the islet periphery (Figure 10; Teitelman et al., 1998). However, in another model of β-cell death (tamoxifen-treated *RIP-cMycER* mice), pScs were reported to initially decrease in number but return to their normal state as β-cells were repopulated (Burris and Hebrok, 2007). Interestingly, pSC localization was unchanged in hyperglycemic *ob/ob* mice (Teitelman et al., 1998). These data suggest that pScs have context-dependent responses to islet damage; however, these responses remain to be defined.

Molecular mechanisms directing pancreatic innervation

Little is known about the mechanisms that determine pancreatic and islet innervation during development. The neural crest cells that form pancreatic nerves and glia originate in the foregut (Kirchgessner et al., 1992). The migration of neural crest cells from the foregut into the pancreas involves chemoattractant signaling from the guidance molecules netrin 1 and netrin 3, which are produced by the exocrine pancreas, to DCC receptors on the neural crest-derived cells. While DCC knockout mice show neural crest cell colonization of the gut, they lack pancreatic nerves (Jiang et al., 2003). Therefore, netrin-DCC signaling appears to be critical for the initial establishment of pancreatic innervation.

A transgenic mouse model demonstrated that overexpression of nerve growth factor (NGF) by pancreatic β-cells induces islet hyperinnervation. Specifically, islets contained more sympathetic nerve fibers, which are very dependent on NGF signaling during early postnatal life and may have outcompeted other nerve fiber types for the excess NGF. While increased islet NGF expression was detected in late embryogenesis

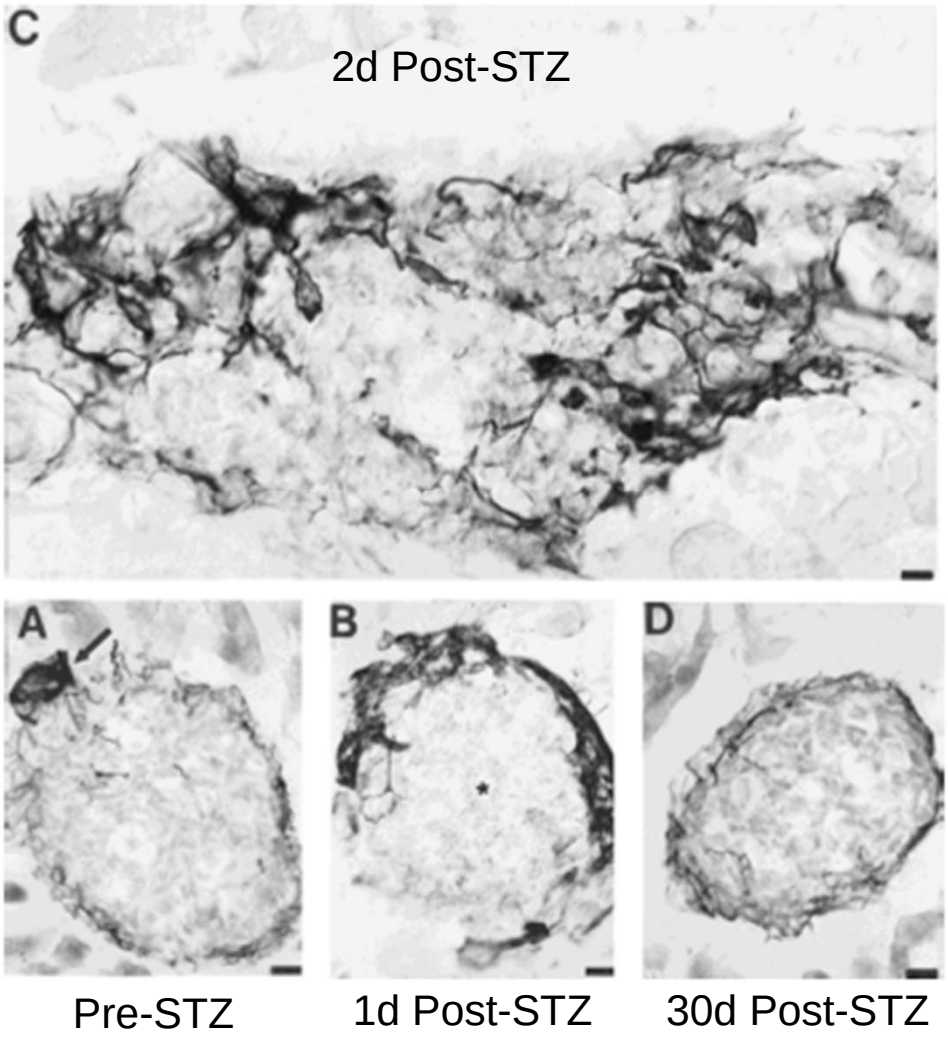

Figure 10. Peri-islet Schwann cells undergo reactive gliosis following islet injury with streptozotocin (STZ). "Histological sections of pancreas immunostained with GFAP antiserum. (A) An adult mouse islet surrounded by a sheath of GFAP+ cells. The islet also contains a polar ''neuroinsular complex'' (arrow), formed by neurons and glial cells. Bar = 40 μm. (B) Pancreatic islet at 1 day post-[STZ]. Note increased GFAP immunoreactivity in peri-islet cells. Cells in the center of the islet (asterisk) are necrotic. Bar = 40 μm. (C) Pancreatic islet of 2 days post-[STZ] mice illustrates the presence of GFAP-reactive Schwann cells. Bar = 20 μm. (D) Pancreatic islet at 30 days post-[STZ]. In some islets, peri-islet glial cells have decreased GFAP immunoreactivity. Bar = 40 μm." From Teitelman et al. (1998).

and early postnatal life, the precise timing of islet hyperinnervation was not investigated (Edwards et al., 1989). A further study demonstrated expression of NGF in β-cells and intraislet endothelial cells throughout late embryonic and postnatal development, and proposed that the decrease in NGF secretion with age contributes to remodeling of islet sympathetic innervation (Cabrera-Vasquez et al., 2009).

In another genetic mouse model, it was found that the GDNF family receptor GFRα2, which mediates development of parasympathetic neurons in the enteric nervous system through neurturin signaling, is also important for development of islet parasympathetic innervation. While GFRα2 knockout mice showed normal glucose tolerance, they had dramatically impaired secretion of islet hormones in response to neuroglucopenic stress (Rossi et al., 2005).

More recently, the cell adhesion molecule 1 (CADM1) was implicated in nerve-islet interactions. The simultaneous expression of CADM1 by both islet nerve fibers and endocrine cells suggested a potential mechanism for intercellular interactions between the two cell types. Further *in vitro* analyses showed that anti-CADM1 antibodies could block the attachment of cells from the αTC6 α-cell line to cultured neurites from superior cervical ganglia (Koma et al., 2008). A follow-up study demonstrated that this distribution of CADM1 (also called SynCAM) is present in the developing pancreas during late embryogenesis, when neural crest cell derivatives first become spatially aligned with α-cells (Shimada et al., 2012).

Islet innervation is important in islet development and function, but knowledge on the mechanisms directing islet innervation is incomplete. Therefore, investigating the ability of other islet-derived neurotrophic factors to mediate islet innervation will

improve our understanding of islet physiology. This Dissertation will highlight the role of VEGF-A.

Vascular Endothelial Growth Factor A (VEGF-A)

Structure and signaling

VEGF-A is the original member of the vascular endothelial growth factor family, which includes VEGF-B, VEGF-C, VEGF-D, and placental growth factor (Matsumoto and Claesson-Welsh, 2001). VEGF-A, originally termed vascular permeability factor (VPF), is the most potent angiogenic factor in the family (Nagy et al., 2007). In contrast, VEGF-C and VEGF-D are more important in promoting lymphangiogenesis, and VEGF-B and placental growth factor have more limited roles in normal vessel formation (Takahashi and Shibuya, 2005). All members of the VEGF family are expressed by mouse pancreatic islets (Inoue et al., 2002).

The *Vegfa* mRNA transcript is alternately spliced to yield several isoforms. These isoforms differ in their receptor specificities and in their ability to bind the ECM, which limits their migration from the cell of origin (Cébe-Suarez et al., 2006; Takahashi and Shibuya, 2005). The mouse and human sequences of VEGF-A are highly homologous, with the latter demonstrating splice isoforms that differ only in the addition of a single amino acid (Tischer et al., 1991). VEGF-$A_{164/5}$, which contains 164 amino acids in the mouse isoform and 165 in the human, is the most important for vascular development, and is sufficient to induce pathological angiogenesis (Nagy et al., 2007). Other common VEGF-A isoforms include VEGF-$A_{120/1}$, and VEGF-$A_{188/9}$ (Takahashi and Shibuya, 2005). VEGF-A assembles as a homodimer that forms a cysteine knot motif (Matsumoto and Claesson-Welsh, 2001).

Signals from VEGF family members are transmitted through several cell surface receptors (Figure 11). The primary VEGF receptors (VEGFRs) are tyrosine kinases and include VEGFR1 (also known as FLT1), VEGFR2 (also known as KDR or FLK1), and VEGFR3 (also known as FLT4). Additionally, the nonkinase receptors neuropilin 1 (NRP1) and neuropilin 2 (NRP2), which are also receptors for the semaphorin family of axon guidance molecules, are VEGFR coreceptors that bind specific VEGF family members, including VEGF-$A_{164/5}$ (Cébe-Suarez et al., 2006). VEGF-A isoforms preferentially bind to VEGFR1, VEGFR2, NRP1, and NRP2 (Nagy et al., 2007).

Role of VEGF-A in the cardiovascular system

VEGF-A was first discovered as a critical signaling protein for endothelial cells, and its role in promoting normal and pathological angiogenesis throughout the body has been well studied (Bautch, 2012; Ferrara, 2004; Nagy et al., 2007). VEGF-A-to-VEGFR2 signaling in endothelial cells stimulates vasculogenesis and angiogenesis by inducing cell proliferation, migration, and survival; it also enhances vessel permeability. In contrast, VEGF-A-to-VEGFR1 signaling in endothelial cells limits developmental angiogenesis but promotes pathological angiogenesis (Cébe-Suarez et al., 2006; Takahashi and Shibuya, 2005).

Disruption of VEGF-A signaling has extremely deleterious effects during development. Two independently generated mouse models showed that global inactivation of a single *Vegfa* allele is embryonic lethal between E11 and E12, because of impaired angiogenesis that results in growth retardation and several developmental anomalies (Carmeliet et al., 1996; Ferrara et al., 1996). Inducible genetic inactivation of

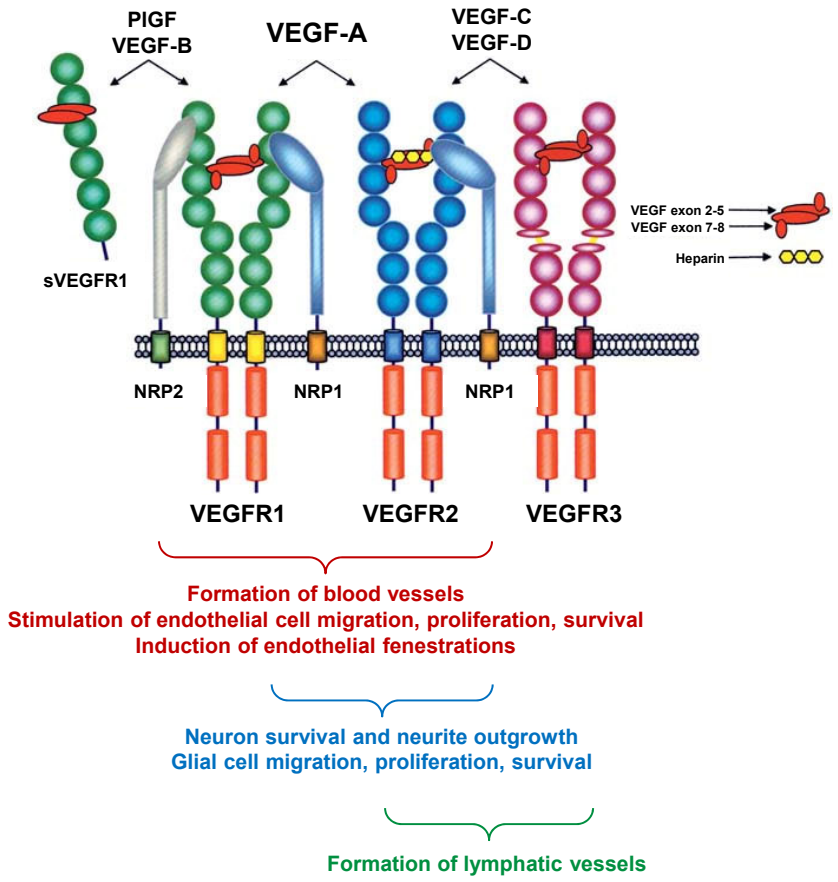

Figure 11. Summary of the roles of VEGF family member receptors in the vascular and nervous systems. Adapted from Cébe-Suarez et al. (2006).

both *Vegfa* alleles in neonatal mice also impaired body growth and organ development, resulting in premature mortality (Gerber et al., 1999). Furthermore, global inactivation of both *Kdr* alleles (encoding VEGFR2) results in embryonic lethality between E8.5 and E9.5, because of impaired hematopoietic cell and endothelial cell differentiation and the inability to form organized blood vessels (Shalaby et al., 1995). Embryos lacking VEGFR1 do not develop past E8.5, showing endothelial cell differentiation but abnormal vessel development (Fong et al., 1995). However, when only the kinase portion of VEGFR1 is deleted, vascular development is normal, suggesting that the most important role for VEGFR1 is to antagonize VEGFR2 signaling (Koch and Claesson-Welsh, 2012). Finally, while genetic deletion of *Nrp1* profoundly affects cardiovascular development (Kawasaki et al., 1999), mice lacking NRP2 are viable and show defects limited to lymphatic vessels and capillaries (Yuan et al., 2002).

VEGF-A signaling also promotes endothelial cell survival and permeability in mature vessels (Betsholtz and Armulik, 2006). Using multiple methods to inhibit global VEGF signaling, including VEGFR tyrosine kinase inhibitors and soluble VEGF-A decoy receptors, it was unexpectedly found that several vascular beds in the adult mouse are dependent on VEGF, including vasculature of the pancreatic islets, thyroid, adrenal cortex, pituitary, and villi of the small intestine (Inai et al., 2004; Kamba et al., 2006). Vessels affected by VEGF inhibitors rapidly lost patency and showed endothelial cell apoptosis within one day of treatment. Over the next few weeks, pericytes migrated away from the endothelial cell-depleted vessels, leaving just the basement membrane (Baffert et al., 2006). These VEGF signaling inhibitors have served as effective antiangiogenic therapy for proliferative retinopathy and certain cancers (Carmeliet and Jain, 2011), but

not without side effects, including cardiovascular dysfunction and renal toxicity (Chen and Cleck, 2009).

Role of VEGF-A in the nervous system

In more recent years, it was discovered VEGF-A can also signal directly to several cell types in the central and peripheral nervous systems, including neurons, glia, and neural stem cells, through expression of the endothelial cell-shared receptors VEGFR2 and NRP1 (Storkebaum et al., 2004). For example, in an *in vivo* model of peripheral nerve injury, VEGF-A pretreatment of acellular nerve grafts enhanced the inward migration of VEGFR2-expressing Schwann cells, in addition to stimulating angiogenesis (Sondell et al., 1999). Similarly, VEGF-A-to-VEGFR2 signaling enhanced axonal outgrowth in cultured neurons (Sondell et al., 2000) and in commissural axons of the brain (Ruiz de Almodovar et al., 2011). VEGF-A-to-NRP1 signaling may also be sufficient for some positive effects in neurons, as it is responsible for guiding the migration of cranial neural crest cells into branchial arch 2 (McLennan et al., 2010) and promoting the survival of migrating gonadotropin-releasing hormone neurons during development of the hypothalamus (Cariboni et al., 2011). The expression of VEGFR2 and NRP1 in motor neurons of adult mice suggests that VEGF-A is even important for homeostasis in mature nerves (Oosthuyse et al., 2001). In all, VEGF-A has been shown to stimulate neurite outgrowth, induce migration of Schwann cells and neural progenitor cells, promote neural cell survival, stimulate neurogenesis, and regulate synaptic plasticity (Ruiz de Almodovar et al., 2009; Storkebaum et al., 2004).

VEGF-A also mediates synaptogenesis of nerve fibers innervating the vasculature (Storkebaum and Carmeliet, 2011). VEGF-A produced by vascular smooth muscle cells

signals through VEGFR2 to promote vascular sympathetic innervation during neonatal development and following experimental denervation of femoral arteries. In addition, VEGF-A antagonizes semaphorin 3A signaling in cocultured neurons, preventing growth cone collapse, and increases growth cone area through VEGFR1 signaling (Marko and Damon, 2008). However, a further study demonstrated that vessels that are sparsely innervated *in vivo* show higher levels of semaphorin 3A (a chemorepellant), but similar levels of VEGF-A, when compared to highly innervated vessels (Long et al., 2009). Finally, mice with genetic or pharmacologic inhibition of VEGF-A signaling show altered morphology of neuroeffector junctions in resistance arteries, leading to dysfunctional blood flow regulation (Storkebaum et al., 2010).

Role of VEGF-A in islet development and function

Islet endocrine cells express VEGF-A in greater quantities than exocrine cells of the pancreas (Brissova et al., 2006; Christofori et al., 1995), allowing for the specialization of the intraislet vasculature (Brissova et al., 2006; Henderson and Moss, 1985). Specifically, normal mouse islets express the VEGF-A_{120} and VEGF-A_{164} isoforms, and their expression is upregulated in insulinoma tumors (Christofori et al., 1995). Intraislet capillaries demonstrate expression of the VEGFR1, VEGFR2 and NRP1 receptors (Brissova et al., 2006; Christofori et al., 1995), while VEGFR2 is downregulated in exocrine capillaries and larger pancreatic vessels (Brissova et al., 2006).

VEGF-A is the main angiogenic factor involved in recruiting endothelial cells during early pancreas development. Increased VEGF-A expression in transgenic *Pdx1-Vegfa*^{164} mice enhanced pancreatic vascularization and resulted in a three-fold increase in

islet area (Lammert et al., 2001). In contrast, genetic inactivation of *Vegfa* in the newly formed pancreas of *Pdx1-Cre;Vegfa*$^{fl/fl}$ mice results in dramatic hypovascularization and retarded growth of the gland (Lammert et al., 2003b; Pierreux et al., 2010). In this model, exocrine capillary density is slightly reduced, but intraislet capillary density is reduced by 70%. Instead of the fenestrated endothelium present in normal islet capillaries, endothelial cells in VEGF-A-deficient islets are thicker and show many caveolae (Lammert et al., 2003b). *Pdx1-Cre;Vegfa*$^{fl/fl}$ mice also show severe glucose intolerance, partly from reduced β-cell proliferation and mass (Reinert and Brissova et al., manuscript in preparation), and partly from reduced insulin secretion, as shown by pancreatic perfusion *in situ* (Jabs et al., 2008). A summary of the findings in *Pdx1-Cre;Vegfa*$^{fl/fl}$ mice is shown in Figure 12.

Unlike the dramatic changes in the pancreas-wide VEGF-A inactivation model, genetic deletion of *Vegfa* in newly formed β-cells is less detrimental to islet development (Brissova et al., 2006; Inoue et al., 2002; Iwashita et al., 2007). Inactivation of β-cell-derived VEGF-A results in about a 50% reduction in intraislet vessel density, but β-cell mass in *RIP-Cre;Vegfa*$^{fl/fl}$ mice is unchanged (Brissova et al., 2006). While *RIP-Cre;Vegfa*$^{fl/fl}$ mice show impaired glucose tolerance and reduced insulin secretion *in vivo*, isolated islets demonstrated normal to enhanced insulin secretion, and increased expression of factors important in β-cell function, including *Ins1*, *Pdx1*, and genes encoding the secretory machinery (Brissova et al., 2006; Iwashita et al., 2007). Similar to the pancreas-wide knockout, intraislet capillaries in *RIP-Cre;Vegfa*$^{fl/fl}$ mice lacked fenestrations and showed more caveolae (Brissova et al., 2006; Iwashita et al., 2007). Interestingly, HFD-fed *RIP-Cre;Vegfa*$^{fl/fl}$ mice showed an increase in β-cell mass,

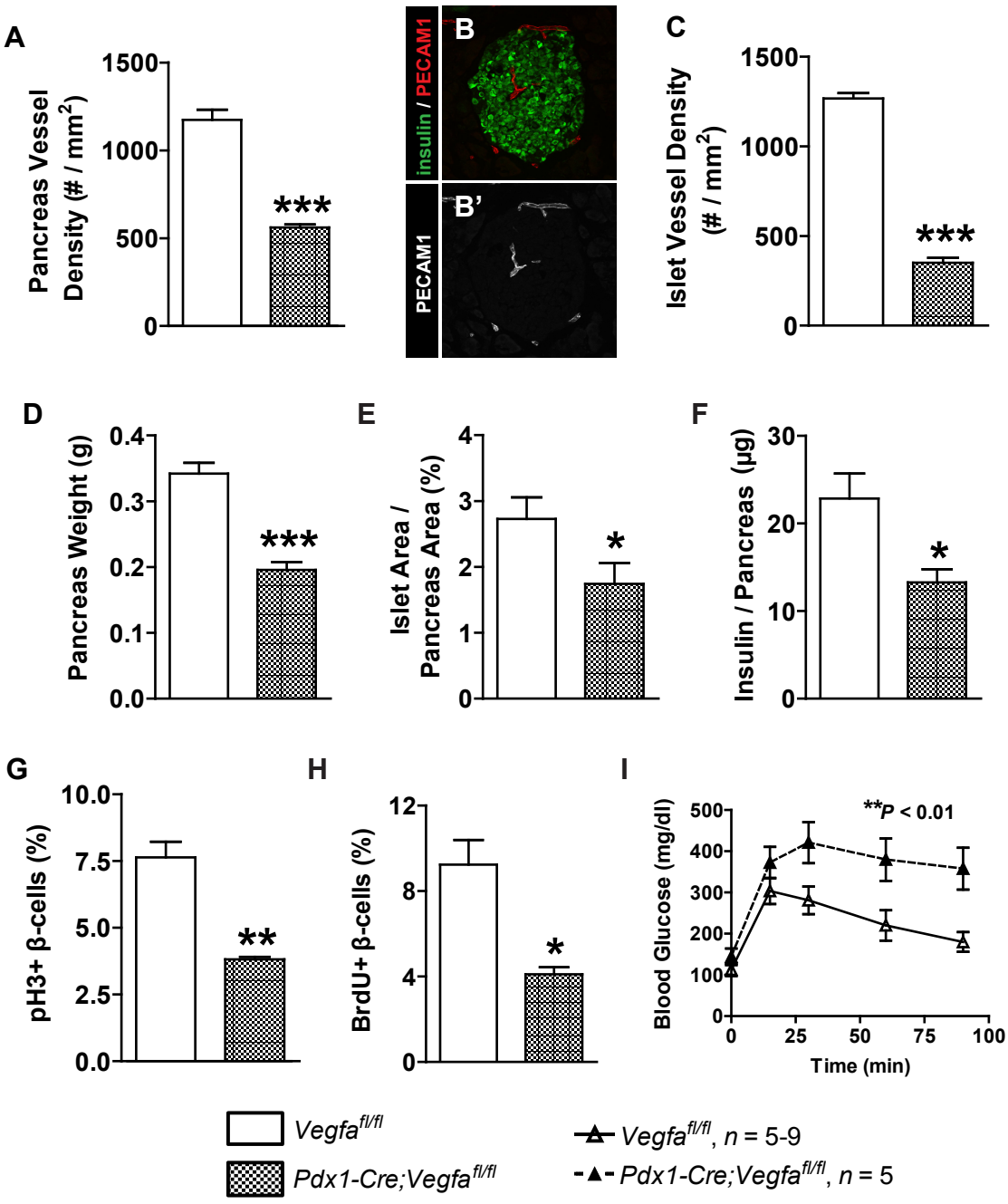

Figure 12. Pancreas-wide inactivation of VEGF-A during embryogenesis impairs development of the endocrine pancreas. *Pdx1-Cre;Vegfa*$^{fl/fl}$ mice demonstrate reduced pancreatic vessel density as early as E14.5 (**A**) and reduced islet vascularity throughout life (data from adult mice shown in **B-C**). The hypovascularized pancreas of adult *Pdx1-Cre;Vegfa*$^{fl/fl}$ mice is hypoplastic (**D**), with reduced islet mass (**E**) and insulin content (**F**), in part due to reduced β-cell proliferation as measured by phospho-histone H3 (pH3) at postnatal day 1 (**G**) and BrdU incorporation in adults (**H**). Adult *Pdx1-Cre;Vegfa*$^{fl/fl}$ mice display significantly impaired glucose tolerance (**I**). Data are from Reinert and Brissova et al. (manuscript in preparation).

compared to both HFD-fed *Vegfa*$^{fl/fl}$ mice and chow-fed controls (Toyofuku et al., 2009), indicating that the extensive vascularization of normal adult islets is not necessary for β-cell mass expansion in maturity.

These genetic models of VEGF-A inactivation clearly demonstrated that VEGF-A plays a key role in islet vascularization. However, because the defects in islet formation were initiated early in development, the true role of endothelial cells in mature islet function could not be definitively determined. Therefore, the role of VEGF-A in mature islets was studied by administering VEGF inhibitors to adult mice. This approach dramatically reduced the number of angiogenic islets and reduced tumor burden in the *RIP1-Tag2* mouse, a model of β-cell carcinoma (Inoue et al., 2002). In wild-type mice, inhibition of VEGF signaling decreased islet vascular density by half and reduced islet vessel permeability. Interestingly, these VEGF receptor inhibitor-treated mice also showed a significant improvement in glucose clearance following glucose tolerance tests, without alterations in insulin sensitivity (Kamba et al., 2006). Nevertheless, the broad actions of VEGF inhibitors following systemic administration still precluded a proper evaluation of the role of VEGF-A in mature islets, which is another subject of this Dissertation.

In an attempt to improve islet transplantation outcomes, VEGF-A has been extensively studied in islet revascularization. Islet VEGF-A expression is required for the revascularization of transplanted islets, because grafts of *RIP-Cre;Vegfa*$^{fl/fl}$ islets fail to attain the same vessel density as control grafts (Brissova et al., 2006). On the other hand, several studies have shown improved transplantation outcomes when graft VEGF-A expression is enhanced. In diabetic mice receiving mouse islets transduced with an

adenovirus containing cDNA for the human VEGF-A_{165} isoform, islet grafts showed increased endothelial cell area and enhanced insulin content and secretion, and were able to normalize the recipient's blood glucose levels (Zhang et al., 2004). In a similar approach, islets from transgenic *RIP-Vegfa* mice transplanted under the kidney capsule of diabetic recipients showed increased vessel density and blood flow, and increased insulin content and β-cell proliferation over control grafts. Furthermore, recipients of *RIP-Vegfa* islet grafts were more likely to experience normalization of blood glucose (Lai et al., 2005). Similarly, diabetic rats showed normalization of blood glucose following transplantation of a marginal mass of islets with transfected vascular endothelial cells expressing VEGF-A_{165}, but not with a marginal mass of islets alone (Cheng et al., 2007). Finally, experiments using transplanted β-cell clusters previously transduced with a tetracycline-inducible VEGF-A_{164} sequence demonstrated that increased VEGF-A expression enhanced graft revascularization and function in the first few weeks after transplantation, but was unnecessary in vascularized grafts (Mathe et al., 2006).

While the use of VEGF-A in improving revascularization of islet grafts seems promising, several mouse models of pancreas-specific or β-cell-specific overexpression of VEGF-A caution that disruption of normal expression of angiogenic factors may be detrimental to islet endocrine cells. Overexpression of VEGF-A in the developing pancreas of *Pdx1-tTA;TetO-Vegfa* mice impaired pancreas growth by restricting tip cell formation and blocking branching morphogenesis within the gland (Magenheim et al., 2011). In a similar model, β-cell-specific overexpression of VEGF-A was induced in doxycycline (Dox)-treated *RIP-rtTA;TetO-hVegfa* mice. Islets that overexpressed VEGF-A throughout embryonic development were hypervascularized and displayed

dramatically impaired islet endocrine cell formation and clustering (Figure 13; Cai et al., 2012). Excessive vascularization is not only harmful to developing islets, as Dox-induced overexpression of VEGF-A in islets of adult *RIP-rtTA;TetO-hVegfa* mice also leads to enhanced endothelial cell proliferation and mass at the expense of the β-cell population (Brissova et. al, manuscript in preparation). At any stage, Dox-treated *RIP-rtTA;TetO-hVegfa* mice show an inverse relationship between β-cell and endothelial cell proliferation (Cai et al., 2012; Brissova et. al, manuscript in preparation).

The work presented in this Dissertation aims to enhance our understanding of islet-derived VEGF-A and its roles in pancreatic islet vascularization and innervation.

Commonalities in Blood Vessel and Nerve Development

Structural alignment and functional coordination of blood vessels and nerves

The common branching pattern of the cardiovascular and nervous systems was described centuries ago, as noted in sixteenth-century drawings by the anatomist Andreas Vesalius (Ruiz de Almodovar et al., 2009). More recently, the microscopic structural alignment of blood vessels and nerves has been documented for several tissues, including skin (Bates et al., 2003; Mukouyama et al., 2005; Mukouyama et al., 2002), skeletal muscle (Bearden and Segal, 2005; Correa and Segal, 2012), gut (Nagy et al., 2009; Stapor and Murfee, 2012), and brain (Stubbs et al., 2009). Importantly, the mechanisms underlying the development and maintenance of these relationships are beginning to be uncovered.

The structural alignment of the vascular and nervous systems has physiologic implications, because the two structures are functionally interconnected. Blood vessels

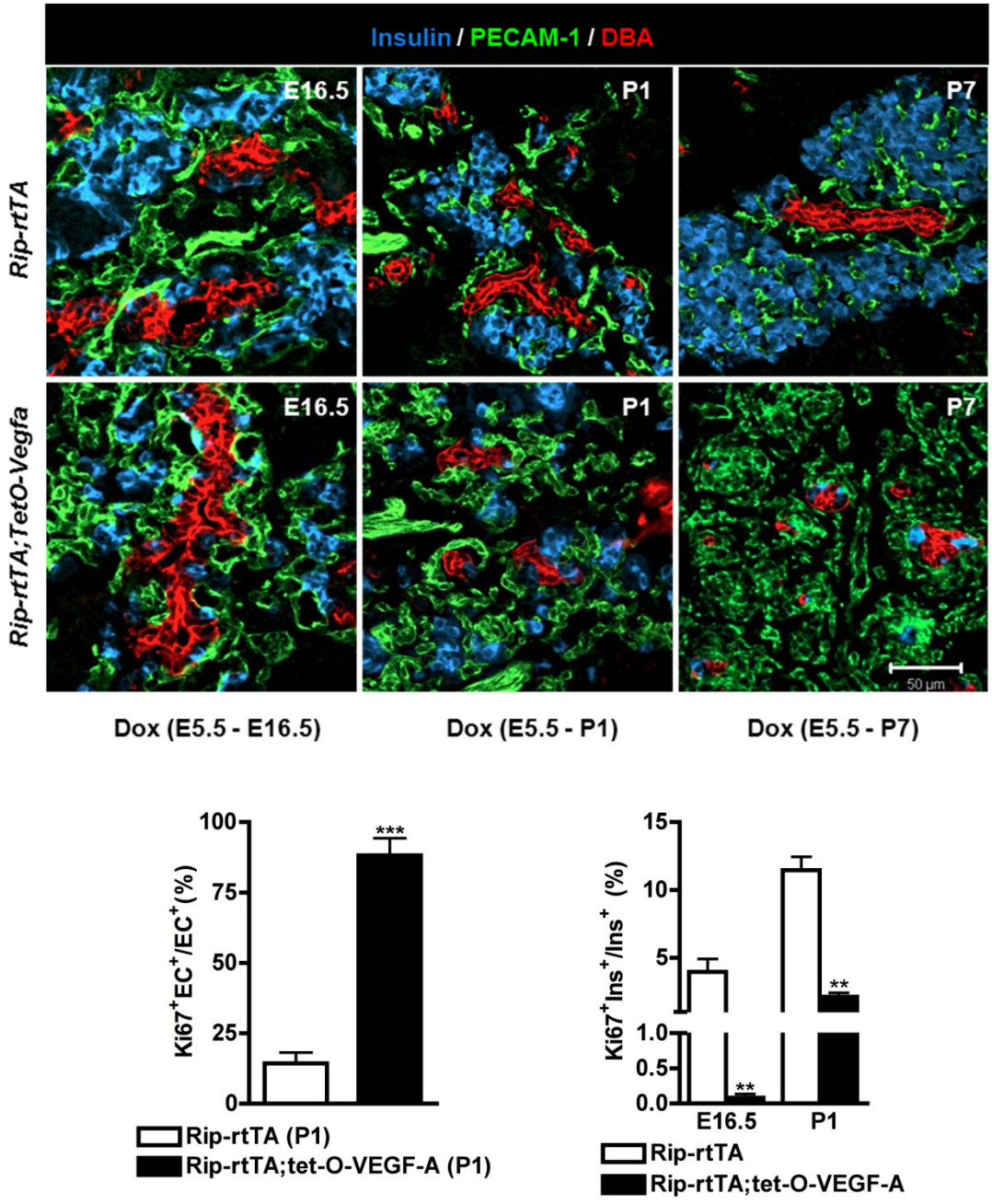

Figure 13. β-cell-specific overexpression of VEGF-A increases islet vascularization but disrupts islet formation. Top, "Pancreatic sections of *Rip-rtTA* and *Rip-rtTA;TetO-Vegfa* mice at E16.5, P1 and P7 were labeled for insulin (blue), PECAM-1 (green), and DBA ductal marker (red)." **Bottom**, endothelial cell proliferation is increased while insulin+ (Ins) cell proliferation is decreased following VEGF-A overexpression, as measured by labeling for the proliferation marker Ki67. From Cai et al. (2012).

and blood flow are intricately regulated by input from the nervous system. Throughout the body, sympathetic and sensorimotor nerves signal to vascular smooth muscle cells on arteries and veins to regulate blood flow through arterioles (Storkebaum and Carmeliet, 2011). Therefore, the close alignment between nerves and arterioles of the diaphragm was also proposed to facilitate the enhancement of blood flow following the recruitment of muscle fibers in actively working skeletal muscle (Correa and Segal, 2012). Conversely, nerves require adequate blood supply for cell survival. Mice in which the hypoxia response element was genetically deleted from the *Vegfa* promoter showed decreased circulating VEGF-A levels and adult-onset motor neuron degeneration, partly from reduced vascular perfusion (Oosthuyse et al., 2001).

Mutual guidance of blood vessels and nerves

Multiple mechanisms are involved in the co-development and subsequent structural alignment of blood vessels and nerves (Carmeliet and Tessier-Lavigne, 2005). First, vessels and nerves can respond similarly to a particular signal derived from the target tissue. Alternatively, the cells that form blood vessels and nerves may release reciprocal guidance cues in a process termed "mutual guidance" (Figure 14). The formation of blood vessels and nerves within a particular tissue may occur simultaneously, or one set of structures may be established before directing the developmental organization of the other. Examples of how tissues utilize these mechanisms to coordinate their vessel and nerve patterning are described below.

Blood vessels and nerves share several classes of signaling molecules, including angiogenic factors (VEGF-A and ephrins), neurotrophic factors (members of the NGF

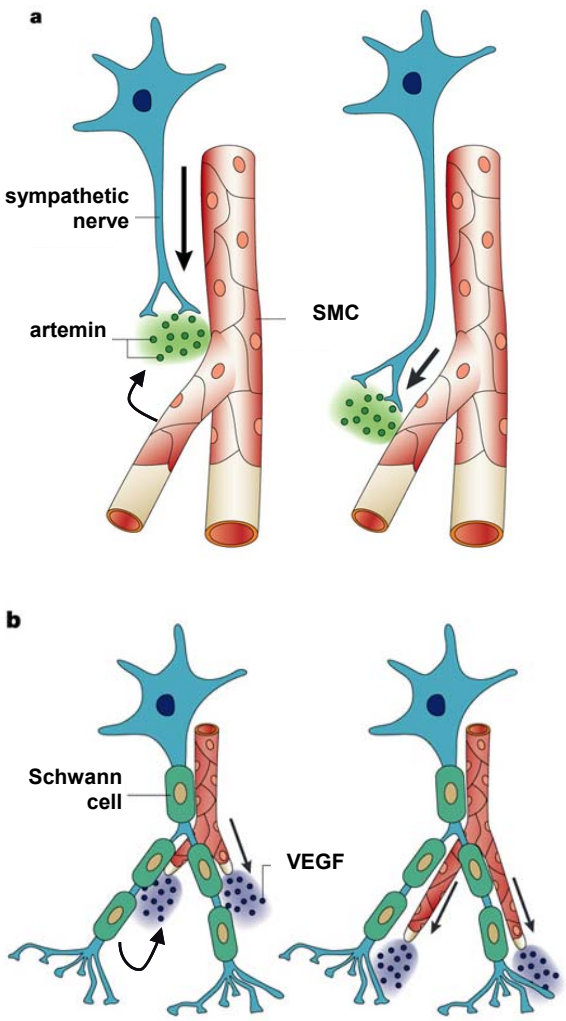

Figure 14. Mechanisms promoting neurovascular congruence. Adapted from Carmeliet (2003): "(a) Artemin is a vessel-derived neurotropic guidance signal for sympathetic nerve axons; its expression in the vascular smooth muscle cells (SMCs), from which it is secreted, gradually shifts distally and thereby guides the sympathetic nerve fibre to the target organ. (b) Vascular endothelial growth factor (VEGF) is a nerve-derived arteriotropic guidance signal for small arteries; its expression in, and secretion from, Schwann cells attracts and induces arteries, but not veins, to track alongside the nerve fibres." Alternatively, blood vessels and nerves may be recruited by identical tissue-derived factors during development.

and GDNF families), and axon guidance molecules (netrins, semaphorins, and slits) (Carmeliet and Tessier-Lavigne, 2005; Gelfand et al., 2009; Quaegebeur et al., 2011; Segura et al., 2009). During development, blood vessels and nerves respond to a variety of these attractive and repulsive cues to properly supply vascular and nervous input to the target tissue. For example, large blood vessels and nerves both follow semaphorin 3A gradients in developing quail forelimb, without any interdependence between the two structures. In this model, experimental induction of hypovascularization or hypervascularization had no effect on nerve patterning (Bates et al., 2003).

In some cases, the nervous system directs patterning of the vasculature (James and Mukouyama, 2011). In embryonic mouse limb skin, nerves induce remodeling of the primary capillary plexus into its final formation and stimulate differentiation of small arteries from that plexus; arterial vessels then serve as a source of NGF to maintain this relationship. Using mutant embryos, it was found that a lack of sensory nerves prevented arterial differentation. In contrast, a mutant with a disorganized nerve pattern showed differentiation of arteries that still demonstrated a close relationship with nerves (Mukouyama et al., 2002). A further analysis of this model showed that VEGF-A secretion by sensory nerves and their myelinating Schwann cells is responsible for nerve-driven arterial differentiation in limb skin, through NRP1 signaling to endothelial cells. However, nerve-vessel alignment was still observed in mutants lacking VEGF-A expression in nerves, suggesting a VEGF-A-independent mechanism was responsible for this patterning (Mukouyama et al., 2005).

Conversely, blood vessels provide signals to and a substrate for developing nerves. For example, genetic inactivation of the neurotropic factor artemin or its receptor GFRα3

disrupts axonal patterning throughout the sympathetic nervous system of mice. Because artemin is produced by vascular smooth muscle cells, these data demonstrate that the vasculature is an important intermediate in nerve pathfinding during development (Honma et al., 2002). A further study demonstrated that highly innervated arterial vessels express artemin to promote sympathetic nerve growth during vascular innervation, but only in the presence of NGF (Damon et al., 2007). Vascular-derived neurotrophin 3 may also guide sympathetic neurons during the development of vascular innervation (Kuruvilla et al., 2004), in addition to HGF, GDNF, and endothelin 3 (Storkebaum and Carmeliet, 2011). Finally, the vascular ECM may serve as a substrate for cells of the nervous system, because enteric neural crest cells expressing β1 integrin interact with ECM proteins to migrate along the intestinal vasculature during avian development. In that study, experimental disruption of the gut vasculature severely affected formation of the enteric nervous system, resulting in aganglionosis of the distal gut (Nagy et al., 2009).

In all, these data demonstrate that a wide variety of signals and mechanisms are responsible for directing and coordinating the development of the vascular and nervous systems.

Aims of Dissertation

The primary goal of this Dissertation is to advance understanding of the roles of VEGF-A and endothelial cells in the pancreatic islet. Islet-derived VEGF-A is critical for directing islet vascularization during development, and reciprocal signaling between endocrine cells and endothelial cells is essential for islet formation and function (Brissova et al., 2006; Lammert et al., 2001; Lammert et al., 2003b; Yoshitomi and Zaret, 2004).

Furthermore, it has been proposed that intraislet endothelial cells provide important signals for islet endocrine cells throughout life (Olsson and Carlsson, 2006). However, several critical questions regarding the role of VEGF-A and endothelial cells in islet development and maintenance remain unanswered, including: (1) might VEGF-A also act as a neurotrophic signal for islet nerves? (2) alternatively, are endothelial cells important in directing islet innervation? and (3) what is the role of VEGF-A in maintaining the vascularization and function of mature islets? These questions will be addressed in the following Chapters.

The mechanisms directing islet innervation are largely unknown, but VEGF-A, the main factor responsible in directing islet vascularization and a proven neurotrophic factor, is a prime candidate for study. Because mature islets are both highly vascularized and richly innervated, it was hypothesized that intraislet vessels and nerves either shared a common developmental mechanism to direct their patterning, such as VEGF-A, or were interdependent structures during islet development. These possibilities are considered in Chapter III. After establishing the temporal nature of the development of islet innervation, genetic mouse models of altered VEGF-A expression defined the role of the intraislet vasculature in determining islet innervation patterns.

While much is known about the role of VEGF-A in directing pancreatic vascularization during development, the specific function of VEGF-A and endothelial cells in mature islets has not been directly studied. *In vivo* experiments using VEGF signaling inhibitors demonstrated a role for VEGF-A in maintaining endothelial cells of the intraislet vasculature, but these inhibitors had effects on diverse capillary beds throughout the body (Kamba et al., 2006). Chapter IV describes the development of a

model of tamoxifen-inducible inactivation of VEGF-A to define how endothelial cells affect the maintenance of islet morphology and function in adult mice.

In the course of these experiments, several important experimental considerations for the use of genetic mouse models were discovered. First, it was unexpectedly found that two of the mouse models used in this Dissertation, which were reported to direct transgene expression to the pancreas (Gu et al., 2002; Zhang et al., 2005), actually demonstrated ectopic transgene expression in the brain. This work is described in Chapter IV. Additionally, the presence of long-term side effects in mice treated with tamoxifen drew concerns that there could be prolonged tamoxifen-induced recombination in transgenic mouse models. Prior work defined a 48-hour window of tamoxifen-induced recombination in mouse embryos (Hayashi and McMahon, 2002), but the precise timing of tamoxifen action in adult transgenic mice remained unknown. Therefore, Chapter V describes the development of a bioassay to define the temporal nature of tamoxifen-inducible Cre-*loxP* recombination *in vivo*. Together, these experiments aimed to improve our understanding of the parameters controlling Cre-*loxP* recombination *in vivo*.

Finally, the role of peri-islet Schwann cells is poorly understood (Tsui et al., 2008b). Therefore, Chapter VI describes preliminary attempts to develop a model in which pancreatic Schwann cells are chemically ablated to study their role in islet formation and function.

The materials and methods used in these studies are summarized in Chapter II. Finally, the significance of this work and future directions are presented in Chapter VII.

CHAPTER II

MATERIALS AND METHODS

Mouse Models

Animal studies were approved by the Institutional Animal Care and Use Committee at Vanderbilt University Medical Center, and were performed in accordance with the *Guide for the Care and Use of Laboratory Animals of the National Institutes of Health*. Animals were monitored by the Vanderbilt University Division of Animal Care. Animals were kept on a 12-hr light/12-hr dark schedule, and were allowed free access to standard chow and water, except where noted.

Vegfa^{tm2Gne} (abbreviated *Vegfa*$^{fl/fl}$) mice on a C57BL/6J background were generously provided by Napoleone Ferrara of Genentech, and have been described previously (Gerber et al., 1999). In these mice, exon 3 of the endogenous *Vegfa* gene is flanked by *loxP* sites ("floxed") so that Cre-mediated recombination prevents expression of functional VEGF-A protein.#

Tg(Pdx1-cre)$^{89.1Dam}$ (abbreviated *Pdx1-Cre*) mice were generously provided by Guoqiang Gu of Vanderbilt University, and have been previously described (Gu et al., 2002). In these transgenic mice, expression of Cre recombinase is driven by a 5.5 kb region of the *Pdx1* promoter, thus targeting the entire pancreatic epithelium, as well as portions of the stomach and duodenum. For a model of reduced pancreatic VEGF-A expression (abbreviated ↓VEGF-A, Chapter III), male hemizygous *Pdx1-Cre* mice were bred with female *Vegfa*$^{fl/fl}$ mice, and their offspring were crossed to obtain litters of mice

homozygous for the *Vegfa-loxP* allele. In this model, *Pdx1-Cre;Vegfa*$^{fl/fl}$ mice were compared to *Vegfa*$^{fl/fl}$ littermate controls.

For a model of inducible overexpression of VEGF-A in β-cells (abbreviated ↑VEGF-A, Chapter III), *Tg(Ins2-rtTA)*^{2Efr} mice (called *RIP-rtTA* mice in this Dissertation) were bred with *TetO-hVegfa* mice and treated with doxycycline as described below. *RIP-rtTA* mice were a generous gift from Shimon Efrat of Tel Aviv University, and have been described previously (Milo-Landesman et al., 2001). In this transgenic model, the tetracycline-responsive rtTA transactivator is expressed under control of the rat *Ins2* promoter (*RIP*) and is thus targeted to pancreatic β-cells. In the presence of doxycycline, the rtTA protein undergoes a conformational change and binds the tetracycline operator (*TetO*) to induce expression of target genes (Bockamp et al., 2002). *TetO-hVegfa* mice were generously provided by Peter Campochiaro of Johns Hopkins University, and have been described (Ohno-Matsui et al., 2002). In this model, expression of the human VEGF-A_{165} protein is induced in cells in which the doxycycline-activated rtTA protein binds the *TetO* operator.

Neural crest-derived cells were genetically labeled in the pancreas by breeding male hemizygous *Tg(Wnt1-cre)*^{11Rth} (abbreviated *Wnt1-Cre*) mice with female *Gt(ROSA)26Sor*$^{tm1(EYFP)Cos}$ (abbreviated *R26-EYFP*) reporter mice (Chapter III). *Wnt1-Cre* mice were generously provided by Michelle Southard-Smith of Vanderbilt University, and have been previously described (Danielian et al., 1998). In these transgenic mice, expression of Cre recombinase is driven by the *Wnt1* enhancer, thus targeting neural crest-derived cells beginning around E8.5. *R26-EYFP* reporter mice were obtained from The Jackson Laboratory (stock number 006148), and have been previously

described (Srinivas et al., 2001). In this model, the *loxP*-STOP-*loxP-EYFP* sequence is ubiquitously expressed from the *ROSA26* (*R26*) locus. Cre-*loxP* recombination removes the stop sequence and leads to expression of EYFP, enhanced yellow fluorescent protein.

For a model of neural crest cell ablation (described in Chapter III), late-stage *Wnt1-Cre*;*Foxd3*$^{fl/-}$ embryos were generously provided by Trish Labosky of Vanderbilt University. FOXD3 is a transcriptional repressor required to maintain the neural crest cell population (Teng et al., 2008). In the absence of FOXD3, there is a widespread loss of neural crest-derived cells, including nerves and glia of the pancreas (Plank et al., 2011).

Leptin-deficient *Lep*^{ob} mice (abbreviated *ob/ob*) on a C57BL/6J background were obtained from The Jackson Laboratory (stock number 000632), and were compared to wild-type C57BL/6J controls (abbreviated *wt/wt*; stock number 000664).

For a model of inducible gene inactivation in β-cells of adult mice, *Tg(Pdx1-cre/ERT)*^{1Mga} (abbreviated *Pdx1*^{PB}-*CreER*^{Tm}) mice on a mixed background were generously provided by Maureen Gannon and Chris Wright of Vanderbilt University. In this model, a β-cell-specific fragment of the *Pdx1* enhancer (Gannon et al., 2001) drives expression of a Cre recombinase fused to a mutated estrogen receptor (Danielian et al., 1998), resulting in expression of a tamoxifen-inducible Cre in the majority of β-cells and in a subset of non-β endocrine cells in adult mice (Zhang et al., 2005). To enable genetic deletion of *Vegfa* (Chapter IV), male hemizygous transgenic *Pdx1*^{PB}-*CreER*^{Tm} mice were bred with female *Vegfa*$^{fl/fl}$ mice, and their offspring were crossed to obtain litters of mice homozygous for the *Vegfa-loxP* allele. Adult *Pdx1*^{PB}-*CreER*^{Tm};*Vegfa*$^{fl/fl}$ mice and *Vegfa*$^{fl/fl}$ controls were treated with tamoxifen as described below.

Gt(ROSA)26Sor^{tm1Sor} (abbreviated *R26-lacZ*) reporter mice on a C57BL/6J background were obtained from The Jackson Laboratory (stock number 003474), and have been previously described (Soriano, 1999). In this model, the *loxP*-STOP-*loxP*-*lacZ* sequence is ubiquitously expressed from the *ROSA26* (*R26*) locus. Cre-*loxP* recombination removes the stop sequence and leads to expression of *lacZ*, the gene encoding β-galactosidase. For the islet transplantation bioassay described in Chapter V, male hemizygous transgenic *Pdx1*^{PB}-*CreER*^{Tm} mice were bred with female *R26-lacZ* mice.

Tg(Ins2-cre)^{1Herr} (abbreviated *Ins2-Cre*) mice were generously provided by Pedro Herrera of the University of Geneva, and have been previously described (Herrera, 2000). In this strain, expression of Cre recombinase is driven by a 0.6 kb fragment of the promoter for the *Ins2* gene and is thus targeted to insulin-expressing pancreatic β-cells.

Tg(Plp1-cre/ERT)^{3Pop} (abbreviated *Plp1-CreER*^{T2}) mice were obtained from The Jackson Laboratory (stock number 005975), and have been previously described (Doerflinger et al., 2003). In this strain, a tamoxifen-inducible Cre recombinase is expressed in cells in which transcription of the gene encoding proteolipid protein 1 is also active, including Schwann cell precursors, before they differentiate into myelinating and non-myelinating Schwann cells.

Gt(ROSA)26Sor$^{tm1(HBEGF)Awai}$ (abbreviated *R26-DTR*) mice on a C57BL/6J background were obtained from The Jackson Laboratory (stock number 007900), and have been previously described (Buch et al., 2005). In this model, the *loxP*-STOP-*loxP*-*DTR* sequence is ubiquitously expressed from the *ROSA26* (*R26*) locus. Cre-*loxP* recombination removes the stop sequence and leads to expression of the simian gene for heparin-binding EGF-like growth factor (HBEGF), also known as the diphtheria toxin

receptor (DTR). Cells expressing DTR can bind and internalize diphtheria toxin (DT) by receptor-mediated endocytosis; once in the cytoplasm, DT inactivates elongation factor 2 to terminate protein synthesis and initiate cell death by apoptosis (Buch et al., 2005). Because the endogenous mouse HBEGF does not bind DT, administration of the toxin to *R26-DTR* mice will target only cells that express DTR following Cre-mediated recombination. To induce DTR expression in various cell types and test the ability of intrapancreatic DT injection to cause cell death (see Chapter VI), male Cre-positive mice were bred with female *R26-DTR* mice.

A summary of the mouse strains used is provided in Table 1. For all developmental studies, noon of the date of the observed vaginal plug was considered to be 0.5 days post coitum (embryonic day [E] 0.5). Mice were considered adults at ten weeks of age. Before all terminal procedures and survival surgeries, mice were anesthetized with a solution of 90 mg/kg ketamine and 10 mg/kg xylazine (Henry Schein). Unless otherwise stated, age-matched littermate mice are shown as controls.

DNA Extraction and Genotyping

DNA was extracted from embryonic tails or postnatal tail biopsies using a Wizard Genomic DNA Purification Kit (Promega, catalog #A1120), according to the manufacturer's protocol, with the addition of Proteinase K (Sigma-Aldrich, catalog #P4850). Extracted DNA was typically diluted 1:20 before PCR analysis.

Alternatively, DNA was isolated from earpunch biopsies from weaned mice. Earpunch biopsies were boiled in a 100°C heat block for 20 minutes in 50 µl of a solution containing 25 mM NaOH and 0.2 mM EDTA, until tissue was mostly digested. After the

Table 1. Mouse models.

MGI Nomenclature	Abbreviation	Reference	Genotyping Primers
Foxd3^{tm1Lby}, *Foxd3*^{tm2Lby}, *Foxd3*^{tm3Lby}	*Foxd3*$^{fl/-}$	Teng et al., 2008	See Reference
Tg(Ins2-cre)^{1Herr}	*Ins2-Cre*	Herrera, 2000	5'- TGC CAC GAC CAA GTG ACA GC -3' (forward) 5'- CCA GGT TAC GGA TAT AGT TCA TG -3' (reverse)
Lep^{ob}	*ob/ob*	Coleman, 1978	5'- TGT CCA AGA TGG ACC AGA CTC -3' 5'- ACT GGT CTG AGG CAG GGA GCA -3'
Tg(Plp1-cre/ERT)^{3Pop}	*Plp1-CreER*^{T2}	Doerflinger et al., 2003	5'- TGC CAC GAC CAA GTG ACA GC -3' (forward) 5'- CCA GGT TAC GGA TAT AGT TCA TG -3' (reverse)
Tg(Pdx1-cre)$^{89.1Dam}$	*Pdx1-Cre*	Gu et al., 2002	5'- TGC CAC GAC CAA GTG ACA GC -3' (forward) 5'- CCA GGT TAC GGA TAT AGT TCA TG -3' (reverse)
Tg(Pdx1-cre/ERT)^{1Mga}	*Pdx1*^{PB}*-CreER*^{Tm}	Zhang et al., 2005	5'- TGC CAC GAC CAA GTG ACA GC -3' (forward) 5'- CCA GGT TAC GGA TAT AGT TCA TG -3' (reverse)
Gt(ROSA)26Sor$^{tm1(HBEGF)Awai}$	*R26-DTR*	Buch et al., 2005	5'- AAA GTC GCT CTG AGT TGT TAT -3' (common forward) 5'- GGA GCG GGA GAA ATG GAT ATG -3' (wild-type reverse) 5'- CAT CAA GGA AAC CCT GGA CTA CTG -3' (mutant reverse)
Gt(ROSA)26Sor$^{tm1(EYFP)Cos}$	*R26-EYFP*	Srinivas et al., 2001	5'- GGA GCG GGA GAA ATG GAT ATG -3' (wild-type reverse) 5'- AAA GTC GCT CTG AGT TGT TAT -3' (common forward) 5'- AAG ACC GCG AAG AGT TTG TC -3' (mutant reverse)
Gt(ROSA)26Sor^{tm1Sor}	*R26-lacZ*	Soriano, 1999	5'- AAA GTC GCT CTG AGT TGT TAT -3' (common) 5'- GCG AAG AGT TTG TCC TCA ACC -3' (mutant reverse) 5'- GGA GCG GGA GAA ATG GAT ATG -3' (wild-type reverse)
Tg(Ins2-rtTA)^{2Efr}	*RIP-rtTA*	Milo-Landesman et al., 2001	5'- GTG AAG TGG GTC CGC GTA CAG -3' 5'- GTA CTC GTC AAT TCC AAG GGC ATC G -3'
Unlisted	*TetO-hVegfa*	Ohno-Matsui et al., 2002	5'- TCG AGT AGG CGT GTA CGG -3' 5'- GCA GCA GCC CCC GCA TCG -3'
Vegfa^{tm2Gne}	*Vegfa*$^{fl/fl}$	Gerber et al., 1999	5'- CCT GGC CCT CAA GTA CAC CTT -3' (forward) 5'- TCC GTA CGA CGC ATT TCT AG -3' (reverse)
Tg(Wnt1-cre)^{11Rth}	*Wnt1-Cre*	Danielian et al., 1998	5'- TGC CAC GAC CAA GTG ACA GC -3' (forward) 5'- CCA GGT TAC GGA TAT AGT TCA TG -3' (reverse)

samples cooled to room temperature, 50 µl of 40 mM Tris HCl was added. Samples were briefly vortexed and centrifuged at 14000 RPM for 6 minutes. The sample supernatant was transferred to a clean tube and stored at -20°C. DNA obtained from earpunch biopsies was used undiluted in PCR reactions.

PCR primers for genotyping were obtained from Integrated DNA Technologies. Upon receipt, primers were reconstituted in DNase-free water at a concentration of 100 µM, diluted (typically 15 µl primer plus 85 µl water), and stored at -20°C until use. Primer sequences are shown in Table 1. Following preparation of the reaction mixtures described below, target DNA was amplified using the thermal cycler conditions shown in Table 2. PCR products were resolved on a 1% agarose gel in 1X TBE buffer containing 100 ng/ml ethidium bromide, unless stated otherwise.

PCR genotyping for the presence of Cre recombinase transgenes was performed using generic Cre primers to amplify a 675 bp DNA product (Le Marchand and Piston, 2010). First, a 5X master mix containing 25 µl of each primer, 25 µl of PCR nucleotide mix (Promega, catalog #C1141), 400 µl of 10X PCR Buffer I with $MgCl_2$ (Applied Biosystems), and 425 µl of DNase-free water was made and stored at -20°C for subsequent experiments. Each final reaction contained 4 µl of the 5X master mix, 0.06 µl of AmpliTaq DNA polymerase (Applied Biosystems, catalog #N8080171), 14.94 µl of DNase-free water, and 1 µl of genomic DNA.

PCR genotyping was used to differentiate the wild-type *Vegfa* and *Vegfa-loxP* (floxed) alleles, using primers described (Gerber et al., 1999). Each reaction contained 1 µl of combined forward and reverse primers, 1 µl of PCR nucleotide mix (Promega, catalog #C1141), 5 µl of PCR buffer without $MgCl_2$ (Applied Biosystems), 4 µl of

Table 2. PCR conditions for genotyping.

	All Cre transgenes	***Vegfa, Vegfa-loxP***	***R26-EYFP***	***R26-DTR***	***R26-lacZ***
PCR Reaction Mix	AmpliTaq	AmpliTaq Gold	FailSafe	ReadyMix	ReadyMix
Initiation Step	3' at 93°C	2' at 50°C then 10' at 95°C	3' at 94°C	3' at 94°C	2' at 93°C
Denaturing Step	20'' at 93°C	15'' at 95°C	30'' at 94°C	30'' at 94°C	30'' at 93°C
Annealing Step	20'' at 60°C	1' at 55°C	1' at 58°C	1' at 61°C	30'' at 58°C
Elongation Step	45'' at 72°C	2' at 72°C	1' at 72°C	1' at 72°C	1' at 65°C
Amplification Cycles	30	32	35	35	40
Final Elongation Step	5' at 72°C	3' at 72°C	2' at 72°C	2' at 72°C	5' at 65°C
Final Hold	4°C	4°C	10°C	10°C	6°C
Expected Products	675 bp for Cre+ mice	150 bp for *Vegfa-loxP* 100 bp for *Vegfa*	600 bp for wild-type *R26* 320 bp for *R26-EYFP*	603 bp for wild-type *R26* 242 bp for *R26-DTR*	500 bp for wild-type *R26* 250 bp for *R26-lacZ*
Gel Electrophoresis	1% agarose	2.5% agarose	1.5% agarose	1% agarose	1% agarose

25 mM $MgCl_2$, 0.25 µl of AmpliTaq Gold DNA polymerase (Applied Biosystems, catalog #4311806), 36.5 µl of DNase-free water, and 1 µl of genomic DNA. A 148 bp band was amplified when the *Vegfa-loxP* allele was present, and a 40 bp PCR product was amplified in the presence of a wild-type *Vegfa* allele. PCR products were separated on a 2.5% agarose gel.

PCR genotyping for the *R26-EYFP* allele was performed using the primers suggested by The Jackson Laboratory. A 320 bp amplification product was generated in the presence of the mutant allele, while the wild-type allele generated a 600 bp product. Each reaction contained 1 µl each of the three primers, 10 µl of 2X FailSafe PCR mix (Epicentre, catalog #FSP995E), 0.5 µl of FailSafe DNA polymerase (Epicentre, catalog #FSE51100), 5.5 µl of DNase-free water, and 1 µl genomic DNA. PCR products were separated on a 1.5% agarose gel.

PCR genotyping for the *R26-lacZ* and *R26-DTR* alleles were performed with primers described (Soriano, 1999) or suggested (The Jackson Laboratory). Each reaction contained 5 µl of ReadyMix Taq PCR Reaction Mix (Sigma-Aldrich, catalog #P4600), 1 µl each of the three respective primers, 1.5 µl of DNase-free water, and 1 µl of genomic DNA. The *R26-lacZ* allele produced a 250 bp amplification product, while the wild-type allele produced a 500 bp product (Soriano, 1999). The *R26-DTR* product was 242 bp, while the wild-type allele was 603 bp (The Jackson Laboratory).

Doxycycline Preparation and Administration

Doxycycline (Dox, Sigma-Aldrich, catalog #D9891) was dissolved in drinking water containing 1% Splenda (zero-calorie sucralose sweetener) for a final Dox

concentration of 2 mg/ml. Dox water was freshly prepared every other day and administered in light-protected containers. For developmental studies, Dox was administered from 5.5 days post coitum to ensure that embryos would be exposed to Dox as soon as the *Ins2* gene became transcriptionally active. Adult (ten-week-old) mice were treated with Dox for one week.

Tamoxifen Preparation and Administration

Corn oil (Sigma-Aldrich, catalog #C8267) was sterilized using a Steriflip vacuum-assisted filter unit (Millipore, catalog #SCGP00525). Tamoxifen (Tm, Sigma-Aldrich, catalog #T5648) was dissolved in filter-sterilized corn oil to make solutions of 10 mg/ml or 20 mg/ml, which were subsequently protected from light. Tm solutions were freshly prepared the day prior to each injection and placed on a nutator to dissolve overnight at room temperature.

Before treatment, excess fur was shaved from the backs of recipient mice under isoflurane anesthesia, to provide an accessible injection site that could be neatly sealed with tissue glue. Using a 23-gauge needle (Becton Dickinson & Co., catalog #305145), recipient mice were given subcutaneous injections of 1 mg Tm (100 µl volume), 8 mg Tm (400 µl volume), or corn oil vehicle every 48 hours, for a total of 3 doses over a 5-day period. Injection sites were sealed with Vetbond tissue adhesive (3M, catalog #1469SB) to prevent oil leakage. Following Tm or vehicle administration, mice were housed individually to prevent cross-contamination (Brake et al., 2004).

Diphtheria Toxin Preparation and Intrapancreatic Administration

Diphtheria toxin (DT, List Biological Laboratories, Inc., catalog #150) was hydrated in sterile 1X PBS at a concentration of 1000 ng/µl and stored in aliquots at -20°C. Immediately before use, DT was diluted in sterile 1X PBS at the indicated concentration and injected.

Adult mice to be injected intrapancreatically with DT or saline vehicle were anesthetized with ketamine/xylazine. Once the mice were unresponsive to a toe pinch, the abdomen was shaved and sterilized with a dilute chlorhexidine solution (1 oz of 2% chlorhexidine in 128 oz water, Henry Schein). A 1-cm midline incision was made in the abdomen, about 1 cm below the sternum. Intestinal loops were gently externalized until the duodenal portion of the pancreas was visualized within the peritoneal cavity. A 31-gauge insulin syringe (Becton Dickinson & Co., catalog #305937) was used to administer DT or saline focally into the pancreas, until the tissue was visibly inflated. The intestinal loops were then manipulated to expose the splenic portion of the pancreas, which was also injected, and then the intestines were gently returned to the peritoneal cavity. The total volume injected into the pancreas was 50-100 µl. The abdominal muscle incision was sutured (5-0 vicryl sutures, Ethicon, catalog #J493G) and the skin opening was closed with 7 mm staples (Reflex Skin Closure System, Braintree Scientific, Inc., catalog #RF7 KIT). Mice were wrapped in sterile gauze and placed under a warm lamp until recovery from anesthesia. Mice were monitored for infection or pain each day following the surgery. Random (non-fasting) blood glucose values were recorded before the surgery and every day thereafter. Staples were removed two weeks after surgery.

Islet Isolation

Islet isolation was performed in collaboration with Greg Poffenberger or Anastasia Coldren and Marcela Brissova of the Vanderbilt Islet Procurement and Analysis Core. Islets were isolated by collagenase P digestion, as described (Brissova et al., 2002; Brissova et al., 2004). Anesthetized mice were dissected to expose the pancreas, and the bile duct was visualized and ligated with sutures. Three milliliters of 0.6 mg/ml collagenase P (Roche Molecular Biochemicals) in Hank's balanced salt solution (HBSS, Gibco) was infused directly into the pancreatic tissue by injection into the bile duct. Once inflated, the pancreatic tissue was dissected from the mouse and digested further in 6.7 ml of 0.6 mg/ml collagenase P in HBSS for eight minutes using a wrist-action shaker in a 37°C water bath, followed by two minutes of manual shaking at room temperature. Seven to eight milliliters of ice-cold 10% fetal bovine serum (FBS) in HBSS was then added to inactivate the collagenase. To wash, the digested pancreata were centrifuged at 1000 RPM for two minutes at 4°C, the supernatant was decanted, and 14-15 ml of 10% FBS in HBSS was added. The previous step was repeated for a total of three washes before the pancreatic tissue pellet was resuspended in fresh 10% FBS in HBSS, plated in a Petri dish, and placed on ice. Islets were handpicked to nearly 100% purity under microscopic guidance, using sterile RNase-free pipette tips.

RNA Extraction and Quantitative Real-Time RT-PCR

For quantitative PCR analysis of islet gene expression, RNA was extracted using an Ambion RNAqueous kit (Life Technologies, catalog #AM1912) and trace contaminating DNA was removed with an Ambion TURBO DNA-free kit (Life

Technologies, catalog #AM1907), according to the manufacturer's protocols. Immediately following islet isolation, 150-400 purified islets (from one to five mice) were washed three times in 10 mM PBS, centrifuging for one minute at 1000 RPM between each wash. Following the washes, 350-700 µl of lysis buffer (from the RNAqueous kit) was added to the islet pellet. Samples were vortexed vigorously and stored at -80°C until RNA extraction was to be completed. Following extraction, RNA quality and purity was assessed by the Vanderbilt Genome Sciences Resource using a Nanodrop ND-1000 spectrophotometer and an Agilent 2100 Bioanalyzer. Only RNA samples with a RIN score >7 were used for quantitative real-time RT-PCR.

Purified RNA was reverse transcribed to cDNA using a High-Capacity cDNA Archive Kit with the addition of an RNase inhibitor (Applied Biosystems, catalog #4368814 and #N8080119), according to the manufacturer's protocol. Quantitative PCR was performed using a TaqMan primer/probe approach, using the primer/probes shown in Table 3. Each reaction contained 10 µl of 2X TaqMan PCR Master Mix (Applied Biosystems, catalog #4304437), 1 µl of 20X primer/probe, and 9 µl of equivalent amounts of cDNA (5-10 ng per reaction). Quantitative PCR was performed with an iQ5 Multicolor Real-Time PCR Detection System (Bio-Rad), with the following cycle conditions: 50°C for two minutes, 95°C for ten minutes, then 40 cycles of 95°C for 15 seconds and 60°C for one minute.

Data were analyzed using the $\Delta\Delta C_t$ method (Livak and Schmittgen, 2001), as calculated by the iQ5 system software. Expression of each gene was normalized to either *Rn18s* (encoding 18S ribosomal RNA) or *Tbp* (encoding TATA box binding protein) as reference genes (Dai et al., 2012). In Chapter III, the relative expression of *Tbp*-

Table 3. Primers for quantitative real-time RT-PCR.

Gene Symbol	TaqMan Assay ID
Rn18s	Hs99999901s1
Edn3	Mm00432986_m1
Gdnf	Mm00599849_m1
Gfap	Mm01253033_m1
Ins2	Mm00731595_gh
Kdr	Mm00440099_m1
Mafa	Mm00845209_s1
Ngf	Mm00443039_m1
Pdx1	Mm00435565_m1
Pecam1	Mm01242584_m1
Tbp	Mm00446973_m1
Vegfa (custom-made *loxP* modification)	Mm00437306_m1
Vegfb	Mm00442102_ml

normalized genes in each sample from *Pdx1-Cre;Vegfa*$^{fl/fl}$ mice was compared to each sample of age-matched *Vegfa*$^{fl/fl}$ controls (n = 3–4 islet preparations per group), then averaged. The relative expression of *Tbp*-normalized genes in each sample from one-week-Dox-treated *RIP-rtTA;TetO-hVegfa* mice was compared to each sample of the untreated *RIP-rtTA;TetO-hVegfa* controls (n = 4 islet preparations per group), and averaged. In Chapter IV, the relative expression of *Rn18s*-normalized genes in each sample from Tm-treated *Pdx1*^{PB}*-CreER*^{Tm}*;Vegfa*$^{fl/fl}$ mice was compared to each sample from Tm-treated *Vegfa*$^{fl/fl}$ controls (n = 3 islet preparations per group). Occasional samples were omitted from further analysis after determining that their *Rn18s* Ct was greater than one cycle different than the other samples. Quantitative PCR experiments were performed according to the Minimum Information for Publication of Quantitative Real-Time PCR Experiments (MIQE) guidelines (Bustin et al., 2009).

RNA Sequencing

For RNA sequencing analysis, islets were harvested from two untreated *RIP-rtTA;TetO-hVegfa* mice and two *RIP-rtTA;TetO-hVegfa* mice treated with Dox for one week. Purified islets were combined into one sample per genotype, and RNA was extracted and assessed for quality as described above. Samples were sent to the HudsonAlpha Institute for Biotechnology (Huntsville, Alabama) for RNA amplification and RNA sequencing. RNA amplification was performed on a 30 ng sample of total RNA using the NuGEN Ovation RNA amplification system optimized for RNA sequencing. Sequencing reactions were then performed with the Illumina HiSeq (v3 chemistry) using modified standard Illumina methods as described (Mortazavi et al., 2008).

Following RNA sequencing, data were analyzed using Avadis NGS software (Strand Scientific Intelligence) by Kristie Aamodt and Marcela Brissova. Genes previously described to be important in nerve growth and axonal guidance were identified through a literature search, and their expression levels (expressed as reads per kilobase per million, or RPKM) and relative fold changes are listed in Tables 6–8 of Chapter III. Genes with less than 20 reads were eliminated by an expression filter in Avadis, and are labeled as "low expression."

ELISA

For quantification of islet VEGF-A production, aliquots of 70 size-matched, purified islets were cultured in an eight-well chamber slide (Nalge Nunc International, catalog #154534) in 480 µl RPMI-1640 medium containing 10% FBS and 11 µM glucose for 48 hours at 37ºC. Following incubation, the media supernatants were collected and assayed for VEGF-A by ELISA (R&D Systems, catalog #MMV00), according to the manufacturer's protocol.

Islet Perifusion

Insulin secretion by aliquots of 30 size-matched islets (53 islet equivalents) from Tm-treated *Vegfa*$^{fl/fl}$ and *Pdx1*^{PB}-*CreER*^{Tm};*Vegfa*$^{fl/fl}$ mice was assessed using a dynamic cell perifusion system (modified from Wang et al., 1997). The base perifusion medium was freshly prepared on the day of the experiment by emptying the contents of a 1 g bottle of Dulbecco's modified Eagle's medium powder (DMEM, Sigma-Aldrich, catalog #D5030) into 1 L of deionized water and adding 3.2 g $NaHCO_3$ (Sigma-Aldrich, catalog

#S6014), 0.58 g L-glutamine (Sigma-Aldrich, catalog #G8540), 0.11 g sodium pyruvate (Sigma-Aldrich, catalog #P2256), 1.11 g HEPES (Sigma-Aldrich, catalog #H7523), 1 g of RIA-grade BSA (Sigma-Aldrich, catalog #A7888), and 3 ml of 0.5% phenol red (Sigma-Aldrich, catalog #P0290). The medium was then vacuum-filtered (Millipore, catalog #SCGPU05RE) and de-gassed at 37°C for 30 minutes. To the base perifusion medium, D-glucose (Sigma-Aldrich, catalog #G8270) was added to a final concentration of 5.6 mM (to measure basal insulin secretion) or 16.7 mM (to measure glucose-stimulated insulin secretion). To enhance glucose-stimulated insulin secretion, 100 μM 3-isobutyl-1-methylxanthine (IBMX, Sigma-Aldrich, catalog #I5879), a phosphodiesterase inhibitor that increases intracellular cAMP, was added to a solution of 16.7 mM D-glucose.

Following isolation, islets were placed in the perifusion chamber, submersed in a 37°C water bath, and perifused with medium at a flow rate of 1 ml/min. Islets were first washed with 5.6 mM D-glucose in base perifusion medium for 30 minutes, discarding the effluent. Throughout the remainder of the experiment, one 3-ml effluent fraction was collected for every three minutes of perifusion. Islets were perifused with media containing 5.6 mM D-glucose for 30 minutes, 16.7 mM D-glucose for 9 minutes, 5.6 mM D-glucose for 21 minutes, 16.7 mM D-glucose plus IBMX for 9 minutes, then 5.6 mM D-glucose for 21 minutes. Each effluent fraction was assayed for insulin content by the Vanderbilt University Hormone Assay and Analytical Services Core, using a liquid-phase radioimmunoassay (Rat Insulin RIA Kit by Linco/Millipore, catalog #RI-13K).

Islet Transplantation

Islet transplant experiments in *R26-lacZ* and *Pdx1*^{PB}-*CreER*^{Tm};*R26-lacZ* mice were performed with littermate donors and recipients, from 6 to 17 weeks of age, as described (Brissova et al., 2004). Recipient mice were treated with Tm or vehicle, with the last dose injected 48 hours, 1 week, 2 weeks, or 4 weeks before islet transplantation was performed. On the day of transplantation, islets were isolated from donor mice by collagenase P digestion and handpicked to nearly 100% purity. Islets were washed three times in sterile 10 mM PBS containing 1% serum (obtained from the donor mouse), and then loaded into P10 tubing (connected to a 1 ml syringe via a gel loading tip), in preparation for transplantation by Greg Poffenberger. Littermate recipient mice were anesthetized and prepared for surgery by shaving the flank, draping the surgical site, and sterilizing the flank skin with a dilute chlorhexidine solution. Once unresponsive to a toe pinch, the flank skin and underlying muscle layer were opened to expose the kidney. A 23-gauge butterfly needle was used to gently separate the kidney capsule from the parenchyma, creating a channel through which the P10 tubing was inserted. Islets were carefully injected beneath the renal capsule, creating an easily identifiable mass of pale tissue. Following removal of the needle, a tiny drop of tissue glue was used to seal the site where the capsule was punctured, located ~0.5 cm away from the graft. The muscle layer was sutured, the skin opening was stapled, and the mice were allowed to recover from anesthesia wrapped in sterile gauze under a warm lamp. Mice were monitored for infection or pain each day following the surgery. Each graft contained 50 to 150 islets from a single littermate donor mouse. Graft-bearing kidneys were harvested two weeks after islet transplantation.

Glucose Tolerance Test (GTT)

Mice were fasted overnight for 16 hours, and weighed at the start of the experiment, around 9 a.m. Tail veins were nicked to obtain a basal blood glucose measurement with a Contour glucometer (Bayer HealthCare LLC). Mice were given an intraperitoneal injection of 10% D-glucose in 10 mM PBS (sterilized using a 0.2 μm polyethersulfone syringe filter, Thermo Scientific/Nalgene, catalog #194-2520), using a 27-gauge needle (Becton Dickinson & Co., catalog #305109), at a dose of 2 g/kg body weight. Blood glucose measurements were repeated 15, 30, 60, 90, and 120 minutes following the glucose injection.

Hyperglycemic Clamp

Hyperglycemic clamps were performed by the Vanderbilt Mouse Metabolic Phenotyping Center (MMPC), according to established protocols (Berglund et al., 2008; Niswender et al., 1997). Briefly, six-month-old Tm-treated male mice underwent surgery to implant catheters in the carotid arteries and jugular veins. One week later, mice were fasted for 6 hours before performing the clamp. The target blood glucose level was ~200 mg/dl. With the time of glucose infusion being t = 0', arterial blood samples were taken at t = -15', -5', 2', 3', 4', 5', 10', 20', 30', 40', 50', 60', 70', 80', and 90'. Arterial blood was assessed for blood glucose, serum insulin and C-peptide levels. The glucose infusion rate (GIR) was also recorded.

High Fat Diet

Some Tm-treated female mice were also placed on a high-fat diet (HFD, with 60% of kcals from fat; Bio-Serv), beginning one month after Tm treatment. Following 16 weeks on the diet, body composition was assessed by nuclear magnetic resonance (NMR) spectroscopy using a Minispec mq 7.5MHz analyzer (Bruker Instruments) in the Vanderbilt MMPC.

Pancreatic Insulin Content

Pancreata were harvested from anesthetized mice before cervical dislocation. Dissected pancreata were rinsed in 10 mM PBS, blotted on filter paper, weighed, and placed in 2 ml acid alcohol (a solution of 1 ml of 10N HCl + 110 ml 95% ethanol) on ice. Pancreata were homogenized using a Polytron PT 10/35 homogenizer (Brinkmann Instruments), and an additional 3 ml acid alcohol was added to the homogenate. Tubes were placed on a rotator at 4ºC for 48 hours to extract insulin, then centrifuged at 2500 rpm for 30 min. The supernatant was collected and stored at -20ºC. Insulin content was analyzed in diluted (1:1000) samples by the Vanderbilt University Hormone Assay and Analytical Services Core, using a liquid-phase radioimmunoassay (Rat Insulin RIA Kit by Linco/Millipore, catalog #RI-13K).

Tissue Collection, Fixation, and Preparation

Pancreata and graft-bearing kidneys were harvested from anesthetized mice before cervical dislocation. Tissues were further dissected and washed in ice-cold 10 mM phosphate-buffered saline (PBS) before fixation in a freshly made solution of

4% paraformaldehyde (Electron Microscopy Sciences, catalog #15710) in 0.1 M PBS (12.07 g dibasic Na_2HPO_4, 2.04 g monobasic KH_2PO_4, 8.0 g NaCl, and 2.0 g KCl in Milli-Q purified water). Tissues were fixed for 90 minutes (on ice) and washed 3–4 times in 0.1 M PBS over the next two hours (on ice). Fixed tissues were cryoprotected by immersion in 30% w/w sucrose overnight at 4°C.

To collect embryos, the uterus of an anesthetized pregnant dam was removed and rinsed in 10 mM PBS. Embryos were dissected from the placenta and sacrificed by decapitation before the abdominal organs were carefully removed. The stomach, pancreas, spleen and duodenum were gently isolated from any other attached tissues using Dumont super fine #5SF forceps (Roboz, catalog #RS-4955). For cryosectioning, organs were fixed in freshly made 4% paraformaldehyde in 10 mM PBS for four hours, washed three times in 10 mM PBS (15 minutes each), and cryoprotected overnight at 4°C in 30% w/w sucrose in 10 mM PBS. For whole mount immunohistochemistry, organs were placed in cryogenic vials and fixed in 4:1 methanol:dimethyl sulfoxide (DMSO) overnight (on a rocker at 4°C), washed twice with 100% methanol (over one hour at 4°C), and stored in methanol at -20ºC until further use. Alternatively, some tissues for whole-mount immunohistochemistry were fixed in 4% paraformaldehyde overnight at 4°C, washed in 10 mM PBS, and used within a few days of harvesting the tissue.

For cryosectioning, cryoprotected tissues were blotted and mounted in Tissue-Tek cryomolds containing Tissue-Tek Optimal Cutting Temperature (OCT) compound (VWR Scientific Products, catalog #25608-916 and #25608-930). Prior to mounting, a scalpel was used to carefully cut graft-bearing kidneys in a transverse plane, adjacent to the islet graft, to obtain cross-sections of the graft atop the kidney parenchyma. Mounted tissues

were frozen at -80°C before cryosectioning. Five- to 30-µm sections were cut on a Leica CM1950 cryostat and affixed to Superfrost Plus Gold slides (Fisher Scientific, catalog #15-188-48). Slides were stored at -80°C until use.

Dissected brains were fixed in freshly prepared 1% paraformaldehyde overnight at 4°C and cut in 2-mm coronal sections using a brain slicer before whole-mount X-gal enzymatic staining was performed.

Reproductive organs dissected from Tm- and vehicle-treated mice were fixed in 4% paraformaldehyde for 90 minutes and dehydrated in an ethanol series (35%, 50%, and 70% for 30 minutes each). Subsequent paraffin embedding, preparation of 5-µm tissue sections, and hematoxylin and eosin staining were performed by the Vanderbilt Translational Pathology Shared Resource. Pathology expertise was contributed by Joyce E. Johnson of Vanderbilt University.

X-Gal Enzymatic Staining

X-gal enzymatic staining was used to detect β-galactosidase activity, as found in cells expressing the bacterial *lacZ* gene following Cre-mediated recombination, or in senescent cells. In preparation for staining, permeabilization solution and staining buffer were made as stock solutions and stored at room temperature for one to two months, protected from light. Permeabilization solution contained 2 mM $MgCl_2$, 0.01% sodium deoxycholate, and 0.02% Nonidet P-40 in 10 mM PBS. Staining buffer contained 2 mM $MgCl_2$, 5 mM potassium ferricyanide, and 5 mM potassium ferrocyanide in 100 mM Tris buffer. For typical X-gal staining, Tris buffer was prepared at pH 7.3. For detection of senescence-associated β-galactosidase activity, Tris buffer was prepared at pH 6.0

(Beattie 1994). Immediately before use, X-gal (5-bromo-4-chloro-indolyl-β-D-galactopyranoside, Research Products International, catalog #B71800) was solubilized in dimethylformamide (DMFA) at a concentration of 1 mg X-gal per 20 µl DMFA and added to the staining buffer, for a final concentration of 1 mg/ml. Samples in X-gal staining solution were protected from light.

Cryosections were subjected to X-gal enzymatic staining, as described (Brissova et al., 2004). Sections were thawed and post-fixed in freshly prepared 0.2% glutaraldehyde/1% paraformaldehyde in 10 mM PBS for 15 minutes at room temperature, then washed three times in 10 mM PBS (five minutes each). Permeabilization solution was applied for ten minutes at room temperature. Slides were placed in a humidified chamber and incubated in X-gal staining solution at 37°C, lasting from several hours to overnight, depending on when the reaction was complete. Slides were washed three times in 10 mM PBS (five minutes each) and mounted with Aqua-Poly/Mount (Polysciences, Inc., catalog #18606).

Fixed brain slices (cut with an adult mouse brain slicer) were subjected to X-gal enzymatic staining in whole mount, as described (Wicksteed et al., 2010). Slices were placed in permeabilization solution for five hours at 4°C, then placed in a modified X-gal staining solution (2 mM $MgCl_2$, 5 mM potassium ferricyanide, 5 mM potassium ferrocyanide, 1 mg/ml X-gal, 0.01% sodium deoxycholate, and 0.02% NP-40 in 10 mM PBS, pH 7.4) overnight at room temperature. Slices were then washed three times in 10 mM PBS (20 minutes each), post-fixed in 4% paraformaldehyde for one hour, washed again three times in 10 mM PBS (20 minutes each), then placed into 70% ethanol. Slices

were photographed using an Olympus SZX12 dissecting microscope connected to a DP12 digital camera (Olympus America).

Immunohistochemistry

Five- to 10-μm cryosections were labeled by immunohistochemistry as described previously (Brissova et al., 2004), using the primary and secondary antibodies listed in Tables 4-5. Cryosections were thawed and allowed to air dry before being encircled with a Super PAP Pen HT hydrophobic marker (Research Products International, catalog #195505). Embryonic and perinatal tissue sections were post-fixed with 1% paraformaldehyde in 10 mM PBS for five to ten minutes. Sections were prepared for immunolabeling by washing three times in 10 mM PBS (five minutes each), permeabilizing in 0.2% Triton X-100 in 10 mM PBS (ten minutes each), washing again three times in 10 mM PBS (five minutes each), then blocking in 5% normal donkey serum in 10 mM PBS (60–90 minutes in a humidified chamber). Primary antibodies were diluted in 0.1% Triton X-100/1% bovine serum albumin (BSA) in 10 mM PBS and placed on the cryosections overnight at 4°C. Sections were washed three times in 0.1% Triton X-100 in 10 mM PBS (ten minutes each) before adding the secondary antibodies, diluted in 0.1% Triton X-100/1% BSA in 10 mM PBS, for one hour at room temperature. Sections were washed three times in 0.1% Triton X-100 in 10 mM PBS (15 minutes each) and washed again three times in 10 mM PBS (five minutes each). Slides were mounted with SlowFade Gold antifade reagent (Invitrogen, catalog #S36938) and sealed with fingernail polish before imaging.

Table 4. Primary antibodies for immunohistochemistry.

Antigen	Host Species	Working Dilutions		Source	Catalog #
		Cryosections	Whole Mount		
Amylase	rabbit	1:1000	-	Sigma	A8273-1VL
β-galactosidase	rabbit	1:10000	-	MP Biomedical (formerly Cappel, ICN Pharmaceuticals)	55976
Cre recombinase	rabbit	1:10000	-	EMD4Biosciences (formerly Novagen)	69050
FABP7	goat	1:250-1:500	-	R&D Systems	AF3166
Glial Fibrillary Acidic Protein (GFAP)	rabbit	1:200	-	Covance	SIG-3471
Glucagon	guinea pig	-	1:10000	Linco	4031-01F
Glucagon	rabbit	1:100	-	Linco/Millipore	4030-01F
Green Fluorescent Protein (GFP)	chicken	1:1000	-	Abcam	ab13970
Insulin	guinea pig	1:200	-	Linco	4011-01F
Insulin	guinea pig	1:500	-	Dako	A0564
Ki67	rabbit	1:500	-	Abcam	ab15580
MafA	rabbit	1:50000	-	Roland Stein (Vanderbilt University)	-
Neuronal Class III β-Tubulin (TUJ1)	rabbit	1:20000	1:5000	Covance	MRB-435P
Neuropilin-1 (NRP1)	rabbit	1:50000	(1:10000)	Alex L. Kolodkin (Johns Hopkins University)	(serum)
proNGF	rabbit	1:1000	-	Millipore	04-1142
PDX1	goat	1:10000	1:5000	Christopher V.E. Wright (Vanderbilt University)	-
mouse PECAM1 (a.k.a. CD31)	rat	1:50	1:100	BD Pharmingen	550274
Somatostatin	sheep	1:500	-	American Research Products	13-2366
Synapsin-1, -2	rabbit	1:2000	-	Synaptic Systems	106 002
Tyrosine Hydroxylase (TH)	rabbit	1:1000	-	Millipore	AB152
Vesicular Acetylcholine Transporter (VAChT)	rabbit	1:2000	-	Synaptic Systems	139 103
rat VEGF-A	goat	1:100	-	R&D Systems	AF564
VEGFR2 (a.k.a. FLK1, KDR)	rabbit	1:2000	(1:2000)	Rolf A. Brekken (UT Southwestern)	T014

Table 5. Secondary antibodies for immunohistochemistry.

Host Species	Primary Ab Species	Fluorophore	Working Dilutions		Vendor	Catalog #
			Cryosections	Whole Mount		
donkey	rabbit	Cy2	1:200	1:200	Jackson Labs	711-225-152
donkey		Cy3	1:500	1:500	Jackson Labs	711-165-152
donkey		Cy5	1:200	1:500	Jackson Labs	711-175-152
donkey	goat	Cy3	-	1:500	Jackson Labs	705-165-147
donkey	rat	Cy2	1:200	1:200	Jackson Labs	712-225-153
donkey		DyLight649	-	1:500	Jackson Labs	712-495-153
donkey	chicken	Cy2	1:200	-	Jackson Labs	703-225-155
donkey		Cy3	1:500	-	Jackson Labs	703-165-155
donkey	guinea pig	Cy2	1:200	-	Jackson Labs	706-225-148
donkey		Cy3	1:500	-	Jackson Labs	706-165-148
donkey		Cy5	1:200	1:500	Jackson Labs	706-175-148

Thick (30 μm) cryosections were immunolabeled using an extended protocol. Air-dried cryosections were encircled with a PAP pen and hydrated in three washes of 10 mM PBS (15 minutes each). Sections were then permeabilized in 0.3% Triton X-100 in 10 mM PBS for three to four hours at room temperature before blocking with 5% normal donkey serum in 0.15% Triton X-100 in 10 mM PBS overnight at 4°C. Sections were washed twice in antibody incubation buffer (0.2% Triton X-100/1% BSA in 10 mM PBS) for 20 minutes each. Primary antibodies were diluted in antibody incubation buffer and placed on the cryosections overnight at 4°C. Sections were washed three times in 0.2% Triton X-100 in 10 mM PBS (30 minutes each) before incubating in the appropriate secondary antibodies diluted in incubation buffer overnight at 4°C. Sections were washed three to four times in 0.2% Triton X-100 in 10 mM PBS (30 minutes each) before mounting in SlowFade and sealing the coverslip with nail polish.

For whole-mount imaging, embryonic tissues in cryogenic vials were rocked at 4ºC in each of the following steps. Before immunolabeling, methanol-fixed tissues were rehydrated (washed once in 50% methanol for 30 minutes and twice in 10 mM PBS for 30 minutes each). Methanol- or paraformaldehyde-fixed tissues were then blocked and permeabilized in PBSBT (10 mM PBS with 2% BSA and 0.5% Triton X-100) in two washes over two hours. The primary and secondary antibodies used are listed in Table 4 and Table 5. On consecutive days, tissues were incubated overnight with primary or secondary antibodies diluted in PBSBT. After each antibody step, tissues were rinsed and washed three to four times with PBSBT for one hour each. Before imaging, immunolabeled tissues were dehydrated (washed once each in 50% and 80% methanol for 30 minutes, and washed twice in 100% methanol over one hour), optically cleared in

a 1:2 solution of benzyl alcohol:benzyl benzoate (BABB; Sigma-Aldrich), and placed on a glass coverslip.

Imaging

Tissue images collected for morphometric analysis were obtained at 20X magnification using an Olympus BX41 epifluorescence microscope connected to a MicroFire camera (Olympus America) or a Leica DMI 6000 B inverted microscope (Leica Microsystems).

Confocal imaging was performed through the Vanderbilt University Cell Imaging Shared Resource with a Zeiss LSM 510 META laser scanning microscope equipped with Argon/2, HeNe1 and HeNe2 lasers (Carl Zeiss Microimaging). Optical sections were obtained with a 20X Plan-Apochromat lens (numerical aperture of 0.75) and subjected to 3D reconstruction with LSM software (Carl Zeiss Microimaging).

Whole-slide scanning was performed through the Vanderbilt Islet Procurement and Analysis Core with a ScanScope CS or ScanScope FL (Aperio Technologies, Inc.). Images were obtained at 20X magnification and analyzed with ImageScope software (Aperio Technologies, Inc.).

Adobe Photoshop software (Adobe Systems Incorporated) was used to crop and adjust levels in images, for display purposes only.

Transmission Electron Microscopy

Transmission electron microscopy was performed on pancreata from *Vegfa*$^{fl/fl}$ and *Pdx1*^{PB}-*CreER*^{Tm};*Vegfa*$^{fl/fl}$ mice one month after Tm treatment, as described (Brissova et

al., 2006), with the assistance of the Vanderbilt University Cell Imaging Shared Resource. To initiate fixation, anesthetized mice were perfused intracardially with fixative (2% paraformaldehyde/2.5% glutaraldehyde in 0.1M sodium cacodylate/1% $CaCl_2$, pH 7.4) by Masakazu Shiota. Dissected pancreata were minced in 0.1M sodium cacodylate/ 1% $CaCl_2$ and placed in fixative for 1 hr at room temperature. Samples were kept in fixative overnight at 4°C before being post-fixed with 1% osmium tetroxide, dehydrated in an ethanol series (25% ethanol for ten minutes, 50% ethanol for ten minutes, 70% ethanol for ten minutes, twice in 95% ethanol for ten minutes each, and three times in 100% ethanol for five minutes each), and then embedded in Spurr resin. Five hundred nm-thick semi-thin sections were stained with toluidine blue and islets were identified by light microscopy. From those blocks, 60–70 nm ultrathin sections were placed on slot grids and stained with uranyl acetate and lead citrate. Islet endocrine cells and intraislet capillaries were visualized on a Phillips CM-12 Transmission Electron Microscope at an operating voltage of 80 KeV and images were captured with an AMT digital camera system.

Morphometric Analysis

Quantification of immunohistochemistry was performed on original, unadjusted images with MetaMorph software (Universal Imaging). Morphometric analysis was performed on at least 30 islets per mouse, with $n \geq 3$ mice per group (except where noted).

In Chapters III and IV, analyses of vessel density and size were performed by immunolabeling PECAM1+ endothelial cells. In adult pancreatic sections, regions of interest were drawn around the insulin+ area of individual islets, and intraislet capillaries

were thresholded for PECAM1+ cells. Vessel density and the area per vessel were calculated using integrated morphometry analysis (Brissova et al., 2006). To assess vascularization in whole mount-labeled *Wnt1-Cre*;*Foxd3*$^{fl/-}$ and *Foxd3*$^{fl/-}$ embryonic pancreata, images were thresholded to measure the number of PECAM1+ vessels and the area of PDX1+ pancreatic epithelial cells, and the ratio was calculated for pancreatic vessel density. Vessel density was measured in every other optical section from individual confocal z-stacks, totaling more than 30 slices analyzed per sample.

In Chapter III, global islet innervation was quantified by calculating both the number and the length of TUJ1+ fibers within the insulin+ islet area, using integrated morphometric analysis. Changes in Schwann cell localization were quantified by thresholding the GFAP+ fiber area as a percentage of the insulin+ islet area. In the case of hypervascularized islets of mice, islets were defined as a continuous object of insulin+ β-cells and PECAM1+ endothelial cells, around which a region of interest was drawn. Islet parasympathetic innervation in *ob/ob* mice was quantified by calculating both the number of VAChT+ varicosities per insulin+ area and the VAChT+ area as a percentage of insulin+ islet area. To accurately represent innervation within islet centers, only islets with a cross-sectional diameter greater than 100 μm were included in the analysis.

In Chapter IV, pancreatic β-cell area and islet β-cell area measurements were performed using an Aperio FL fluorescence-based slide scanner and ImageScope software (Aperio Technologies, Inc.). For pancreatic β-cell area, four pancreatic sections (at least 200 μm apart) were immunolabeled for insulin and the acinar tissue enzyme amylase, counterstained with the nuclear label DAPI, and scanned at 20X magnification. ImageScope software was used to calculate the insulin+ and amylase+ areas of each

cross-section, and the pancreatic β-cell area was defined as insulin+ area / (insulin+ area plus amylase+ area). For islet β-cell area, ImageScope software was used to measure insulin+ and glucagon+ areas of islets, and islet β-cell area was defined as insulin+ area / (insulin+ area plus glucagon+ area).

In Chapter V, insulin+ and β-galactosidase+ (β-gal+) cells were counted manually with the aid of MetaMorph software. At least three cross-sections were counted for each islet graft (200-3000 total insulin+ cells counted per graft), and at least ten islet cross-sections were counted per pancreas (300-500 insulin+ cells counted per mouse). The percentage of insulin+ β-cells expressing β-gal was calculated for each cross-section, and averaged for each graft or pancreas sample. Two to four tissue samples were obtained for each treatment group or time point.

Statistical Analysis

Statistics were performed with Prism software (GraphPad), using Student's *t*-test to compare two groups, or one-way ANOVA to compare three or more groups. For the high fat diet study in Chapter IV, two-way ANOVA was used to assess the effects of diet, genotype, and their interaction. Data are summarized as mean ± standard error of the mean (SEM), and assigned statistical significance at $P < 0.05$.

CHAPTER III

INVESTIGATING THE ROLE OF VEGF-A IN ISLET INNERVATION

Introduction

With the knowledge that peripheral nerves and blood vessels are closely aligned, in part by sharing potential guidance molecules such as VEGF-A, it was hypothesized that intraislet VEGF-A expression and/or its effects on islet vascularization were responsible for directing islet innervation (Figure 15). In this Chapter, the relationship between VEGF-A, vascularization, and innervation in the pancreatic islet was explored by addressing the following questions: (1) How are islet vascularization and innervation developmentally related? (2) Does VEGF-A and islet vascularization influence islet innervation? (3) Conversely, does islet innervation influence islet vascularization? and (4) Can VEGF-A signal directly to neural crest-derived neurons and glia in the islet? Using mouse models of increased or decreased VEGF-A expression within pancreatic islets, it was found that islet innervation follows islet vascularization during development, in both a temporal and spatial manner. However, intraislet VEGF-A expression indirectly affects neural crest-derived cells of the islet, because only endothelial cells of the islet express VEGF-A receptors during the postnatal maturation of islet innervation. These results show that islet vascularization and innervation are developmentally interconnected, and that islet-derived VEGF-A acts as a principal coordinator of islet morphology and function.

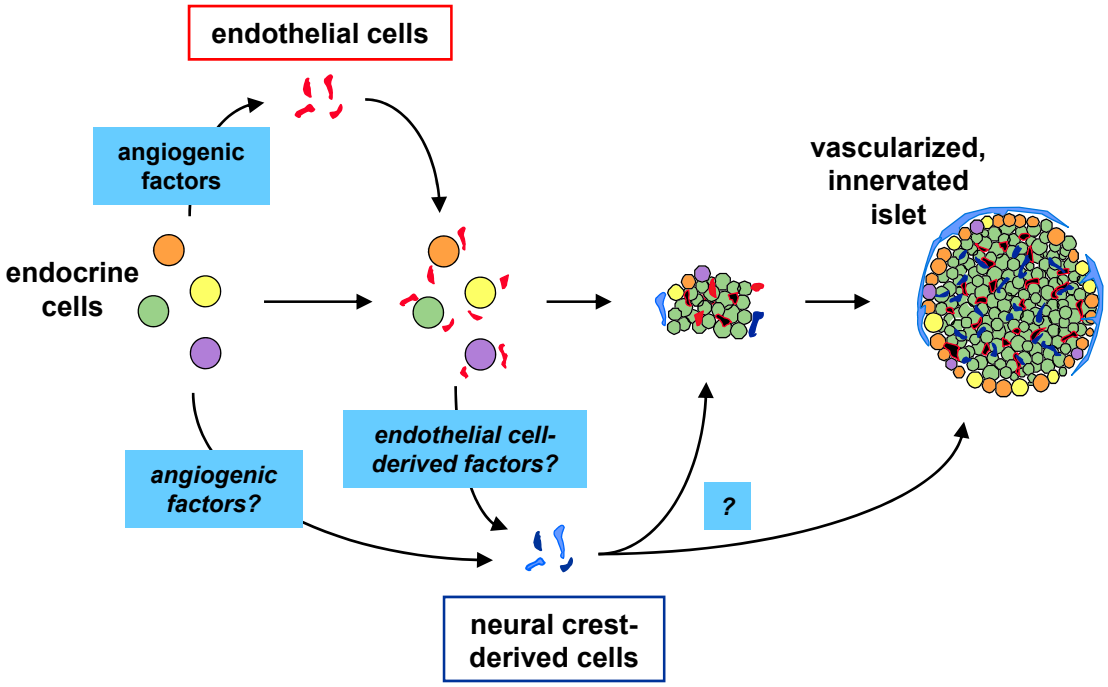

Figure 15. Potential model of the development of islet vascularization and innervation. During embryogenesis and postnatal life, the development of islet vasculature occurs concomitantly with islet morphogenesis. Additionally, neural crest-derived cells enter the pancreas and differentiate into nerves and glia that eventually innervate mature islets. However, the temporal nature of islet innervation and the mechanisms governing this process remain unclear. This is the basis for the studies described in Chapter III.

Results

Pancreatic islets are highly vascularized and richly innervated

To investigate pancreatic innervation and explore its relationship with vascularization, immunofluorescence labeling was performed on pancreatic sections from adult mice, using markers for nerve fibers (neuronal class III β-tubulin, TUJ1), peri-islet Schwann cells (glial fibrillary acidic protein, GFAP), and endothelial cells (platelet endothelial cell adhesion molecule 1, PECAM1). As expected, pancreatic islets (labeled for insulin+ β-cells) displayed a dense capillary network of PECAM1+ endothelial cells (Figure 16A and C; Brissova et al., 2006; Lammert et al., 2003b; Murakami et al., 1993; Vetterlein et al., 1987). Similarly, islets were richly innervated, with many thin TUJ1+ fibers intermingled with insulin+ β-cells at the islet core (Figure 16A). A subset of these TUJ1+ fibers were aligned with PECAM1+ capillaries (Figure 16B, closed arrowheads), but many TUJ1+ fibers were not adjacent to endothelial cells, as assessed by confocal microscopy (Figure 16B, open arrowheads). Both capillaries and fine nerve fibers were more numerous within islets compared to the acinar tissue of the exocrine pancreas, though pancreatic ducts were also highly innervated (denoted by asterisks in Figures 16-17). On some pancreatic cross-sections, large nerve bundles and/or nerve cell bodies were found adjacent to an islet, forming a neuroinsular complex (arrows in Figure 16A). In contrast to TUJ1+ nerve fibers, GFAP+ peri-islet Schwann cells of the pancreas were almost exclusively found at the border of the endocrine and exocrine pancreas, in many cases encircling the islets (Figure 16C). Occasionally, glial cell processes would extend into the insulin+ area of the islet, often alongside a capillary (Figure 16D). As with TUJ1+ nerve fibers, GFAP+ Schwann cells in the pancreas were much more likely

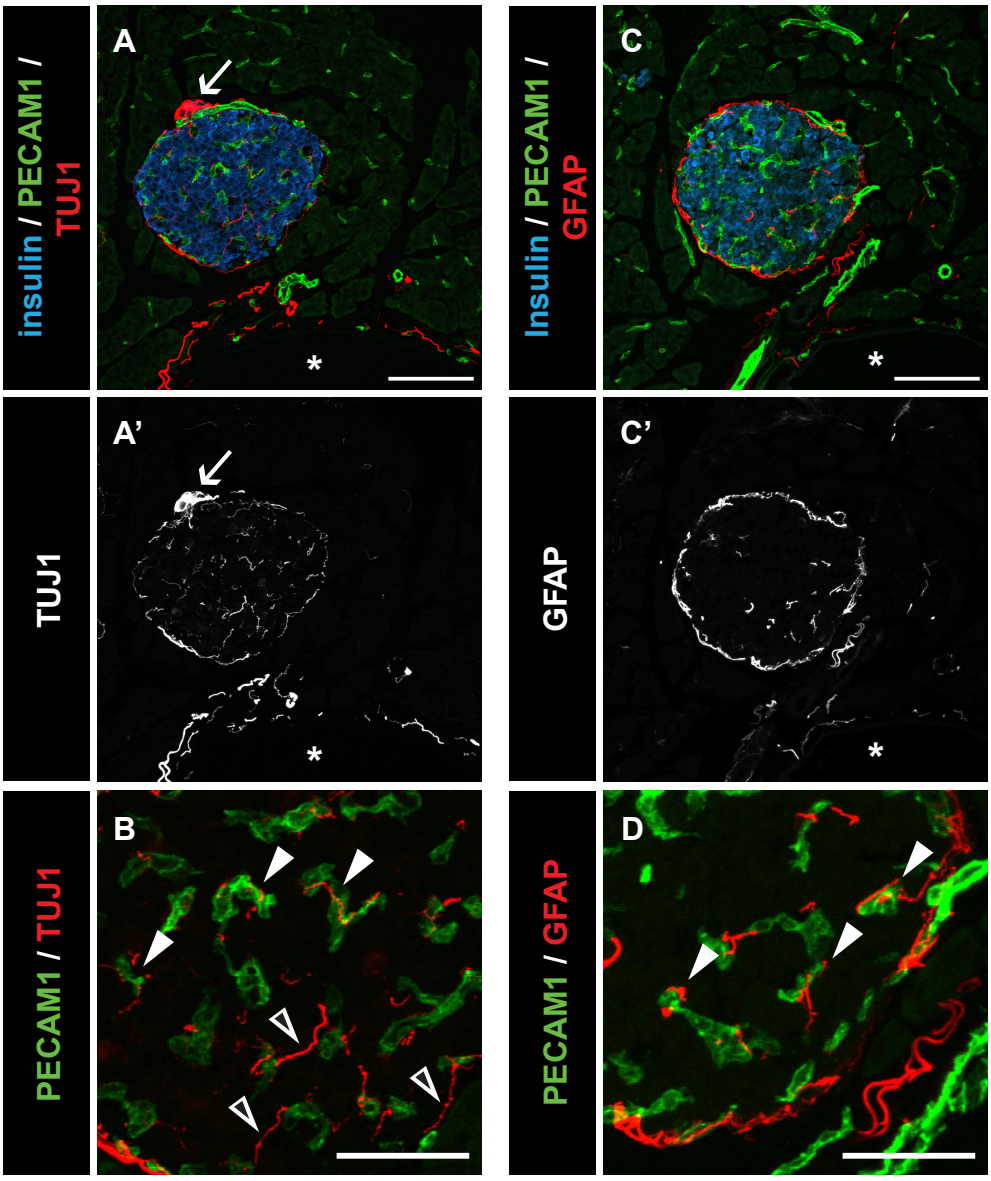

Figure 16. Pancreatic islets are highly vascularized and richly innervated. **A-B**. Representative wild-type adult pancreas immunolabeled for insulin (blue), endothelial cells (PECAM1, green), and nerve fibers (TUJ1, red/grayscale). **C-D**. Representative wild-type pancreas immunolabeled for insulin (blue), endothelial cells (PECAM1, green), and peri-islet Schwann cells (GFAP, red/grayscale). Scale bars in **A** and **C** are 100 μm, and scale bars in **B** and **D** (2x zoom of islets in **A** and **C**, respectively) are 50 μm. Arrow denotes a neuroinsular complex, * denotes a duct lumen, closed arrowheads denote closely aligned blood vessels and nerve fibers or Schwann cells, open arrowheads denote nerve fibers not aligned with blood vessels.

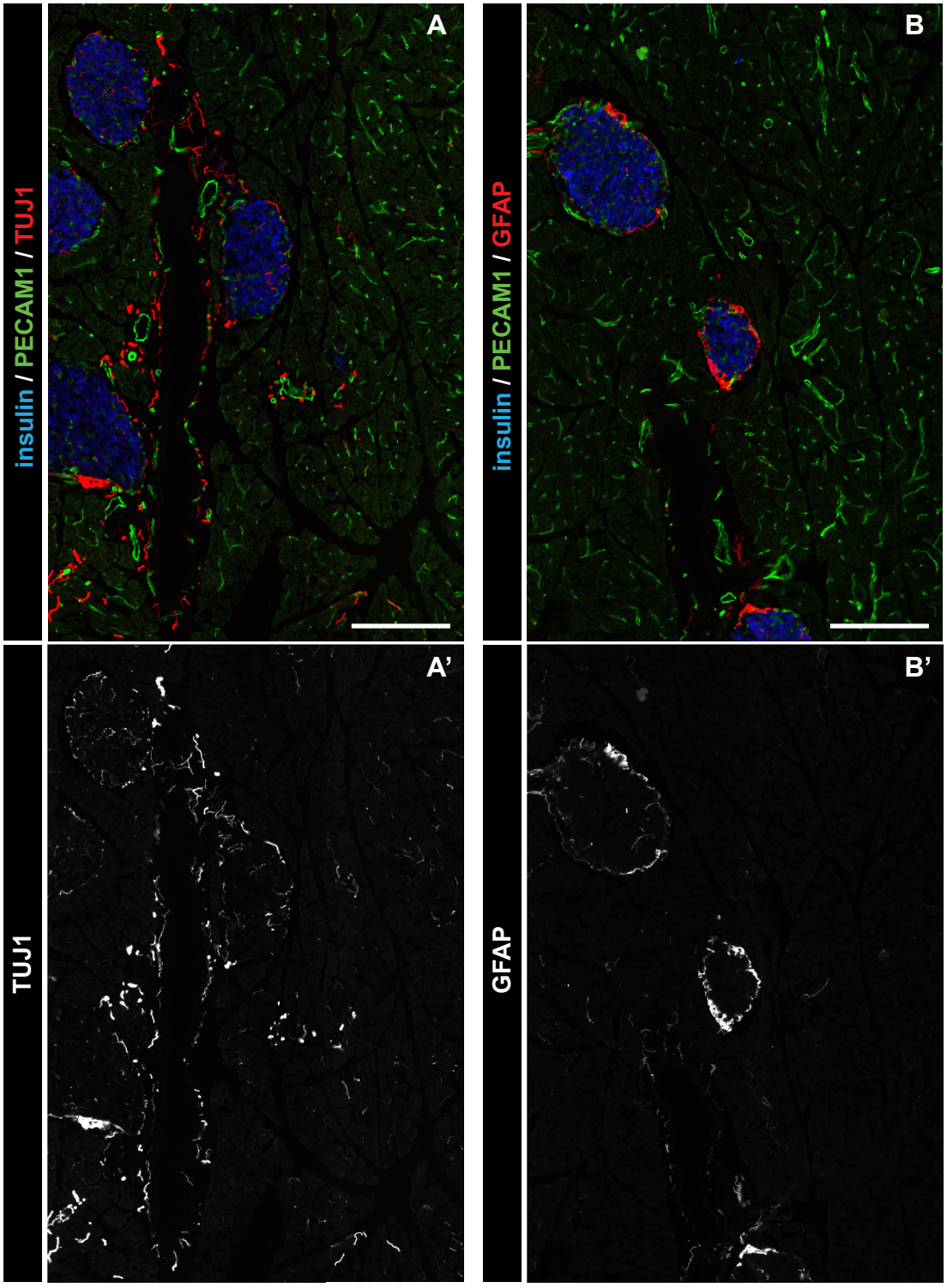

Figure 17. Pancreatic islets are more vascularized and innervated than pancreatic acinar tissue. A-B. Representative wild-type adult pancreas immunolabeled for insulin (blue), endothelial cells (PECAM1, green), and nerve fibers (TUJ1; red/grayscale in **A**) or Schwann cells (GFAP; red/grayscale in **B**). Scale bars are 200 μm. * denotes a duct lumen.

to be associated with islets or ducts than with acinar cells (Figures 16C, 17B). Because capillaries, nerve fibers, and Schwann cells were highly concentrated in islets and often in close proximity with one another, the relationship between islet vascularization and innervation was investigated further.

Islet VEGF-A expression influences both islet vascularization and innervation

To determine if islet innervation was affected by changes in islet vascularization, islet innervation patterns were examined in mouse models with altered VEGF-A production. For a model of reduced pancreatic vascularization, *Pdx1-Cre;Vegfa*$^{fl/fl}$ (abbreviated ↓VEGF-A) mice were used. In this model, VEGF-A is genetically inactivated throughout the pancreas during embryogenesis, resulting in a nearly 90% decrease in islet vascularization (Jabs et al., 2008; Lammert et al., 2003b; Reinert and Brissova et al., manuscript in preparation). To increase islet vascularization, a Tet-on inducible genetic mouse model, in which treatment with doxycycline (Dox) induces expression of VEGF-A in insulin+ β-cells, was used. Adult *RIP-rtTA*;*TetO-hVegfa* mice were treated with Dox for one week (abbreviated ↑VEGF-A), which led to a 100-fold increase in VEGF-A secretion from isolated islet clusters, a dramatic expansion of intraislet endothelial cells (a four-fold increase in the intraislet endothelial cell area), and a reduction in β-cell number (Brissova et al., manuscript in preparation). Compared to littermate controls (Figure 18A), islets in adult ↓VEGF-A mice showed reduced innervation (Figure 18B), as measured by a 52% reduction in the number of TUJ1+ nerve fibers present within the insulin+ area of the islet (Figure 18D), as well as a 50% reduction in the length of those fibers (Figure 18E). In contrast, hypervascularized islet

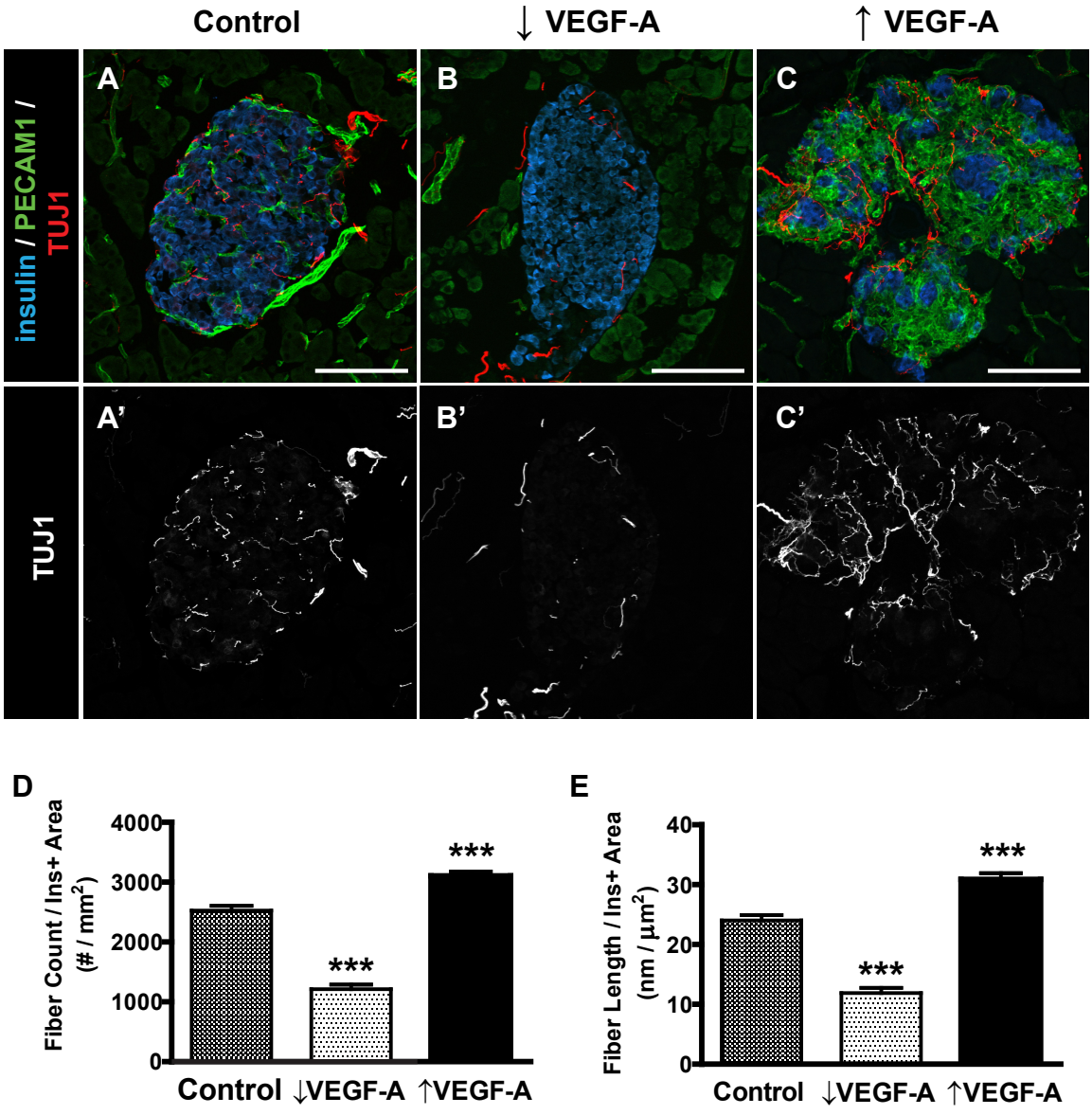

Figure 18. Islet innervation follows islet VEGF-A production and vascularization. **A-C.** Representative islets from adult *Vegfa*$^{fl/fl}$ control (**A**), *Pdx1-Cre;Vegfa*$^{fl/fl}$ (↓VEGF-A; **B**), and doxycycline-treated (for one week) *RIP-rtTA;TetO-hVegfa* (↑VEGF-A; **C**) mice, immunolabeled for insulin (blue), PECAM1 (green) and TUJ1 (red/grayscale). Scale bars are 100 µm. **D-E**. Morphometric quantification of TUJ1+ fiber density (**D**) and fiber length (**E**). ***$P < 0.001$ vs. control group.

clusters in ↑VEGF-A mice were highly innervated, though nerve fibers were found more closely associated with endothelial cells than with β-cells (Figure 18C). VEGF-A-overexpressing islet clusters showed a 23% increase in the number of TUJ1+ nerve fibers (Figure 18D) and a 29% increase in fiber length (Figure 18E). A very similar innervation pattern was observed in islets from ↓VEGF-A and ↑VEGF-A mice labeled with antibodies to synapsin-1 and -2 (Figure 19). These data suggest that islet innervation closely follows islet vascularization and/or islet VEGF-A expression.

The development of pancreatic innervation during embryogenesis does not require VEGF-A

Next, several important stages in pancreas and islet development were evaluated to determine when VEGF-A plays an important role in islet innervation. Because differentiated neural crest-derived cells begin to associate with developing islets of the pancreatic epithelium after E15.5 (Burris and Hebrok, 2007; Nekrep et al., 2008; Plank et al., 2011), pancreatic innervation was evaluated beginning in late embryogenesis, when differentiated endocrine cells are beginning to cluster and delaminate from the ductal epithelium (Pan and Wright, 2011). At E16.5, the developing pancreas and islets were already well vascularized by PECAM1+ endothelial cells (Figure 20A''; Brissova et al., 2006; Reinert and Brissova et al., manuscript in preparation). Control pancreata were also well innervated at this stage, containing a network of TUJ1+ nerve fibers (Figure 20A'''). Analysis using confocal microscopy revealed that developing islets (visualized by labeling for glucagon+ endocrine cells) were interconnected by the network, with nerve fibers traveling between clusters of endocrine cells (Figure 21). During embryogenesis,

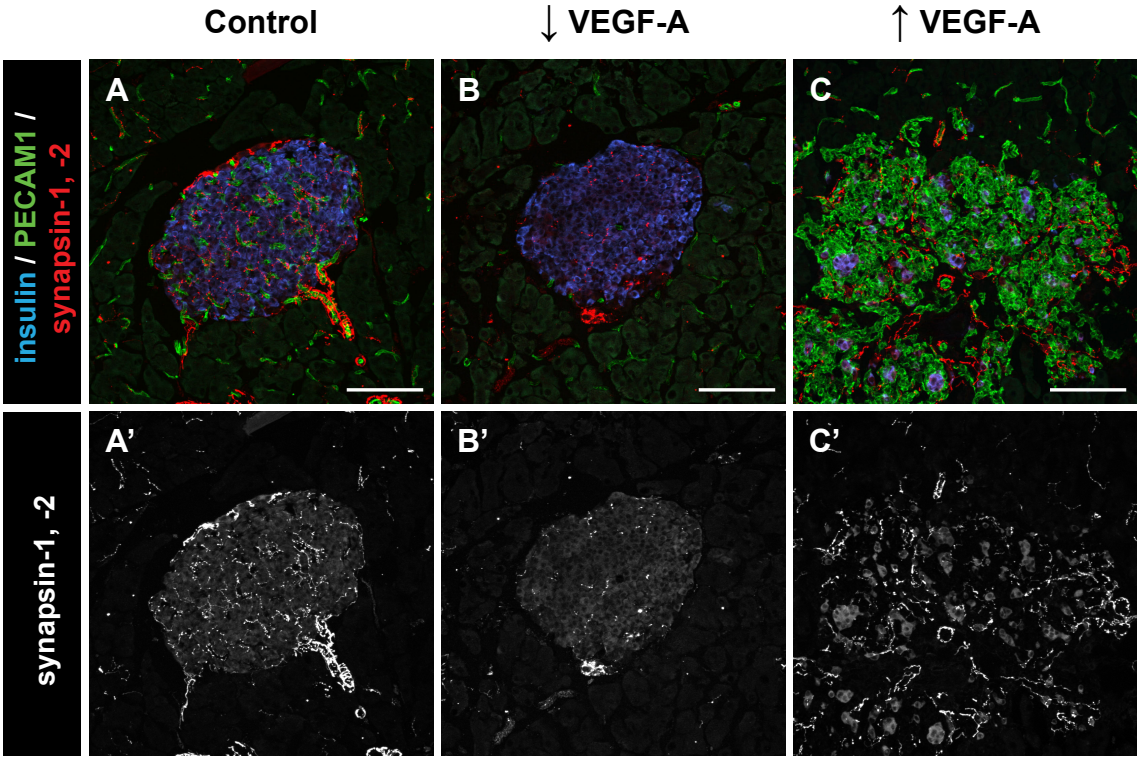

Figure 19. Islet innervation follows islet VEGF-A production and vascularization. **A-C.** Representative islets from adult *Vegfa*$^{fl/fl}$ control (**A**), *Pdx1-Cre;Vegfa*$^{fl/fl}$ (↓VEGF-A; **B**), and doxycycline-treated (for one week) *RIP-rtTA;TetO-hVegfa* (↑VEGF-A; **C**) mice, immunolabeled for insulin (blue), PECAM1 (green) and synapsin-1, -2 (red/grayscale). Scale bars are 100 μm.

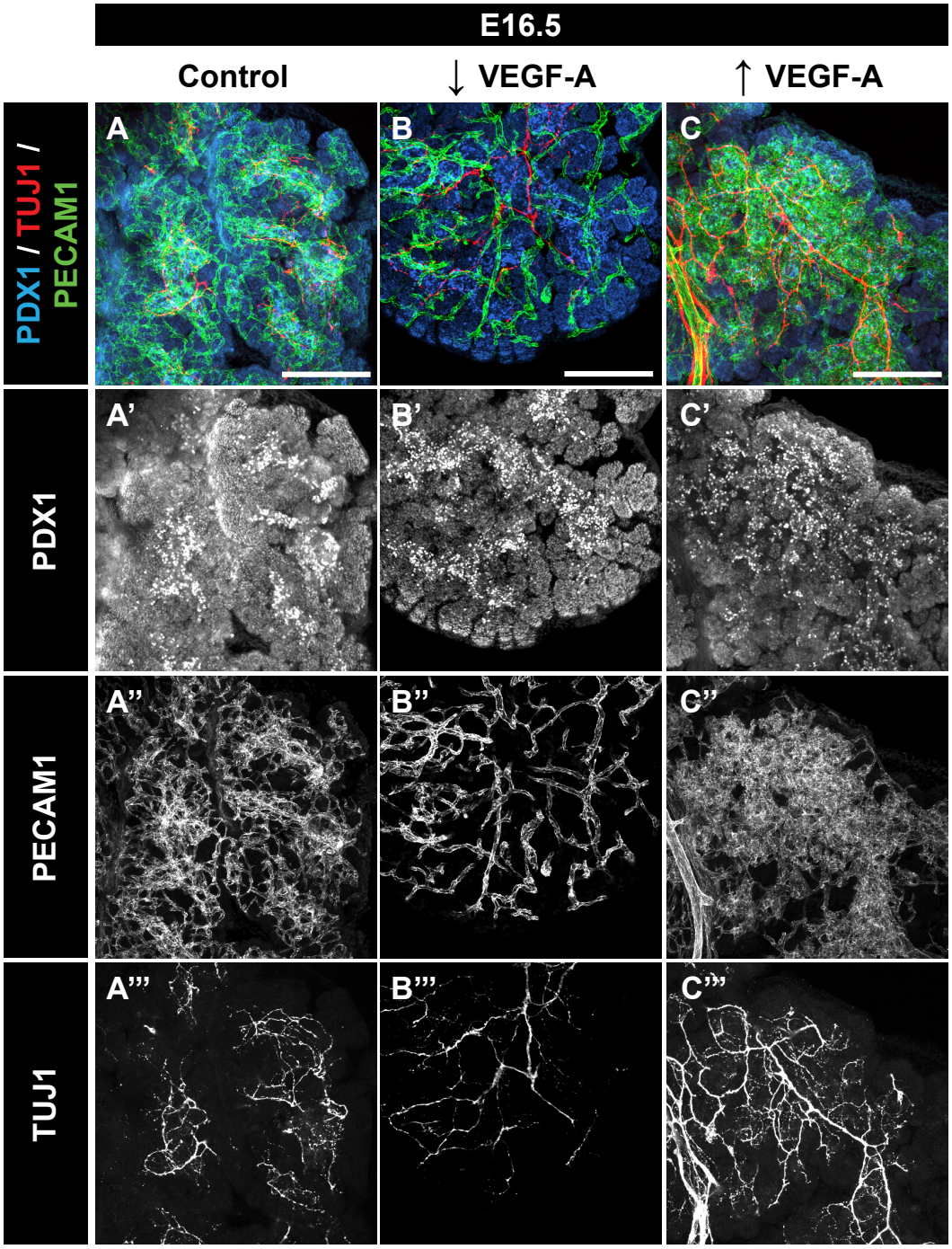

Figure 20. VEGF-A is not required for, but enhances, pancreatic innervation during embryogenesis. Images are 3D reconstructions of confocal z-stacks (30 μm thick) of embryonic day 16.5 (E16.5) pancreata from untreated *RIP-rtTA;TetO-hVegfa* control (**A**), *Pdx1-Cre;Vegfa*$^{fl/fl}$ (↓VEGF-A; **B**), and doxycycline-treated (from E5.5) *RIP-rtTA; TetO-hVegfa* (↑VEGF-A; **C**) mice. Pancreata were immunolabeled in whole mount with antibodies to PDX1 (blue), PECAM1 (green), and TUJ1 (red). Scale bars in **A-C** are 100 μm, and correspond to all panels below.

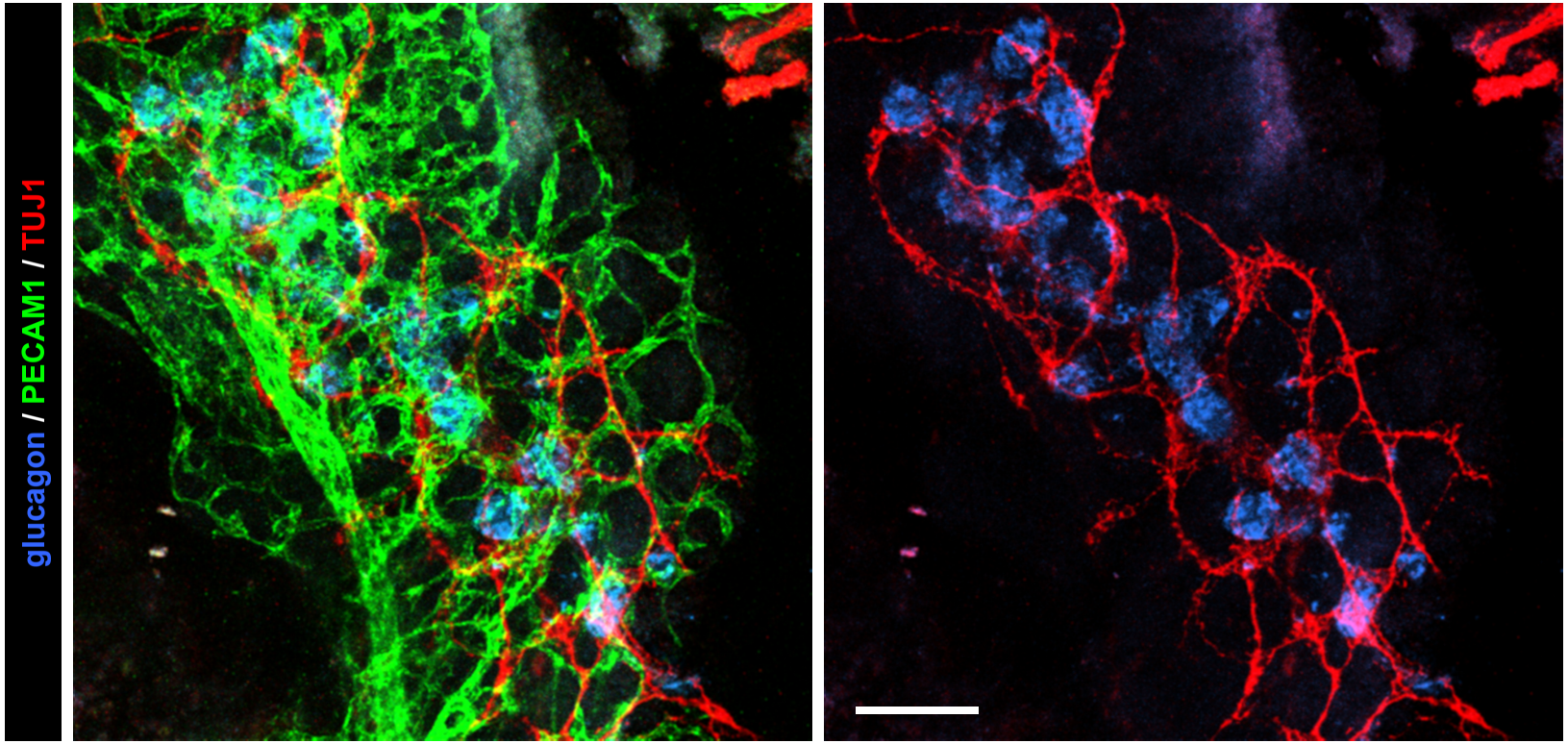

Figure 21. Developing pancreatic islets are interconnected by a network of nerves during embryogenesis. Image is a 3D reconstruction of confocal z-stacks (25 μm thick) from an embryonic pancreas at embryonic day 14.5, immunolabeled for glucagon (blue), PECAM1 (green), and TUJ1 (red). Scale bar is 100 μm and applies to both panels. Image courtesy of Marcela Brissova.

however, nerve fibers did not penetrate into the core of islets, but remained localized to the periphery of endocrine cell clusters. While pancreata from ↓VEGF-A mice showed a dramatic reduction in vascularization (Figure 20B; Reinert and Brissova et al., manuscript in preparation), VEGF-A was not required for the establishment of pancreatic innervation, because TUJ1+ nerve fibers were found throughout the pancreata of ↓VEGF-A embryos (Figure 20B'''). This pattern of pancreatic vascularization and innervation was also observed at E14.5, when endocrine cell differentiation is still very active, and at E18.5, when individual islets can be found (Figure 22). In contrast, E16.5 pancreata from ↑VEGF-A mice (treated with Dox from E5.5) were dramatically hypervascularized and highly innervated (Figure 20C).

Pancreatic vascularization is not altered by reduced innervation

To determine if nerve fibers in the developing pancreas influence vascular patterning, *Wnt1-Cre;Foxd3*$^{fl/-}$ mice were used as a model of neural crest cell ablation (Plank et al., 2011; Teng et al., 2008). Because these mice die perinatally, pancreatic vascularization was evaluated in embryos at E16.5. As expected, the pancreatic epithelium in *Wnt1-Cre;Foxd3*$^{fl/-}$ embryos was depleted of TUJ1+ nerve fibers (Figure 23B). In contrast, PECAM1+ endothelial cells formed a dense capillary network in *Wnt1-Cre;Foxd3*$^{fl/-}$ embryos, unchanged from controls (Figure 23C). This indicates that the lack of neural crest-derived nerves and glia does not impair pancreatic vascularization.

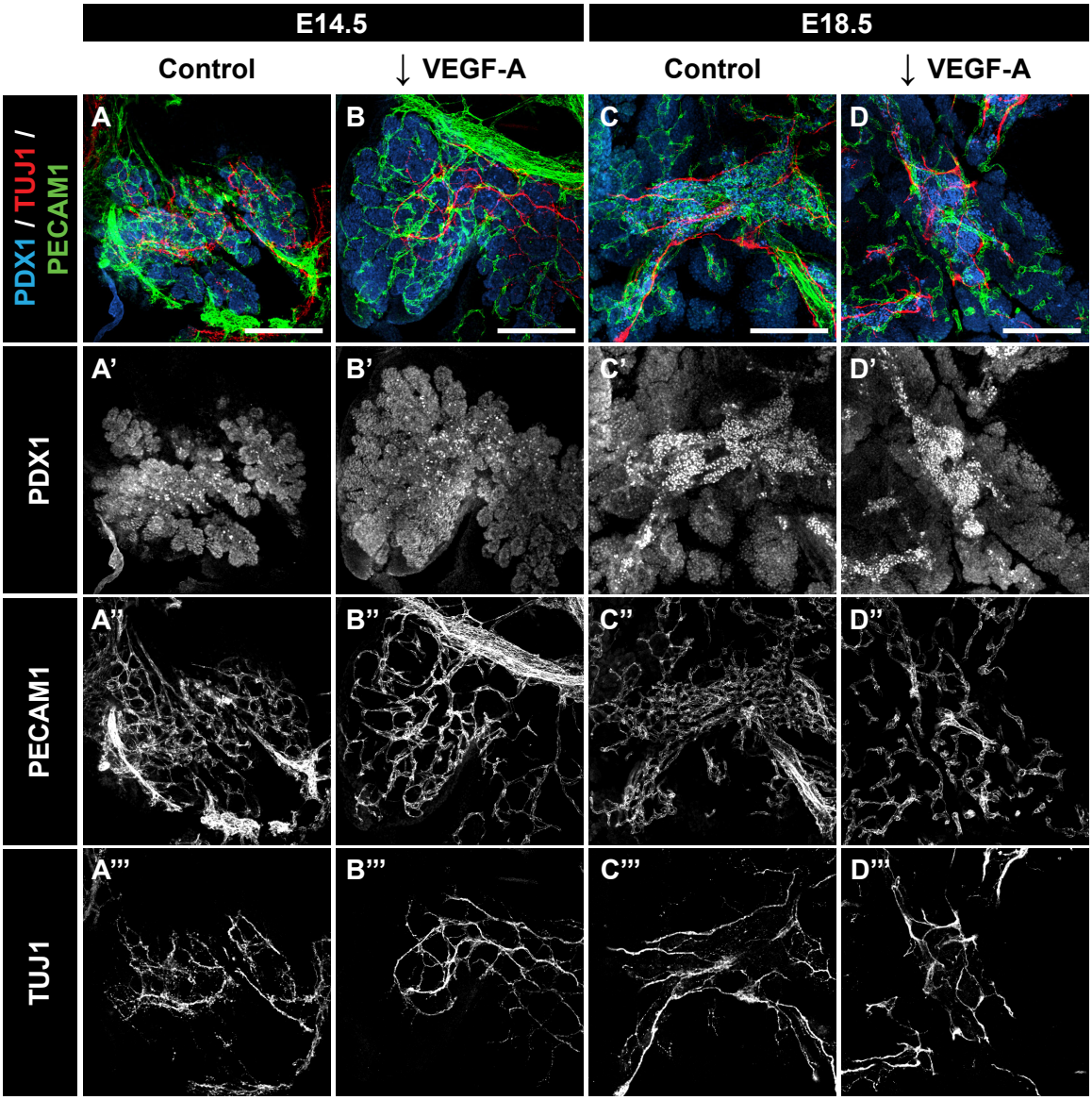

Figure 22. VEGF-A is not required for pancreatic innervation during embryogenesis. A-D. Images are 3D reconstructions of confocal z-stacks (30 μm thick) of embryonic pancreata from *Vegfa*$^{fl/fl}$ control (**A, C**) and *Pdx1-Cre;Vegfa*$^{fl/fl}$ (↓VEGF-A; **B, D**) mice at embryonic day 14.5 (E14.5; **A, B**) and E18.5 (**C, D**). Pancreata were immunolabeled in whole mount with antibodies to PDX1 (blue), PECAM1 (green), and TUJ1 (red). Scale bars in **A-D** are 100 μm, and correspond to all panels below.

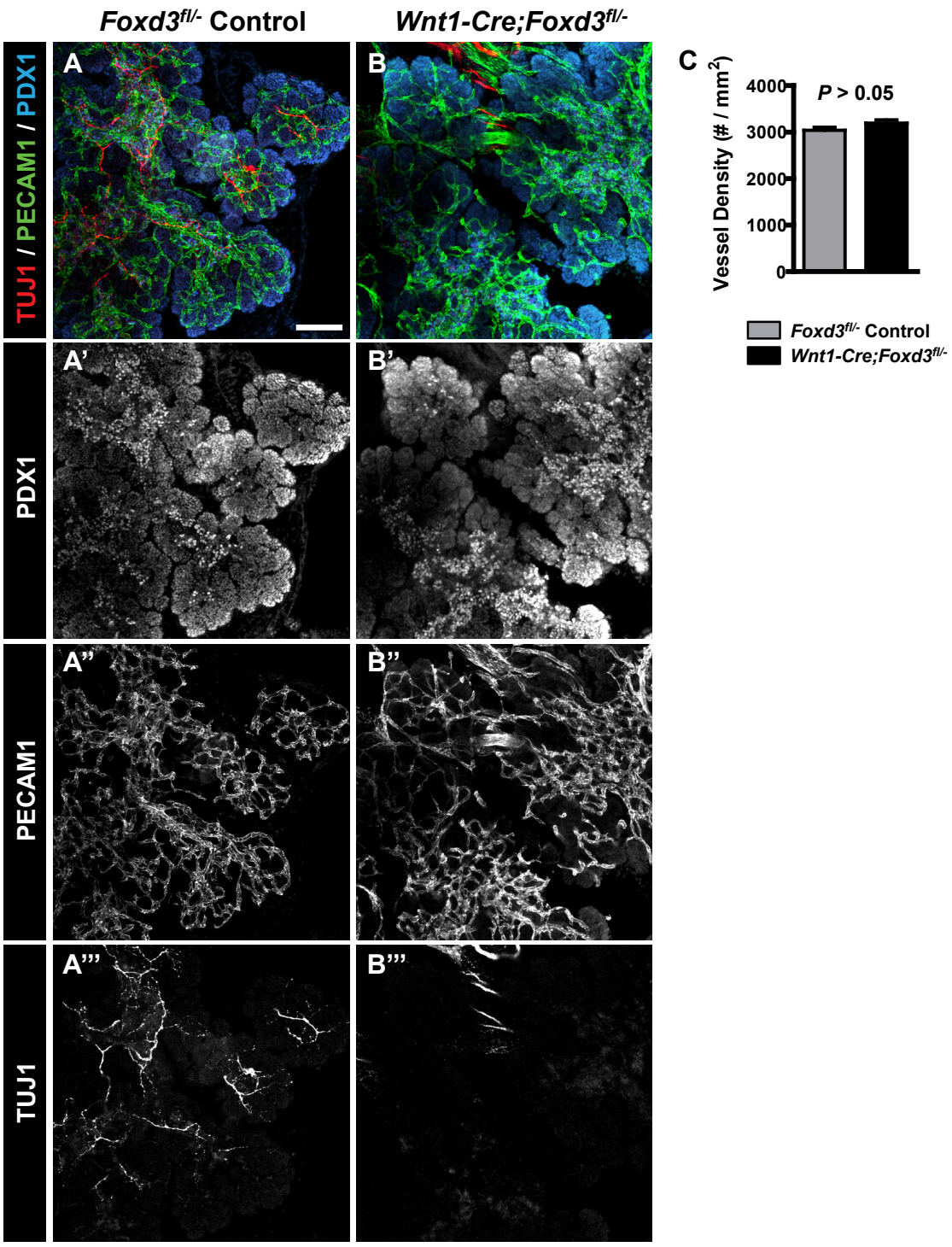

Figure 23. Pancreatic vascularization is not altered by reduced innervation. **A-B.** Images are 3D reconstructions of confocal z-stacks (15 µm thick) of embryonic pancreata from *Foxd3*$^{fl/-}$ (**A**) and *Wnt1-Cre;Foxd3*$^{fl/-}$ (**B**) mice at embryonic day 16.5 (E16.5), immunolabeled in whole mount with antibodies to PDX1 (blue), PECAM1 (green), and TUJ1 (red). Scale bar in **A** is 50 µm, and corresponds to all other panels. **C.** Quantification of vessel density.

Islet innervation matures postnatally, and is dependent on VEGF-A

Because nerve fibers in the embryonic pancreas remained localized to the periphery of developing endocrine clusters, islet innervation patterns were examined during postnatal islet development. At postnatal day 1 (P1) and P7, insulin+ cell clusters in control pancreata displayed a mature capillary network (Figure 24A, D), while islets in ↓VEGF-A mice were depleted of capillaries (Figure 24B, E). In contrast to mature islets in adult mice, TUJ1+ fibers remained localized to the islet periphery in both control and ↓VEGF-A pancreata at P1 and P7, and no differences in islet innervation were apparent between the two genotypes at these times (Figure 24A, B, D, E). In fact, islet innervation did not mature until weaning (P21), when TUJ1+ fibers penetrated the insulin+ islet core in control (Figure 25A) but not ↓VEGF-A (Figure 25B) pancreata. In contrast to the clusters of insulin+ β-cells in islets of control and ↓VEGF-A mice, β-cell-specific VEGF-A overexpression during pancreas development profoundly affected islet formation (Cai et al., 2012). Islet clusters in ↑VEGF-A mice showed a dramatic increase in the number of PECAM1+ endothelial cells (Figures 24C, 24F, and 25C). Additionally, insulin+ β-cells were no longer clustered in typical islet shapes, but instead were dispersed throughout the endothelial cell masses (Cai et al., 2012). However, at each time point, these clusters of endocrine and endothelial cells were highly innervated, containing a dense network of TUJ1+ nerve fibers (Figures 24C, 24F, and 25C). These data indicate that islet innervation matures postnatally and normal islet VEGF-A production is critical for this process.

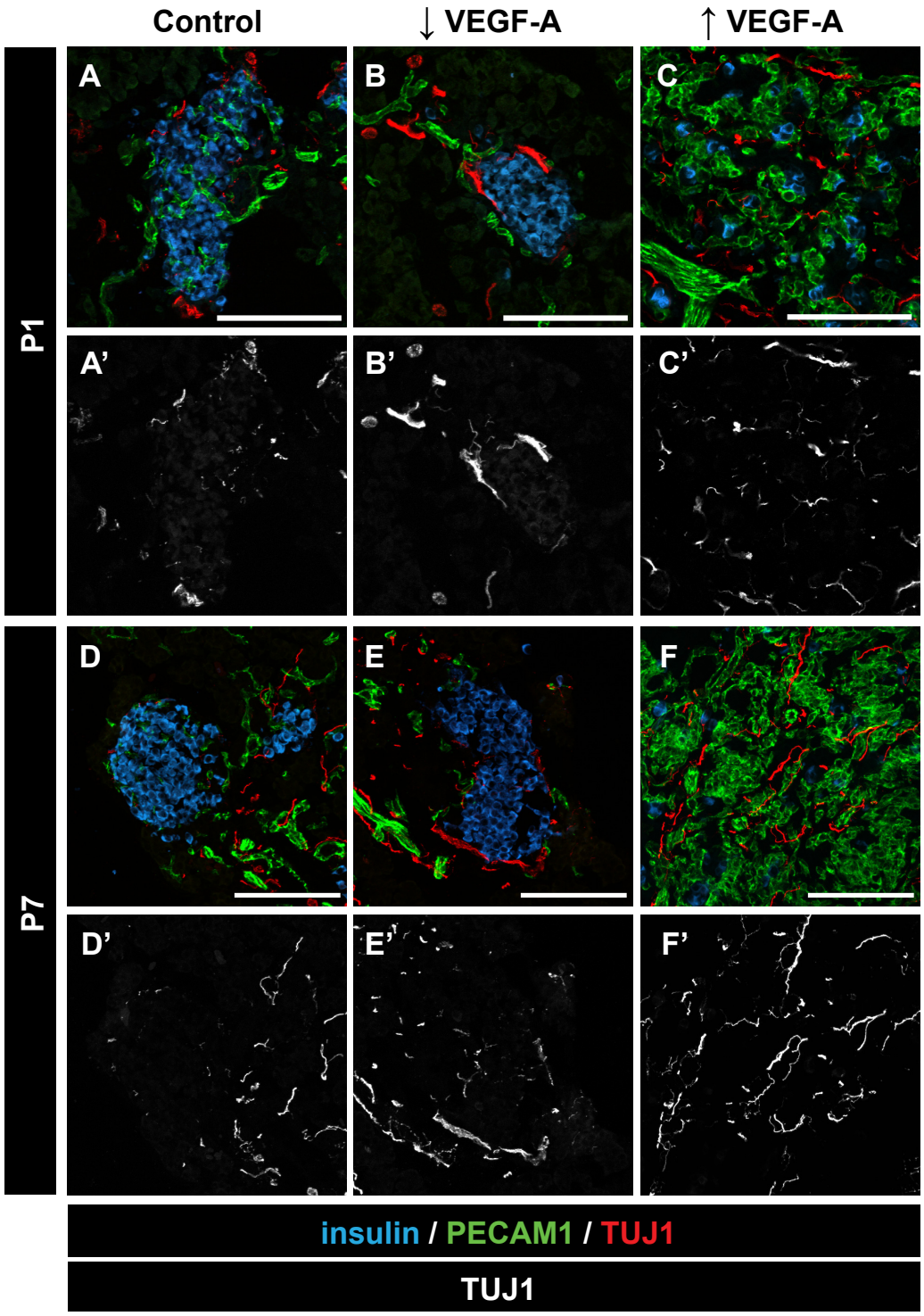

Figure 24. Pancreatic islet innervation is not mature in early postnatal life. Representative islets from *Vegfa*$^{fl/fl}$ control (**A, D**), *Pdx1-Cre;Vegfa*$^{fl/fl}$ (↓VEGF-A; **B, E**), and doxycycline-treated (from E5.5) *RIP-rtTA;TetO-hVegfa* (↑VEGF-A; **C, F**) mice at postnatal day 1 (P1; **A-C**) and P7 (**D-F**), immunolabeled for insulin (blue), PECAM1 (green) and TUJ1 (red/grayscale). Scale bars are 100 μm.

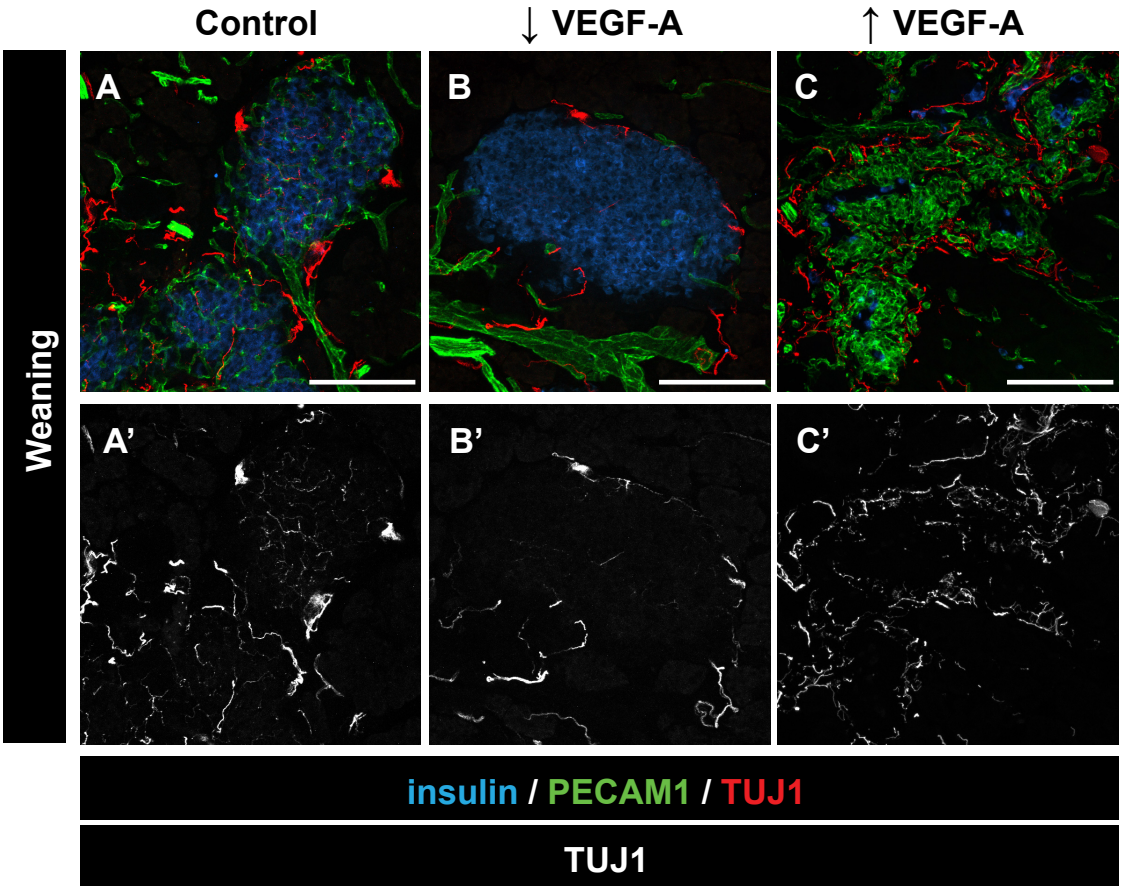

Figure 25. Pancreatic islet innervation matures around weaning, and depends on VEGF-A expression. Representative islets from *Vegfa*$^{fl/fl}$ control (**A**), *Pdx1-Cre;Vegfa*$^{fl/fl}$ (↓VEGF-A; **B**), and doxycycline-treated (from E5.5) *RIP-rtTA;TetO-hVegfa* (↑VEGF-A; **C**) mice at weaning (postnatal day [P]21-P28), immunolabeled for insulin (blue), PECAM1 (green) and TUJ1 (red/grayscale). Scale bars are 100 μm.

Both sympathetic and parasympathetic nerve fibers are affected by changes in VEGF-A expression

To determine if the changes in islet innervation following altered VEGF-A expression affected all nerve fiber types in the islet, or only a specific subset of nerve fibers, pancreata from both ↓VEGF-A and ↑VEGF-A mice (and their respective controls) were labeled for markers of sympathetic, parasympathetic, and sensory nerve fibers. Because sensory nerve fibers were found to be very rare in islets of all experimental groups, the remainder of the analysis was focused on autonomic nerve fibers.

To label sympathetic nerve fibers, an antibody to tyrosine hydroxylase (TH), the rate-limiting enzyme in catecholamine biosynthesis, was used. In control islets, TH labeled many nerve fibers, but also labeled a few insulin+ β-cells (Figure 26A). Surprisingly, VEGF-A-deficient islets showed a dramatic increase in the number of endocrine cells expressing TH (Figure 26B). The robust expression of TH in endocrine cells precluded the morphometric quantification of TH+ fibers in VEGF-A-deficient islets, but few TH+ fibers were observed. Unlike VEGF-A-deficient islets, islet clusters in ↑VEGF-A mice showed rare TH+ β-cells but had an abundance of TH+ fibers following induction of VEGF-A overexpression (Figure 26C). Because the expression of TH in β-cells has been suggested to be a marker of senescent cells (Teitelman et al., 1998), X-gal staining was performed on pancreatic cryosections to evaluate for acid β-galactosidase activity (Beattie et al., 1994). Islets from six-month-old ↓VEGF-A mice and *Vegfa*$^{fl/fl}$ controls showed equal X-gal staining (Figure 27), though acinar tissue in ↓VEGF-A mice showed much greater X-gal staining than acinar tissue in *Vegfa*$^{fl/fl}$ controls (Figure 27, circles).

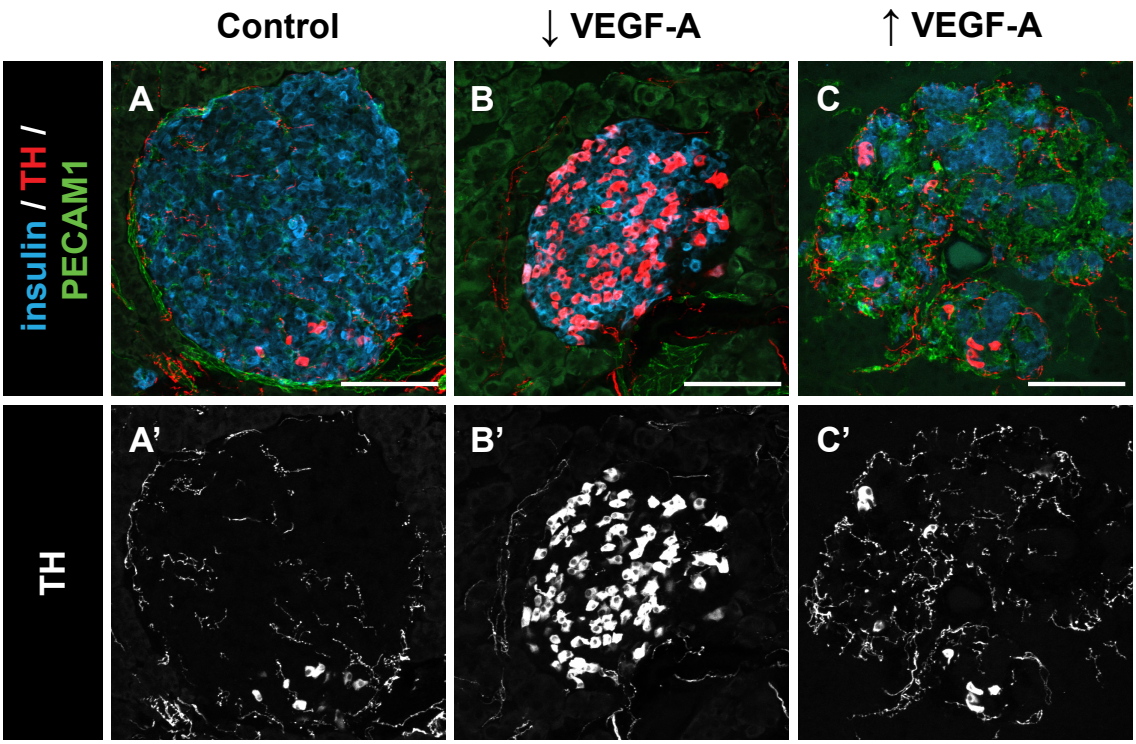

Figure 26. Islet VEGF-A production influences islet sympathetic innervation. Representative islets from adult *Vegfa*$^{fl/fl}$ control (**A**), *Pdx1-Cre;Vegfa*$^{fl/fl}$ (↓VEGF-A; **B**), and doxycycline-treated (for one week) *RIP-rtTA;TetO-hVegfa* (↑VEGF-A; **C**) mice, immunolabeled for insulin (blue), PECAM1 (green) and tyrosine hydroxylase (TH; red/grayscale). Scale bars are 100 μm.

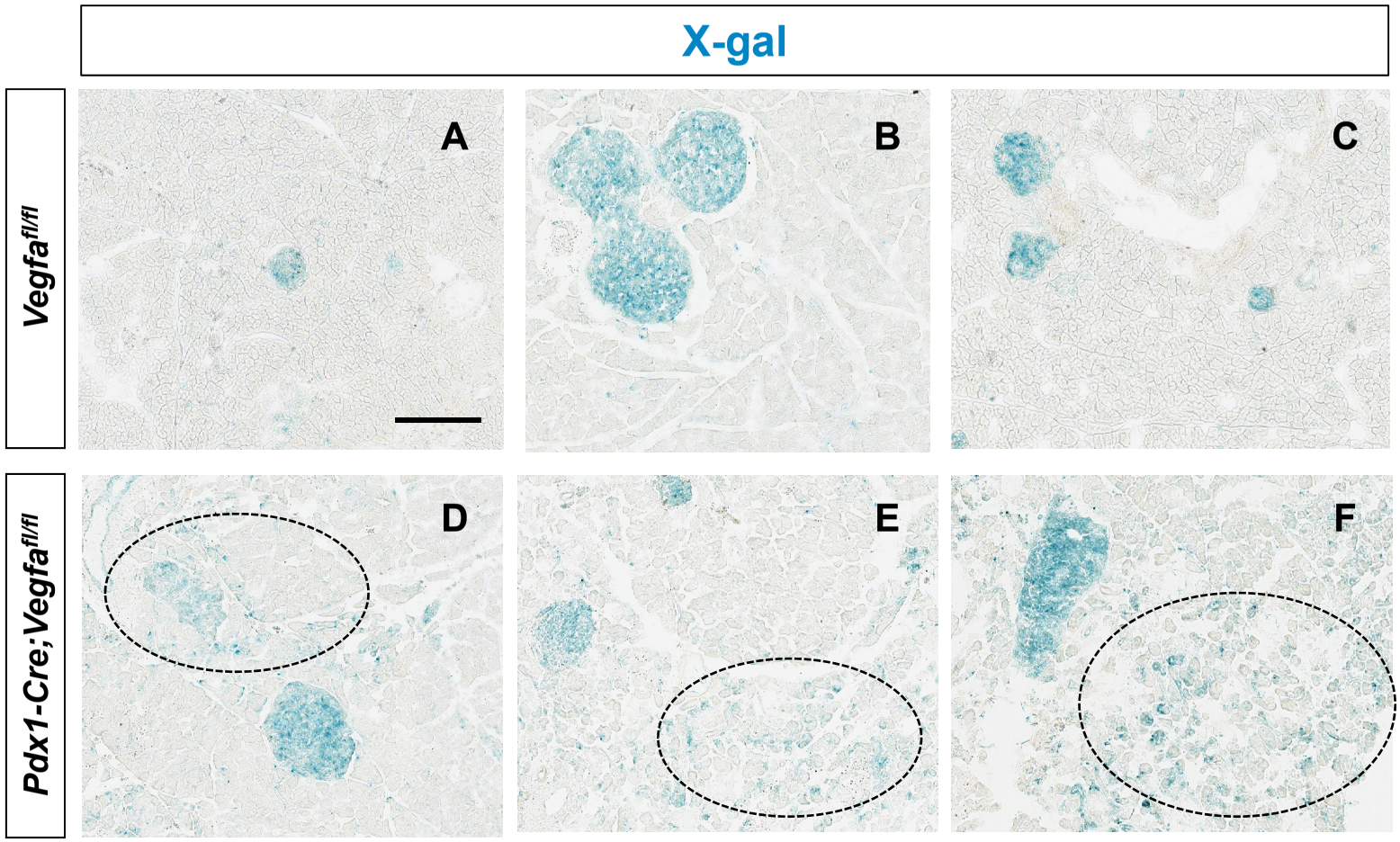

Figure 27. Senescence-associated β-galactosidase is elevated in VEGF-A-deficient pancreata but not in VEGF-A-deficient islets. Senescence-associated β-galactosidase expression, as indicated by acidic X-gal staining, is not increased in *Pdx1-Cre;Vegfa*$^{fl/fl}$ islets (**D-F**) compared to *Vegfa*$^{fl/fl}$ controls (**A-C**), at six months of age. However, increased X-gal staining was observed in the exocrine pancreas in *Pdx1-Cre;Vegfa*$^{fl/fl}$ mice (dotted lines). Scale bar in **A** is 250 μm, and applies to all panels.

To determine when the increase in TH+ β-cells in VEGF-A-deficient islets is first evident, TH expression was examined at multiple stages of development in ↓VEGF-A mice. At E14.5, E17.5, and P1, few insulin+ β-cells were TH+ in control or ↓VEGF-A mice (Figure 28A-C, F-H). At P7, when few TUJ1+ or TH+ nerves were present within the islet core, TH+ β-cells were readily found in control islets (Figure 28D). Only a few TH+ β-cells remain in islets of control mice after weaning, when TUJ1+ fibers are consistently found within the islet core (Figure 28E). Interestingly, islets in ↓VEGF-A mice showed more TH+ β-cells at both P7 and P21 than littermate controls (Figure 28I, J). In contrast, while hypervascularized islet clusters from ↑VEGF-A mice (treated with Dox from E5.5) show many TH+ fibers at P7, almost no β-cells express TH (Figure 28K).

Finally, an antibody to the vesicular acetylcholine transporter (VAChT) was used to mark cholinergic fibers of the parasympathetic nervous system. Islets from control mice showed many VAChT+ nerve fibers, and no evidence of VAChT labeling in endocrine cells (Figure 29A). Similar to the decrease in TH+ islet fibers in ↓VEGF-A mice, VEGF-A-deficient islets also showed fewer VAChT+ nerve fibers (Figure 29B). In contrast, the highly innervated islet clusters in ↑VEGF-A mice expressed numerous VAChT+ fibers (Figure 29C). In all, these data show that islet VEGF-A expression determines islet autonomic innervation patterns.

Peri-islet Schwann cells undergo reactive gliosis when islet VEGF-A expression is decreased

In contrast to nerve fibers, Schwann cells showed a surprisingly similar dramatic change in morphology following both VEGF-A inactivation and overexpression. While

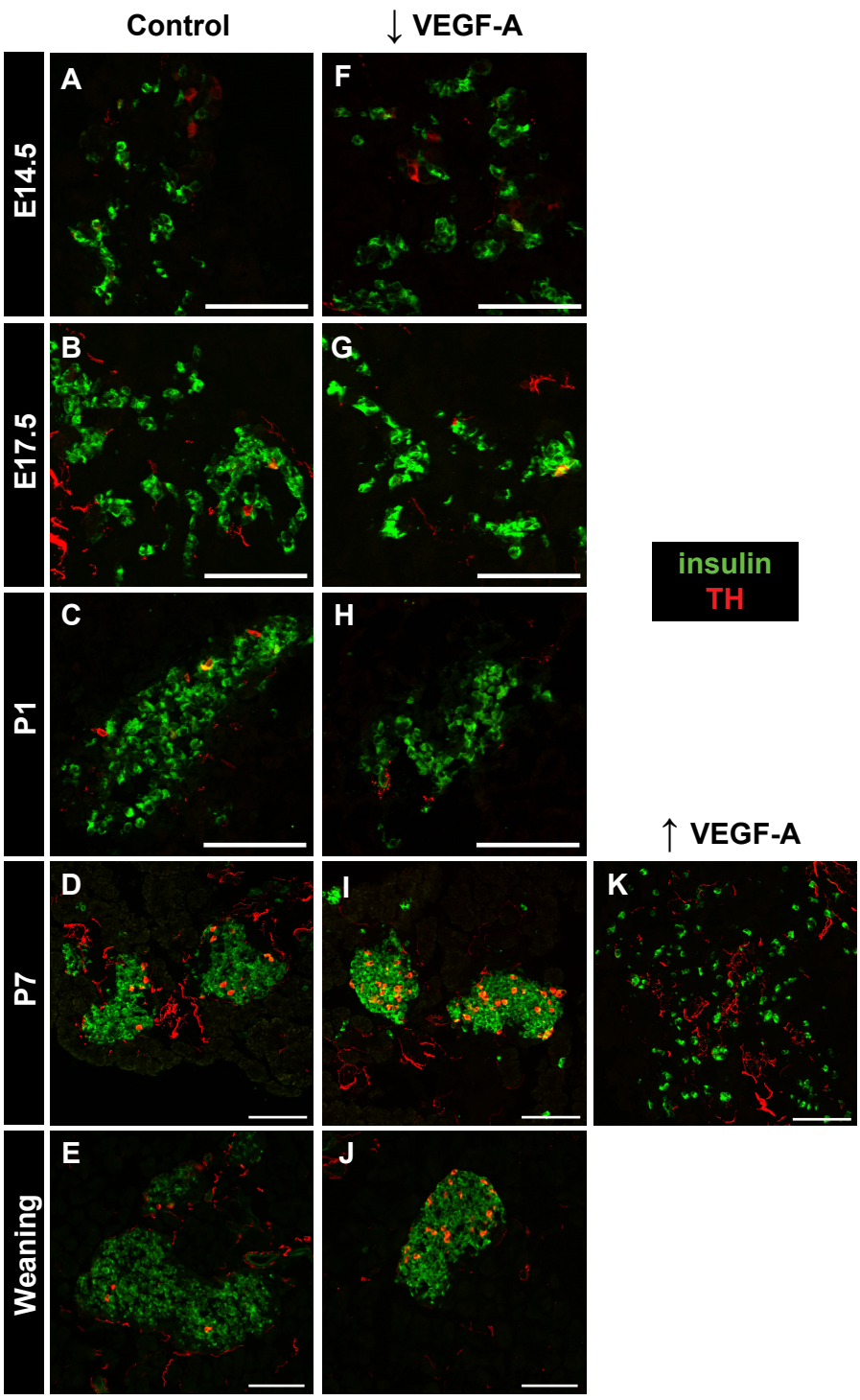

Figure 28. The proportion of β-cells expressing tyrosine hydroxylase is elevated in VEGF-A-deficient islets during postnatal development. A-J. Representative islets from *Vegfa*$^{fl/fl}$ (**A-E**), *Pdx1-Cre;Vegfa*$^{fl/fl}$ (↓VEGF-A; **F-J**), and doxycycline-treated (from E5.5) *RIP-rtTA;TetO-hVegfa* (↑VEGF-A; **K**) mice at embryonic day 14.5 (E14.5; **A, F**), E17.5 (**B, G**), postnatal day 1 (P1; **C, H**), P7 (**D, I, K**) and weaning (**E, J**), immunolabeled for insulin (green) and TH (red). Scale bars are 100 μm.

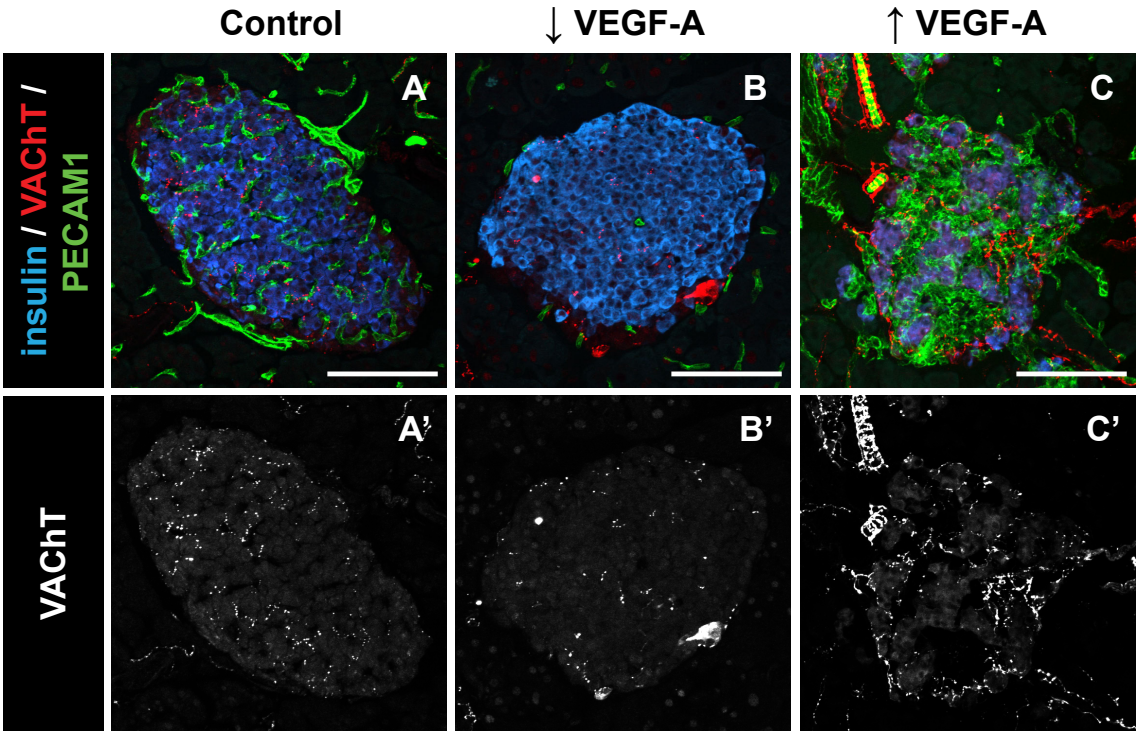

Figure 29. Islet VEGF-A production influences islet parasympathetic innervation. Representative islets from adult *Vegfa*$^{fl/fl}$ control (**A**), *Pdx1-Cre;Vegfa*$^{fl/fl}$ (↓VEGF-A; **B**), and doxycycline-treated (for one week) *RIP-rtTA;TetO-hVegfa* (↑VEGF-A; **C**) mice, immunolabeled for insulin (blue), PECAM1 (green) and the vesicular acetylcholine transporter (VAChT; red/grayscale). Scale bars are 100 μm.

Schwann cells in control pancreata were located at the islet periphery (Figure 30A), GFAP+ Schwann cell processes were found mainly intercalated between insulin+ cells in islets of adult ↓VEGF-A mice (Figure 30B). By morphometry, this was measured as a three-fold increase in the GFAP+ fiber area within the insulin+ islet area (Figure 30D), which correlated with a 600% increase in *Gfap* mRNA expression in isolated islets from adult ↓VEGF-A mice (Figure 30E). Islet clusters in ↑VEGF-A mice showed a similar redistribution of GFAP+ Schwann cell processes into the islet core (Figure 30C), though many of the Schwann cell processes were broader in shape and displayed less intense GFAP immunofluorescence than GFAP+ fibers in control and ↓VEGF-A islets. Islet clusters in ↑VEGF-A mice showed a seven-fold increase in the islet area occupied by GFAP+ Schwann cells compared to controls (Figure 30D), but showed a 70% decrease in *Gfap* mRNA (Figure 30E). GFAP+ Schwann cells began to display the morphology seen in mature islets in ↓VEGF-A and ↑VEGF-A mice around weaning (Figure 31). While Schwann cells in ↑VEGF islets appear to simply alter their morphology in the changing islet microenvironment, the increased GFAP expression in Schwann cells of ↓VEGF islets is indicative of reactive gliosis, an adaptive response by glia of the nervous system in the setting of nerve injury.

Islet neural crest-derived cells do not express VEGF-A receptors during the postnatal maturation of islet innervation

To determine if VEGF-A signaling directly regulates islet innervation, nerves and Schwann cells were examined for expression of two VEGF-A receptors important in mediating its positive effects of cells of the nervous system, the VEGF receptor 2

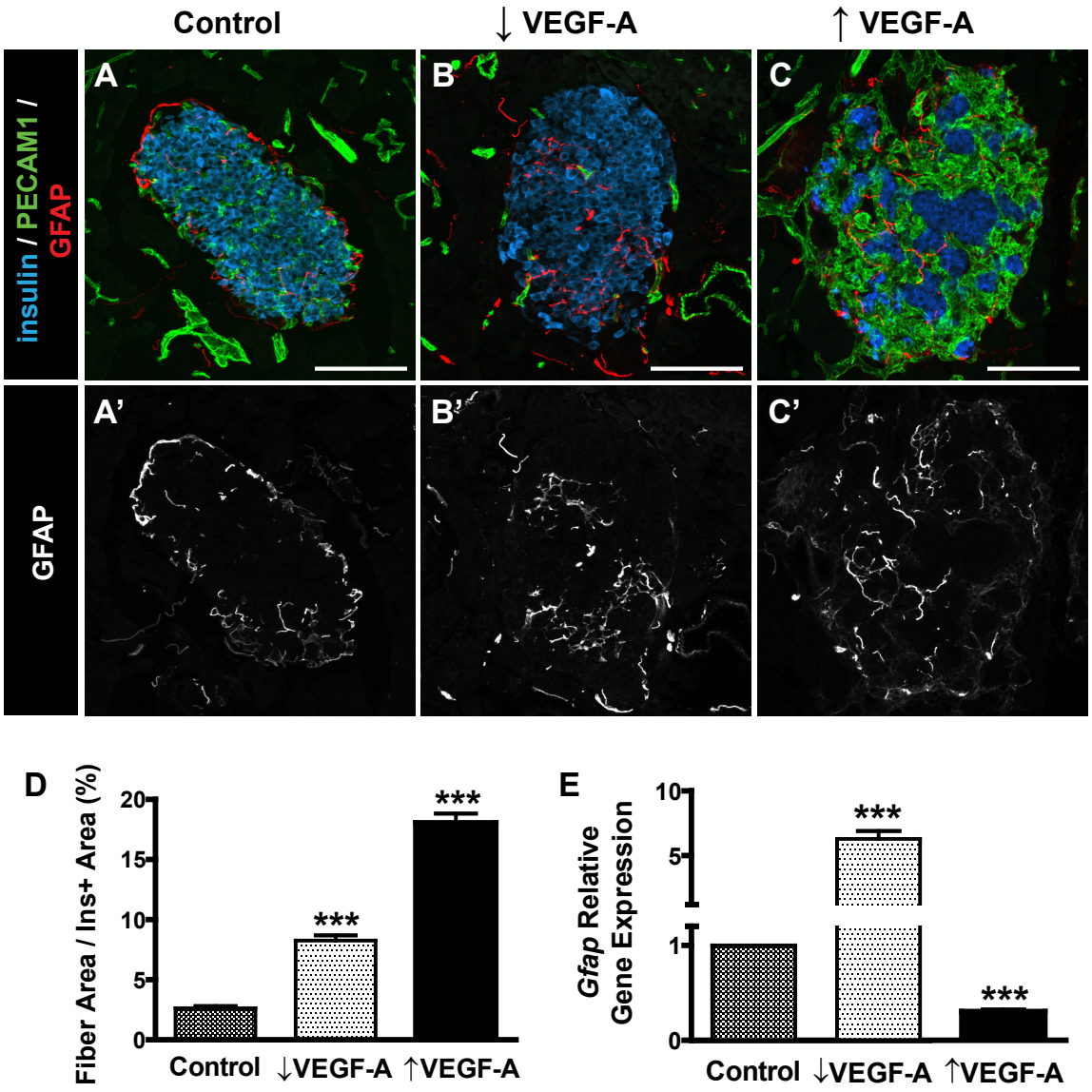

Figure 30. Peri-islet Schwann cells demonstrate altered morphology following changes in VEGF-A expression and islet vascularization. A-C. Representative islets from adult *Vegfa*$^{fl/fl}$ control (**A**), *Pdx1-Cre;Vegfa*$^{fl/fl}$ (↓VEGF-A; **B**), and doxycycline-treated (for one week) *RIP-rtTA;TetO-hVegfa* (↑VEGF-A; **C**) mice, immunolabeled for insulin (blue), PECAM1 (green) and GFAP (red/grayscale). Scale bars are 100 μm. **D**. Morphometric quantification of GFAP+ fiber area in adult islets. **E.** Relative expression of *Gfap* mRNA in isolated islets. ***$P < 0.001$ vs. control group.

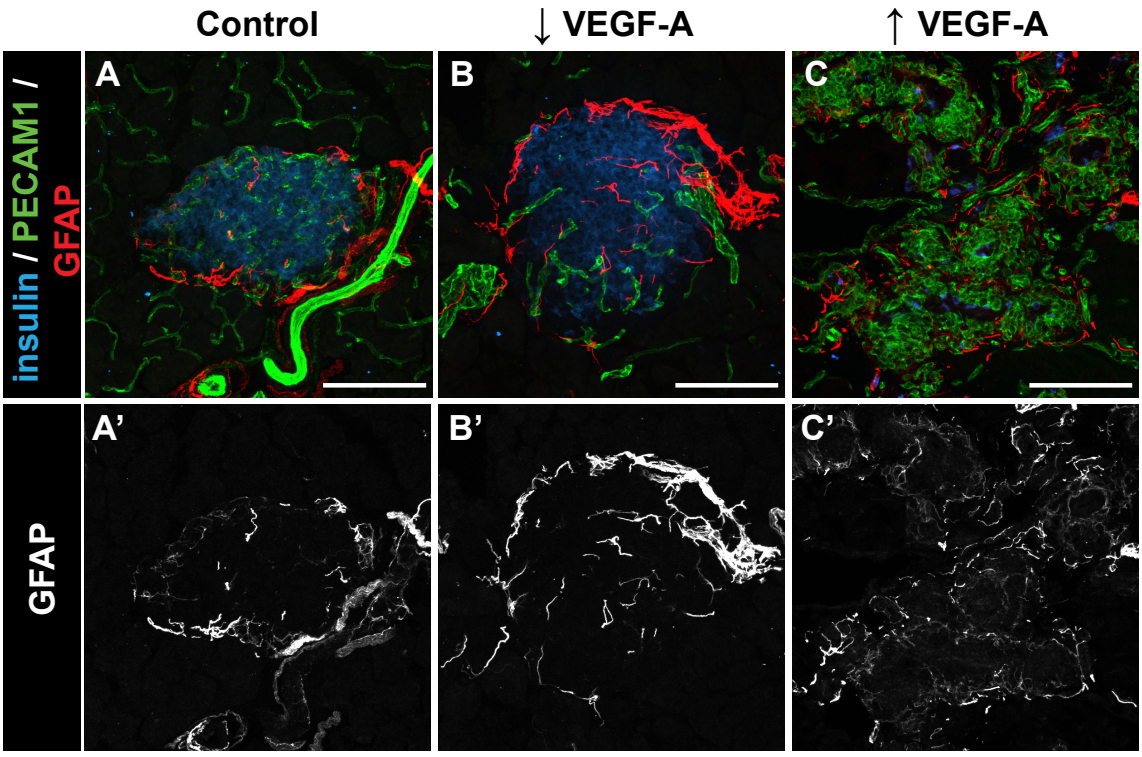

Figure 31. Disrupted Schwann cell morphology following altered VEGF-A expression is present by weaning. A-C. Representative islets from *Vegfa*$^{fl/fl}$ control (**A**), *Pdx1-Cre;Vegfa*$^{fl/fl}$ (↓VEGF-A; **B**), and doxycycline-treated (from E5.5) *RIP-rtTA;TetO-hVegfa* (↑VEGF-A; **C**) mice at weaning (postnatal day [P]21-P28), immunolabeled for insulin (blue), PECAM1 (green) and GFAP (red/grayscale). Scale bars are 100 μm.

(VEGFR2) and neuropilin 1 (NRP1). In this experiment, *Wnt1-Cre;R26-EYFP* mice, in which neural crest-derived cells are indelibly labeled with YFP (Plank et al., 2011), were used to co-label VEGF-A receptors with pancreatic nerves and Schwann cells. Both VEGFR2 and NRP1 displayed strong colocalization with PECAM1+ capillaries in control and hypervascularized islets (Figure 32). In contrast, coexpression of YFP+ neural crest cells with either VEGF-A receptor was not observed during the postnatal maturation of islet innervation (P7, weaning, and adult, Figures 33-34; P1, Figure 35B). However, a few YFP+ neural crest cells expressed NRP1, but not VEGFR2, at E16.5 (Figure 35A and C, arrowheads). Therefore, VEGF-A does not appear to signal to intraislet nerves during the postnatal maturation of islet innervation.

Gene expression changes following VEGF-A deficiency or overexpression

To investigate the ability of intraislet endothelial cells to enhance islet innervation, RNA sequencing was performed on isolated islet clusters from ↑VEGF-A mice treated with Dox for one week (in which the majority of cells are endothelial cells; Brissova et al., manuscript in preparation) and untreated controls. Hypervascularized islet clusters showed upregulation of a few known neurotrophic factors, including nerve growth factor (NGF; Table 6), and upregulation of axon guidance factors (Table 7). Furthermore, several extracellular matrix (ECM) components showed changes in expression, indicative of ECM remodeling (Table 8). For example, VEGF-A-overexpressing islet clusters showed a five-fold increase in the collagen IV isoforms α1 and α2, a six-fold increase in laminin-411 (α4, β1, and γ1 chains), and an 11-fold increase in fibronectin 1,

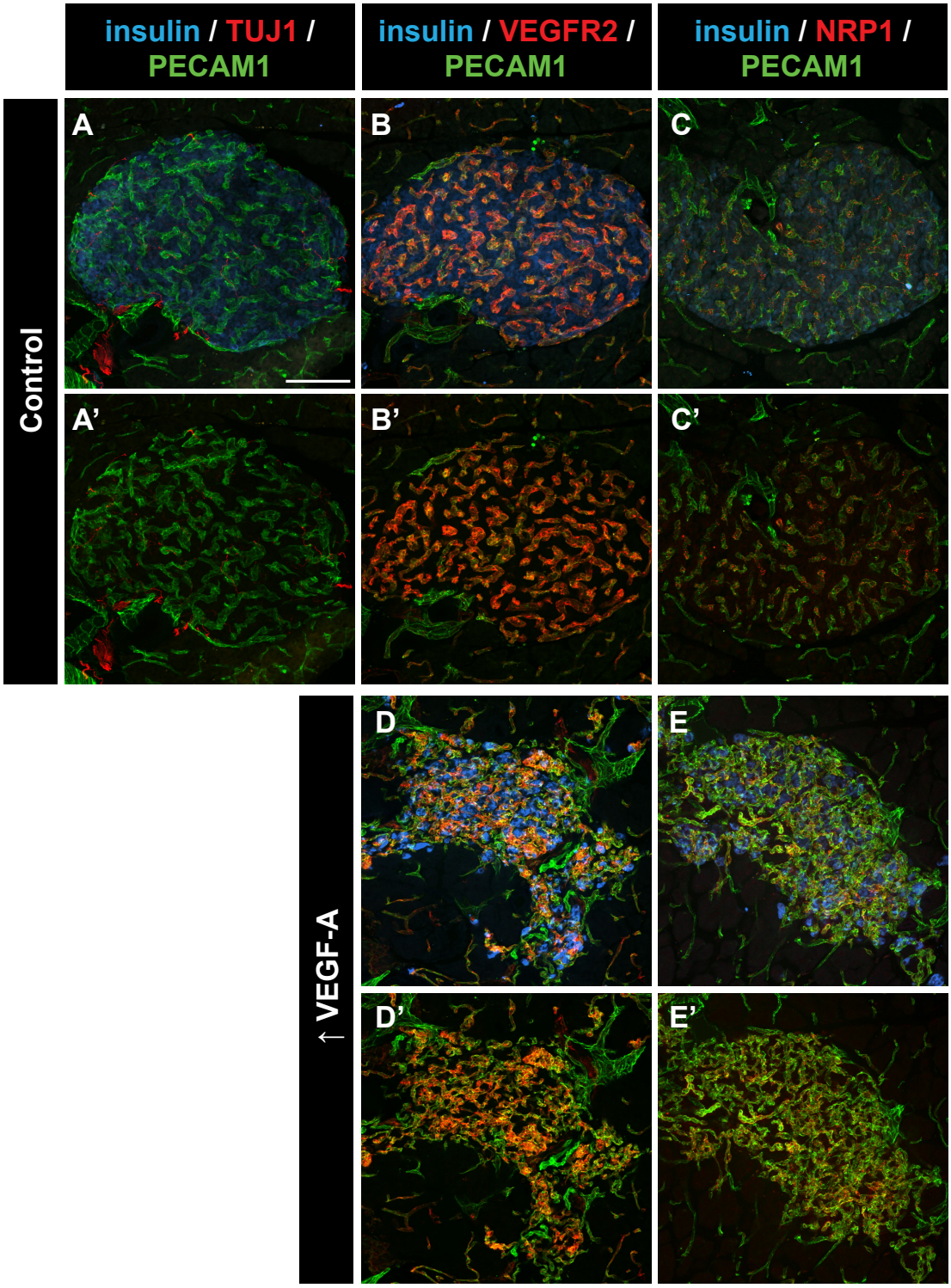

Figure 32. Intraislet capillaries express VEGF-A receptors. Representative islets from adult *Vegfa*$^{fl/fl}$ (control) and doxycycline-treated (for one week) *RIP-rtTA; TetO-hVegfa* (↑VEGF-A) mice, immunolabeled for insulin (blue), PECAM1 (green), and TUJ1 (red; A), VEGFR2 (red; **B, D**) or neuropilin-1 (NRP1, red; **C, E**). Scale bar in **A** is 100 μm and applies to all other panels.

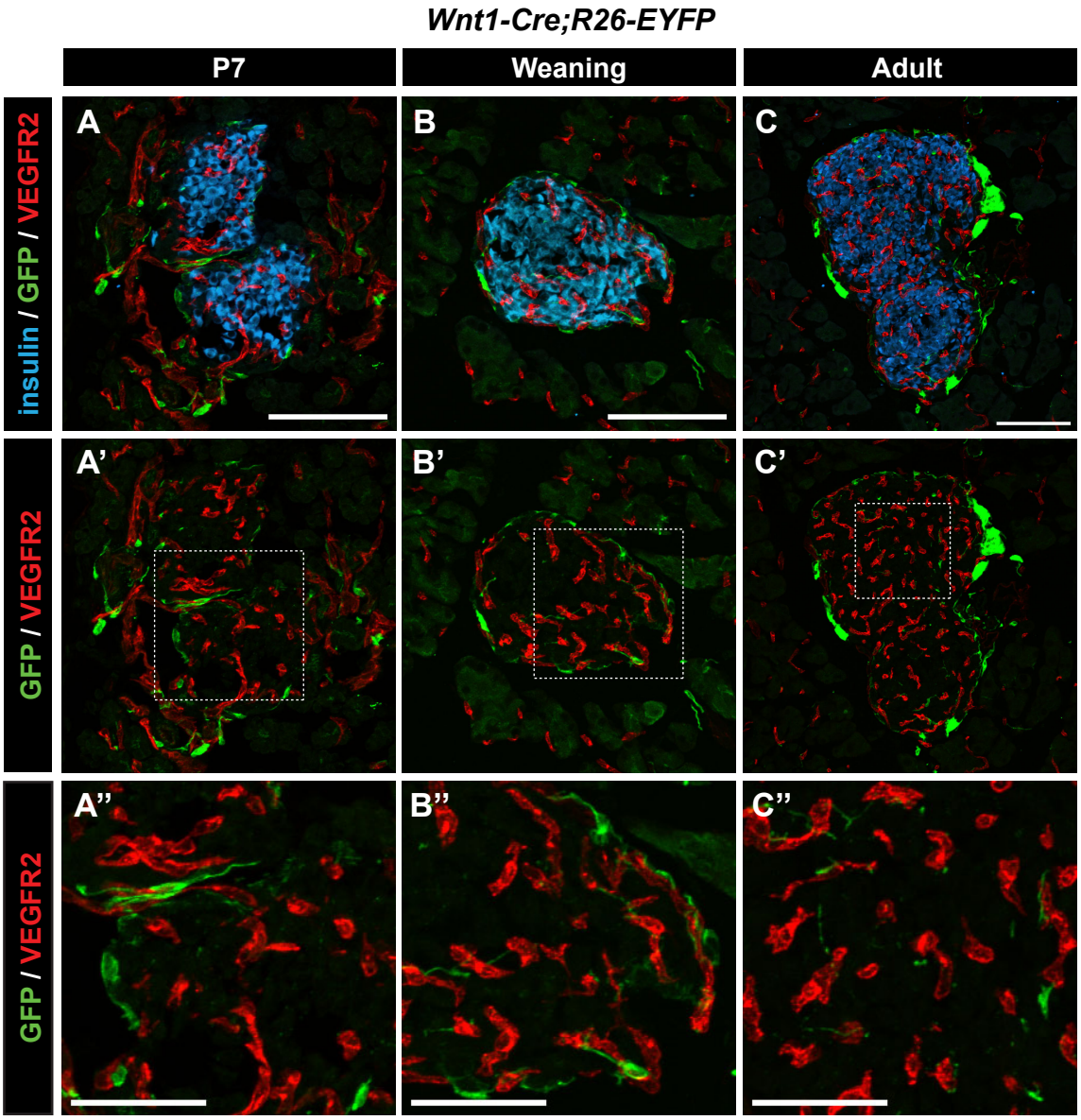

Figure 33. Islet neural crest-derived cells do not express the VEGF receptor 2 in postnatal life. Representative islets from *Wnt1-Cre;R26R-EYFP* mice at postnatal day 7 (P7; **A**), weaning (P21; **B**), and adult (**C**) stages labeled for insulin (blue), GFP (green), and VEGFR2 (red). Scale bars in **A, B** and **C** are 100 μm. Regions denoted by the dotted line in **A', B'**, and **C'** are shown in **A", B"** and **C"**, respectively. Scale bars in **A", B"**, and **C"** are 50 μm.

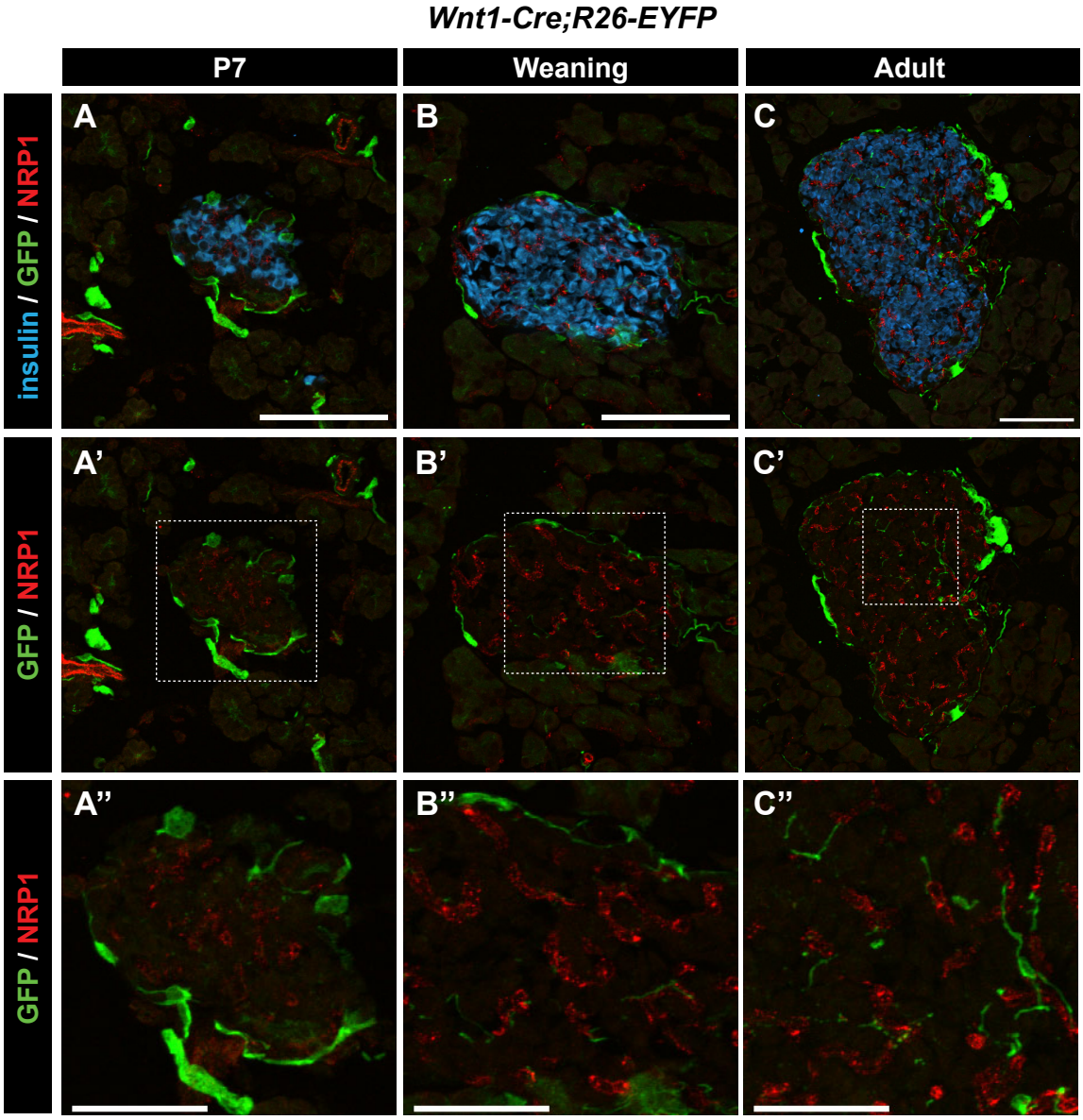

Figure 34. Islet neural crest-derived cells do not express the VEGF receptor neuropilin 1 in postnatal life. Representative islets from *Wnt1-Cre;R26R-EYFP* mice at postnatal day 7 (P7; **A**), weaning (P21; **B**), and adult (**C**) stages labeled for insulin (blue), GFP (green), and neuropilin 1 (NRP1; red). Scale bars in **A, B** and **C** are 100 µm. Regions denoted by the dotted line in **A', B'**, and **C'** are shown in **A", B"** and **C"**, respectively. Scale bars in **A", B"**, and **C"** are 50 µm.

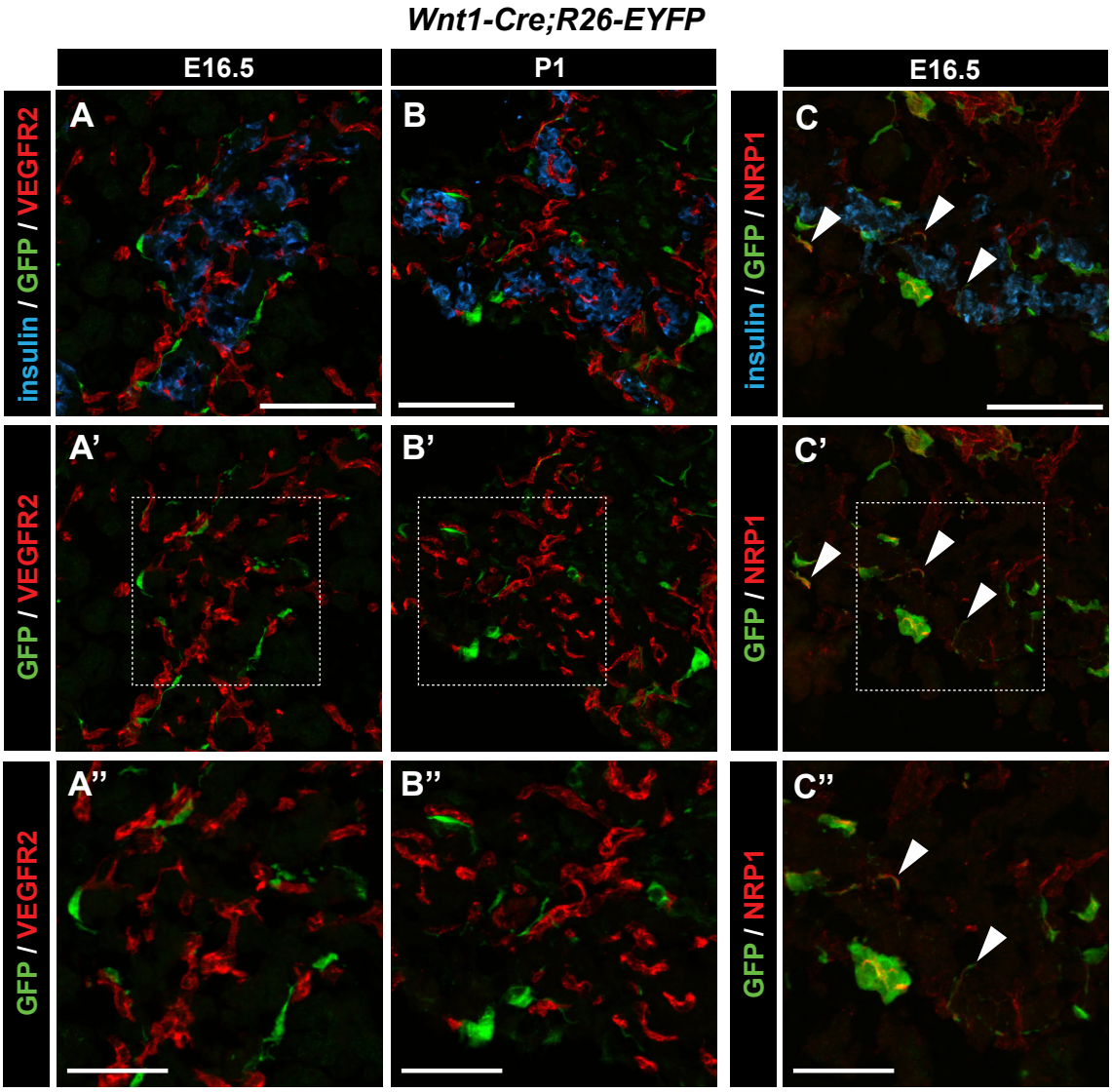

Figure 35. Some neural crest derived-cells express neuropilin-1, but not VEGFR2, during pancreas development. Representative islets from *Wnt1-Cre;R26R-EYFP* mice at embryonic day 16.5 (E16.5; **A, C**) and postnatal day 1 (P1; **B**). Images are labeled for insulin (blue), GFP (green), and VEGFR2 (red in **A-B**) or neuropilin 1 (NRP1, red in **C**). Regions denoted by the dotted line in **A', B'**, and **C'** are shown in **A", B"** and **C"**, respectively. Arrowheads in **C** denote fibers with colocalization of GFP and NRP1. Scale bars in **A, B,** and **C** are 100 μm. Scale bars in **A", B"**, and **C"** are 50 μm.

Table 6. Gene expression of neurotrophic factors and their receptors in isolated islets after one week of VEGF-A overexpression. LO, low expression; relative fold changes were not calculated for genes with low expression (-).

Gene Symbol	Fold Change	No Dox RPKM	1 wk Dox RPKM	Gene Name
Artn	-	LO	LO	artemin
Bdnf	1.14	0.57	0.66	brain derived neurotrophic factor
Bmp1	1.79	4.41	7.94	bone morphogenetic protein 1
Bmp2	3.96	0.38	1.57	bone morphogenetic protein 2
Bmp3	1.17	1.36	1.61	bone morphogenetic protein 3
Bmp4	1.04	2.72	2.86	bone morphogenetic protein 4
Bmp5	2.47	7.70	19.14	bone morphogenetic protein 5
Bmp6	1.21	0.64	0.78	bone morphogenetic protein 6
Bmp7	1.16	0.27	0.32	bone morphogenetic protein 7
Bmp8	-	LO	LO	bone morphogenetic protein 8
Bmp15	-	LO	LO	bone morphogenetic protein 15
Bmpr1a	-1.26	25.58	20.42	bone morphogenetic protein receptor, type 1A
Bmpr1b	-1.18	1.87	1.59	bone morphogenetic protein receptor, type 1B
Bmpr2	2.14	49.68	107.26	bone morphogenic protein receptor, type II (serine/threonine kinase)
Edn1	2.25	0.60	1.40	endothelin 1
Edn3	-2.30	4.38	1.91	endothelin 3
Ednra	4.35	8.49	37.24	endothelin receptor type A
Ednrb	3.56	56.83	203.91	endothelin receptor type B
Gdnf	-	LO	LO	glial cell line derived neurotrophic factor
Gfra1	-2.29	3.97	1.74	glial cell line derived neurotrophic factor family receptor alpha 1
Gfra2	2.32	4.50	10.54	glial cell line derived neurotrophic factor family receptor alpha 2
Gfra3	-	LO	LO	glial cell line derived neurotrophic factor family receptor alpha 3
Hgf	1.07	1.29	1.38	hepatocyte growth factor
Igf1	5.00	4.25	21.45	insulin-like growth factor 1
Igf1r	-1.31	14.07	10.77	insulin-like growth factor I receptor
Igf2	-1.57	6.60	4.23	insulin-like growth factor 2
Igf2r	1.16	16.05	18.69	insulin-like growth factor 2 receptor
Ngf	3.96	3.74	15.09	nerve growth factor
Ngfr	1.40	1.89	2.67	nerve growth factor receptor (TNFR superfamily, member 16)
Ntf3	-	LO	LO	neurotrophin 3
Ntf5	-	LO	LO	neurotrophin 5
Ntrk1	-	LO	LO	neurotrophic tyrosine kinase, receptor, type 1 (TrkA)
Ntrk2	-2.97	17.52	5.94	neurotrophic tyrosine kinase, receptor, type 2
Ntrk3	2.46	0.09	0.24	neurotrophic tyrosine kinase, receptor, type 3
Pspn	-	LO	LO	persephin
Ret	-3.00	11.54	3.86	ret proto-oncogene

Table 7. Gene expression of axon guidance factors and their receptors in isolated islets after one week of VEGF-A overexpression. LO, low expression; relative fold changes were not calculated for genes with low expression (-).

Gene Symbol	Fold Change	No Dox RPKM	1 wk Dox RPKM	Gene Name
Dcc	-	LO	LO	deleted in colorectal carcinoma
Efna1	4.38	1.20	5.41	ephrin A1
Efna2	-1.22	1.10	0.91	ephrin A2
Efna3	-	LO	LO	ephrin A3
Efna4	7.67	0.25	2.23	ephrin A4
Efna5	-3.48	5.67	1.63	ephrin A5
Efnb1	1.18	1.36	1.63	ephrin B1
Efnb2	3.17	22.04	70.45	ephrin B2
Efnb3	1.03	1.29	1.34	ephrin B3
Epha1	-1.42	0.82	0.58	Eph receptor A1
Epha2	4.09	1.72	7.12	Eph receptor A2
Epha3	2.08	1.15	2.42	Eph receptor A3
Epha4	2.55	3.50	8.99	Eph receptor A4
Epha5	-1.23	0.37	0.30	Eph receptor A5
Epha7	-2.83	3.56	1.26	Eph receptor A7
Ephb1	5.27	0.69	3.72	Eph receptor B1
Ephb2	-2.18	0.51	0.24	Eph receptor B2
Ephb3	3.37	0.22	0.79	Eph receptor B3
Ephb4	2.74	3.59	9.92	Eph receptor B4
Fgf2	7.54	0.19	1.66	fibroblast growth factor 2
Nrp1	2.24	31.39	70.75	neuropilin 1
Nrp2	4.23	19.26	82.05	neuropilin 2
Ntn1	8.27	0.03	0.35	netrin 1
Ntn3	-2.19	0.31	0.14	netrin 3
Ntn4	-1.03	6.07	5.95	netrin 4
Ntng2	4.25	0.12	0.59	netrin G2
Plxna1	1.84	1.93	3.58	plexin A1
Plxna2	1.52	6.78	10.40	plexin A2
Plxna3	-2.63	1.29	0.49	plexin A3
Plxna4	2.04	2.13	4.37	plexin A4
Plxnb1	1.13	2.62	2.98	plexin B1
Plxnb2	-1.14	12.76	11.30	plexin B2
Plxnc1	2.16	0.32	0.72	plexin C1
Plxnd1	5.36	3.09	16.71	plexin D1
Robo1	-1.89	7.01	3.73	roundabout homolog 1 (Drosophila)
Robo2	-3.82	16.15	4.26	roundabout homolog 2 (Drosophila)
Robo3	2.31	0.16	0.39	roundabout homolog 3 (Drosophila)
Robo4	3.15	7.38	23.46	roundabout homolog 4 (Drosophila)
Sema3a	-	LO	LO	sema domain, immunoglobulin domain (Ig), short basic domain, secreted, (semaphorin) 3A
Sema3b	1.95	0.93	1.85	sema domain, immunoglobulin domain (Ig), short basic domain, secreted, (semaphorin) 3B
Sema3c	1.17	1.07	1.26	sema domain, immunoglobulin domain (Ig), short basic domain, secreted, (semaphorin) 3C
Sema3d	1.89	0.21	0.41	sema domain, immunoglobulin domain (Ig), short basic domain, secreted, (semaphorin) 3D
Sema3e	-1.49	0.91	0.61	sema domain, immunoglobulin domain (Ig), short basic domain, secreted, (semaphorin) 3E
Sema3g	1.57	4.53	7.18	sema domain, immunoglobulin domain (Ig), short basic domain, secreted, (semaphorin) 3G

Table 7, continued.

Gene Symbol	Fold Change	No Dox RPKM	1 wk Dox RPKM	Gene Name
Sema4a	-1.56	0.69	0.44	sema domain, immunoglobulin domain (Ig), transmembrane domain (TM) and short cytoplasmic domain, (semaphorin) 4A
Sema4b	1.10	3.79	4.21	sema domain, immunoglobulin domain (Ig), transmembrane domain (TM) and short cytoplasmic domain, (semaphorin) 4B
Sema4c	3.95	1.18	4.72	sema domain, immunoglobulin domain (Ig), transmembrane domain (TM) and short cytoplasmic domain, (semaphorin) 4C
Sema4d	-1.57	4.07	2.61	sema domain, immunoglobulin domain (Ig), transmembrane domain (TM) and short cytoplasmic domain, (semaphorin) 4D
Sema4f	-1.50	1.28	0.86	sema domain, immunoglobulin domain (Ig), TM domain, and short cytoplasmic domain
Sema4g	2.28	0.21	0.50	sema domain, immunoglobulin domain (Ig), transmembrane domain (TM) and short cytoplasmic domain, (semaphorin) 4G
Sema5a	2.66	4.68	12.52	sema domain, seven thrombospondin repeats (type 1 and type 1-like), transmembrane domain (TM) and short cytoplasmic domain, (semaphorin) 5A
Sema5b	3.92	0.24	0.97	sema domain, seven thrombospondin repeats (type 1 and type 1-like), transmembrane domain (TM) and short cytoplasmic domain, (semaphorin) 5B
Sema6a	2.55	2.83	7.27	sema domain, transmembrane domain (TM), and cytoplasmic domain, (semaphorin) 6A
Sema6b	2.13	1.91	4.12	sema domain, transmembrane domain (TM), and cytoplasmic domain, (semaphorin) 6B
Sema6c	-	LO	LO	sema domain, transmembrane domain (TM), and cytoplasmic domain, (semaphorin) 6C
Sema6d	3.97	16.10	64.37	sema domain, transmembrane domain (TM), and cytoplasmic domain, (semaphorin) 6D
Sema7a	2.32	5.00	11.73	sema domain, immunoglobulin domain (Ig), and GPI membrane anchor, (semaphorin) 7A
Slit1	-	LO	LO	slit homolog 1
Slit2	1.46	1.38	2.03	slit homolog 2 (Drosophila)
Slit3	2.33	4.94	11.58	slit homolog 3 (Drosophila)
Tgfb1	4.34	5.96	26.15	transforming growth factor, beta 1
Tgfb2	1.94	5.78	11.28	transforming growth factor, beta 2
Tgfb3	3.47	4.85	16.98	transforming growth factor, beta 3
Tgfbr1	-1.00	10.62	10.68	transforming growth factor, beta receptor I
Tgfbr2	2.06	5.78	12.00	transforming growth factor, beta receptor II
Tgfbr3	-1.21	11.76	9.78	transforming growth factor, beta receptor III
Unc119b	-1.19	2.47	2.09	unc-119 homolog B (C. elegans)
Unc13a	-2.89	6.06	2.10	unc-13 homolog A (C. elegans)
Unc13b	-2.80	2.70	0.97	unc-13 homolog B (C. elegans)
Unc45a	1.12	1.36	1.54	unc-45 homolog A (C. elegans)
Unc45b	1.98	5.21	10.37	unc-45 homolog B (C. elegans)
Unc50	-1.35	40.54	30.18	unc-50 homolog (C. elegans)
Unc5a	-1.36	1.88	1.39	unc-5 homolog A (C. elegans)
Unc5b	4.33	1.67	7.31	unc-5 homolog B (C. elegans)
Unc5c	-3.40	1.63	0.48	unc-5 homolog C (C. elegans)
Unc79	-3.77	5.29	1.41	unc-79 homolog (C. elegans)
Unc80	-3.14	18.08	5.79	unc-80 homolog (C. elegans)
Unc93b1	2.28	2.06	4.77	unc-93 homolog B1 (C. elegans)

Table 8. Gene expression of extracellular matrix proteins in isolated islets after one week of VEGF-A overexpression. LO, low expression; relative fold changes were not calculated for genes with low expression (-).

Gene Symbol	Fold Change	No Dox RPKM	1 wk Dox RPKM	Gene Name
Col10a1	15.70	0.13	2.36	collagen, type X, alpha 1
Col11a1	6.89	0.09	0.67	collagen, type XI, alpha 1
Col12a1	9.61	0.42	4.09	collagen, type XII, alpha 1
Col13a1	2.40	3.40	8.23	collagen, type XIII, alpha 1
Col14a1	1.65	6.86	11.42	collagen, type XIV, alpha 1
Col15a1	4.43	15.34	68.43	collagen, type XV, alpha 1
Col16a1	2.38	0.20	0.49	collagen, type XVI, alpha 1
Col18a1	10.37	0.46	4.94	collagen, type XVIII, alpha 1
Col19a1	3.97	0.12	0.49	collagen, type XIX, alpha 1 [
Col1a1	3.55	35.00	124.95	collagen, type I, alpha 1
Col1a2	3.83	15.31	59.00	collagen, type I, alpha 2
Col25a1	1.13	0.24	0.27	collagen, type XXV, alpha 1
Col27a1	1.52	2.16	3.32	collagen, type XXVII, alpha 1
Col28a1	1.57	0.66	1.05	collagen, type XXVIII, alpha 1
Col3a1	2.63	22.06	58.33	collagen, type III, alpha 1
Col4a1	5.12	41.47	213.50	collagen, type IV, alpha 1
Col4a2	5.90	10.78	64.02	collagen, type IV, alpha 2
Col4a3	1.73	3.06	5.32	collagen, type IV, alpha 3
Col4a4	2.08	0.59	1.24	collagen, type IV, alpha 4
Col4a5	5.64	0.33	1.92	collagen, type IV, alpha 5
Col5a1	3.66	1.73	6.41	collagen, type V, alpha 1
Col5a2	4.83	0.94	4.60	collagen, type V, alpha 2
Col5a3	7.55	0.66	5.05	collagen, type V, alpha 3
Col6a1	2.81	5.95	16.88	collagen, type VI, alpha 1
Col6a2	4.12	2.50	10.40	collagen, type VI, alpha 2
Col6a3	4.91	1.91	9.46	collagen, type VI, alpha 3
Col6a5	-3.28	0.44	0.13	collagen, type VI, alpha 5
Col6a6	-1.97	3.00	1.53	collagen, type VI, alpha 6
Col8a1	4.70	10.59	50.09	collagen, type VIII, alpha 1
Col9a2	-2.35	0.43	0.18	collagen, type IX, alpha 2

Table 8, continued.

Gene Symbol	Fold Change	No Dox RPKM	1 wk Dox RPKM	Gene Name
Fn1	11.39	2.25	25.91	fibronectin 1
Itga1	3.77	7.93	30.14	integrin alpha 1
Itga10	3.24	0.06	0.24	integrin, alpha 10
Itga11	2.40	0.28	0.70	integrin alpha 11
Itga2	2.79	0.81	2.31	integrin alpha 2
Itga2b	4.02	0.06	0.29	integrin alpha 2b
Itga3	1.22	2.84	3.51	integrin alpha 3
Itga4	1.04	4.50	4.70	integrin alpha 4
Itga5	9.73	0.43	4.32	integrin alpha 5 (fibronectin receptor alpha)
Itga6	3.32	18.00	60.09	integrin alpha 6
Itga7	4.44	0.47	2.15	integrin alpha 7
Itga8	3.09	1.15	3.60	integrin alpha 8
Itga9	3.78	2.64	10.06	integrin alpha 9
Itgad	-48.38	0.65	0.00	integrin, alpha D
Itgae	2.91	0.16	0.50	integrin alpha E, epithelial-associated
Itgal	2.86	0.45	1.31	integrin alpha L
Itgam	2.24	1.57	3.55	integrin alpha M
Itgav	-1.27	13.64	10.81	integrin alpha V
Itgax	1.83	2.62	4.84	integrin alpha X
Itgb1	2.20	110.44	244.48	integrin beta 1 (fibronectin receptor beta)
Itgb2	2.31	3.30	7.72	integrin beta 2
Itgb3	6.27	9.08	57.40	integrin beta 3
Itgb4	2.07	0.30	0.63	integrin beta 4
Itgb5	1.52	5.24	8.04	integrin beta 5
Itgb6	1.79	0.26	0.48	integrin beta 6
Itgb7	2.27	0.56	1.32	integrin beta 7
Itgb8	-1.90	2.77	1.46	integrin beta 8
Itgbl1	1.10	5.24	5.82	integrin, beta-like 1
Lama2	2.44	4.89	12.04	laminin, alpha 2
Lama3	1.56	4.41	6.92	laminin, alpha 3
Lama4	6.38	8.00	51.43	laminin, alpha 4
Lama5	2.43	1.13	2.77	laminin, alpha 5
Lamb1	6.98	5.94	41.78	laminin B1
Lamb2	2.06	4.34	8.99	laminin, beta 2
Lamc1	5.26	27.39	145.00	laminin, gamma 1
Lamc2	-2.80	3.27	1.17	laminin, gamma 2
Lamc3	7.38	0.03	0.32	laminin gamma 3

all previously shown to be major components of the intraislet vascular basement membrane (Nikolova et al., 2006).

To confirm that NGF expression was increased in intraislet endothelial cells following VEGF-A overexpression, quantitative RT-PCR and immunohistochemistry was performed. Compared to untreated *RIP-rtTA*;*TetO-hVegfa* controls, β-cell-specific VEGF-A overexpression in ↑VEGF-A mice led to a three-fold increase in *Ngf* mRNA in isolated islet clusters (Figure 36B). In contrast, *Ngf* was unchanged in ↓VEGF-A islets, compared to $Vegfa^{fl/fl}$ controls (Figure 36A). As expected, expression of the endothelial cell marker *Kdr* (encoding VEGFR2) was dramatically reduced in ↓VEGF-A islets, but expression of *Pecam1* (encoding PECAM1) was elevated three-fold in ↑VEGF-A islet clusters (Figure 36A-B). In contrast, *Ins2* (encoding insulin) expression was unchanged in ↓VEGF-A islets and significantly reduced in ↑VEGF-A islet clusters (Figure 36A-B). Immunohistochemistry showed that NGF expression did not localize to any particular cell type, but was broadly expressed throughout the islet in all groups (Figure 36C-E). These data suggest that the VEGF-A-induced expansion of the intraislet endothelial cell population contributes to islet hyperinnervation through expression of NGF.

β-cell hyperplasia may enhance islet innervation

To determine if β-cell mass also influences the extent of islet innervation, the adult *ob/ob* mouse was used as a model of β-cell hyperplasia. Islets in adult *ob/ob* mice have a greater than three-fold increase in islet area compared to littermate *wt/wt* control mice, and an altered intraislet vasculature, including reduced vessel density but increased

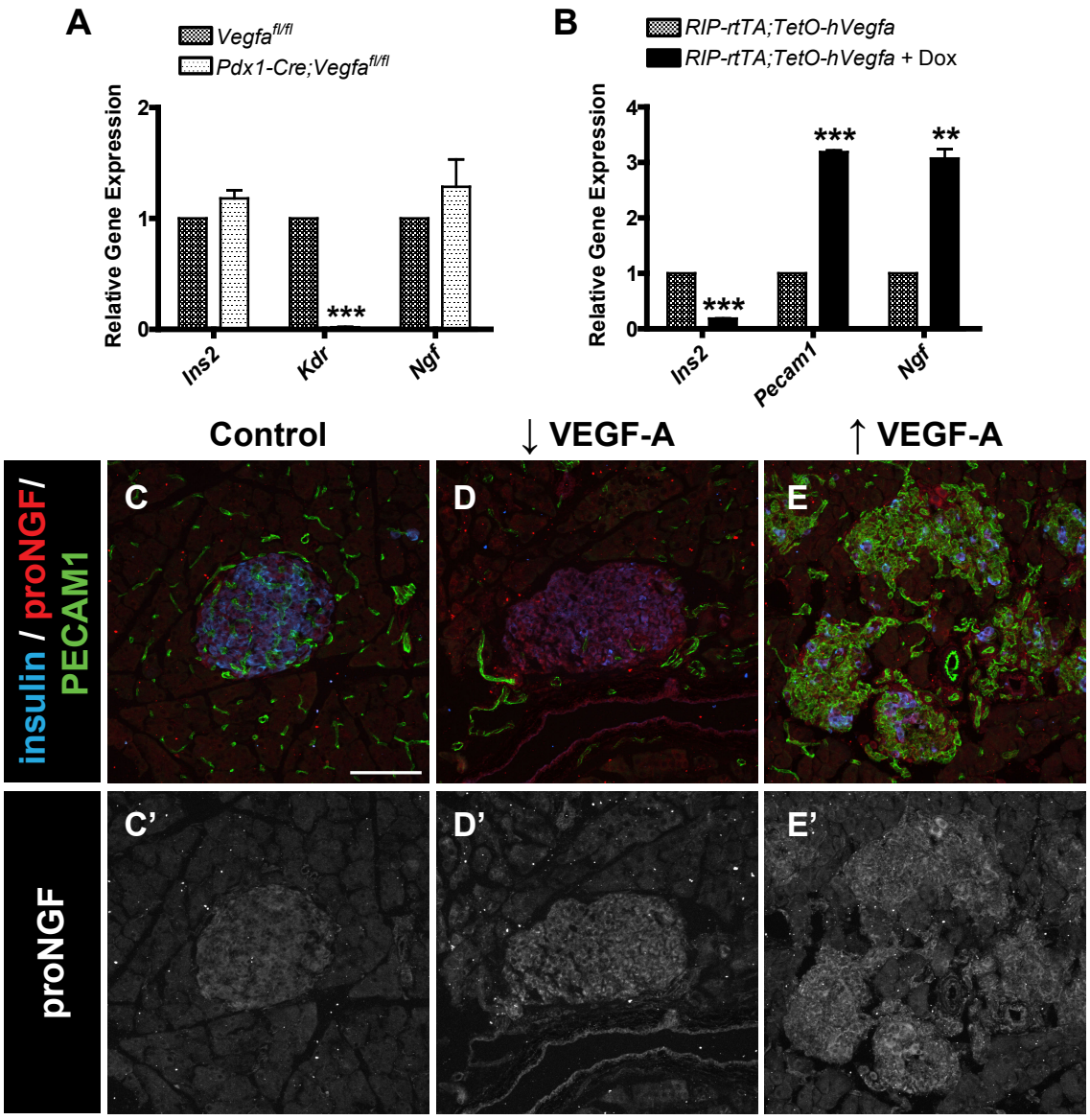

Figure 36. Islet NGF expression is increased following VEGF-A overexpression. **A.** Relative gene expression of *Ins2* (encoding insulin), *Kdr* (encoding VEGFR2), and *Ngf* (encoding NGF) in islets from *Pdx1-Cre;Vegfa*$^{fl/fl}$ mice compared to *Vegfa*$^{fl/fl}$ controls, evaluated by quantitative PCR. Values are 1.181 ± 0.144 for *Ins2* (n = 4; P > 0.05 vs. control), 0.020 ± 0.006 for *Kdr* (n = 4; ***P < 0.001 vs. control) and 1.285 ± 0.494 for *Ngf* (n = 4; P > 0.05 vs. control). **B.** Relative gene expression of *Ins2*, *Pecam1* (encoding PECAM1), and *Ngf* in islets from doxycycline-treated (for one week) *RIP-rtTA;TetO-hVegfa* mice compared to untreated *RIP-rtTA;TetO-hVegfa* controls, evaluated by quantitative PCR. Values are 0.184 ± 0.005 for *Ins2* (n = 4; ***P < 0.001 vs. control), 3.188 ± 0.058 for *Pecam1* (n = 4; ***P < 0.001 vs. control) and 3.072 ± 0.341 for *Ngf* (n = 4; **P = 0.0089 vs. control). **C-E**. Representative islets from adult control (**C**),*Pdx1-Cre;Vegfa*$^{fl/fl}$ (↓VEGF-A; **D**), and doxycycline-treated (for one week) *RIP-rtTA;TetO-hVegfa* (↑VEGF-A; **E**) mice, immunolabeled for insulin (blue), PECAM1 (green) and proNGF (red/grayscale). Scale bar in **C** is 100 μm and applies to **D-E**.

vessel diameter and increased blood flow (Dai et al., manuscript in preparation). Global islet innervation was slightly increased in hyperplastic *ob/ob* islets (Figure 37A-B), as quantified by the density of TUJ1+ nerve fibers (Figure 37C). In contrast, GFAP+ Schwann cells in *ob/ob* pancreata displayed a normal peri-islet morphology (Figure 38).

Surprisingly, *ob/ob* islets displayed evidence of fiber-type specific changes in autonomic innervation. Islets in *ob/ob* mice showed dense parasympathetic innervation (Figure 39A-B), with an increased density of VAChT+ varicosities and increased VAChT+ area (Figure 39E-F). This observation was not solely a reflection of the increased number of large islets in *ob/ob* mice, as larger islets in *wt/wt* mice did not show a similar increase in VAChT+ nerve fibers (Figure 39C-D). In contrast to parasympathetic innervation, islet sympathetic innervation was unchanged, or perhaps even decreased, in *ob/ob* mice. Islets from *ob/ob* and *wt/wt* mice showed a comparable number of TH+ nerve fibers within the insulin+ islet core (Figure 39G-H). Similarly, both *ob/ob* and *wt/wt* showed a few TH+ β-cells per islet (Figure 39G-H, arrows). These data show that *ob/ob* islets have enhanced parasympathetic, but not sympathetic, innervation.

In contrast to the *ob/ob* model, no changes in islet innervation were observed in either ↓VEGF-A mice or $Vegfa^{fl/fl}$ controls in the late stages of pregnancy, another model of β-cell hyperplasia (Figure 40).

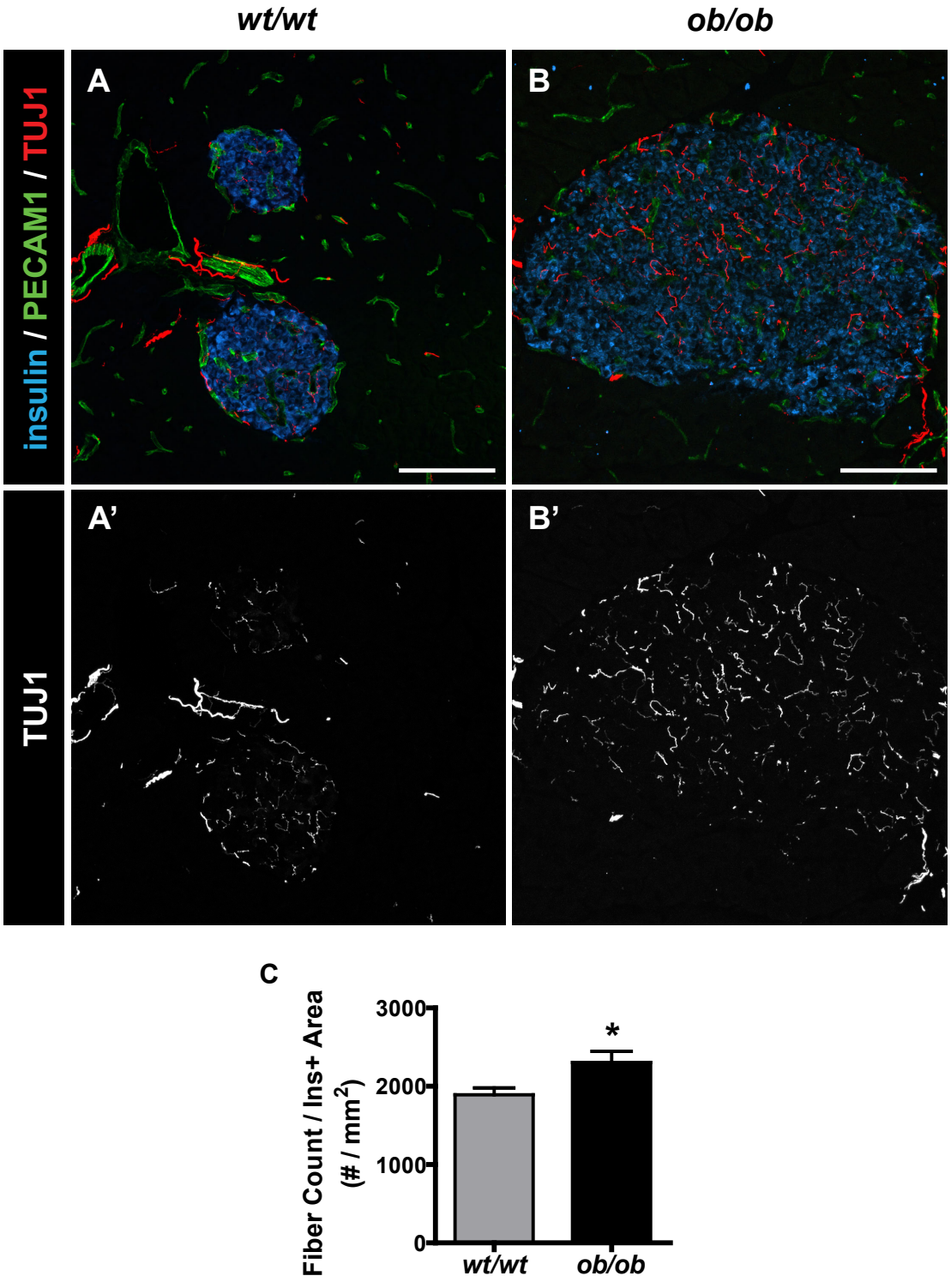

Figure 37. Islet innervation is enhanced in *ob/ob* mice. A-B. Representative islets immunolabeled for insulin (blue), PECAM1 (green), and TUJ1 (red/grayscale). **C**. Quantification of islet TUJ1+ nerve fiber density. *$P < 0.05$. Scale bars are 100 μm.

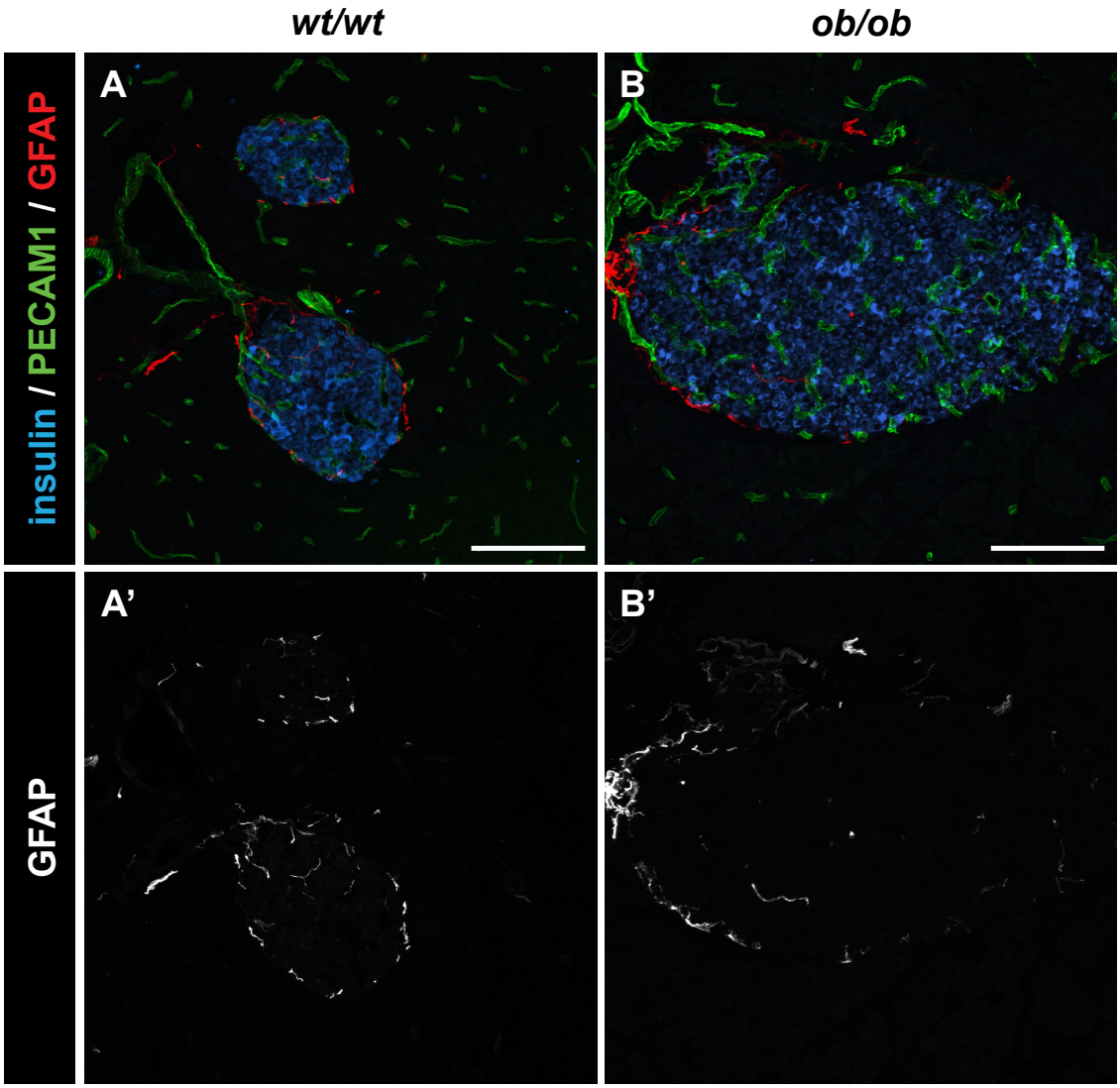

Figure 38. Peri-islet Schwann cells are unchanged in *ob/ob* mice. A-B. Representative islets immunolabeled for insulin (blue), PECAM1 (green), and GFAP (red/grayscale). Scale bars are 100 μm.

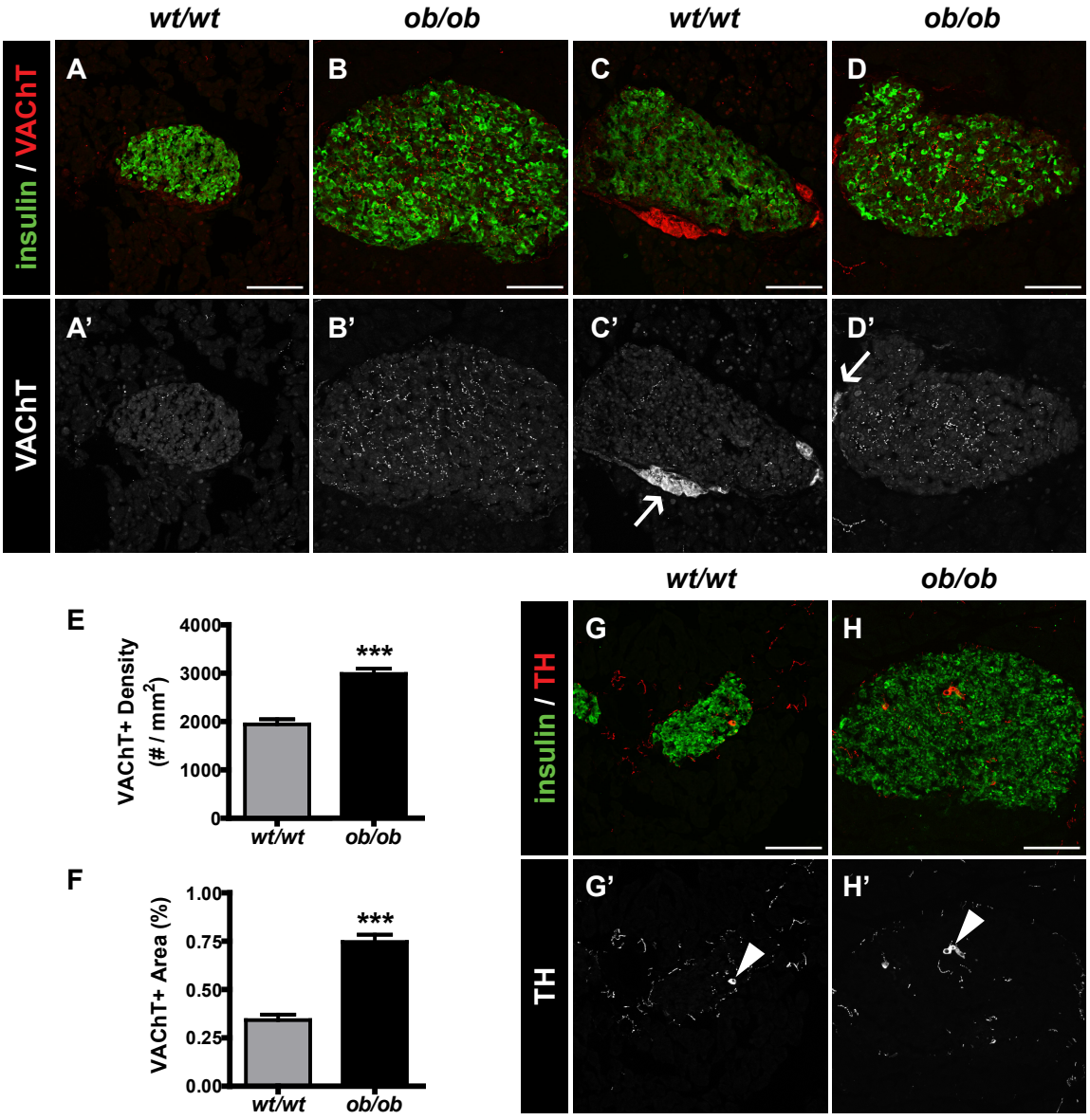

Figure 39. Islet parasympathetic, but not sympathetic, innervation is enhanced in *ob/ob* mice. A-D. Representative islets immunolabeled for insulin (green) and the vesicular acetylcholine transporter (VAChT; red/grayscale). Arrows in **C** and **D** denote neuroinsular complexes. **E.** Quantification of islet VAChT+ varicosity density. **F**. Quantification of islet VAChT+ area. **G-H**. Representative islets immunolabeled for insulin (green) and tyrosine hydroxylase (TH; red/grayscale). Arrowheads denote TH+ β-cells. Scale bars are 100 μm.

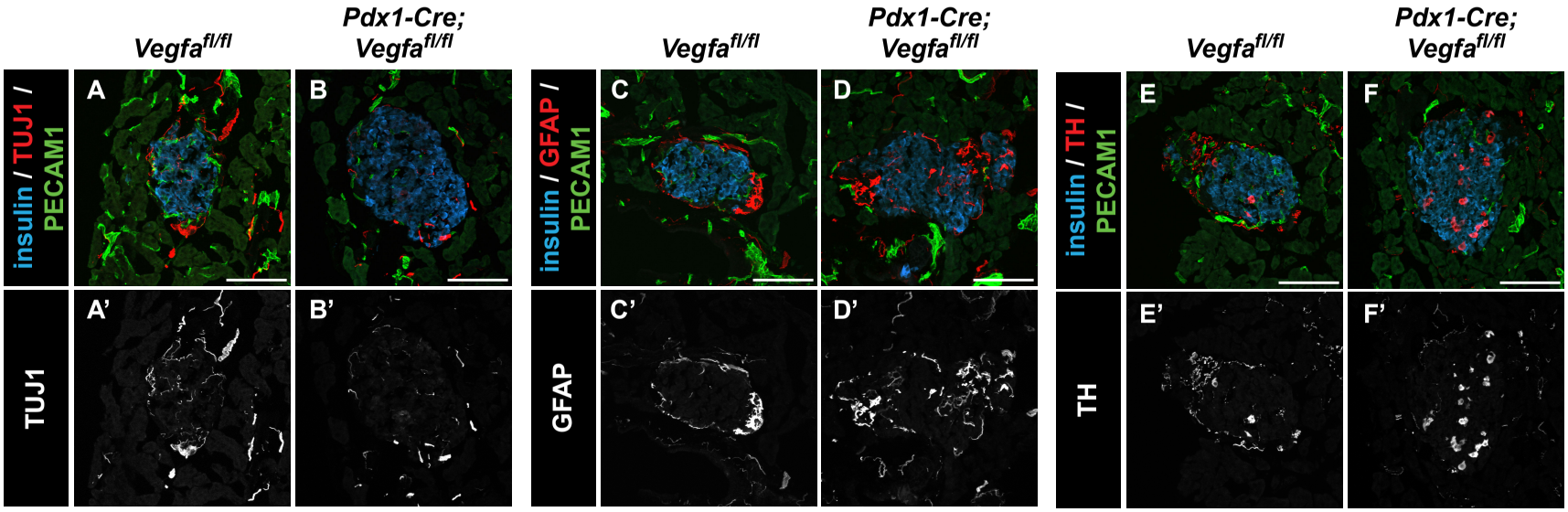

Figure 40. Islet innervation is unchanged in late pregnancy. Islet innervation in pregnant (16.5 days post coitum) *Vegfa*$^{fl/fl}$ and *Pdx1-Cre;Vegfa*$^{fl/fl}$ mice is similar to their respective non-pregnant controls. **A-B.** Representative islets immunolabeled for insulin (blue), PECAM1 (green), and TUJ1 (red/grayscale). **C-D**. Representative islets immunolabeled for insulin (blue), PECAM1 (green) and GFAP (red/grayscale). **E-F**. Representative islets immunolabeled for insulin (blue), PECAM1 (green), and tyrosine hydroxylase (TH, red/grayscale). Scale bars are 100 μm.

Discussion

Pancreatic islets are highly vascularized and richly innervated, two features that are essential for the fine regulation of blood glucose. The close physical relationship between islet nerves and blood vessels has been noted (Burris and Hebrok, 2007; Cabrera-Vasquez et al., 2009; Lindsay et al., 2006; Rodriguez-Diaz et al., 2011a; Shimada et al., 2012), but the molecular mechanisms involved in directing this relationship are incompletely defined. The data presented in this Chapter showed for the first time that (1) establishment of the intraislet vasculature by VEGF-A is critical for the postnatal maturation of islet innervation, and (2) intraislet endothelial cells provide important signals for nerves through expression of NGF.

Islet innervation follows islet vascularization during development

VEGF-A is critical in recruiting endothelial cells to the developing pancreas, allowing for endocrine cell clusters to become vascularized and exposed to blood flow as early as E13.5 (Brissova et al., 2006; Shah et al., 2011). In contrast, while the pancreas contains differentiated nerve fibers as early as E14.5, these fibers are only peripherally associated with clusters of developing endocrine cells until early postnatal life. Islet nerve fibers are not consistently found interspersed with β-cells of vascularized islets until the weaning stage, around three weeks after birth. The data presented in this Chapter support prior observations that islet innervation occurs late in islet maturation (Burris and Hebrok, 2007; Cabrera-Vasquez et al., 2009), but also demonstrate that the VEGF-A-directed formation of the intraislet vasculature is crucial for the final development of islet innervation. Islet nerves serve a modulatory role in islet function, and this relatively late

maturation of islet innervation coincides with developmental changes in the life of the mouse, such as weaning (Aguayo-Mazzucato et al., 2006). In fact, β-cells do not show mature glucose-stimulated insulin secretion or normal glucose tolerance until several weeks after birth (Lavine et al., 1971). As β-cells in newborn rodents do not show adult β-cell gene expression (Aguayo-Mazzucato et al., 2011; Jermendy et al., 2011), it is possible that the maturation of islet innervation that occurs in early postnatal life plays a key role in final β-cell development. While a lack of neural crest-derived cells in the embryonic pancreas impairs endocrine cell development (Nekrep et al., 2008; Plank et al., 2011), it will be interesting to explore the precise role of nerves and Schwann cells during the postnatal maturation of the pancreas, following the development of models that will allow us to address this issue.

Intraislet vessels are crucial for islet nerve pathfinding during development

While neurovascular alignment is a common theme among tissues, multiple mechanisms may be used to achieve this arrangement. These data show that the initialization of pancreatic innervation and the maturation of islet innervation occur by distinct processes that are differentially dependent on VEGF-A and vascularization. Neural crest-derived cells arrive in the embryonic pancreas and associate with islet clusters independent of VEGF-A signaling, in part recruited by pancreas-derived netrin signaling (Jiang et al., 2003). Later in development, differentiated nerves fail to penetrate the islet without an established, VEGF-A-directed intraislet vascular plexus. This VEGF-A requirement appears to be indirect, because pancreatic neural crest-derived cells

did not express the VEGF-A receptors VEGFR2 or NRP1 in during the postnatal maturation of islet innervation.

The requirement for vessels in the final maturation of islet innervation is similar to the avian enteric nervous system, in which the experimental disruption of gut endothelial cells prevented the migration of undifferentiated neural crest cells and impaired formation of the enteric nervous system (Nagy et al., 2009). In that study, it was found that signaling through β1 integrin, a receptor for ECM components, was crucial for the interaction between neural crest cells and endothelial cells. This interaction is likely paralleled in islet development, in which endothelial cells form the basement membrane (Nikolova et al., 2006). Data obtained from RNA sequencing of hypervascularized, hyperinnervated islets demonstrated an increase in several components of the ECM, including collagen IV α1, collagen IV α2, laminin-411, and fibronectin 1. In this way, islet innervation may require a mature intraislet vascular network to function as a scaffold for neurite penetration into the islet.

Whether vessels themselves provide the predominant signals that recruit neurites during normal islet development remains unclear. The incomplete alignment of capillaries and nerve endings in adult islets suggests that β-cells also provide important signals to mediate the final development of islet innervation. Both endocrine and endothelial cells express NGF during development (Cabrera-Vasquez et al., 2009). In addition, β-cells are more efficient than non-β endocrine cells in promoting reinnervation of transplanted islet cell grafts (Myrsén et al., 1996). Here, two different models of β-cell hyperplasia were used to determine whether more β-cells enhanced islet innervation. During late-stage pregnancy, a short-term model of β-cell hyperplasia, no changes were

evident in innervation. However, islet innervation was enhanced in *ob/ob* mice, which display dramatic β-cell hyperplasia in the setting of long-term insulin resistance. Therefore, the ability of β-cells to signal to nerve endings appears to depend on specific circumstances.

In contrast to the lack of expression of VEGF receptors in neural crest-derived cells of the postnatal islet, NRP1 expression was observed in some YFP+ neural crest-derived cells at E16.5. While NRP1 interacts with VEGFR2 to mediate VEGF-A signaling in endothelial cells, NRP1 also interacts with plexin receptors that bind axonal guidance molecules in the semaphorin family (Gu et al., 2003; Schwarz et al., 2009). Because these NRP1+ neural crest-derived cells did not coexpress VEGFR2, it is possible that they are receiving guidance signals from semaphorins instead of VEGF-A; however, VEGF-A-to-NRP1 signaling may help mediate neuron survival, as it does in the hypothalamus (Cariboni et al., 2011). The potential role of semaphorins in pancreas development remains to be determined.

Intraislet vessels are neurotrophic in mature islets

A variety of blood vessel-derived factors are implicated in signaling to nerves. During development, endothelial cells express BDNF and BMPs 2, 4, and 7, which mediate neuronal differentiation (Lammert et al., 2003a). Additionally, there are multiple factors involved in directing the autonomic innervation of vessels that may also be candidates for mediating neurite growth in islets, such as HGF, GDNF, artemin, neurotrophin 3, NGF, and endothelin 3 (Storkebaum and Carmeliet, 2011).

Here, β-cell-specific VEGF-A overexpression led to hypervascularization followed by hyperinnervation of pancreatic islets, both during development and following a one-week period in the mature animal. In a model of inducible angiogenesis in the rat mesentery, neurite growth slowly followed the pattern of new vessels, resulting in neurovascular alignment down to the capillary level, though the molecular mechanisms mediating this relationship remain unclear (Stapor and Murfee, 2012). However, an examination of factors involved in nerve regeneration in skin wounds found that microvascular endothelial cells were a source of NGF (Gibran et al., 2003). To better understand what factors might mediate the hyperinnervation following VEGF-A overexpression, RNA sequencing was performed on ↑VEGF-A islet clusters isolated after one week of VEGF-A induction, when endothelial cells form the most abundant islet cell population. Only a limited number of neurotrophic factors were upregulated. Further quantitative RT-PCR analysis of isolated islets confirmed upregulation of NGF, a factor known to be important in islet physiology. One recent study showed that pro-NGF was expressed by islet endothelial cells to help direct sympathetic innervation during development (Cabrera-Vasquez et al., 2009). Additionally, overexpression of NGF by β-cells led to sympathetic hyperinnervation of the islet (Edwards et al., 1989). These data suggest that intraislet endothelial cells are important in directing islet innervation through production of NGF.

β-cells in hypoinnervated islets show neuro-islet plasticity

The significance of tyrosine hydroxylase (TH) expression by β-cells remains unclear. The presence of occasional TH+ β-cells was documented in both the endogenous

pancreas (Iturriza and Thibault, 1993; Karlsson et al., 1997; Lindsay et al., 2006) and in transplanted islets (Korsgren et al., 1992; Persson-Sjögren et al., 1998; Persson-Sjögren et al., 2002; Persson-Sjögren et al., 2001a). TH expression in β-cells has been proposed to be a marker of endocrine precursor cells during early pancreas development (Alpert et al., 1988; Teitelman and Lee, 1987; Teitelman et al., 1993), a marker of post-proliferative β-cells on the path to senescence (Teitelman et al., 1988), or an indicator of synthesis of endogenous islet catecholamines (Borelli and Gagliardino, 2001; Borelli et al., 2003). These data do not support the hypothesis that TH+ β-cells are post-proliferative, because there was no increase in TH+ β-cells in islets in pregnant mice or in leptin-deficient *ob/ob* mice. It is possible that the dramatic increase in the number of TH+ β-cells in VEGF-A-deficient pancreata marks an increased number of senescent cells in these islets, in agreement with the >50% reduction in β-cell proliferation observed in these mice at P1 and adult stages (Reinert and Brissova et al., manuscript in preparation). However, no change was observed in senescence-associated β-galactosidase staining. The number of TH+ β-cells in ↓VEGF-A islets begins to increase postnatally, when islet innervation should be reaching its mature state. Thus, another possibility is that these hypoinnervated, hypovascularized islets detect a lack of neuronal input and some β-cells are taking on the role of catecholamine synthesis in compensation. Normal β-cells are known to express several neuronal markers, including glutamic acid decarboxylase (GAD) and several neurotrophin receptors (Atouf et al., 1997; Scharfmann, 1997), and have been proposed to function like neurons (Fujita and Kobayashi, 1979; reviewed in Arntfield and van der Kooy, 2011). Furthermore, human α-cells express VAChT and produce acetylcholine that functions as a paracrine signal to enhance islet hormone secretion (Rodriguez-Diaz et al.,

2011b). Therefore, TH expression in endocrine cells may be an indicator of neuro-islet plasticity, similar to other rodent models of diabetes in which endocrine cells assume expression of neurotransmitters in attempt to normalize glucose homeostasis (Ahrén et al., 2006).

Peri-islet Schwann cells sense islet injury following a disruption in islet morphology

The precise role of peri-islet Schwann cells (pScs) and the significance of their localization at the endocrine/exocrine interface of the pancreas are unknown. The redistribution of pScs to islet centers observed in VEGF-A-deficient islets most closely resembles the reactive gliosis observed in injured islets of mice treated with streptozotocin (STZ; Teitelman et al., 1998). In this model, the reactive glial cells expressed NGF and endocrine cells increased expression of the NGF receptor TrkA. Following the STZ injury, recovered islets with regenerated β-cells displayed a normal, peri-islet morphology of glial cells (Teitelman et al., 1998). These data suggested that pScs detect a disruption in islet morphology and/or function and may aid in the regeneration process. In contrast to the transient gliosis observed in the STZ model, VEGF-A-deficient islets demonstrate gliosis well into adulthood, suggesting that a persistent, as-yet undefined signal triggers a reaction in pScs that may serve to promote nerve regeneration. However, the fact that VEGF-deficient islets contained fewer nerves throughout life emphasizes the importance of the vascular scaffold for nerve penetration into islets.

Islet parasympathetic innervation is enhanced in the setting of insulin resistance

The autonomic nervous system plays critical roles in regulating energy homeostasis (Lustig, 2003; Marino et al., 2011) and in determining blood vessel tone and blood pressure (Storkebaum and Carmeliet, 2011). The increased density of cholinergic nerves observed in *ob/ob* islets is consistent with multiple studies demonstrating the importance of the parasympathetic nervous system in mediating the increased insulin secretion and islet blood flow in obese mice and rats. For example, administration of the cholinergic signaling antagonist methylatropine induced a dramatic and sustained reduction in plasma insulin levels in *ob/ob* mice, compared to the slight, brief reduction in lean controls, suggesting that *ob/ob* mice have an enhanced cholinergic tone (Ahrén and Lundquist, 1982). Similarly, perifused pancreas from five-day-old preobese Zucker Diabetic Fatty (ZDF) rats, which are homozygous for a mutation in the leptin receptor, showed a greater enhancement in glucose-stimulated insulin secretion in the presence of ACh but not arginine (Atef et al., 1991). While parasympathetic innervation is a critical component of the hyperinsulinemia observed in these rodent models of obesity, parasympathetic nerves are also involved in increasing islet blood flow. Rats with either genetic (ZDF) or surgically induced (ventromedial hypothalamus lesioning) obesity show increased islet blood flow compared to their respective controls, and this effect is reversed by vagotomy (Atef et al., 1992). The parasympathetic nervous system is also important in relaying the message to selectively increase islet blood flow when the brain or gut detects hyperglycemia. When glucose is infused to increase blood glucose levels specifically in the brain (without inducing peripheral hyperglycemia), signals from the central nervous system are transmitted through the vagus nerves to enhance islet blood

flow (Jansson and Hellerström, 1986). Furthermore, rats previously exposed to a period of continuous hyperglycemia (via a 48-hour glucose infusion) demonstrate a prolonged heightened sensitivity to glucose, through enhanced insulin secretion and increased islet blood flow; this "memory" effect is also dependent on intact vagal signaling (Atef et al., 1997). Additionally, glucose infusion directly into the duodenum triggers a vagal relay to induce insulin secretion and enhance islet blood flow (Carlsson et al., 1999). In all, these data indicate that parasympathetic innervation is enhanced in *ob/ob* islets to augment insulin secretion and promote increased blood flow (see model in Figure 41).

Model of pancreatic islet development

The data presented here support a model in which VEGF-A and its patterning of islet vascularization are critical for the final maturation of islet innervation (Figure 42). Endothelial cells are required for induction of the pancreatic buds starting at E8.5 (Lammert et al., 2001), and neural crest-derived cells arrive in the pancreatic epithelium around E10.0 (Plank et al., 2011). By E13.5, VEGF-A-expressing endocrine cells have recruited endothelial cells to form the early islet vascular plexus and provide blood flow (Brissova et al., 2006). Differentiated nerves and glia associate with developing islet clusters between E13.5 and E15.5 (Plank et al., 2011), independent of VEGF-A expression and islet vascularization, but remain localized to the islet periphery (Burris and Hebrok, 2007; Nekrep et al., 2008; Plank et al., 2011; Shimada et al., 2012). Postnatally, endocrine cell- and endothelial cell-derived factors (such as NGF) signal to nerve fibers to follow capillaries into the islet core. Islet innervation reaches its mature

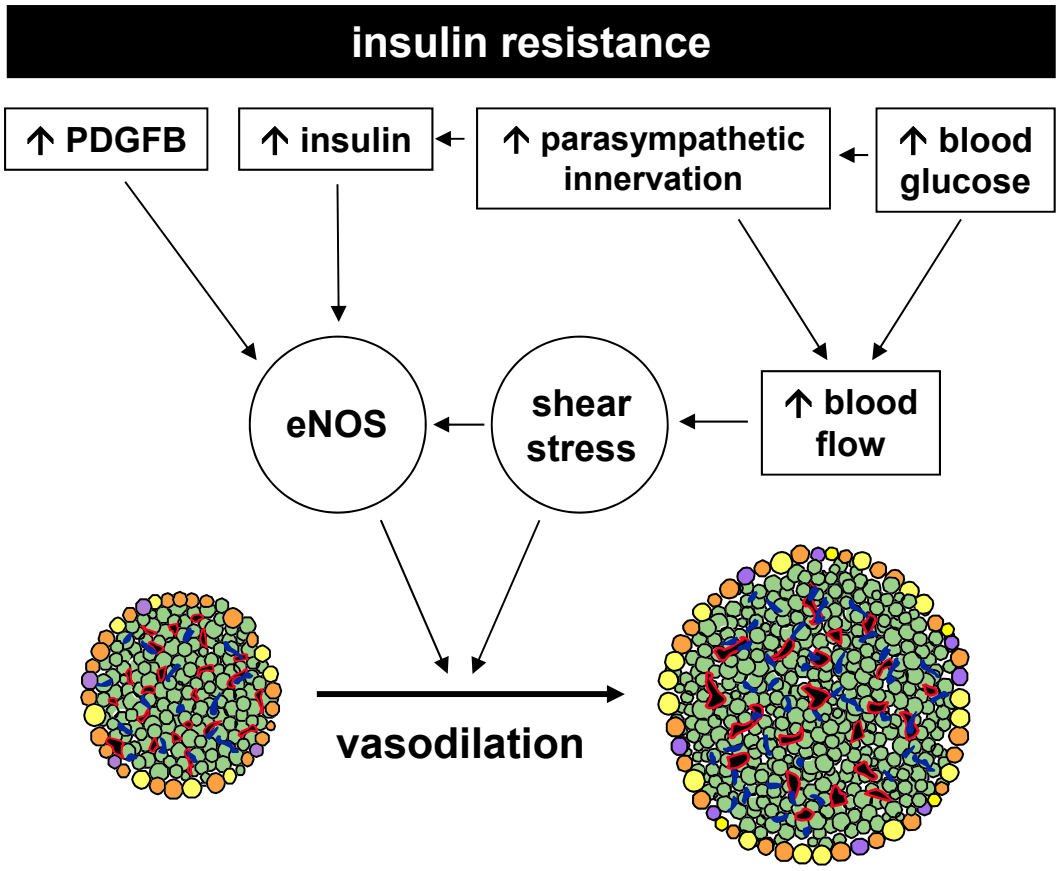

Figure 41. Summary of changes in pancreatic islet vascularization and innervation in the *ob/ob* mouse. Enhanced parasympathetic innervation contributes to insulin hypersecretion, increased blood flow, and vasodilation in hyperplastic islets of *ob/ob* mice. Model refers to data from Dai et al. (manuscript in preparation).

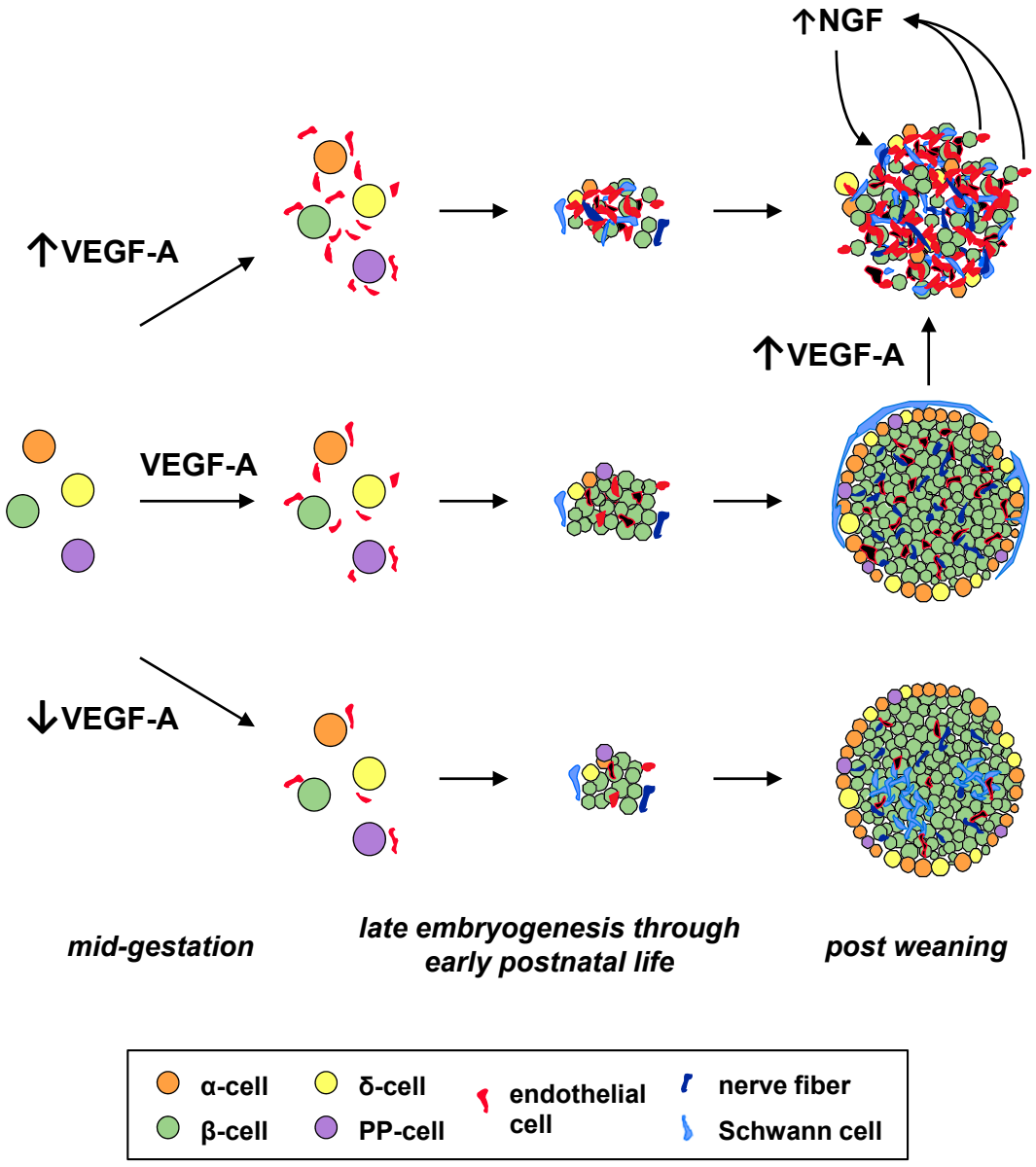

Figure 42. Model of pancreatic islet development. In the normal pancreas, islet-derived VEGF-A recruits endothelial cells that form the intraislet capillary plexus during embryogenesis. Formation of this plexus is required for islet innervation to fully develop, as VEGF-A-deficient islets are both hypovascularized and hypoinnervated. In contrast, VEGF-A excess leads to islet hypervascularization and hyperinnervation, in part through enhanced expression of nerve growth factor (NGF). From Reinert et al. (manuscript submitted).

state around the time of weaning, three weeks after birth, when nerve fibers and capillaries are intermingled with endocrine cells, and Schwann cells localize to the islet periphery. In the VEGF-A-deficient pancreas, the impaired recruitment of endothelial cells results in hypovascularized islets. While neural crest-derived cells do associate with developing endocrine cell clusters, nerve fibers fail to penetrate the islet core during postnatal development. Instead, Schwann cells, normally localized to the islet periphery, are redistributed to the islet core in a state that resembles reactive gliosis. In contrast, when VEGF-A expression by β-cells is increased, a dramatic expansion of endothelial cells leads to rapid islet hypervascularization. These highly vascularized islet clusters become densely innervated yet also show altered Schwann cell morphology.

Several groups have noted differences in endocrine cell arrangements of human and mouse islets (Brissova et al., 2005; Cabrera et al., 2006; Steiner et al., 2010), but only recently has the morphology of human islet innervation been explored (Rodriguez-Diaz et al., 2011a). While human islets display fewer nerve fibers than mouse islets, those nerve fibers appear to be more closely associated with intraislet capillaries than with endocrine cells themselves. In fact, it was suggested that this arrangement allows islet neurotransmitters to signal first to arterial smooth muscle cells, thus allowing changes in blood flow to regulate islet function. Alternatively, islet neurotransmitters may be released into the bloodstream before they reach endocrine cells (Rodriguez-Diaz et al., 2011a). Because the close physical relationship between the intraislet vascular and nervous systems is maintained in human islets, it is promising that the vascular-mediated nerve patterning observed in mouse islets is a mechanism conserved in humans.

In conclusion, these data show that capillaries and nerve fibers are intimately related within the pancreatic islet, and that islet innervation is highly dependent on islet vascularization. Although VEGF-A does not signal directly to islet neural elements, perturbations in islet VEGF-A expression induce dramatic changes in islet vascularization, which has a profound impact on the ingrowth of islet nerve fibers, the structural arrangement of peri-islet Schwann cells, and the expression of neuronal genes by endocrine cells. It is concluded that VEGF-A is a master coordinator of islet neurovascular development.

CHAPTER IV

INVESTIGATING THE ROLE OF VEGF-A IN THE MAINTENANCE OF ISLET VASCULARIZATION

Some data in this Chapter have been published (Figure 54; Wicksteed et al., 2010).

Introduction

Pancreatic islets are intimately connected to the vasculature, and disruption of this relationship has been hypothesized to contribute to diabetes (Lammert, 2008). Furthermore, it has been proposed that the decreased vessel density (Mattsson et al., 2002) and oxygen tension (Carlsson et al., 2001; Carlsson et al., 2000) in islet grafts is a major reason for islet transplantation failure. Therefore, a basic understanding of the role of the intraislet vasculature in islet formation and function may lead to improved therapies for diabetes.

In order to understand the mechanisms directing normal islet vascularization, much work has focused on the role of islet-derived angiogenic factors. When VEGF-A is inactivated either in the early pancreas or in newly formed β-cells, the intraislet capillary plexus fails to become fully established, resulting in substantial defects in insulin secretion *in vivo*, glucose intolerance, and, in the case of the pancreas-wide knockout, reduced β-cell proliferation and mass (Brissova et al., 2006; Lammert et al., 2003b; Reinert and Brissova et al., manuscript in preparation). Similarly, overexpression of VEGF-A in developing pancreata (Magenheim et al., 2011) or β-cells (Cai et al., 2012) is

detrimental to endocrine cell differentiation and islet formation. Therefore, VEGF-A expression must be precisely controlled in the developing pancreas for proper islet development and function.

While existing genetic mouse models demonstrated a role for VEGF-A and endothelial cells in islet formation, the precise role of VEGF-A in mature islets is unclear (Figure 43). The prior approaches inactivated VEGF-A in embryogenesis, thus making it difficult to identify which phenotypes in adult mice were the result of developmental defects in hypovascularized islets and which reflected the role of VEGF-A and endothelial cells in mature islets. In an alternate approach, studies in which VEGF signaling inhibitors were administered to adult mice demonstrated the importance of VEGF-A in maintaining the density and permeability of the intraislet vasculature, but, surprisingly, showed that interrupting global VEGF-A signaling improved glucose tolerance (Kamba et al., 2006). However, the effects of VEGF inhibitors on the vasculature of multiple tissues again prevented a full understanding of the role of endothelial cells in established islets.

Here, a tamoxifen-inducible Cre-*loxP* mouse model was used to genetically delete *Vegfa* in β-cells of adult mice and precisely define the role of VEGF-A and intraislet endothelial cells in the maintenance of islet morphology and function in maturity. It was found that mature pancreatic β-cells could tolerate a significant and prolonged reduction in intraislet capillary density and still maintain relatively normal function. By comparison, inactivation of VEGF-A in early pancreas development resulted in hypovascularized islets with a sustained reduction in β-cell proliferation and mass (Reinert and Brissova et al., manuscript in preparation). These data show that intraislet endothelial cells play a

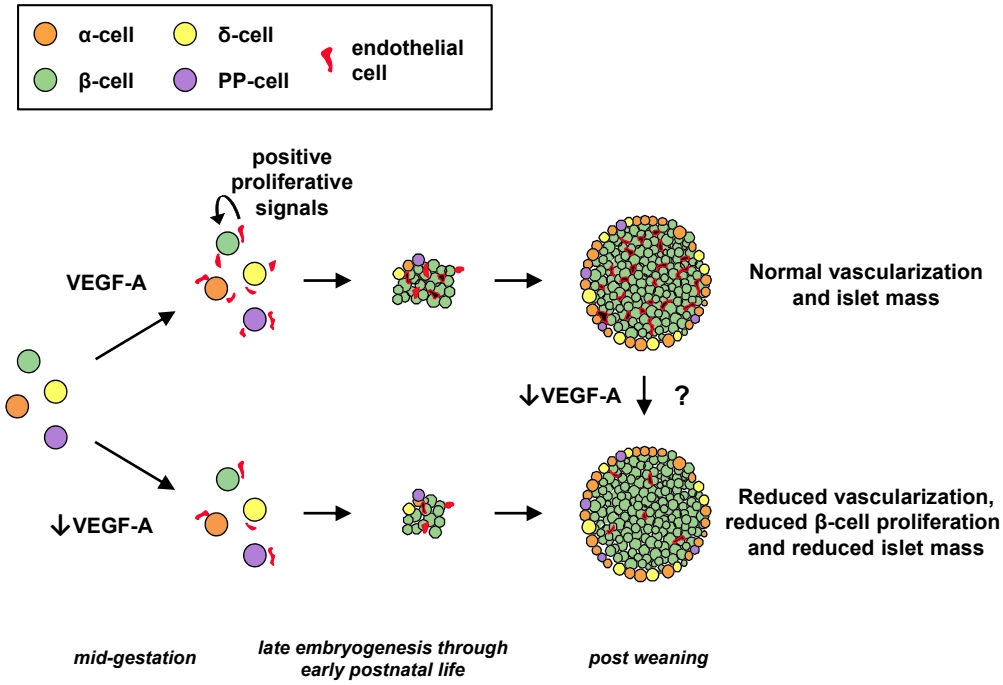

Figure 43. Defining the role of VEGF-A in mature islets. Current evidence shows that islet-derived VEGF-A and its effects on islet vascularization are crucial for β-cell proliferation and islet development (Reinert and Brissova et al., manuscript in preparation). However, it is unknown whether inactivation of VEGF-A specifically in mature islets will have similar effects on islet vascularization and function. This is the basis for the studies performed in Chapter IV.

lesser role in maintaining mature islets than in directing islet development.

Results

Evaluating an inducible Cre-loxP model to inactivate Vegfa in β-cells of adult mice

To reduce VEGF-A production in mature islets, a tamoxifen (Tm)-inducible Cre-*loxP* mouse model was used. *Vegfa*$^{fl/fl}$ mice were crossed with *Pdx1*^{PB}-*CreER*^{Tm} mice, in which a Tm-inducible form of Cre recombinase is expressed in β-cells (and in a small subset of non-β endocrine cells) of the islet (Zhang et al., 2005). First, the Tm dose that effectively reduced VEGF-A expression with minimal toxicity was determined. While a 3 x 8 mg Tm dose was required for widespread recombination of the *R26-lacZ* reporter allele in β-cells, and also induced effective recombination of the conditional *Vegfa* allele (Reinert et al., 2012), much lower Tm doses were able to inactivate VEGF-A production in β-cells of *Pdx1*^{PB}-*CreER*^{Tm};*Vegfa*$^{fl/fl}$ mice. Adult mice were injected with three doses of 2 mg, 1 mg, or 0.1 mg Tm, and sacrificed one week after the final Tm injection to assess islet VEGF-A production over 48 hours in culture. Control islets from vehicle-treated *Pdx1*^{PB}-*CreER*^{Tm};*Vegfa*$^{fl/fl}$ mice and from Tm-treated *Vegfa*$^{fl/fl}$ mice showed a similar amount of VEGF-A release into the culture media, as quantified by ELISA (Figure 44B). In contrast, Tm-treated *Pdx1*^{PB}-*CreER*^{Tm};*Vegfa*$^{fl/fl}$ mice showed significantly reduced VEGF-A production, in a dose-dependent manner (Figure 44B). These studies were continued using the 3 x 1 mg Tm dose, which resulted in a 91.4% reduction in islet VEGF-A secretion *in vitro*.

The extent of islet VEGF-A inactivation was also assessed using immunohistochemistry. Compared to pancreatic acinar tissue, islet endocrine cells from adult vehicle-treated and Tm-treated *Vegfa*$^{fl/fl}$ mice and from vehicle-treated

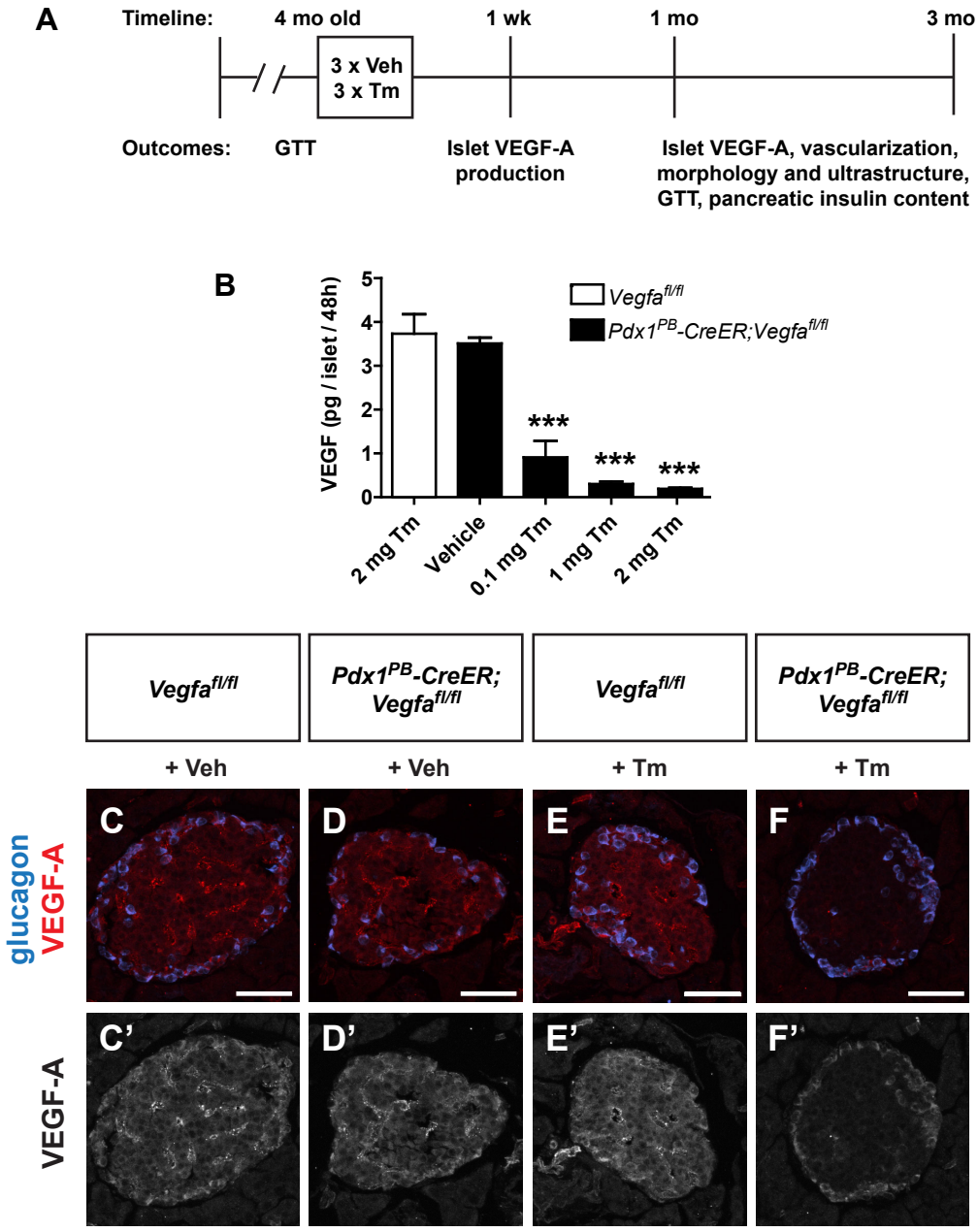

Figure 44. Tamoxifen-induced inactivation of VEGF-A in adult islets. A. Four month-old *Vegfa*$^{fl/fl}$ and *Pdx1*^{PB}*-CreER;Vegfa*$^{fl/fl}$ mice were treated with three injections of tamoxifen (Tm) or corn oil vehicle (Veh) and evaluated for islet VEGF-A production, vascularization, and function. **B.** VEGF-A secretion from cultured islets was analyzed using an ELISA one week after treating mice with Tm or Veh. ***$P < 0.001$ vs. Tm-treated *Vegfa*$^{fl/fl}$ islets and vs. vehicle-treated *Pdx1*^{PB}*-CreER;Vegfa*$^{fl/fl}$ islets; $n = 3$ per group. **C-F**. Islet VEGF-A expression was evaluated using immunohistochemistry three months after 3 x 1 mg Tm or Veh treatment. VEGF-A, red/grayscale; glucagon, blue. Scale bars are 50 μm**.**

Pdx1^{PB}-*CreER*^{Tm};*Vegfa*$^{fl/fl}$ mice express high levels of VEGF-A (Figure 44C-E). Reduced VEGF-A immunoreactivity was observed in β-cells from adult *Pdx1*^{PB}-*CreER*^{Tm};*Vegfa*$^{fl/fl}$ mice both one and three months after Tm treatment, though VEGF-A was still expressed by α-cells at the islet periphery (Figure 44F and data not shown).

The timeline of experiments performed to evaluate islet morphology and function following VEGF-A inactivation is shown in Figure 44A.

Inactivation of Vegfa in mature islets reduces islet vessel density, vessel size, and endothelial cell fenestrations

To better understand the role of VEGF-A on the mature islet vasculature, the morphology and gene expression of intraislet capillaries were examined in Tm-treated *Vegfa*$^{fl/fl}$ and *Pdx1*^{PB}-*CreER*^{Tm};*Vegfa*$^{fl/fl}$ mice. Intraislet capillaries were labeled by immunohistochemistry using an antibody to the endothelial cell marker PECAM1 (Figure 45A-D), and islet vessel density and size was evaluated using morphometric analysis. Three months after Tm-induced VEGF-A inactivation, the islet vessel density was reduced 53.4% in Tm-treated *Pdx1*^{PB}-*CreER*^{Tm};*Vegfa*$^{fl/fl}$ mice, as compared to Tm-treated *Vegfa*$^{fl/fl}$ mice and vehicle-treated controls (Figure 45E). Furthermore, islet vessel size/branching was also reduced 44.5% in *Pdx1*^{PB}-*CreER*^{Tm};*Vegfa*$^{fl/fl}$ mice three months after Tm treatment, as measured by the area per islet vessel (Figure 45F). Similar changes in the intraislet vasculature were also observed one month following Tm treatment (data not shown).

Next, expression of the angiogenic factors VEGF-A and VEGF-B and their receptor VEGFR2 was examined by quantitative RT-PCR. As expected, expression of

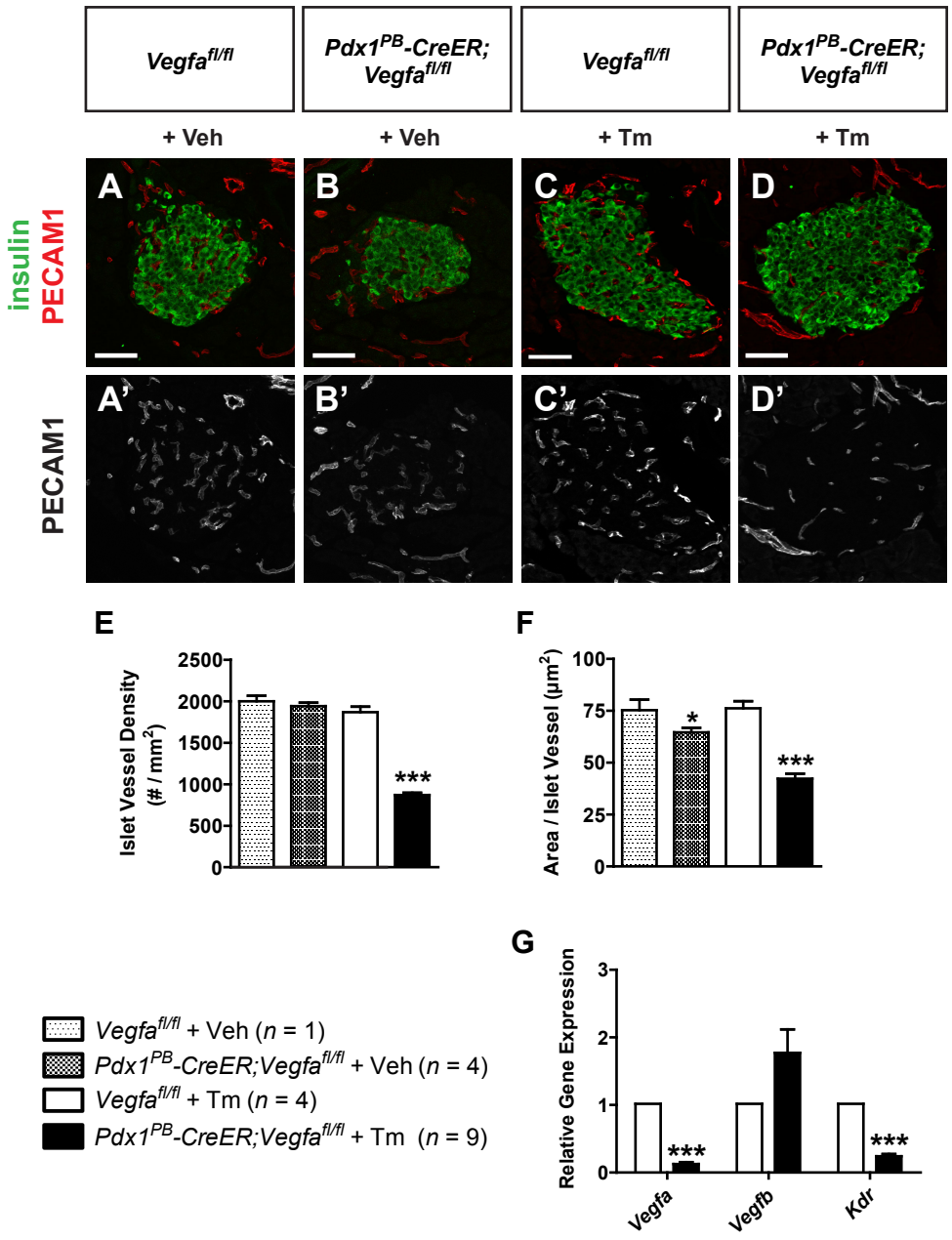

Figure 45. VEGF-A is required to maintain the intraislet vasculature in adult mice. A-D. Immunohistochemistry of *Vegfa*$^{fl/fl}$ and *Pdx1*^{PB}*-CreER;Vegfa*$^{fl/fl}$ islets following tamoxifen (Tm) or vehicle (Veh) treatment. Insulin, green; PECAM1, red/grayscale. Scale bars are 50 µm. **E-F.** Islet vessel density (**E**) and area per islet vessel (**F**) three months after Tm treatment. The number of mice evaluated in each group is listed in the legend. *$P < 0.05$, ***$P < 0.001$. Similar vascular changes were also observed one month after Tm treatment. **G**. Relative gene expression of *Vegfa*, *Vegfb*, and *Kdr* (encoding the VEGF receptor 2) in isolated islets, measured by quantitative PCR. Values are 0.126 ± 0.0275 for *Vegfa* ($n = 3$; ***$P < 0.0001$ vs. control), 1.771 ± 0.349 for *Vegfb* ($n = 3$; $P > 0.05$ vs. control), and 0.241 ± 0.0323 for *Kdr* ($n = 3$; ***$P = 0.0002$ vs. control).

Vegfa mRNA was significantly reduced in Tm-treated *Pdx1*^{PB}-*CreER*^{Tm};*Vegfa*$^{fl/fl}$ islets compared to Tm-treated *Vegfa*$^{fl/fl}$ controls (Figure 45G). In contrast, expression of *Vegfb* was unchanged following VEGF-A inactivation (Figure 45G). Tm-treated *Pdx1*^{PB}-*CreER*^{Tm};*Vegfa*$^{fl/fl}$ islets also showed a reduction in mRNA expression of the gene for the VEGF receptor 2, *Kdr*, in agreement with the reduction in endothelial cells (Figure 45G).

To evaluate whether reduced VEGF-A expression altered the permeability of intraislet capillaries, islets from *Pdx1*^{PB}-*CreER*^{Tm};*Vegfa*$^{fl/fl}$ mice and *Vegfa*$^{fl/fl}$ controls were examined by transmission electron microscopy, one month after Tm treatment. As expected, there were fewer capillaries in islets from *Pdx1*^{PB}-*CreER*^{Tm};*Vegfa*$^{fl/fl}$ mice, and most capillaries were found at the islet periphery. As described previously (Brissova et al., 2006; Lammert et al., 2003b), endothelial cell processes lining the lumen of capillaries in Tm-treated *Vegfa*$^{fl/fl}$ controls were highly fenestrated (Figure 46A-B). Surprisingly, the capillaries in Tm-treated *Pdx1*^{PB}-*CreER*^{Tm};*Vegfa*$^{fl/fl}$ mice displayed a wide range in the degree of fenestrated endothelium in capillary cross-sections. Fenestrations were readily found in capillaries of VEGF-A-deficient islets, though they were less prevalent than in *Vegfa*$^{fl/fl}$ controls (Figure 46C-F). In contrast to previous models of VEGF-A inactivation in developing islets (Brissova et al., 2006; Lammert et al., 2003b), the presence of caveolae in intraislet capillaries of *Pdx1*^{PB}-*CreER*^{Tm};*Vegfa*$^{fl/fl}$ mice was much more variable between individual capillaries, and, when present, was not as thick as in previous models.

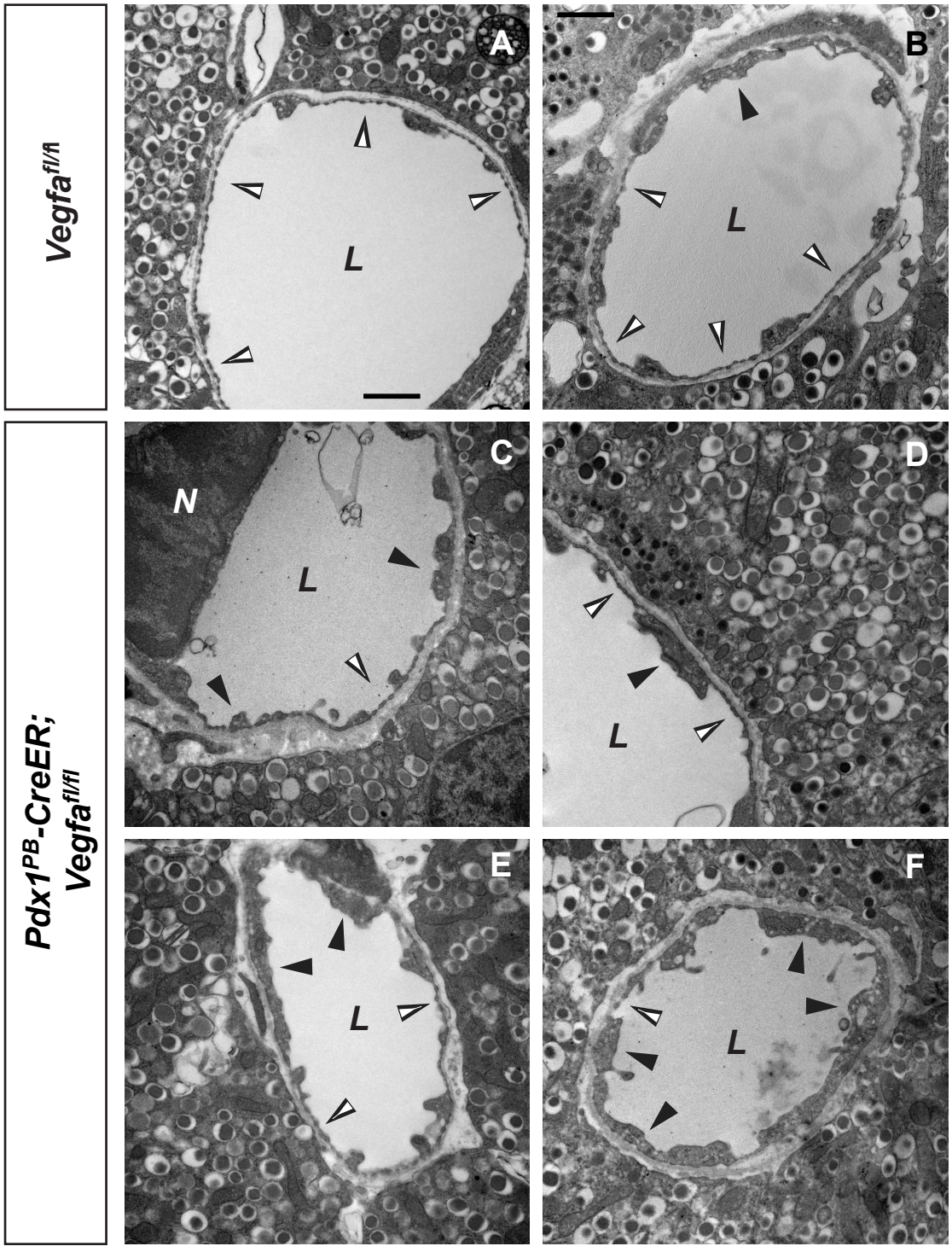

Figure 46. Inactivation of VEGF-A in adult islets has variable effects on endothelial cell fenestrations. Transmission electron micrographs of intraislet capillaries in Tm-treated *Vegfa*$^{fl/fl}$ (**A-B**) and *Pdx1*^{PB}*-CreER;Vegfa*$^{fl/fl}$ (**C-F**) mice. Images were acquired at 15000x magnification. Scale bar in **A** is 100 nm, and applies to **B-F**. *L*, capillary lumen; *N*, endothelial cell nucleus; open arrowheads denote fenestrations and closed arrowheads denote caveolae.

Mature β-cells are maintained in VEGF-A-deficient islets

A variety of studies were performed to evaluate whether a reduction in intraislet endothelial cells in adult mice would affect islet morphology. Islets in Tm-treated *Pdx1*^{PB}-*CreER*^{Tm};*Vegfa*$^{fl/fl}$ mice retained a normal arrangement of endocrine cells, with α-cells and δ-cells located at the islet periphery (Figure 47A-B). Furthermore, there was no change in the proportion of β-cells to α-cells following islet VEGF-A inactivation (Figure 47C). β-cells in Tm-treated *Pdx1*^{PB}-*CreER*^{Tm};*Vegfa*$^{fl/fl}$ mice also displayed normal nuclear expression of the transcription factors MAFA and PDX1 (Figure 47D-E), and did not show changes in expression of *Ins2*, *Mafa*, or *Pdx1* mRNA (Figure 47F). The total pancreatic insulin content was slightly increased in male Tm-treated *Pdx1*^{PB}-*CreER*^{Tm};*Vegfa*$^{fl/fl}$ mice (Figure 47G), but unchanged in was females (Figure 47H). However, both pancreatic β-cell area (Figure 47I) and total pancreatic weight (data not shown) were unchanged in Tm-treated *Pdx1*^{PB}-*CreER*^{Tm};*Vegfa*$^{fl/fl}$ mice. The ultrastructure of β-cells also was unchanged in Tm-treated *Pdx1*^{PB}-*CreER*^{Tm};*Vegfa*$^{fl/fl}$ mice, as evaluated by transmission electron microscopy. β-cells remained densely packed with insulin granules in Tm-treated *Pdx1*^{PB}-*CreER*^{Tm};*Vegfa*$^{fl/fl}$ mice and *Vegfa*$^{fl/fl}$ controls, and β-cell granules retained their characteristic halos following VEGF-A inactivation (Figure 48).

Mice with hypovascularized islets have slightly impaired glucose tolerance but normal insulin secretion

Whole-body glucose homeostasis was examined in Tm-treated mice to evaluate whether depletion of intraislet vessels affected islet function. Before Tm treatment, there was no difference in glucose tolerance between *Pdx1*^{PB}-*CreER*^{Tm};*Vegfa*$^{fl/fl}$ mice and

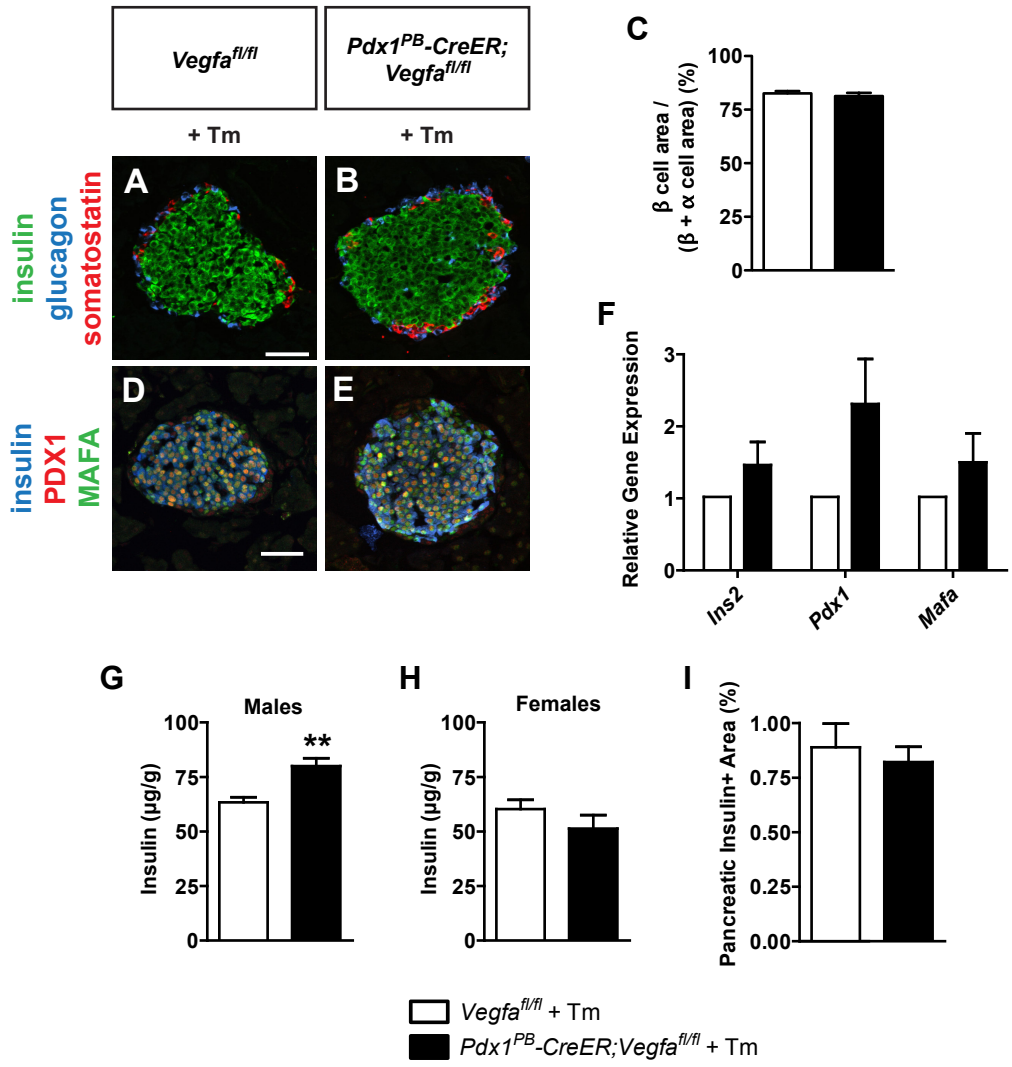

Figure 47. VEGF-A inactivation in adult islets does not impair β-cell gene expression or mass. A-B. Immunohistochemistry of islets three months after tamoxifen (Tm) treatment. Insulin, green; glucagon, blue; somatostatin, red. Scale bar in **A** is 50 µm, and applies to **B. C.** Morphometric quantification of islet β-cell area. $P > 0.05$; $n = 3$ per group. **D-E**. Immunohistochemistry of islets three months after Tm treatment. Insulin, blue; MAFA, green; PDX1, red. Scale bar in **D** is 50 µm, and applies to **E. F.** Relative gene expression of *Ins2*, *Pdx1*, and *Mafa* in islets from Tm-treated mice, evaluated by quantitative PCR. Values are 1.464 ± 0.321 for *Ins2*, 2.311 ± 0.624 for *Pdx1* and 1.502 ± 0.402 for *Mafa*. For all genes, $P > 0.05$ vs. control; $n = 3$ per group. **G.** Pancreatic insulin content in male mice. $^{**}P = 0.0092$; $n = 11$ for Tm-treated *Vegfa*$^{fl/fl}$ mice and $n = 5$ for Tm-treated *Pdx1*^{PB}*-CreER;Vegfa*$^{fl/fl}$ mice. **H.** Pancreatic insulin content in female mice. $P > 0.05$; $n = 2$ for Tm-treated *Vegfa*$^{fl/fl}$ mice and $n = 3$ for Tm-treated *Pdx1*^{PB}*-CreER; Vegfa*$^{fl/fl}$ mice. **I.** Morphometric quantification of pancreatic β-cell area. $P > 0.05$; $n = 3$ per group.

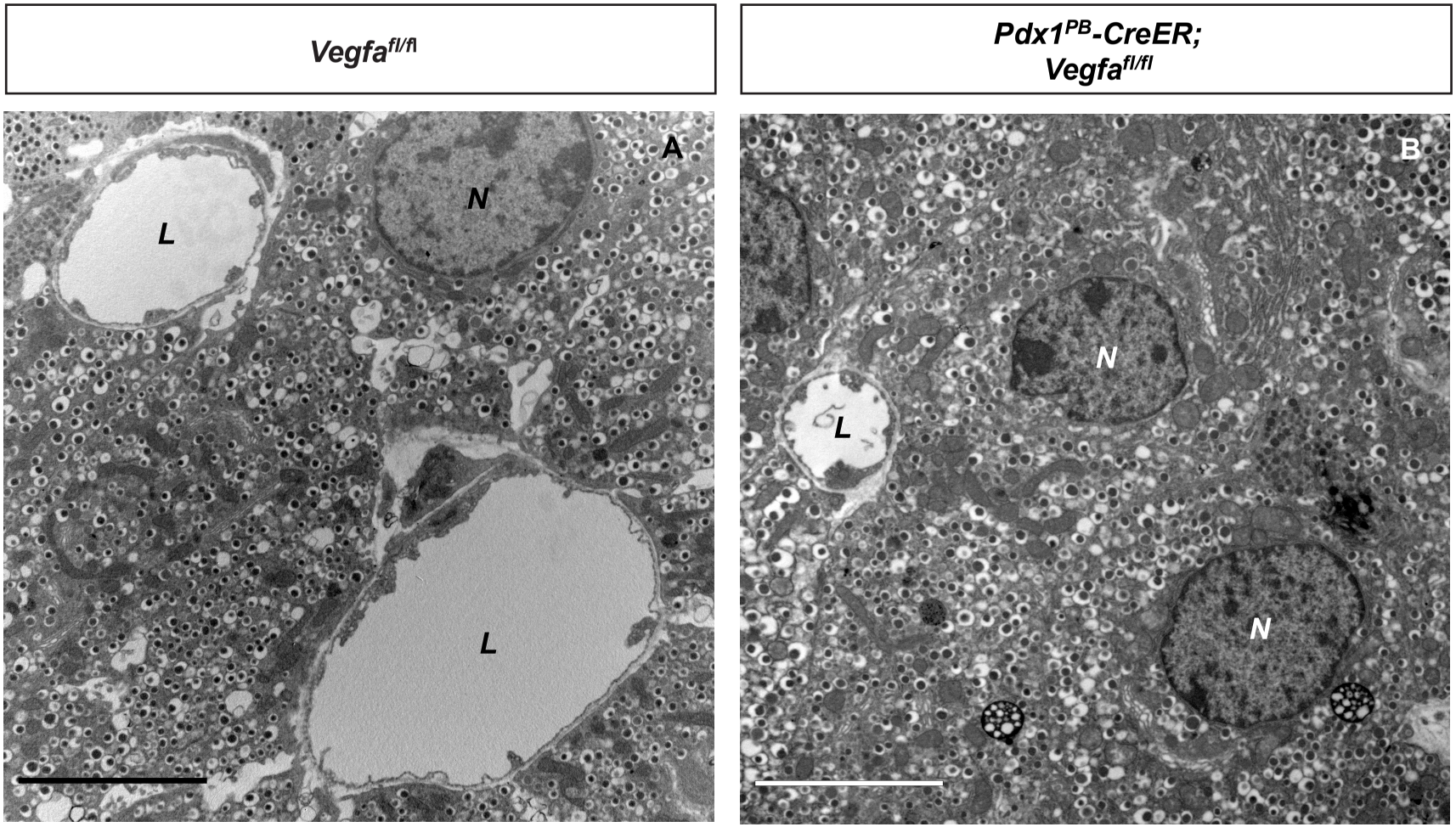

Figure 48. β-cell granulation is normal in VEGF-A-deficient islets. Transmission electron micrographs of islets from Tm-treated *Vegfa*$^{fl/fl}$ (**A**) and *Pdx1*^{PB}*-CreER;Vegfa*$^{fl/fl}$ (**B**) mice revealed normal insulin secretory granule morphology and density. Images were acquired at 5600x magnification. Scale bars are 2 μm. *L*, capillary lumen; *N*, β-cell nucleus.

Vegfa$^{fl/fl}$ controls (Figures 49A and 50A). However, Tm-treated *Pdx1*^{PB}-*CreER*^{Tm};*Vegfa*$^{fl/fl}$ males showed impaired glucose tolerance both one month and three months after VEGF-A inactivation (Figure 49B-C). This phenotype was less pronounced in female mice, and only manifested three months following VEGF-A inactivation (Figure 50B-C).

Next, an *in vitro* perifusion assay was used to determine if VEGF-A inactivation affected insulin secretion independent of blood flow. Compared to *Vegfa*$^{fl/fl}$ controls, islets from *Pdx1*^{PB}-*CreER*^{Tm};*Vegfa*$^{fl/fl}$ mice did not show altered insulin secretion at basal (5.6 mM) glucose levels, or following stimulation with 16.7 mM glucose with or without the secretagogue IBMX (Figure 51).

To determine if VEGF-A inactivation affected insulin secretion *in vivo*, hyperglycemic clamps were performed six weeks after Tm treatment to measure glucose-stimulated insulin secretion. After a six-hour fast, Tm-treated *Pdx1*^{PB}-*CreER*^{Tm};*Vegfa*$^{fl/fl}$ males showed fasting hyperglycemia compared to Tm-treated *Vegfa*$^{fl/fl}$ controls (Figure 52A), so the arterial blood glucose levels were slightly elevated in *Pdx1*^{PB}-*CreER*^{Tm};*Vegfa*$^{fl/fl}$ mice during the early part of the clamp. However, *Pdx1*^{PB}-*CreER*^{Tm};*Vegfa*$^{fl/fl}$ mice were clamped at the same blood glucose level as controls (~200 mg/dl) for the remainder of the experiment. Unexpectedly, *Pdx1*^{PB}-*CreER*^{Tm};*Vegfa*$^{fl/fl}$ mice required a lower glucose infusion rate (GIR) than *Vegfa*$^{fl/fl}$ controls to maintain hyperglycemia (Figure 52B), suggestive of insulin resistance. Tm-treated *Pdx1*^{PB}-*CreER*^{Tm};*Vegfa*$^{fl/fl}$ mice had normal fasting arterial insulin values, but showed a slight elevation in fasting arterial C-peptide, a byproduct of insulin biosynthesis (Figure 52C-D). However, there was no statistically significant difference in arterial insulin values in *Pdx1*^{PB}-*CreER*^{Tm};*Vegfa*$^{fl/fl}$ mice when compared to *Vegfa*$^{fl/fl}$ controls.

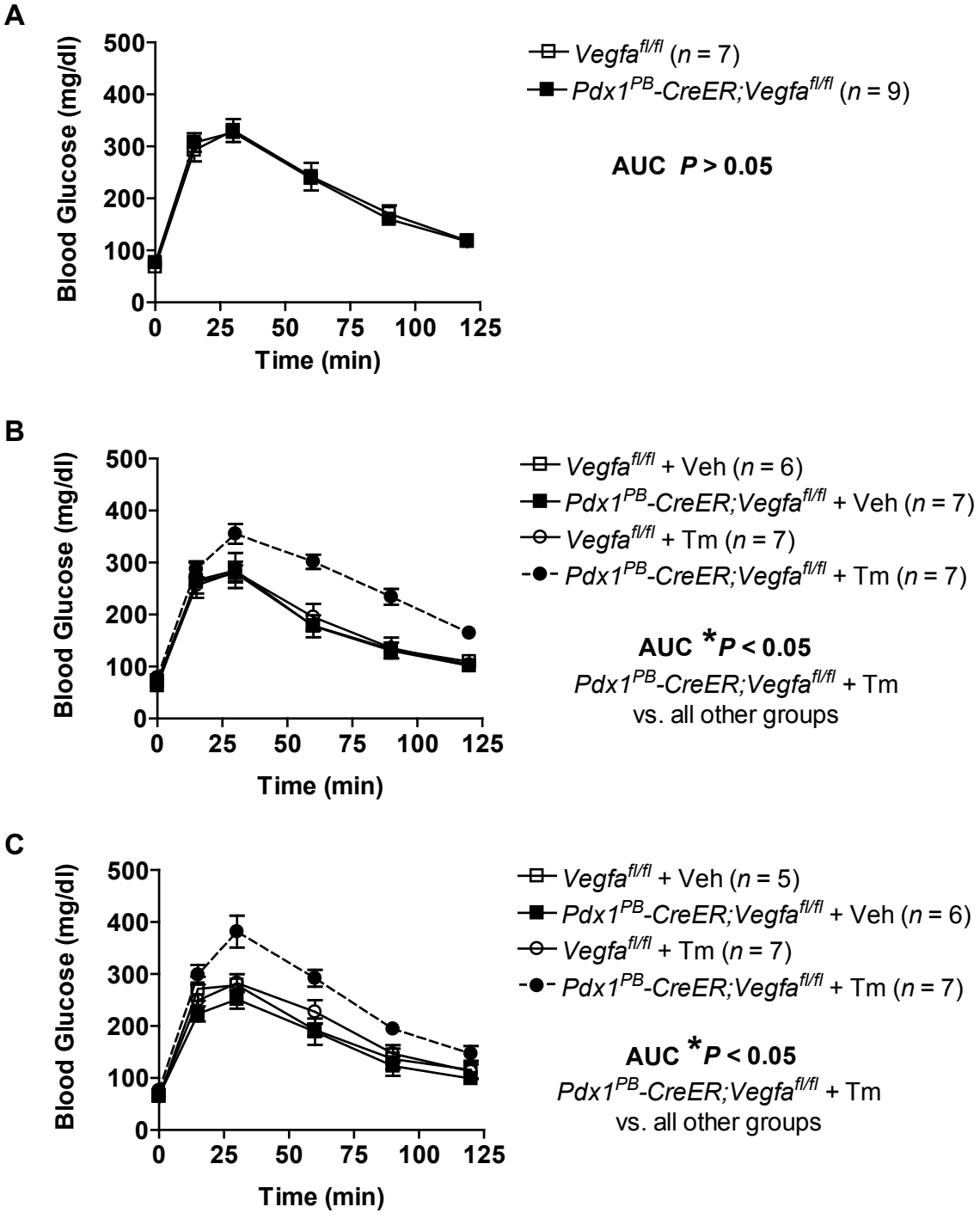

Figure 49. Islet VEGF-A inactivation results in impaired glucose tolerance. Glucose tolerance testing was performed before tamoxifen (Tm) treatment (**A**), and one month (**B**) and three months (**C**) following Tm or vehicle (Veh) treatment. Male mice were fasted for 16 hours before intraperitoneal injection of 2 mg/g glucose. Data were analyzed by one-way ANOVA of the area under the curve (AUC).

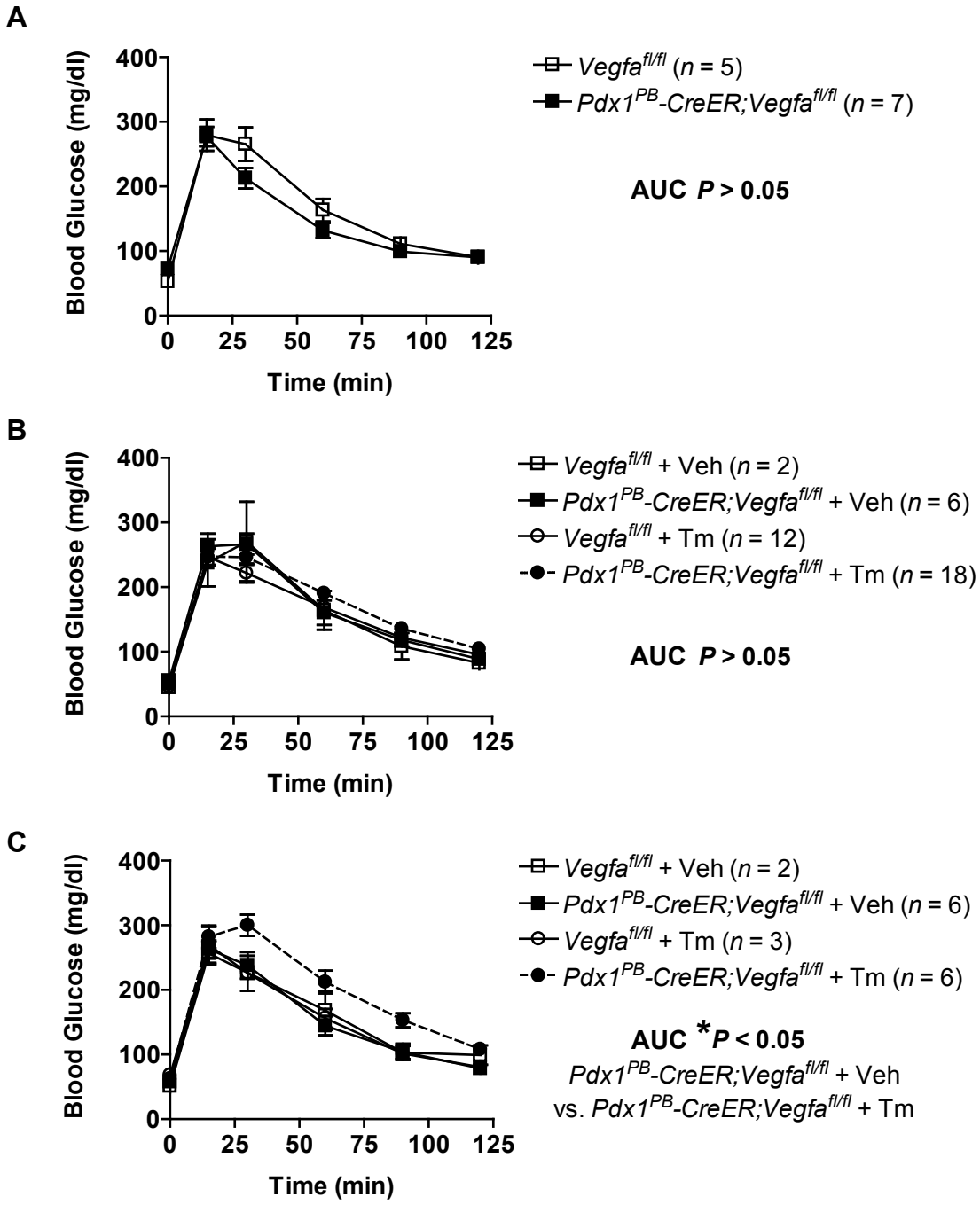

Figure 50. Impaired glucose tolerance developed more slowly in *Pdx1^{PB}-CreER; Vegfa$^{fl/fl}$* female mice. Glucose tolerance testing was performed before tamoxifen (Tm) treatment (**A**), and one month (**B**) and three months (**C**) following Tm or vehicle (Veh) treatment. Female mice were fasted for 16 hours before intraperitoneal injection of 2 mg/g glucose. Data were analyzed by one-way ANOVA of the area under the curve (AUC).

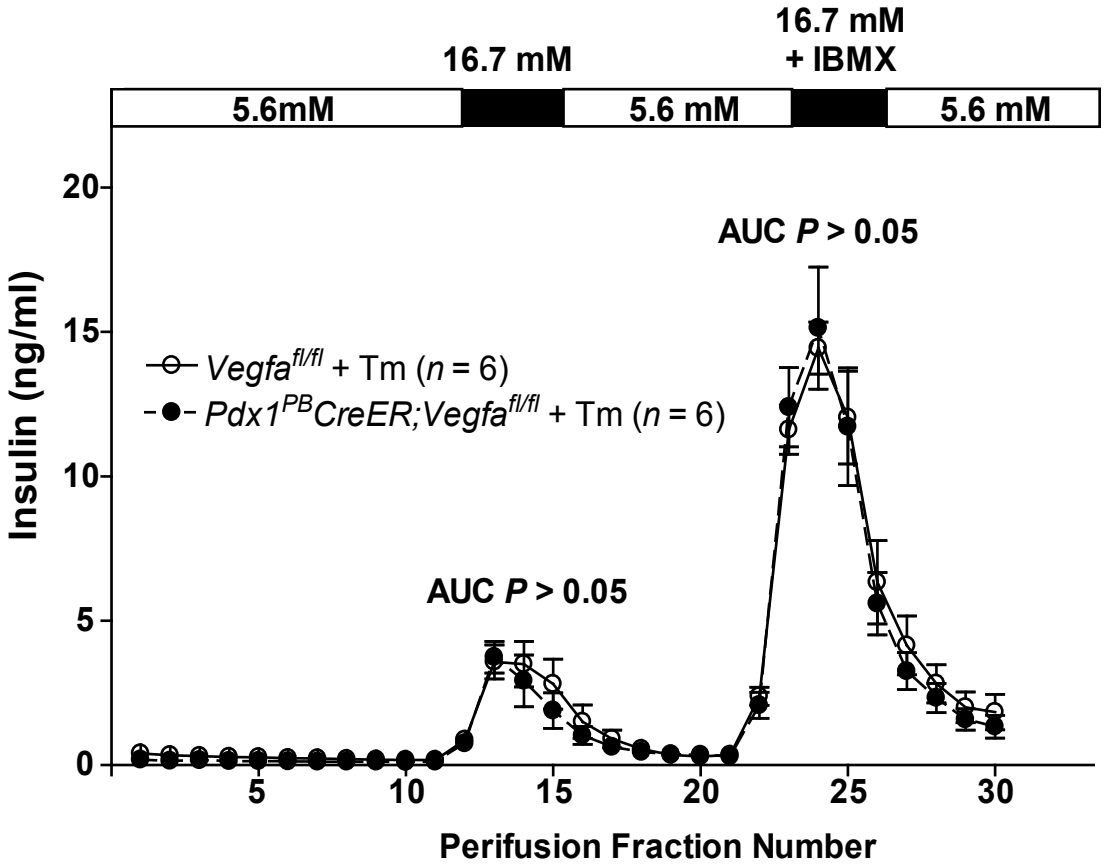

Figure 51. Hypovascularization does not affect insulin secretion *in vitro*. Perifusion of islets isolated from Tm-treated mice. Area under the curve (AUC) values for the 16.7 mM glucose stimulus are 14.32 ± 3.433 ng/ml in Tm-treated *Vegfa*$^{fl/fl}$ mice and 12.04 ± 2.963 ng/ml in Tm-treated *Pdx1*^{PB}*-CreER;Vegfa*$^{fl/fl}$ mice. Area under the curve (AUC) values for the 16.7 mM glucose + IBMX stimulus are 56.86 ± 7.179 ng/ml in Tm-treated *Vegfa*$^{fl/fl}$ mice and 54.88 ± 8.129 ng/ml in Tm-treated *Pdx1*^{PB}*-CreER;Vegfa*$^{fl/fl}$ mice.

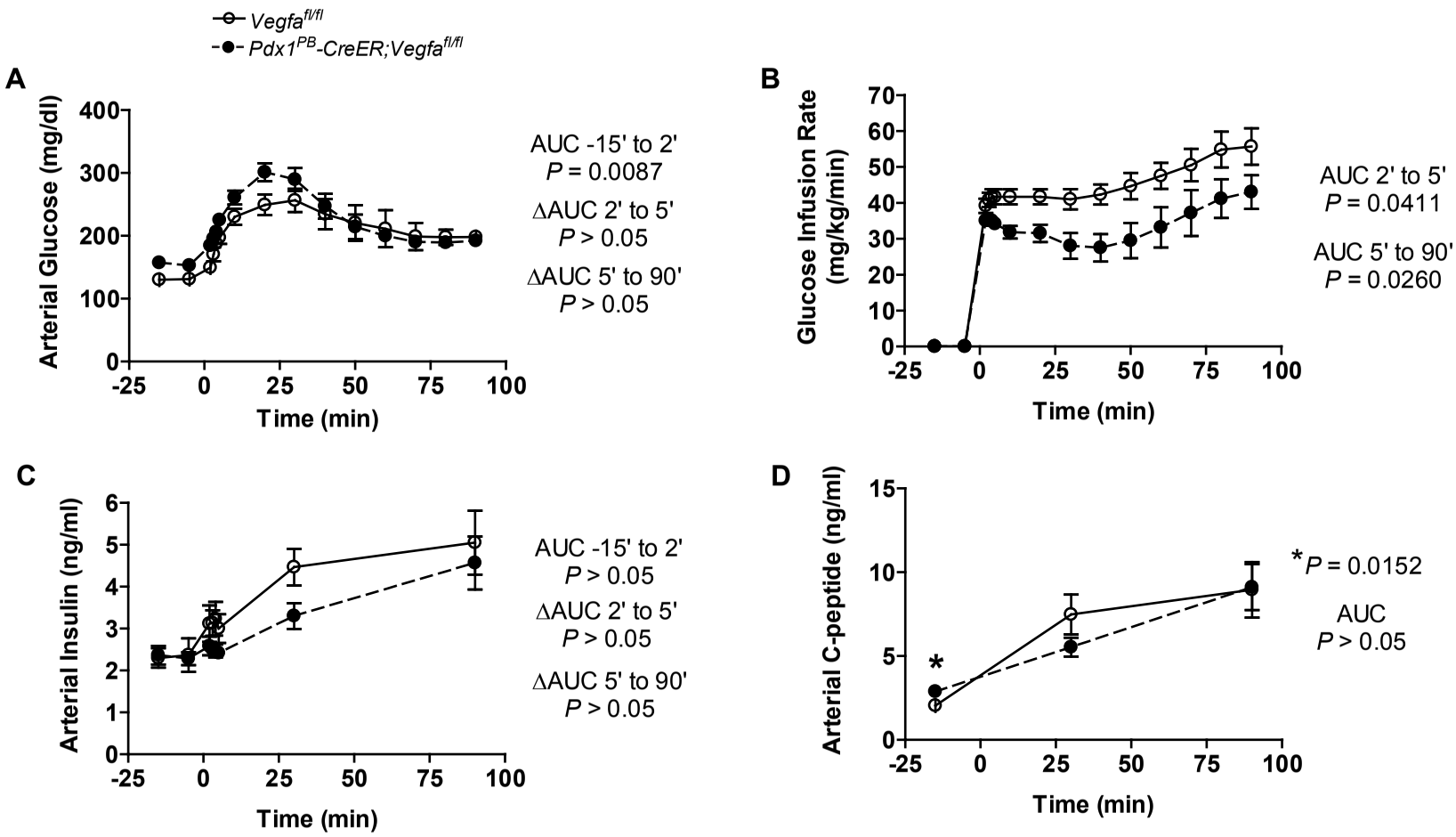

Figure 52. Hyperglycemic clamp on tamoxifen-treated mice. A. Arterial blood glucose values. **B**. Glucose infusion rate. **C.** Serum insulin values. **D.** Serum C-peptide values. In **A-C**, the area under the curve (AUC) was calculated for the basal time period (t = -15' to 2'), and the AUC relative to baseline (ΔAUC) was calculated for the first phase of the clamp (t = 2' to 5') and the second phase of the clamp (t = 5' to 90'). In **D**, data at each time point was compared by Student's t-test, in addition to calculating the AUC.

Similarly, arterial C-peptide levels in Tm-treated *Pdx1*^{PB}*-CreER*^{Tm}*;Vegfa*$^{fl/fl}$ mice were not different from Tm-treated *Vegfa*$^{fl/fl}$ controls in response to increased arterial glucose (Figure 52D).

Hypovascularization does not prevent a high-fat diet-induced increase in pancreatic insulin content

To determine if reduced islet vascularization would impact the islet adaptation to insulin resistance, female Tm-treated *Pdx1*^{PB}*-CreER*^{Tm}*;Vegfa*$^{fl/fl}$ mice were placed on a high-fat diet (HFD) beginning one month following Tm treatment. Surprisingly, neither *Pdx1*^{PB}*-CreER*^{Tm}*;Vegfa*$^{fl/fl}$ mice nor *Vegfa*$^{fl/fl}$ controls showed increased weight gain or impaired glucose tolerance on the HFD compared to chow-fed controls (Figure 53A and data not shown). Similarly, HFD-fed mice showed no changes in lean mass or fat mass after 16 weeks on the diet, compared to chow-fed controls (Figure 53B-C). However, HFD-fed *Vegfa*$^{fl/fl}$ and *Pdx1*^{PB}*-CreER*^{Tm}*;Vegfa*$^{fl/fl}$ mice showed a similar increase in pancreatic insulin content over chow-fed controls (Figure 53D), suggesting that the normal islet vasculature is not required for β-cell adaptation to metabolic stress.

Ectopic expression of Cre recombinase in the brain

During the course of these experiments, it was discovered that Cre recombinase activity was ectopically present in the brain tissue of *Pdx1-Cre* mice (Wicksteed et al., 2010). The possibility that Cre was active in the brain tissue of *Pdx1*^{PB}*-CreER*^{Tm} mice was investigated here, using the *R26-lacZ* reporter mouse strain so that β-galactosidase expression could serve as an indicator of Cre activity. *Pdx1*^{PB}*-CreER*^{Tm}*;R26-lacZ* mice

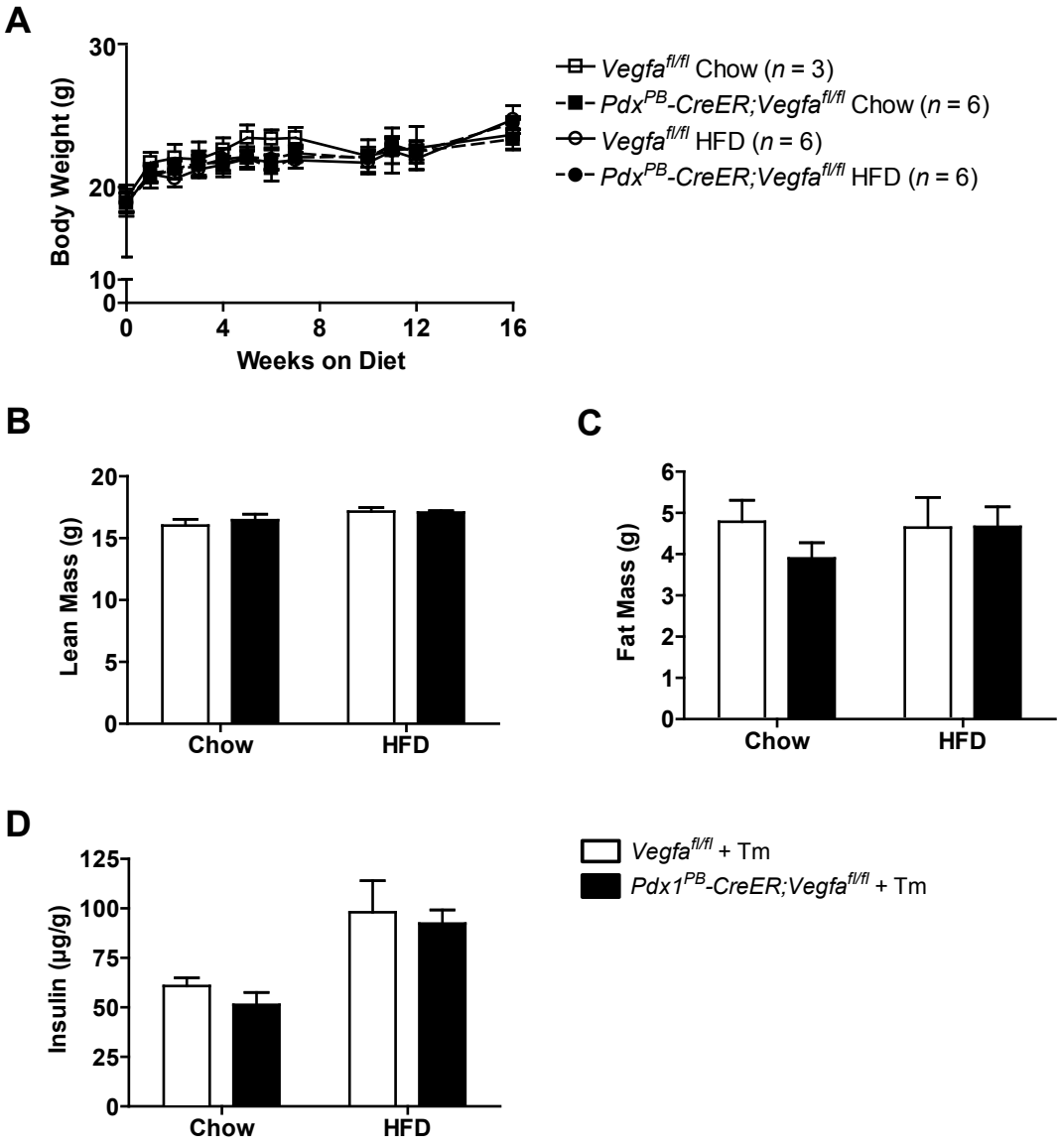

Figure 53. VEGF-A-deficient islets show enhanced insulin expression following a high fat diet, in the absence of changes in body weight, lean mass, or fat mass. Female mice were placed on a high fat diet (HFD) or chow diet for 16 weeks, beginning one month after Tm treatment (at 5 months of age). **A.** Body weight measurements of chow-fed and HFD-fed female *Vegfa*$^{fl/fl}$ and *Pdx1*^{PB}*-CreER;Vegfa*$^{fl/fl}$ mice. **B-C.** Body composition was assessed by NMR spectroscopy to determine lean mass (**B**) and fat mass (**C**) of Tm-treated mice, and analyzed by two-way ANOVA. $P > 0.05$ for diet, genotype, and interaction for both lean mass and fat mass; n = 3-6 per group. **D.** Pancreatic insulin content of HFD-fed and chow-fed *Vegfa*$^{fl/fl}$ and *Pdx1*^{PB}*-CreER;Vegfa*$^{fl/fl}$ mice was assessed after 16 weeks and analyzed by two-way ANOVA. $P = 0.0075$ for diet, and $P > 0.05$ for genotype and interaction; n = 3 per group.

were given either 3 x 1 mg Tm, 3 x 8 mg Tm, or vehicle and assessed for evidence of Cre-mediated recombination.

The pancreas of mice treated with 3 x 8 mg Tm showed scattered islets positive for β-galactosidase, as detected by X-gal staining (Figure 54). The brains of *Pdx1^{PB}-CreER^{Tm};R26-lacZ* mice showed dose-dependent evidence of ectopic recombination. *Pdx1^{PB}-CreER^{Tm};R26-lacZ* mice treated with 3 x 1 mg Tm demonstrated X-gal staining localized to the hypothalamus (Figure 54), similar to the ectopic expression observed in *Pdx1-Cre;R26-lacZ* mice (Wicksteed et al., 2010). However, *Pdx1^{PB}-CreER^{Tm};R26-lacZ* mice treated with 3 x 8 mg Tm showed punctate X-gal staining throughout the brain, but especially within the hypothalamus (Figure 54). As expected, Tm-treated *R26-lacZ* mice and untreated *Pdx1^{PB}-CreER^{Tm};R26-lacZ* mice showed no evidence of recombination in the pancreas or brain (Figure 55).

To evaluate changes in VEGF-A signaling in the brains of Tm-treated *Pdx1^{PB}-CreER^{Tm};Vegfa$^{fl/fl}$* mice, anesthetized mice were infused with a FITC-conjugated tomato lectin that labels the vasculature. No apparent differences were found in the vascular morphology of brain sections from Tm-treated *Pdx1^{PB}-CreER^{Tm};Vegfa$^{fl/fl}$* mice and *Vegfa$^{fl/fl}$* controls (Figure 56). Similarly, no differences were present in *Pdx1-Cre;Vegfa$^{fl/fl}$* mice compared to their controls (Figure 56).

Discussion

VEGF-A is important in islet vascularization, revascularization, and function. However, it was previously unknown whether the impaired function of VEGF-A-deficient islets in adult mice resulted solely from islet hypovascularization or were

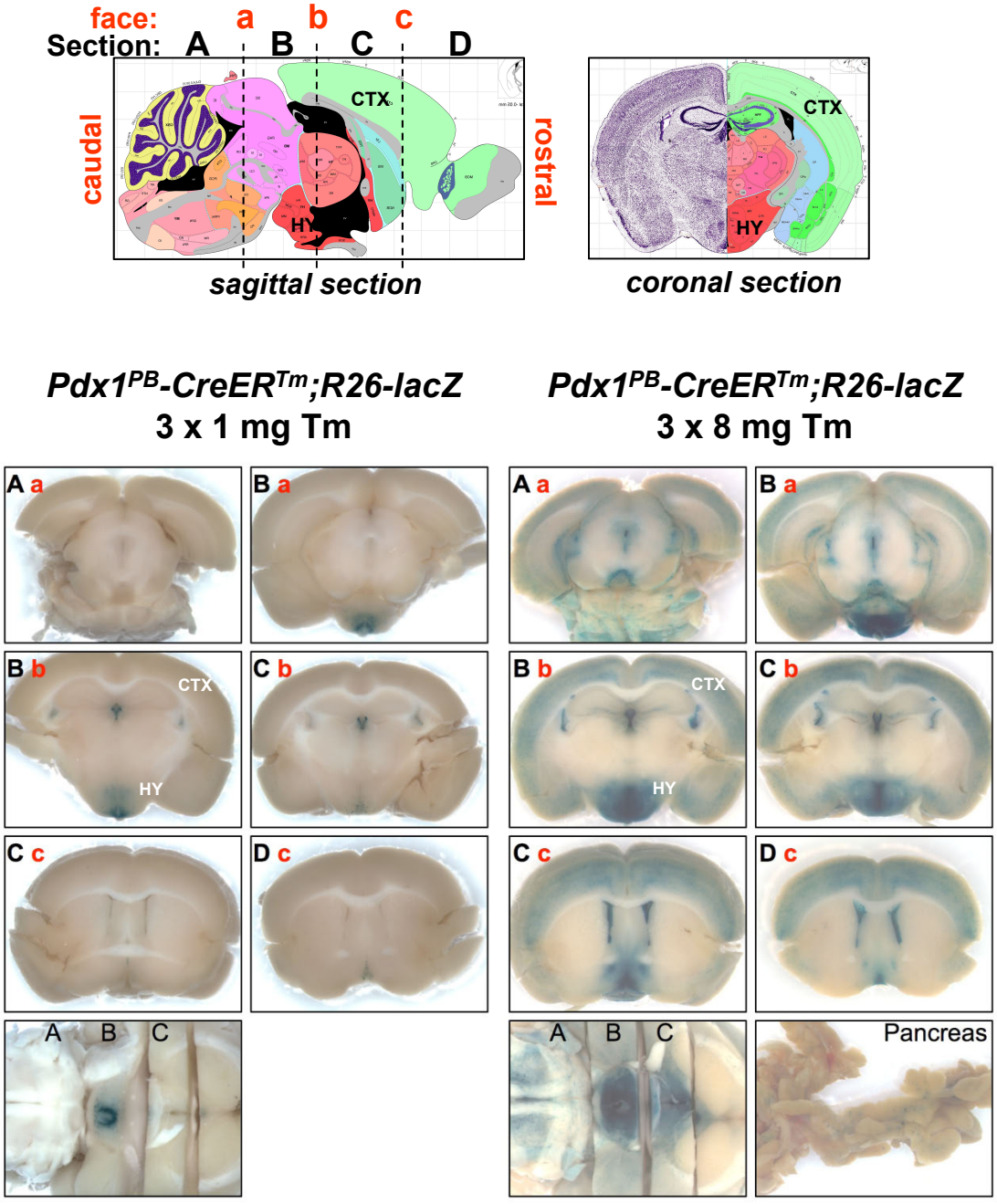

Figure 54. Detection of ectopic Cre-mediated recombination in *Pdx1^{PB}-CreER^{Tm}* brains. Top panel, Schematic of mouse brain in sagittal view (from the Allen Mouse Brain Atlas at http://www.brain-map.org/) with designated brain slices (A-D) and coronal sectioning planes (a-c). Adult *Pdx1^{PB}-CreER^{Tm};R26-lacZ* mice treated with 3 x 1 mg Tm (**left panel**) or 3 x 8 mg Tm (**right panel**) were subjected to X-gal staining in whole mount. CTX, cortex; HY, hypothalamus. From Wicksteed et al. (2010).

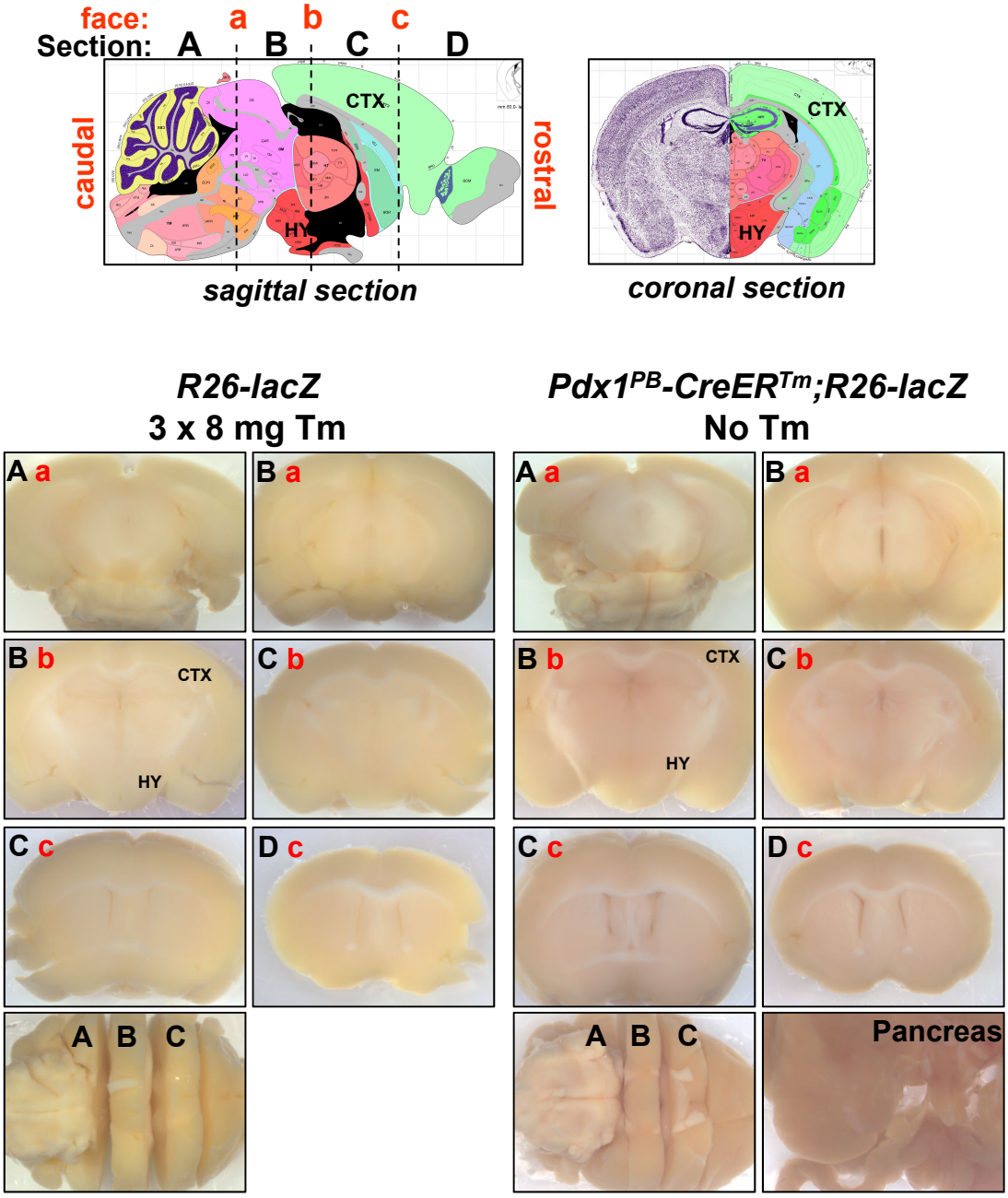

Figure 55. Cre-mediated recombination is not detected in *Pdx1^{PB}-CreER^{Tm}* brains in the absence of tamoxifen. Top panel, Schematic of mouse brain in sagittal view (from the Allen Mouse Brain Atlas at http://www.brain-map.org/) with designated brain slices (A-D) and coronal sectioning planes (a-c). Adult *R26-lacZ* mice treated with 3 x 8 mg Tm (**left panel**) and untreated *Pdx1^{PB}-CreER^{Tm};R26-lacZ* mice (**right panel**) were subjected to X-gal staining in whole mount. CTX, cortex; HY, hypothalamus.

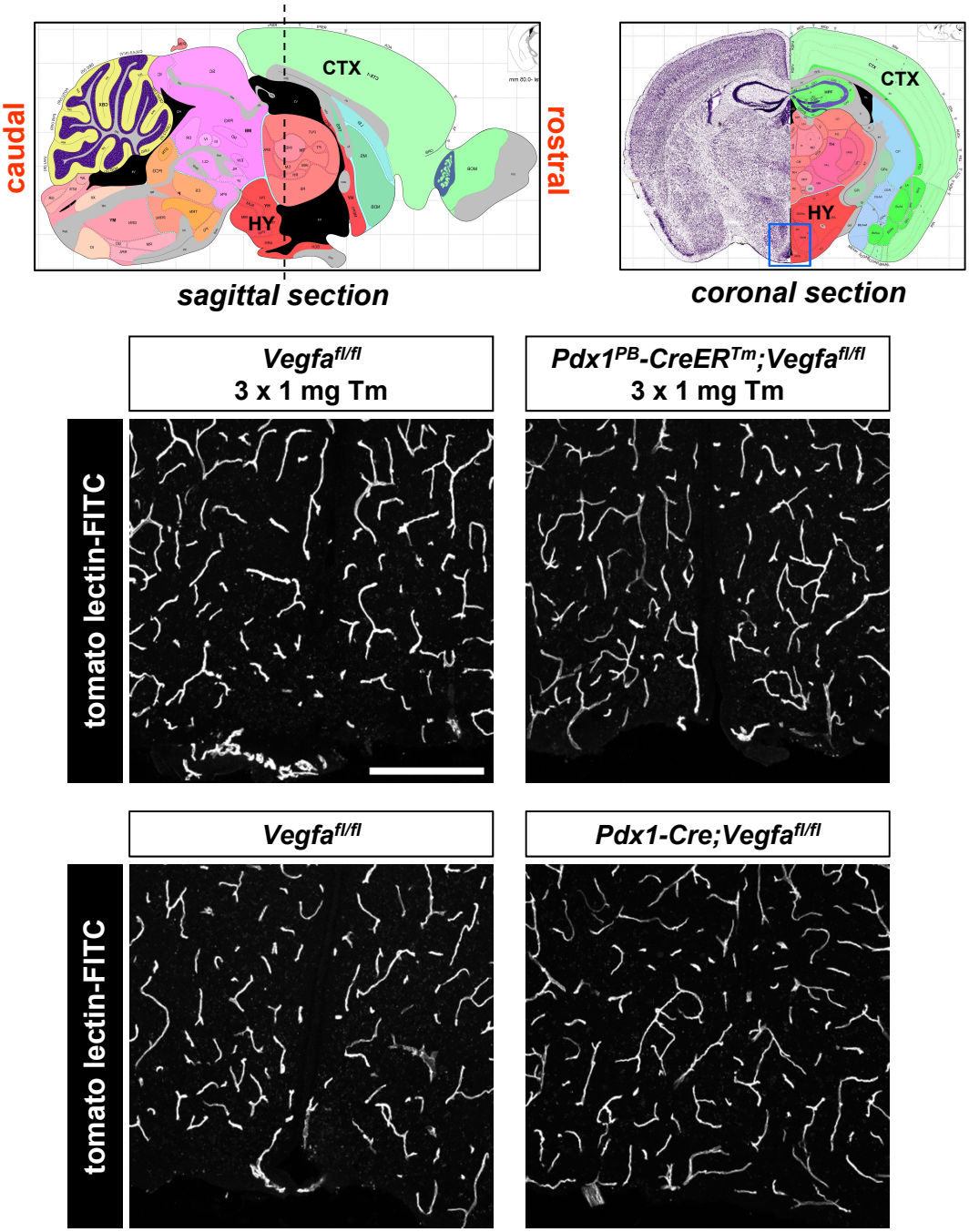

Figure 56. Vascularization is not altered in *Pdx1^{PB}-CreER^{Tm};Vegfa$^{fl/fl}$* and *Pdx1-Cre;Vegfa$^{fl/fl}$* brains. Top panel, Schematic of mouse brain (from the Allen Mouse Brain Atlas at http://www.brain-map.org/) showing the designated coronal sectioning plane (dotted line) and the region of interest (blue box) presented in the panels below. **Bottom panels**, Adult Tm-treated *Pdx1^{PB}-CreER^{Tm};Vegfa$^{fl/fl}$* mice, *Pdx1-Cre;Vegfa$^{fl/fl}$* mice, and their respective littermate controls were infused intravitally with a FITC-conjugated tomato lectin to label the functional vasculature, and 30 µm-thick brain cryosections were imaged by confocal microscopy. Scale bar is 200 µm, and applies to all panels. CTX, cortex; HY, hypothalamus.

manifestations of altered islet development. Surprisingly, even though the present Tm-inducible model induced a substantial and prolonged reduction in VEGF-A production in β-cells of adult Tm-treated *Pdx1*^{PB}-*CreER*^{Tm};*Vegfa*$^{fl/fl}$ mice, no changes were found in β-cell gene expression or mass, and only slight changes were observed in glucose metabolism *in vivo*. These results show that VEGF-A and the intraislet vasculature play a much greater role in promoting islet growth during development (Lammert et al., 2003b; Reinert and Brissova et. al, manuscript in preparation) than in maintaining β-cells in mature islets (Figure 57).

VEGF-A is required to maintain the vascularity of mature islets

Islet vascularization and function in this model was investigated at least one month following VEGF-A inactivation, to focus on the long-term consequences of VEGF-A deficiency and also to avoid any side effects of Tm treatment (as will be described in Chapter V). However, it is likely that changes in the intraislet vasculature occurred rapidly following VEGF-A inactivation, because inhibitors of VEGF signaling have been shown to reverse endothelial cell fenestrations within 24 hours and induce capillary regression within one week of treatment (Inai et al., 2004; Kamba et al., 2006). Both short-term (7 days) and longer (21 days) treatment with a small molecule inhibitor of VEGF receptor tyrosine kinase activity showed about a 50% reduction in islet capillary density (Kamba et al., 2006), similar to the changes observed in *Pdx1*^{PB}-*CreER*^{Tm};*Vegfa*$^{fl/fl}$ mice from one to three months following Tm treatment. These data show that constitutive intraislet VEGF-A signaling is responsible for maintaining the high degree of islet vascularity and permeability. However, the remaining intraislet

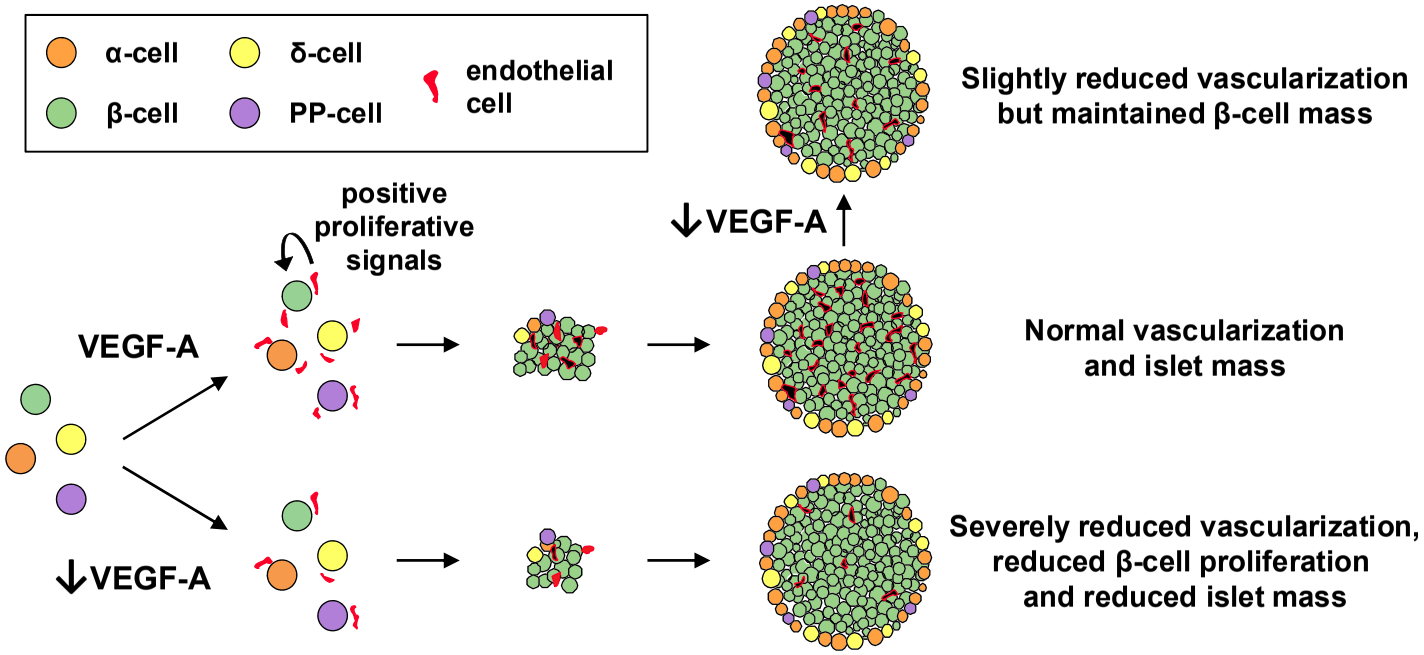

Figure 57. Differential roles for VEGF-A in developing versus mature islets. Inactivation of VEGF-A in the developing pancreas profoundly affects islet vascularization and impairs β-cell proliferation. In contrast, inactivation of VEGF-A in mature islets slightly reduces islet vascularization and has no long-term impact on β-cell mass.

vasculature is stable, likely maintained by VEGF-A derived from non-β-cells of the islet and/or other islet-derived angiogenic factors (Brissova et al., 2006).

Normal islet vascularization is not required to maintain β-cell gene expression and mass

Surprisingly, these data show that the high degree of vascularization found in islets within the pancreas of wild-type mice is not required for the maintenance of β-cell gene expression or mass. Tm-treated *Pdx1*^{PB}*-CreER*^{Tm}*;Vegfa*$^{fl/fl}$ mice showed no changes in expression of the β-cell genes *Ins2*, *Pdx1*, or *Mafa*, and no changes in β-cell area within the pancreas. β-cell proliferation was also examined three months following VEGF-A inactivation, but only rare Ki67+ β-cells were found in pancreata from either Tm-treated *Vegfa*$^{fl/fl}$ or *Pdx1*^{PB}*-CreER*^{Tm}*;Vegfa*$^{fl/fl}$ mice (data not shown). This low basal proliferation rate is expected for 7-month-old mice (Teta et al., 2005), and suggests that if the intraislet vasculature were involved in maintaining β-cell proliferation in mature islets, only minimal changes in proliferation would be detectable in the current model. It is possible that Tm-treated *Pdx1*^{PB}*-CreER*^{Tm}*;Vegfa*$^{fl/fl}$ mice retain a certain threshold of endothelial cells required to maintain basal β-cell proliferation, a threshold not reached by islets in *Pdx1-Cre;Vegfa*$^{fl/fl}$ mice, which show reduced β-cell proliferation (Reinert and Brissova et al., manuscript in preparation). No changes were observed in pancreatic β-cell area even three months following VEGF-A inactivation, so the halving of intraislet vessel density that occurred in this model did not impair β-cell proliferation or cause β-cell loss to a degree that would impair the maintenance of β-cell mass.

These data also show that the normal intraislet vasculature is not required to maintain insulin biosynthesis in β-cells. In fact, pancreatic insulin content was slightly

increased in male *Pdx1^{PB}-CreER^{Tm};Vegfa$^{fl/fl}$* mice, perhaps in response to the insulin resistance uncovered by the hyperglycemic clamp experiment. Additionally, while HFD-fed female *Pdx1^{PB}-CreER^{Tm};Vegfa$^{fl/fl}$* mice surprisingly did not gain any more weight than animals on the regular chow diet, or develop impaired glucose tolerance (data not shown), they did show an increase in pancreatic insulin content. This suggests that β-cells in hypovascularized islets can increase insulin production in response to increased demand. This is in agreement with a report that *RIP-Cre;Vegfa$^{fl/fl}$* mice showed an increase in β-cell mass following a HFD (Toyofuku et al., 2009). In contrast to these data, a study in rats showed that an expansion of endothelial cells precedes the β-cell proliferation that occurs in late pregnancy, and that endothelial cell-derived HGF may be involved in stimulating β-cell proliferation (Johansson et al., 2006b). Therefore, the role of endothelial cells in β-cell expansion may be context-dependent.

The specialized intraislet vasculature is thought to be critical for maintaining a high oxygen tension within the metabolically active endocrine pancreas (Carlsson et al., 1998). It has been proposed that the decreased vessel density (Mattsson et al., 2002) and oxygen tension (Carlsson et al., 1998; Carlsson et al., 2000; Carlsson et al., 2001) in islet grafts is a major reason for islet transplantation failure. The data presented here suggest that mature islets are able to tolerate a two-fold reduction in vessel density and still maintain normal gene expression and insulin production, with only slight defects in islet function. That β-cells can adapt to the lower oxygen tension likely observed in this hypovascularized state may not be surprising, because it was recently found that a reserve pool of pancreatic islets are regularly exposed to low oxygenation. These metabolically dormant islets are recruited into action through increased blood perfusion only when

necessary, such as following an experimental partial pancreatectomy (Olsson and Carlsson, 2011). Therefore, the inability of islet grafts to achieve the highly vascularized state observed in islets within the pancreas may not necessarily be the biggest obstacle for islet transplantation to achieve long-term success.

Islet hypovascularization slightly impairs islet function in vivo, but has no effect on insulin secretion in vitro

The main defect observed in *Pdx1*^{PB}*-CreER*^{Tm}*;Vegfa*$^{fl/fl}$ mice was slightly impaired glucose tolerance following VEGF-A inactivation. This suggests that there is either a delay in the glucose stimulus reaching the β-cells, or a delay in insulin release into the bloodstream. Because β-cells secrete insulin mainly into the interstitium and not directly into capillaries (Takahashi et al., 2002), it is likely that the insulin produced in Tm-treated *Pdx1*^{PB}*-CreER*^{Tm}*;Vegfa*$^{fl/fl}$ mice simply has a longer path to traverse before finding the bloodstream. Indeed, perifusion of islets from Tm-treated *Pdx1*^{PB}*-CreER*^{Tm}*;Vegfa*$^{fl/fl}$ mice showed no changes in glucose-stimulated insulin secretion *in vitro*, while the hyperglycemic clamp data showed that *Pdx*^{PB}*-CreER*^{Tm}*;Vegfa*$^{fl/fl}$ mice had a slight, but not statistically significant, reduction in glucose-stimulated insulin secretion *in vivo*. While any potential defect in early insulin secretion may be masked by the increased blood glucose concentrations during the early phase of the clamp, *Pdx*^{PB}*-CreER*^{Tm}*;Vegfa*$^{fl/fl}$ mice were able to match insulin secretion of the control mice at the end of the clamp, when glucose levels were similar. These data suggest that VEGF-A inactivation is less detrimental to mature islets compared to developing islets.

By comparison, adult *RIP-Cre;Vegfa*$^{fl/fl}$ mice, in which VEGF-A production by β-cells was reduced in embryogenesis, had more severe glucose intolerance and reduced insulin secretion (Brissova et al., 2006). Adult *RIP-Cre;Vegfa*$^{fl/fl}$ mice display a similar reduction in intraislet vessel density as Tm-treated *Pdx*^{PB}*-CreER*^{Tm}*;Vegfa*$^{fl/fl}$ mice, and also show normal β-cell mass. However, *RIP-Cre;Vegfa*$^{fl/fl}$ mice also show dramatic changes in intraislet capillary ultrastructure, displaying few fenestrations and increased caveolae (Brissova et al., 2006), similar to intraislet capillaries in mice treated with VEGF signaling inhibitors (Kamba et al., 2006). In contrast, *Pdx*^{PB}*-CreER*^{Tm}*;Vegfa*$^{fl/fl}$ mice unexpectedly display a mix in capillary ultrastructure, with the preservation of many fenestrations. It is possible that non-β endocrine cells are able to compensate for the lack of VEGF-A production by β-cells in *Pdx1*^{PB}*-CreER*^{Tm}*;Vegfa*$^{fl/fl}$ mice, and that this increased capillary permeability may account for the relatively mild glucose intolerance seen in this model. In all, these data suggest that the VEGF-A-mediated maintenance of islet vascular density and permeability is important for the fine-tuning of islet function *in vivo*, but these parameters are not necessarily required for basic β-cell function.

The metabolic data presented here contrasts with data from mice treated with a VEGF receptor inhibitor, in which fasting blood glucose and glucose tolerance was improved (Kamba et al., 2006). Although the inhibitor led to a similar reduction in pancreatic islet vascular density as in the Tm-inducible model, it also affected the vasculature of multiple other tissues, including the thyroid, pituitary, and adrenal glands, so the precise mechanism leading to improved glucose homeostasis remains unexplained. A similar observation was made in a clinical study in which patients with type 2 diabetes

experienced a reduction in blood glucose levels following treatment with VEGF receptor inhibitors for renal cancer, though again the mechanism remains unclear (Billemont et al., 2008). Some data suggest that inhibition of VEGF signaling in the liver improves hepatic insulin sensitivity through a HIF-2α mechanism, and that liver activation of HIF-2α corrects hyperglycemia in *db/db* mice (Wei, 2011).

One unexplained finding from the clamp study performed in Tm-treated Pdx^{PB}-$CreER^{Tm}$;$Vegfa^{fl/fl}$ mice is the decreased glucose infusion rate required to maintain hyperglycemia, which indicates insulin resistance. The insulin resistance is not a result of Tm treatment itself, because control $Vegfa^{fl/fl}$ mice were also treated with Tm before the hyperglycemic clamp experiment. Because islet-derived VEGF-A is not thought to influence cells outside the islet, as indicated by the sharp demarcation in vascular phenotypes of the endocrine versus exocrine pancreas (Henderson and Moss, 1985), it is unclear how inactivation of VEGF-A solely within β-cells would directly lead to insulin resistance. Since this conditional VEGF-A allele is highly sensitive to Cre-mediated recombination, only requiring low Tm doses to induce recombination, it is possible that even low levels of aberrant Cre expression in other tissues could induce sufficient recombination to affect tissue function. Therefore, one possible explanation is that VEGF-A is inactivated in the hypothalamus following Tm treatment, because Pdx^{PB}-$CreER^{Tm}$ mice were shown to have ectopic Cre-mediated recombination in the brain. No changes were observed in the vascularization of brain sections in either Tm-treated Pdx^{PB}-$CreER^{Tm}$;$Vegfa^{fl/fl}$ or *Pdx1-Cre;*$Vegfa^{fl/fl}$ mice. However, this may not be a sufficiently sensitive indicator of VEGF-A signaling, because few changes were observed in the vasculature of brains in mice treated with VEGF signaling inhibitors (Kamba et al.,

2006). It is possible that VEGF-A inactivation disrupts other aspects in brain function, because VEGF-A can signal directly to adult neurons to mediate their survival (Mackenzie and Ruhrberg, 2012). Alternatively, there may be ectopic inactivation of VEGF-A in insulin-dependent tissues, though the potential impact of VEGF-A inactivation on the vascularization and function of these tissues is less clear. Inhibition of VEGF-A signaling reduces fenestrations of the liver endothelium (Tam et al., 2006), and liver endothelial cells provide important mitogenic signals to hepatocytes, including HGF (LeCouter et al., 2003). But again, inhibition of VEGF signaling in the liver may improve hepatic insulin sensitivity (Wei, 2011). It is also unclear whether VEGF-A inactivation in mature skeletal muscle would affect insulin sensitivity, because this vascular bed may (Tang et al., 2004) or may not (Kamba et al., 2006) be dependent on VEGF-A signaling. Finally, VEGF-A inactivation has variable effects in adipose tissue (Sun et al., 2012). Thus, the etiology of the insulin resistance in our model is not certain and warrants further study.

In conclusion, although VEGF-A is a critical factor for the proper development of islet vascularization and function, VEGF-A and the intraislet vasculature plays a less critical role in mature pancreatic islets. While VEGF-A is required for maintaining the specialized vasculature observed in normal adult islets, mature β-cells can adapt to and survive even long-term reductions in islet vascularity. Importantly, these data suggest that achieving the highly vascularized state of pancreatic islets may not be necessary for the long-term success of transplanted mature islets.

CHAPTER V

ESTIMATING THE TIMELINE OF TAMOXIFEN-INDUCED CRE RECOMBINATION USING AN ISLET TRANSPLANTATION BIOASSAY

While developing the model of inducible islet VEGF-A inactivation described in Chapter IV, long-term side effects were noted in mice treated with tamoxifen (Tm). These initial studies drew concerns about the design and interpretation of some prior studies using Tm-inducible model systems. Experiments performed to address these concerns are described below, following a brief introduction to current issues in the use of Tm-inducible model systems. Data and text within this chapter have been published (Reinert et al., 2012).

Introduction

The advent of Tm-inducible Cre recombinases has greatly improved the ability to temporally control Cre-*loxP* recombination *in vivo*, and has been particularly useful for investigating properties of mature tissues in the adult mouse. Over the past decade, Tm-inducible gene recombination has been used to examine organ maintenance and function through a variety of approaches, including cell lineage tracing (Badea et al., 2003; Bonaguidi et al., 2011; Burns et al., 2007; Dorrell et al., 2011; Hsieh et al., 2007; Ninkovic et al., 2007; Pellegrinet et al., 2011; Rawlins et al., 2009; Rock et al., 2009; Sangiorgi and Capecchi, 2008; Scholten et al., 2010; Zhu et al., 2011), inducible gene expression (Johansson et al., 2007; Mao et al., 2006; Pelengaris et al., 2002; Remedi et al.,

2009; Youssef et al., 2010), and gene inactivation (Lepper et al., 2009; Porat et al., 2011; Salpeter et al., 2011; Yang et al., 2010).

Several studies have described the importance of various parameters in Cre-*loxP* recombination, such as expression of Cre recombinase (Buelow and Scharenberg, 2008; Metzger and Chambon, 2001) and the accessibility of *loxP* sites (Guo et al., 2002; Long and Rossi, 2009). For inducible Cre-*loxP* recombination, one critical parameter that is often poorly described is verification that the Tm dose used is appropriate for the experiment, not only for maximizing the spatial extent of recombination in the target tissue but also by limiting the temporal extent of recombination. Specifically, knowing the timeline of Tm-induced Cre-*loxP* recombination is critical for "pulse-chase" lineage tracing experiments, because a pulse that unknowingly extends into the chase period will continue to label newly generated cells, and lead to the interpretation that all labeled cells are derived from the cell population that existed during the expected pulse period. For example, the current limited knowledge of the Tm pulse period in adult mice may be one factor contributing to the discrepancies observed in recent lineage tracing studies of the pancreas.

In the pancreatic islet biology field, investigators are striving to understand the normal development and maintenance of insulin-producing β-cells and attempting to find sources for creating and regenerating β-cells, with the ultimate goal of treating diabetes. The use of Tm-inducible mouse models for cell lineage tracing has played a key role in advancing our understanding of pancreas biology, although some conflicting results have yet to be resolved. In an adaptation of classic pulse-chase experiments, Dor and colleagues were the first to use a Tm-inducible Cre driver strain to label mature

pancreatic β-cells in adult mice (Dor et al., 2004). After determining that the proportion of labeled β-cells did not change over time, they concluded that pre-existing β-cells were the source of β-cell replenishment in adult mice, and that there was no significant contribution of (unlabeled) stem cells to the β-cell population. This finding was also supported by studies using Tm-inducible systems to demonstrate that all mature β-cells possess a certain replication capacity (Brennand et al., 2007; Nir et al., 2007; Salpeter et al., 2010). In contrast, several other groups have used the same pulse-chase approach and concluded that β-cells can originate from non-β-cell sources, after observing changes in the proportion of labeled β-cells following post-injury regeneration or during pregnancy, when β-cell mass increases (Abouna et al., 2010; Liu et al., 2010a; Nakamura et al., 2011). Further complicating our concept of β-cell turnover, one group reported isolating multipotent, stem-like cells from pancreatic islets, and, using the same lineage tracing methods as Dor et al. (2004), identified insulin+ cells as the source (Smukler et al., 2011).

An alternative lineage tracing approach is to label a given cell type and determine whether or not it has the capacity to mature or transdifferentiate into another cell type. Using this more direct method of tracking cells, β-cells have been reported to originate from pancreatic ductal cells (Inada et al., 2008) and glucagon-producing α-cells (Thorel et al., 2010) in the injured mature pancreas, suggesting that transdifferentiation may occur under specific circumstances. However, the mechanisms involved in this process still require further examination, because several studies have failed to find evidence of β-cell transdifferentiation from acinar cells (Blaine et al., 2010; Desai et al., 2007; Kopinke and Murtaugh, 2010; Sangiorgi and Capecchi, 2009; Strobel et al., 2007a) or

ductal cells (Furuyama et al., 2011; Kopinke et al., 2011; Kopp et al., 2011b; Solar et al., 2009) in the adult pancreas.

While the Tm-inducible genetic models used in these studies have proven to be useful in addressing complex biological questions regarding pancreas development and maintenance, the conflicting results are sometimes difficult to reconcile. The fact that various Cre driver mice and reporter strains were used makes it inherently more difficult to compare different studies, because each model system differs in the specificity of Cre expression and the efficiency of target gene induction (Kopp et al., 2011a; Kushner et al., 2010; Murtaugh, 2011). A recent report that described Tm-independent activity of Cre recombinase in the commonly used β-cell-targeted *RIP-CreER*^{Tm} mouse found that the extent of the "leakiness" varied, depending on the target gene (Liu et al., 2010b). Moreover, a wide range of Tm doses and administration methods have been reported, even for studies using similar Cre driver and reporter mice. In fact, one review questioned whether different Tm doses could account for the conflicting outcomes in two very similar models of pancreatic ductal cell lineage tracing (Kopp et al., 2011a). The need to draw such comparisons between experiments emphasizes the necessity for a full understanding of the parameters controlling recombination in each model system.

While understanding the temporal limits of CreER activity is crucial for the design and interpretation of lineage tracing experiments, the kinetics of Tm activity have been studied almost exclusively in embryonic tissues (Hayashi and McMahon, 2002; Nakamura et al., 2006). Using immunohistochemistry, it was found that Cre localized to the nucleus of embryonic cells 24 hours after administration of Tm to a pregnant dam, but returned to the cytoplasm 48 hours after treatment (Hayashi and McMahon, 2002).

Further studies showed that the extent of recombination events was dramatically different in embryos depending on the developmental stage at which Tm treatment was performed, because of the embryo's rapidly changing gene expression profile. These results suggested that Tm-induced recombination events in the embryo are restricted to a short time frame after drug administration to the dam (Danielian et al., 1998; Gu et al., 2002; Nakamura et al., 2006). Since most tissues in the adult animal do not show frequent, dramatic changes in gene expression or cell turnover, it is not possible to extrapolate the duration of active recombination following Tm administration in embryonic studies to that in adult mice.

In this study, the kinetics of Tm-induced Cre-*loxP* recombination in pancreatic β-cells was defined in adult mice. Because the precise level of circulating Tm necessary for inducing recombination *in vivo* is unknown, pancreatic islet transplantation was used as a bioassay to directly measure recombination at a given time following Tm administration. It was found that significant recombination of reporter alleles can occur for weeks after Tm treatment, and that the length of time that a Tm pulse induces recombination is dose-dependent. Furthermore, Tm-treated male mice experienced side effects that have not been reported in recent literature. These data have considerable implications for the design and interpretation of studies utilizing Tm-inducible systems in adult mice.

Results

High doses of tamoxifen induce prolonged nuclear localization of Cre recombinase in mature β-cells

To estimate the duration of Tm-induced Cre-mediated recombination in adult mice, nuclear localization of Cre recombinase was evaluated in islet β-cells on pancreatic sections collected from transgenic *Pdx1*^{PB}-*CreER*^{Tm};*Vegfa*$^{fl/fl}$ mice at different time points following the administration of 3 x 8 mg Tm. Surprisingly, Cre was found in the β-cell nucleus and cytoplasm in *Pdx1*^{PB}-*CreER*^{Tm};*Vegfa*$^{fl/fl}$ pancreas collected either one week or one month after the final Tm dose (Figure 58D-I). In contrast, vehicle-treated *Pdx1*^{PB}-*CreER*^{Tm};*Vegfa*$^{fl/fl}$ mice displayed strict cytoplasmic localization of Cre in β-cells, as demonstrated by colocalization with insulin (Figure 58A-C). Likewise, β-cells from *Pdx1*^{PB}-*CreER*^{Tm};*Vegfa*$^{fl/fl}$ mice sacrificed three months after the final Tm treatment demonstrated cytoplasmic but not nuclear Cre localization (Figure 58J-L).

High doses of tamoxifen induce a prolonged period of Cre-loxP recombination in adult mice

To better understand how long a given Tm dose is able to induce Cre-mediated recombination *in vivo*, a system was developed to evaluate recombination that occurs at any given time following Tm treatment. It was reasoned that measuring the serum Tm concentration in this model would likely be unhelpful, because the precise level of circulating Tm necessary for inducing recombination is unknown. Therefore, a bioassay was designed using pancreatic islet transplantation to assess recombination in Tm-naïve islet β-cells transplanted into Tm-treated mice. In this model, islets containing a Tm-

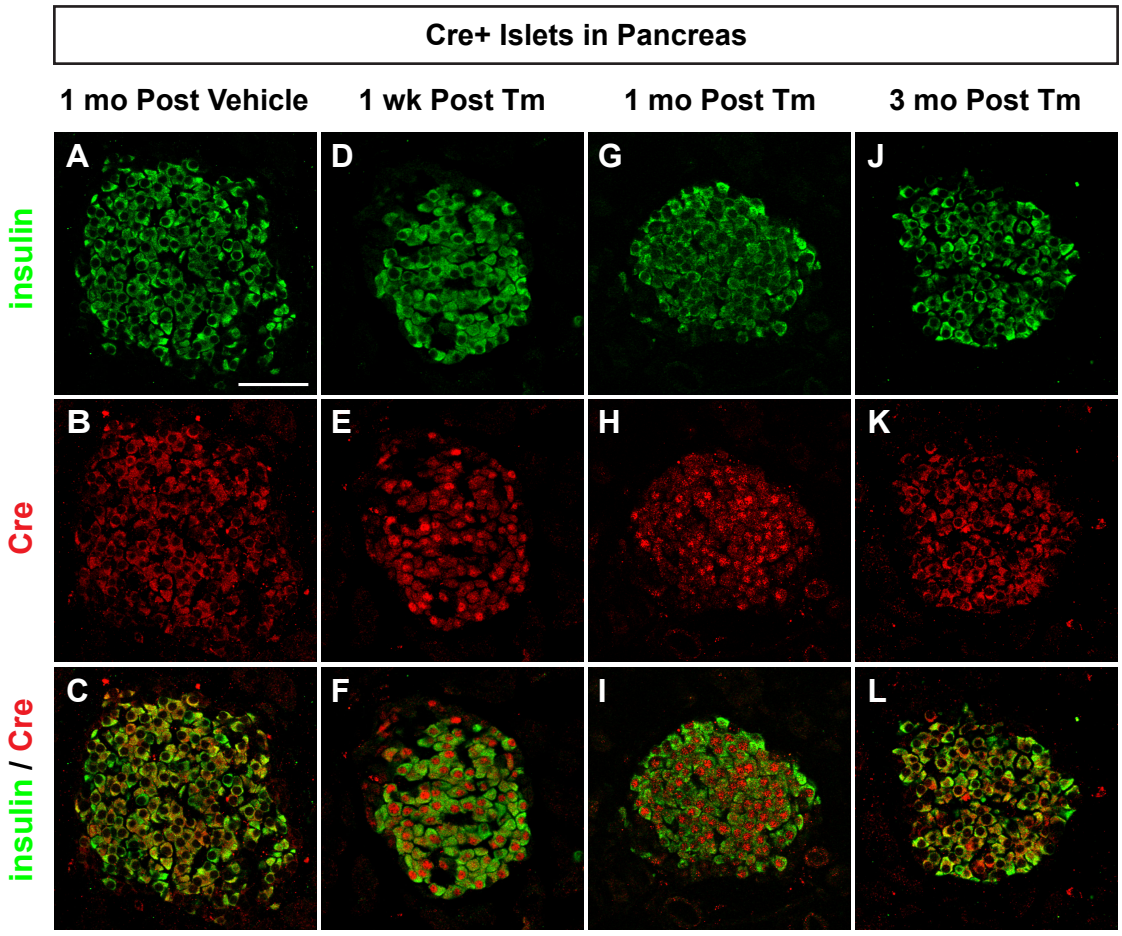

Figure 58. Tamoxifen-induced Cre subcellular localization is time-dependent. Representative islets from adult *Pdx1*^{PB}*-CreER*^{Tm}*;Vegfa*$^{fl/fl}$ mice given 8 mg tamoxifen (Tm, **D-L**) or corn oil vehicle (**A-C**) in three subcutaneous injections. Pancreata were harvested 1 week (**D-F**), 1 month (**G-I**), or 3 months (**J-L**) following the last injection and labeled with antibodies against insulin (green; **A, D, G, J**) and Cre recombinase (red; **B, E, H, K**). Merged images are shown in **C, F, I, L**. Scale bar in **A** is 50 μm, and applies to panels **B-L**.

inducible Cre reporter (from *Pdx1*^{PB}-*CreER*^{Tm};*R26-lacZ* mice) were transplanted beneath the renal capsule of mice treated with different doses of Tm prior to islet transplantation (Figure 59A, 60A). In this way, the relevant endpoint, recombination, served as the metric.

The first dose evaluated was 3 x 8 mg Tm, a dose similar to that used in other studies for lineage tracing of β-cells in adult mice (Abouna et al., 2010; Brennand et al., 2007; Dor et al., 2004; Liu et al., 2010a; Nakamura et al., 2011; Nir et al., 2007; Smukler et al., 2011; Thorel et al., 2010). As expected, islets in Tm-treated *R26-lacZ* mice did not express β-gal, as visualized by immunohistochemistry (Figure 59B). In *Pdx1*^{PB}-*CreER*^{Tm};*R26-lacZ* mice given 3 x 8 mg Tm, 80.1 ± 8.2% of β-cells in pancreatic islets expressed β-gal (Figure 59C). To evaluate this dose in the transplant model, recipient mice were given three subcutaneous injections of Tm or vehicle before receiving a pancreatic islet transplant from Tm-naïve *Pdx1*^{PB}-*CreER*^{Tm};*R26-lacZ* donor mice. Islet grafts were placed 48 hours, 1 week, 2 weeks, or 4 weeks following the final Tm injection (Figure 59A). Significant recombination was observed in *Pdx1*^{PB}-*CreER*^{Tm};*R26-lacZ* islet grafts in mice given 3 x 8 mg Tm for weeks after the final Tm dose. When quantified, 77.9 ± 0.4% of β-cells expressed β-gal when transplanted 48 hours after the final Tm injection (Figure 59F), 46.2 ± 5.0% were β-gal+ 1 week after injection (Figure 59G), and 26.3 ± 7.0% expressed β-gal 2 weeks after injection (Figure 59H). Recombination was also noted in grafts placed 4 weeks after the final Tm injection, with 1.9 ± 0.9% of β-cells positive for β-gal (Figure 59I). In contrast, islet cells from *R26-lacZ* mice transplanted into Tm-treated mice did not express β-gal (Figure 59D). Similarly, most *Pdx1*^{PB}-*CreER*^{Tm};*R26-lacZ* islet cells transplanted into vehicle-treated mice did not

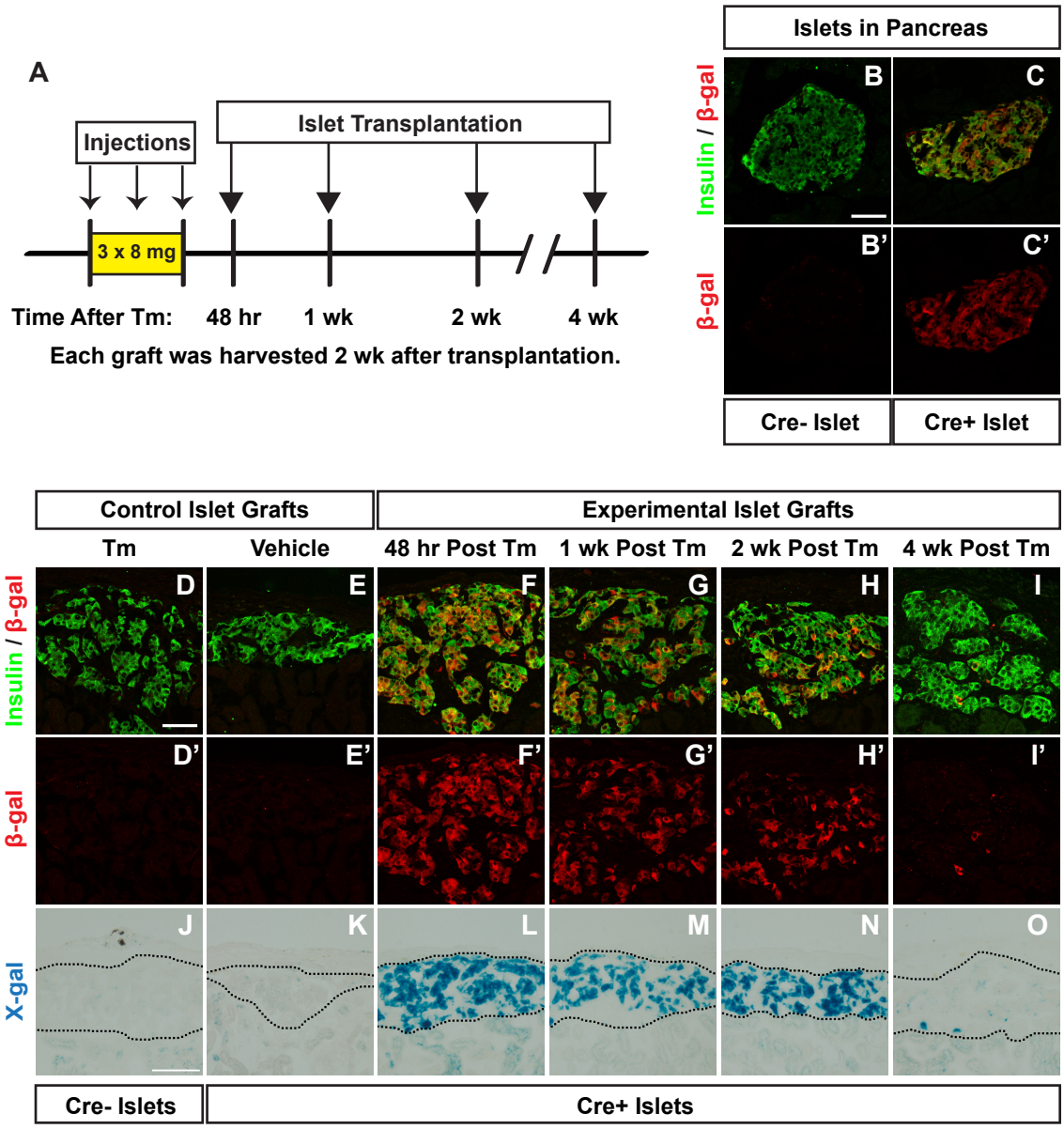

Figure 59. Higher dose tamoxifen induces recombination for weeks following administration. A. Islets from untreated *Pdx1*^{PB}*-CreER*^{Tm}*;R26-lacZ* (Cre+) mice or *R26-lacZ* (Cre-) controls were transplanted into mice given three subcutaneous injections of 8 mg tamoxifen (Tm) or vehicle at the indicated times following the last injection. **B-C.** Representative islets from Cre- (**B**) and Cre+ (**C**) mice treated with 3 x 8 mg Tm, labeled with antibodies to insulin (green) and β-galactosidase (β-gal, red). Scale bar in **B** is 50 μm and applies to panel **C**. **D-I.** Islet graft cryosections were labeled with antibodies to insulin (green) and β-gal (red). Scale bar in **D** is 50 μm, and applies to panels **E-I. J-O**. β-gal activity was evaluated in islet grafts by X-gal staining. Scale bar in **J** is 100 μm, and applies to panels **K-O**.

show signs of recombination (Figure 59E), although a few β-gal+ β-cells were found in one of the grafts (0.6 ± 0.6%). These results were confirmed by X-gal staining (Figure 59J-O).

Lower doses of tamoxifen show a shorter period of Cre-loxP recombination in adult mice

Next, the islet transplantation bioassay was used to test the duration of recombination following 3 x 1 mg Tm (Figure 60A), a dose that induced effective recombination in *Pdx1*^{PB}-*CreER*^{Tm};*Vegfa*$^{fl/fl}$ mice (see Figure 44 in Chapter IV). Compared to mice receiving 3 x 8 mg Tm, treatment with 3 x 1 mg Tm induced less recombination in pancreatic islets of *Pdx1*^{PB}-*CreER*^{Tm};*R26-lacZ* mice (29.8 ± 4.1% of β-cells expressed β-gal, Figure 60B). Likewise, less, but notable, recombination was observed in *Pdx1*^{PB}-*CreER*^{Tm};*R26-lacZ* grafts placed in mice receiving 3 x 1 mg Tm: 4.9 ± 1.7% of β-cells expressed β-gal 48 hours after Tm (Figure 60E), and 4.5 ± 1.9% of β-cells were β-gal+ 1 week after Tm (Figure 60F). No β-gal+ β-cells were noted in control grafts (Figure 60C-D). These results were also confirmed by X-gal staining of the islet grafts (Figure 60G-J).

The duration of tamoxifen-induced gene recombination is dose-dependent

A summary of Tm-induced recombination in *Pdx1*^{PB}-*CreER*^{Tm};*R26-lacZ* pancreatic islets and islet grafts is shown in Figure 61. Recombination of β-cells in both endogenous pancreatic islets (Figure 61A) and in islet grafts (Figure 61B) is dose-dependent. At either dose, recombination in the transplanted islet cells was lower than recombination in pancreatic islets. However, all groups of *Pdx1*^{PB}-*CreER*^{Tm};*R26-lacZ*

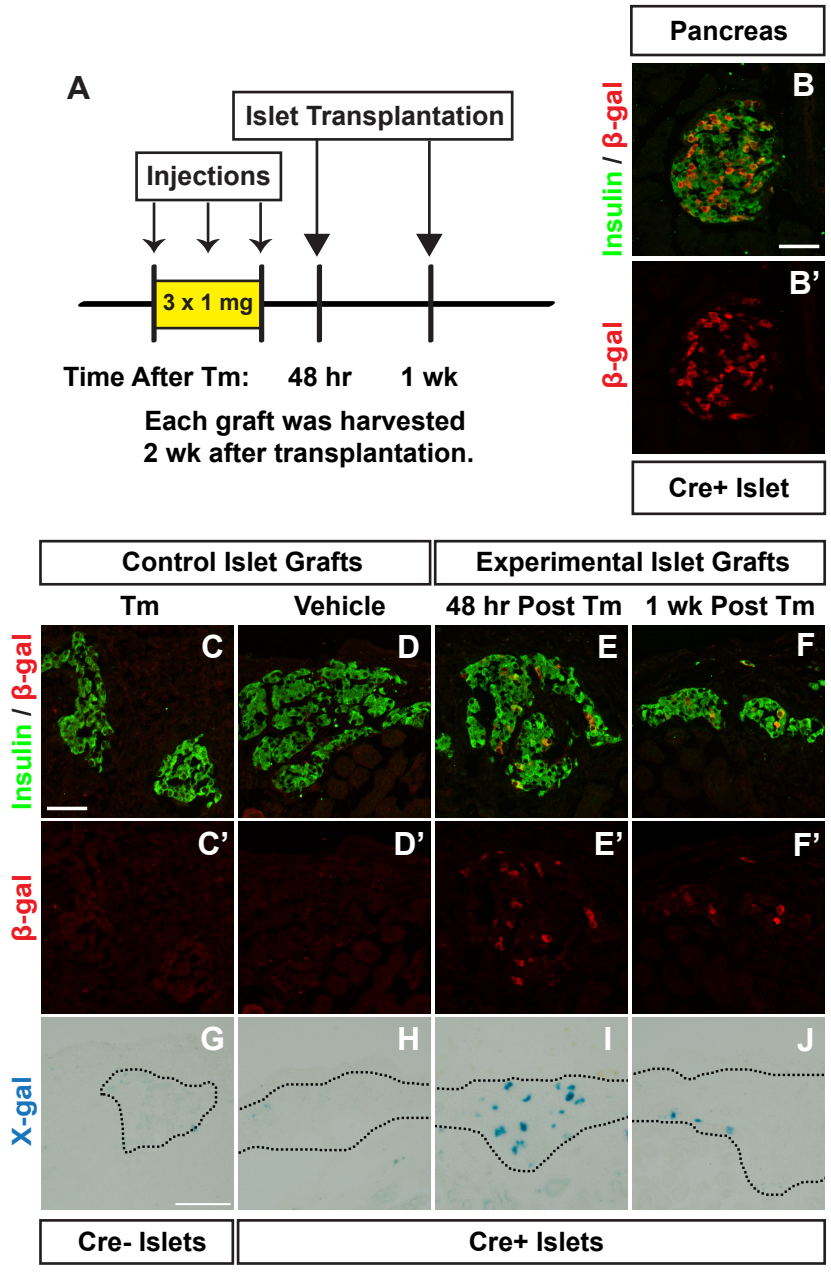

Figure 60. Lower dose tamoxifen induces recombination up to one week following administration. A. Islets from untreated *Pdx1*^{PB}*-CreER*^{Tm}*;R26-lacZ* (Cre+) mice or *R26-lacZ* (Cre-) controls were transplanted into mice given three subcutaneous injections of 1 mg tamoxifen (Tm) or vehicle at the indicated times following the last injection. **B.** Representative islet from a Cre+ mouse treated with 3 x 1 mg Tm, labeled with antibodies to insulin (green) and β-galactosidase (β-gal, red). Scale bar is 50 μm. **C-F.** Islet graft cryosections were labeled with antibodies to insulin (green) and β-gal (red). Scale bar in **C** is 50 μm, and applies to panels **D-F. G-J**. β-gal activity was evaluated in islet grafts by X-gal staining. Scale bar in **G** is 100 μm, and applies to panels **H-J**.

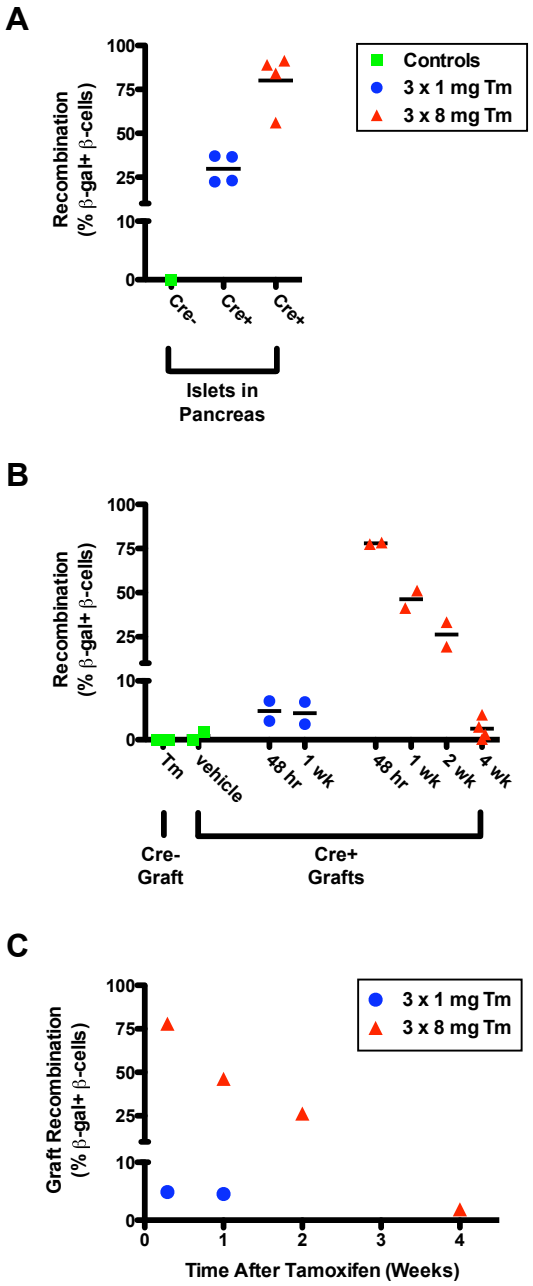

Figure 61. The duration of tamoxifen-induced gene recombination is dose-dependent. The percentage of insulin+ β-cells expressing β-gal in islets from pancreas sections (**A**) and from transplanted islet grafts (**B**) is shown. Each data point represents the percentage of double-positive cells to all insulin+ β-cells counted in a single mouse sample. Cre-, *R26-lacZ* control islets; Cre+, *Pdx1*^{PB}*-CreER*^{Tm}*;R26-lacZ* islets; Tm, tamoxifen. **C**. Amount of recombination observed in islet grafts from mice given either 3 x 1 mg or 3 x 8 mg tamoxifen at the indicated time points following the last tamoxifen injection. Data in **C** is expressed as means of data in **B**.

islets transplanted into Tm-treated mice showed recombination rates higher than vehicle-treated controls, independent of Tm dose or time of transplantation. While recombination in *Pdx1*^{PB}-*CreER*^{Tm};*R26-lacZ* islet grafts from mice receiving 3 x 1 mg Tm was relatively low at both the 48-hour and 1-week post-treatment time points, compared to islets in the pancreas of mice receiving 3 x 1 mg Tm, the recombination seen in *Pdx1*^{PB}-*CreER*^{Tm};*R26-lacZ* islet grafts from mice receiving 3 x 8 mg Tm was substantial for 2 weeks following Tm administration (Figure 61B). Importantly, *Pdx1*^{PB}-*CreER*^{Tm};*R26-lacZ* islet grafts from mice treated with 3 x 8 mg Tm showed recombination at a rate higher than controls even 4 weeks after treatment (Figure 61B). The estimated kinetics of Tm-induced recombination in this model system are plotted in Figure 61C.

Side effects of tamoxifen treatment in adult mice

At both doses, Tm-treated mice experienced major side effects that have not been mentioned in recent publications. The corn oil vehicle itself was incompletely absorbed in some mice, as indicated by subcutaneous masses found in the area of injection in both vehicle-treated and Tm-treated mice (Figure 62A). Upon dissection, these masses contained pockets of transparent oil, with no signs of inflammation or infection. Oil pockets were especially prevalent in female mice, and lasted for weeks or months after Tm administration. Additionally, male mice treated with Tm, but not corn oil vehicle alone, experienced dramatic scrotal enlargement (Figure 62B). This enlargement was first observed one week after Tm administration and lasted for at least three months (the last observed time point). All of the Tm-treated male mice described in this Dissertation developed this abnormality to some degree. While higher Tm doses did cause more

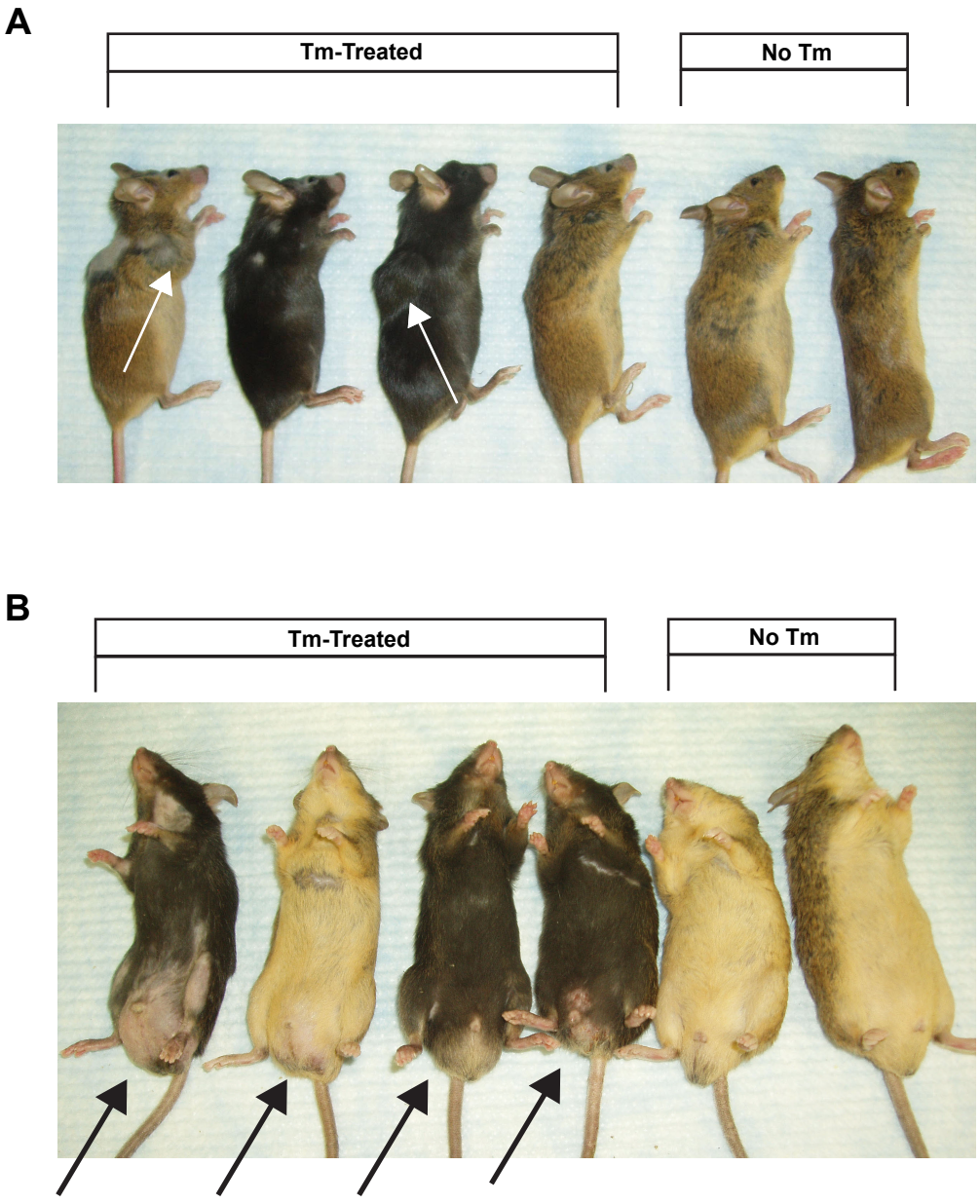

Figure 62. Anatomic changes following tamoxifen treatment. A. Some mice given subcutaneous injections of corn oil vehicle with or without tamoxifen (Tm) had subcutaneous accumulation of oil (white arrows) weeks and months following the last oil injection. **B**. Tm-treated male mice demonstrated scrotal enlargement (black arrows) as early as one week after treatment and lasting for months. Tm-treated mice shown were given 3 x 8 mg Tm, but similar results were observed in mice given 3 x 1 mg Tm.

dramatic anatomic changes, variability was seen between mice given identical doses. Some mice were more bothered by the scrotal changes, and developed self-inflicted wounds. Upon dissection, no changes were observed in the size of male reproductive organs or perigonadal fat pads. However, the fat appeared to envelop the testes more loosely in Tm-treated mice, and in some cases, loops of intestine were found to extend into the scrotum, indicating herniation. Histological examination of the male reproductive tract revealed no changes in reproductive organs, such as testis and epididymis, following Tm treatment (Figure 63A-B). Instead, Tm-treated males showed patches of edematous reactive fat containing spindle cells (Figure 63D). One mouse with extensive self-inflicted wounds showed chronic inflammation and fat necrosis within the preputial gland, located in the subcutaneous tissue adjacent to the penis (Figure 63F).

Discussion

Tm-inducible Cre-*loxP* systems are being used in broad areas of research and are providing important biologic insights in tissue development, maintenance, and function. However, our understanding of the parameters involved in recombination is incomplete. One unresolved issue regarding Cre-*loxP* recombination in adult mice is the length of time that Tm induces recombination. In this study, an *in vivo* bioassay using pancreatic islet transplantation was developed to directly measure recombination at specific times following Tm administration, thereby quantifying the biologic and pharmacologic half-life of Tm. It was found that: (1) administration of high Tm doses leads to extended CreER nuclear localization; (2) Tm administration induces reporter gene recombination for several days or weeks after Tm treatment is completed, depending on the original

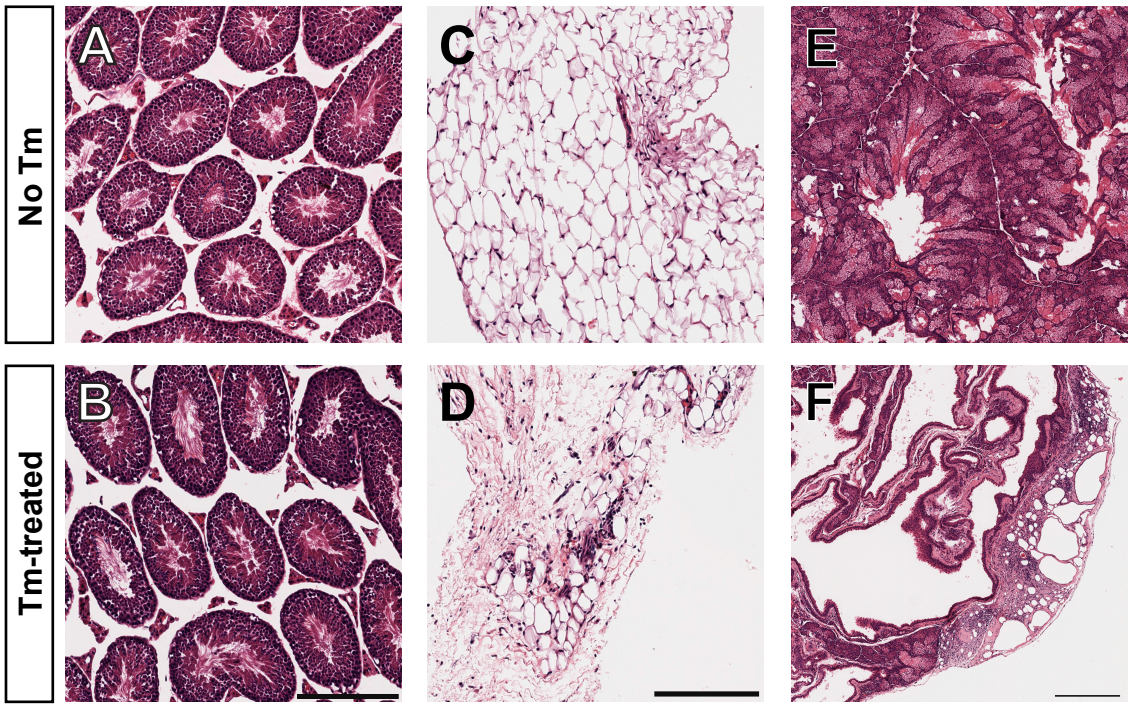

Figure 63. Histologic changes following tamoxifen treatment. A-F. H&E-stained sections of tissue from the scrota of control (**A, C, E**) and Tm-treated (**B, D, F**) male mice. **A-B**. Seminiferous tubules of the testes. Scale bar in **B** is 200 μm, and applies to panel **A. C-D.** Scrotal fat in a control mouse (**C**), compared to the reactive fat observed in a Tm-treated mouse (**D**). Scale bar in **D** is 200 μm, and applies to panel **C. E-F**. One Tm-treated mouse showed chronic inflammation and fat necrosis within the preputial gland (**F**); control gland, **E**. Scale bar in **F** is 400 μm, and applies to panel **E**.

dose administered; and (3) Tm treatment induces side effects that may have physiologic consequences in Tm-inducible models.

Multiple factors are involved in obtaining specific and effective Cre-*loxP* recombination *in vivo*, including (but not limited to) the promoter or enhancer driving expression of Cre recombinase, the accessibility of *loxP* sites in the target gene, and, for inducible systems, the Tm dose used (Buelow and Scharenberg, 2008; Feil et al., 1996; Hayashi and McMahon, 2002; Liu et al., 2010b). First, the chosen promoter or enhancer in a Cre driver mouse ideally targets Cre expression to specific cell types; in reality, transgenic mice do not express Cre in 100% of the targeted cells, and some transgenes show aberrant expression of Cre in untargeted cell types (Song et al., 2010; Wicksteed et al., 2010). Second, the accessibility of target *loxP* alleles to Cre recombinase can also impact recombination efficiency. For example, recombination of the *Z/AP* and *Z/EG* reporters is less efficient than recombination of reporter alleles from the *ROSA26* locus (Badea et al., 2009; Long and Rossi, 2009), and studies with these reporters may not necessarily reflect recombination of other target alleles (Liu et al., 2010b). Third, in addition to the wide range of Tm doses reported in the literature, there are a variety of Tm administration methods, from the use of Tm or its active metabolite 4-hydroxytamoxifen, to the drug preparation (oil suspensions vs. implanted pellets), and the route of administration (subcutaneous vs. intraperitoneal vs. oral). Finally, the data obtained using this bioassay demonstrate that the duration of Tm activity is another important variable to consider for Tm-inducible systems. In all, this wide range in model systems and methodology makes it difficult to compare different studies, and may contribute to the conflicting results reported in the pancreatic β-cell literature.

This bioassay was developed to directly assess the length of time that a given dose of Tm can induce Cre-*loxP* recombination *in vivo*. Early studies on Tm-induced Cre-*loxP* recombination utilized the rapid turnover of keratinocytes in epidermis to show that induction of reporter gene expression was limited to a few days after administration of relatively low doses of Tm (Brocard et al., 1997; Metzger and Chambon, 2001). Reporter gene-expressing keratinocytes that originated in the basal epidermal layer were found to have migrated out within one week of stopping Tm treatment, leaving unlabeled, newly generated cells below. Additionally, subcellular localization of Cre recombinase was correlated with Tm administration, as Cre was found in the keratinocyte nucleus in mice currently undergoing Tm treatment, but was localized to the cytoplasm three days after the final Tm dose.

In contrast to the doses used in those early experiments to evaluate the timeline of Tm activity in skin (Brocard et al., 1997; Metzger and Chambon, 2001), which were similar to the low dose used in this bioassay, many recent studies have used much higher Tm doses to achieve maximal recombination of reporter alleles in target tissues (Bonaguidi et al., 2011; Dorrell et al., 2011; Pellegrinet et al., 2011; Rawlins et al., 2009; Rock et al., 2009; Scholten et al., 2010). The rationale for using a higher Tm dose in studies utilizing Tm-inducible models in the pancreas (Abouna et al., 2010; Brennand et al., 2007; Dor et al., 2004; Liu et al., 2010a; Nakamura et al., 2011; Nir et al., 2007; Smukler et al., 2011; Thorel et al., 2010) include: (1) the transgenic mice commonly used to target pancreatic β-cells (*RIP-CreER*^{Tm} (Dor et al., 2004) and *Pdx1*^{PB}*-CreER*^{Tm} (Zhang et al., 2005) were generated using the *CreER*^{Tm} sequence (Danielian et al., 1998), which has been shown to be less sensitive to Tm than the *CreER*^{T2} sequence (Indra et al., 1999);

and (2) recombination efficiency is influenced by the accessibility of target *loxP* alleles to Cre recombinase (Liu et al., 2010b). The *Z/AP* reporter mouse has been frequently used to label pancreatic β-cells, and recombination of the *Z/AP* and *Z/EG* reporter alleles is less efficient than recombination of reporter alleles in the *ROSA26* locus (Long and Rossi, 2009). Although using the Tm dose that allows for maximal recombination is desirable, these data show that high doses of Tm can induce a prolonged period of Tm-induced Cre activity and unwanted side effects. Therefore, determining the optimal Tm dose for efficacy and safety will be particularly important in characterizing new model systems, including the recently described *MIP-CreER* mouse that targets β-cells (Wicksteed et al., 2010).

The subcellular localization of Cre recombinase was examined to estimate the time frame of potential recombination following Tm treatment. The fact that Cre was detected in nuclei of β-cells in the pancreas up to five weeks following the final Tm dose suggested that administration of Tm to adult mice induces a period of recombination that is much longer than the 12- to 48-hour window originally described in Tm-treated embryos (Gu et al., 2002; Hayashi and McMahon, 2002; Nakamura et al., 2006). Indeed, significant Tm-induced recombination was observed up to four weeks following drug administration, though perhaps to a lower extent than the number of β-cells showing nuclear localization of Cre might suggest. There are several possible reasons for this discrepancy in Cre subcellular localization and target gene recombination. Cre localization was analyzed in endogenous β-cells in the pancreas of transgenic mice, while the islet grafts had been transplanted under the kidney capsule of recipient mice. There may be differences in Tm availability at these two sites, because the pancreas was found

to have unexpectedly high concentrations of Tm compared to other tissues (Furr and Jordan, 1984; Lien et al., 1991). Additionally, the low blood flow experienced by newly transplanted islets may reduce the amount of Tm circulating to the β-cells, because revascularization of islet grafts takes several days to weeks to occur (Brissova et al., 2004). For these reasons, this islet graft model may in fact underestimate the amount of recombination that may occur in endogenous β-cells of Tm-treated mice. Alternatively, there may not be a direct correlation between Cre localization and recombination of target alleles; however, this is difficult to assess, because the amount of nuclear Cre required for inducing recombination is dependent on the sensitivity of the targeted floxed allele (Liu et al., 2010b; Long and Rossi, 2009), and may not necessarily be detected by immunohistochemistry. Importantly, these data show that evaluating Cre subcellular localization alone is not sufficient to estimate active recombination in a given cell.

Here, Tm was administered subcutaneously, as other groups have reported without noting side effects (Kopp et al., 2011b; Nir et al., 2007; Strobel et al., 2007b). While unexpected, the oil pockets observed are consistent with a report that described incomplete absorption of oil vehicles after an attempt to administer hormones subcutaneously to rodents (Deanesly and Parkes, 1933). In that study, the investigators collected the subcutaneous oil that remained days or weeks after injection and found that it still contained biologically active estrins. This observation raises the possibility that Tm itself is slowly and/or incompletely absorbed following subcutaneous injection, which could lead to the prolonged biologic activity observed in this study, and potentially to variability in Tm dosing between mice. Alternative Tm administration methods, such as implanted or food-based pellets, will prevent side effects associated with the oil vehicle.

However, the length of Tm action must still be determined for each of these treatment protocols.

The side effects observed in Tm-treated male mice were also surprising, because there has been little discussion of adverse events following Tm administration to adult transgenic mice (Anastassiadis et al., 2010; Guo et al., 2002; Hall et al., 2011; Vasioukhin et al., 1999). The pathologic changes in the scrota of Tm-treated mice appear to be limited to fat (and in one case, the preputial gland), and not to male reproductive organs. Instead, the scrotal swelling in Tm-treated mice closely resembles the scrotal hernias observed in male mice treated with estrogenic compounds, which were associated with hypertrophy of inguinal and scrotal skeletal muscle (Burrows, 1934; Gardner, 1936; Hazary and Gardner, 1960). Because Tm has mainly estrogenic actions in mice (Furr and Jordan, 1984), the hernias may be an indication that Tm treatment is promoting feminization of male mice. This is potentially concerning for investigators using these models for studies on metabolic diseases like diabetes. It is well known that wild-type male and female mice show differences in glucose tolerance (Bonnevie-Nielsen, 1982; Lavine et al., 1971), and some recent studies have reported that male mice are more susceptible to developing glucose intolerance following Cre-*loxP*-mediated inactivation of critical β-cell genes such as *Foxm1* and *Neurog3* (Wang et al., 2009; Zhang et al., 2006). Thus, it is important not only to include Tm-treated control groups to evaluate the drug's physiologic effects on the mice, but also to limit the Tm dose in order to minimize these effects.

In summary, this bioassay demonstrated that β-cells of adult mice can experience a prolonged period of Tm-induced nuclear localization of Cre recombinase, accompanied

by significant levels of Cre-*loxP* recombination for days and weeks after Tm treatment. These findings have important implications for the design and interpretation of experiments utilizing Tm-inducible systems. While a prolonged period of recombination is not necessarily undesirable in studies in which Tm is used to inactivate target genes, it is a critical parameter in lineage tracing experiments that rely on the induction of a reporter gene during a defined "pulse" period. Because many variables may affect Tm-induced recombination in a given model, the doses and timeline described here cannot be applied as strict guidelines for all Tm-inducible systems. Importantly, these data caution against the use of high Tm doses with the expectation that the effects of Tm are innocuous and short-lived. It is recommended that investigators carefully define the Tm dose and duration of action in each model system.

CHAPTER VI

GENERATING A MODEL OF INDUCIBLE KILLING OF PANCREATIC SCHWANN CELLS

Introduction

Peri-islet Schwann cells (pScs) have been described in multiple morphological studies (Donev, 1984; Smith, 1975; Sunami et al., 2001), and have been shown to be targeted by the immune system in humans with type 1 diabetes and in the non-obese diabetic (NOD) mouse (Tsui et al., 2008a; Winer et al., 2003), but their role in islet physiology remains unknown. The goal of the studies presented in this Chapter was to develop a cell ablation approach that would test the hypothesis that pScs are required for normal islet function *in vivo*.

In the past, *in vivo* cell ablation and inactivation techniques have generally involved the administration of a drug with relative specificity for the targeted cell type. For example, the glucose analogs alloxan and streptozotocin have been used to destroy β-cells in mice to induce hyperglycemia or to study β-cell regeneration. While these drugs have a relative specificity for the GLUT2 glucose transporter on β-cells, renal and hepatic toxicity are associated with treatment (Lenzen, 2008). In studies examining the role of glial cells in the nervous system, fluorocitrate and L-aminoadipic acid are used as gliotoxins to affect cell metabolism and function(Baudoux and Parker, 2008; Paulsen et al., 1987).

The advent of transgenic mouse technology has greatly advanced our ability to develop models of targeted cell ablation. In the *RIP-cMycER* mouse, the rat insulin promoter (*RIP*) drives β-cell-specific expression of a fusion protein composed of the proto-oncogene c-Myc and a mutated estrogen receptor. When tamoxifen is administered, nuclear translocation of c-Myc leads to cell death (Pelengaris et al., 2002). Similarly, the PANIC-ATTAC mouse displays apoptosis of β-cells following chemically induced activation of caspase 8 (Wang et al., 2008).

A similar approach is to target expression of the human diphtheria toxin receptor (DTR) to specific mouse tissues. Because the mouse equivalent of this receptor does not bind DT, DT protein can be administered to the mouse to induce a cell-specific inhibition of protein synthesis and subsequent cell death without any detectable side effects in non-targeted tissues. As an example, male *RIP-DTR* mice, in which most β-cells express DTR, will experience hyperglycemia and almost complete β-cell loss following treatment with DT (Thorel et al., 2010). To increase the utility of this approach, *R26-DTR* mice were generated to allow for the ubiquitous expression of *loxP*-STOP-*loxP*-DTR from the *ROSA26* locus (Buch et al., 2005). Following Cre-mediated recombination and removal of the STOP sequence, DTR is expressed in the target cell type.

In this Chapter, the DT-DTR approach was used to target pScs or neural crest-derived cells using *Plp1-CreER*^{T2};*R26-DTR* or *Wnt1-Cre*;*R26-DTR* mice, respectively (Figure 64). Because these two mouse models demonstrate Cre expression in cells outside of the pancreas, and would likely experience widespread cell death following global administration of DT, a surgical method was developed to administer DT specifically to the pancreas of adult mice.

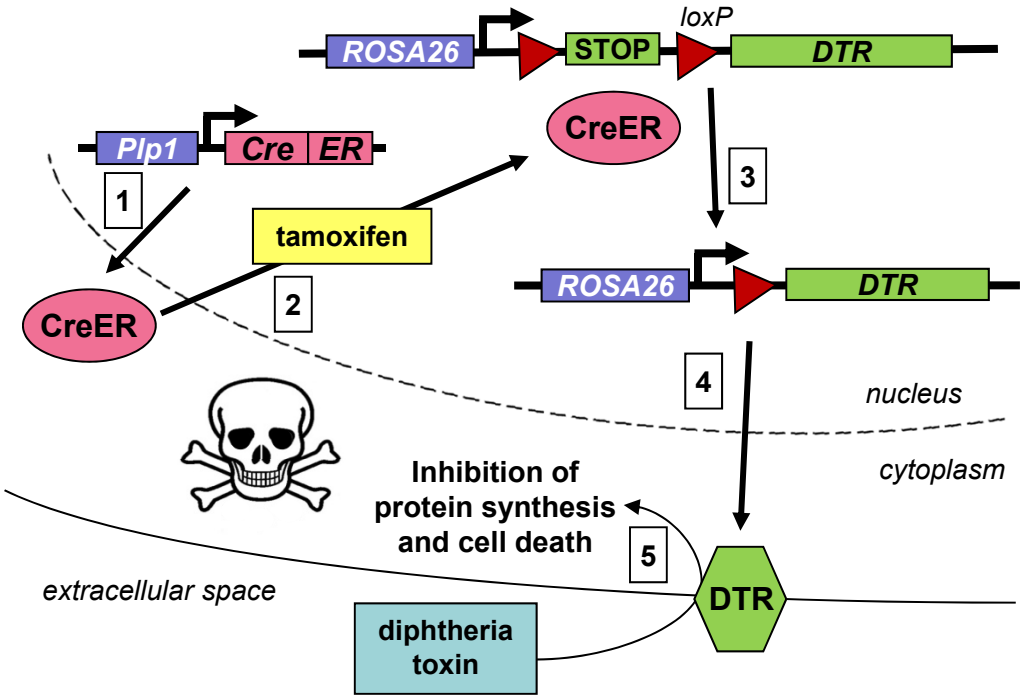

Figure 64. Proposed model for inducible ablation of peri-islet Schwann cells in *Plp1-Cre;R26-DTR* mice.

Results

Validation of intrapancreatic injection of diphtheria toxin

First, the *Ins2-Cre;R26-DTR* mouse model was used to test the concept of intrapancreatic (IPa) injection of DT, as intraperitoneal (IP) injection of DT in this model induces hyperglycemia, a marker of β-cell death. Other controls for this experiment included *R26-DTR* mice given an IPa injection of DT and *Ins2-Cre;R26-DTR* mice that underwent a sham operation with IPa administration of saline.

IPa injections were administered to both the duodenal and splenic portions of the pancreas, as described in Chapter II. Following IPa injection of DT or saline, a focal pocket of clear fluid could be observed within the pancreatic tissue (Figure 65, arrows). On occasion, limited bleeding would occur during the procedure, but overall the procedure was well tolerated by the mice.

In the first round of experiments, mice were given 25 ng of DT, but none of the mice experienced hyperglycemia after one week. When the DT dose was increased to 50 ng, both IPa and IP administration led to hyperglycemia in *Ins2-Cre;R26-DTR* mice but not *R26-DTR* controls. However, blood glucose levels had normalized in these mice ten days after the surgery.

Next, the dose was increased to 1 μg, with the reasoning that excessive doses would not be harmful in this experimental model. With this dose, DT-injected *Ins2-Cre;R26-DTR* mice showed rapid, dramatic hyperglycemia (>600 mg/dl, the upper limit of the glucometer measurement; Figure 66A-B). Both IP and IPa injection of 1 μg DT induced a similar degree of hyperglycemia in *Ins2-Cre;R26-DTR* mice after only a few days. However, in both males and females, the hyperglycemia peaked a few days later in

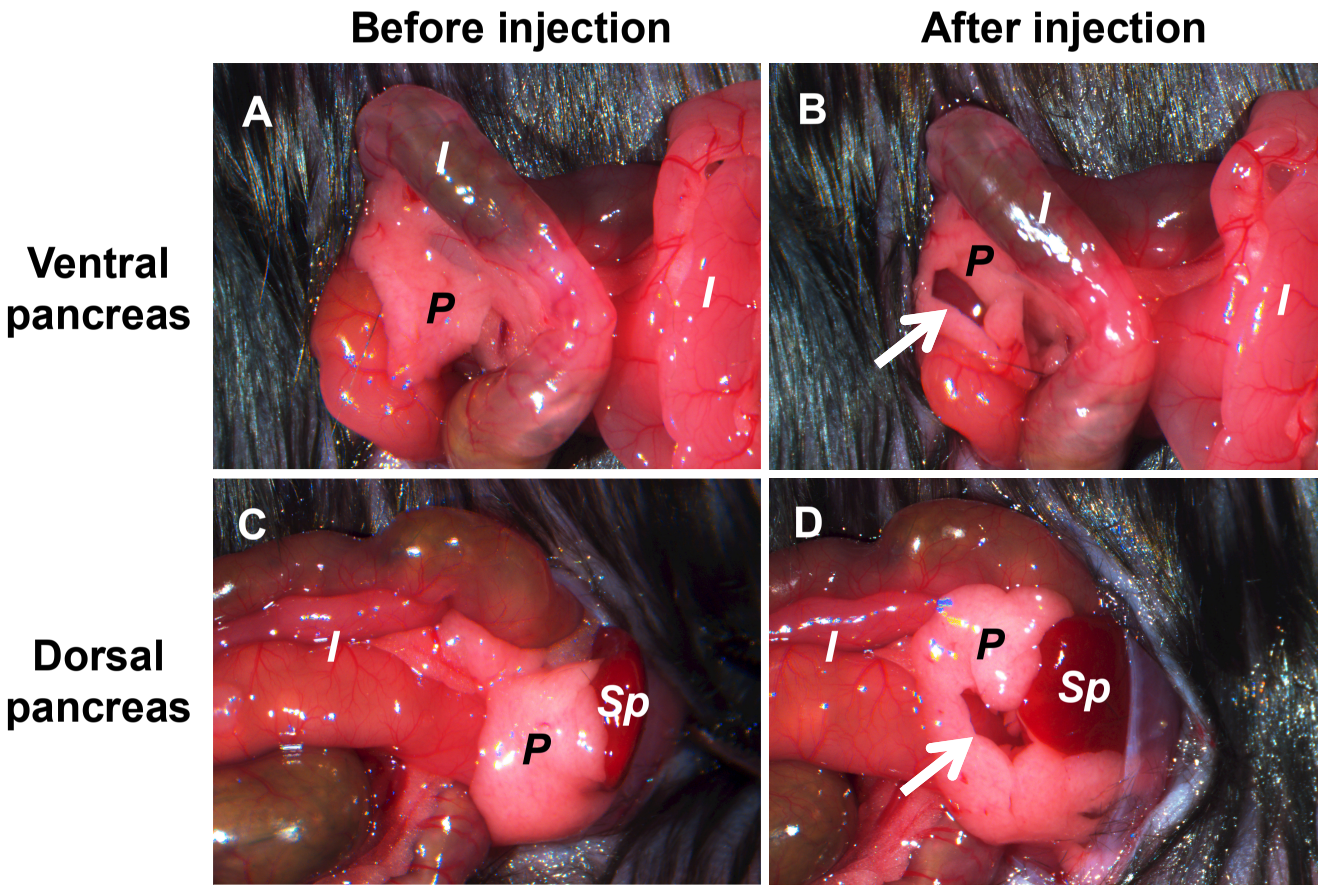

Figure 65. Intrapancreatic administration of diphtheria toxin. The ventral (**A, B**) and dorsal (**C, D**) parts of the pancreas were exposed and carefully injected with a total of 100 µl diphtheria toxin (arrows in **B** and **D**). *P*, pancreas; *I*, intestine; *Sp*, spleen.

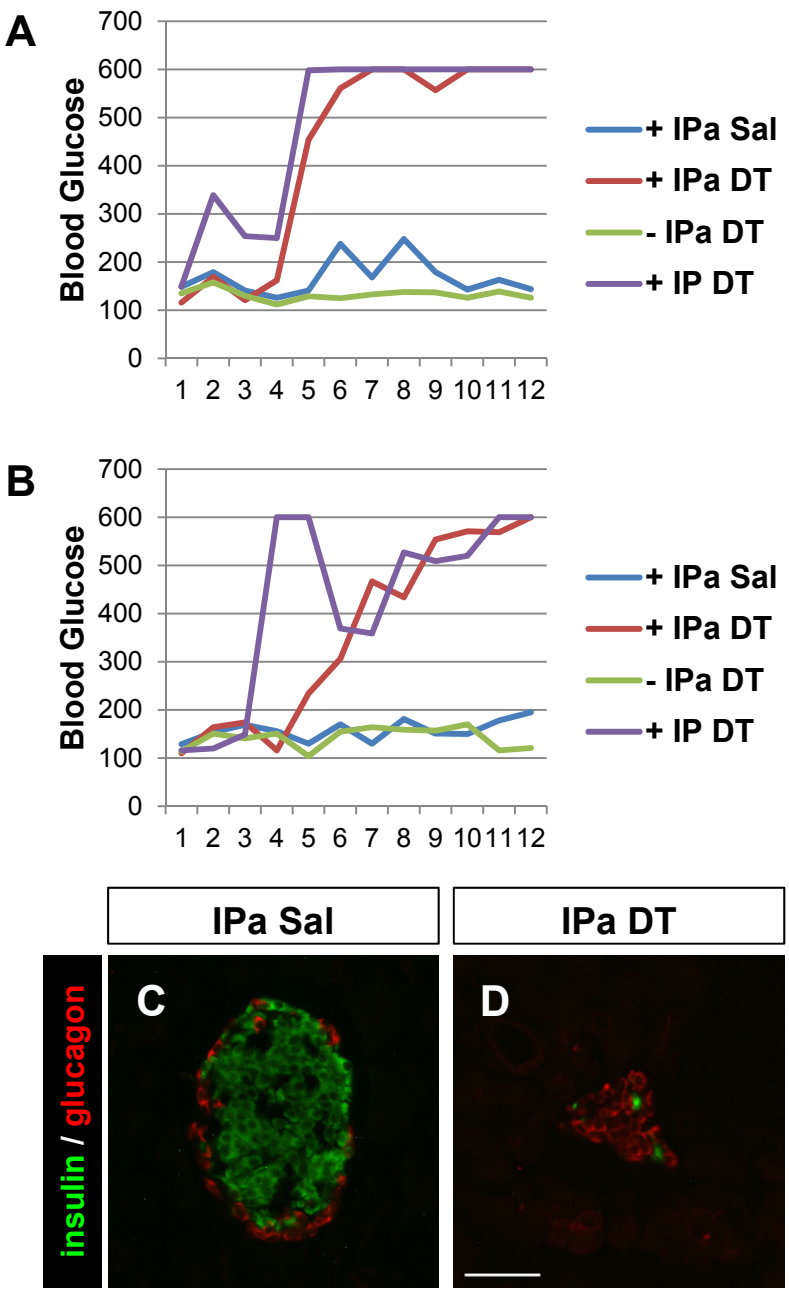

Figure 66. Intrapancreatic administration of diphtheria toxin destroys β-cells in *Ins-Cre;R26-DTR* mice. A-B. Nonfasting blood glucose values following intrapancreatic (IPa) or intraperitoneal (IP) administration of saline (Sal) or diphtheria toxin (DT) to male (**A**) and female (**B**) *Ins-Cre;R26-DTR* (+) mice and *R26-DTR* controls (-). Time points on the X-axis represent measurements taken on separate days. Measurement 1 was taken 4 days before surgery. Measurement 2 was taken on the day of surgery. All remaining values were obtained daily following surgery. Pancreata were harvested after the last reading. **C-D.** Immunohistochemistry of islet morphology following IPa administration of saline (**C**) or DT (**D**). Insulin, green; glucagon, red. Scale bar in **D** is 50 μm, and applies to panel **C**.

mice given IPa DT, perhaps reflecting slower diffusion of DT from the IPa injection. In contrast, IPa saline-treated *Ins2-Cre;R26-DTR* mice and IPa DT-treated *R26-DTR* mice remained normoglycemic throughout the experiment (Figure 66A-B).

To confirm that the hyperglycemia observed in DT-treated *Ins2-Cre;R26-DTR* mice was the result of β-cell loss, pancreatic cryosections were immunolabeled for insulin and glucagon. In contrast to the normal islet morphology observed in *Ins2-Cre;R26-DTR* mice given IPa injections of saline (Figure 66C), very few β-cells were found in *Ins2-Cre;R26-DTR* mice given IPa DT (Figure 66D). These data indicated that IPa injection is an effective method of DT administration.

Attempt to generate an inducible model to target pancreatic Schwann cells

In an attempt to induce expression of the DT receptor in pancreatic Schwann cells, *Plp1-CreER^{T2}* mice were used, because *GFAP-Cre* mice were noted to have surprisingly poor expression of Cre recombinase in nonmyelinating Schwann cells of the peripheral nervous system (Zhuo et al., 2001). Therefore, hemizygous *Plp1-CreER^{T2}* mice were crossed with the *R26-lacZ* reporter strain to evaluate Cre expression in peri-islet Schwann cells. Young *Plp1-CreER^{T2};R26-lacZ* mice were treated with 3 x 2 mg Tm, a dose comparable to that used by those who designed the transgenic line (Doerflinger et al., 2003), to induce nuclear localization of Cre and recombination of the reporter allele. However, no evidence of β-galactosidase expression or X-gal staining was observed (data not shown). Therefore, this Cre line was not usable for the desired studies.

Using a neural crest-specific model to test intrapancreatic injection of diphtheria toxin

Because the proposed *Plp1-CreER*^{T2} model did not immediately show promising results, an alternative approach was pursued using IPa DT injection in *Wnt1-Cre*;*R26-DTR* mice, in which Cre-mediated recombination would induce expression of DTR in peri-islet Schwann cells. However, because *Wnt1-Cre* mice have broad Cre-mediated recombination in neural crest-derived cells (Jiang et al., 2000), this approach would also target several cell types in the body, including nerves and Schwann cells throughout the peripheral nervous system. Therefore, it was used as a proof-of-principle experiment to test whether IPa administration of DT would result in targeted cell death confined to the pancreas.

In the first round of experiments, 500 ng DT was administered IPa to *Wnt1-Cre*;*R26-DTR* mice and *R26-DTR* controls. Surprisingly, IPa-injected *Wnt1-Cre*;*R26-DTR* mice were found dead four days after the surgery, after showing a successful initial recovery from the procedure. Because that dose of DT was suspected to be toxic, a lesser dose of 50 ng DT was tested next. Following IPa DT, one *Wnt1-Cre*;*R26-DTR* mouse demonstrated transient hyperglycemia with a 10% weight loss, and another mouse showed a 22% weight loss six days post surgery. Upon dissection, the second mouse showed a small, very pink pancreas and large, potentially dilated colon. However, no changes were observed in global pancreatic innervation using immunohistochemistry (data not shown).

Next, an intermediate dose of 250 ng was used, but the IPa DT-treated mouse experienced seizures three days after surgery, accompanied by a decreased random blood

glucose level (~90 mg/dl). Finally, a 100 ng dose was found to induce hypoglycemia in one mouse two days after surgery, but also resulted in death one day later.

To evaluate the ability of 100 ng DT to kill neural crest-derived cells in the pancreas, IPa-injected mice were sacrificed at the onset of hypoglycemia, three days after surgery. Before dissection, IPa DT-treated *Wnt1-Cre*;*R26-DTR* mice demonstrated reduced movement within the cage and opacification of the eyes. Upon dissection, the intestines of DT-treated *Wnt1-Cre*;*R26-DTR* mice were dusky, distended, and firm, compared to the pink, soft intestines of saline-treated controls. All other abdominal organs appeared normal. To evaluate the efficacy of DT-induced death of neural crest-derived cells in the pancreas, immunohistochemistry was performed on pancreatic sections from these mice. In DT-treated *Wnt1-Cre;R26-DTR* mice, TUJ1+ nerves and GFAP+ Schwann cells were still present in the pancreas (Figure 67A, C, D, F), though some areas were only sparsely innervated. Interestingly, TH+ nerve fibers were noticeably reduced in the pancreas of DT-treated *Wnt1-Cre;R26-DTR* mice, while DT-treated *R26-DTR* controls showed TH+ fibers throughout the pancreas (Figure 67B, E).

Discussion

The goal of the experiments described in this Chapter was to develop a method in which the role of peri-islet Schwann cells could be targeted for study *in vivo*, by administering diphtheria toxin (DT) to transgenic mice. Because there is no known way to specifically target peri-islet Schwann cells, an intrapancreatic (IPa) injection model was first developed and validated by inducing hyperglycemia in *Ins2-Cre;R26-DTR* mice. Then, IPa injection of DT was evaluated for its ability to kill neural elements in the

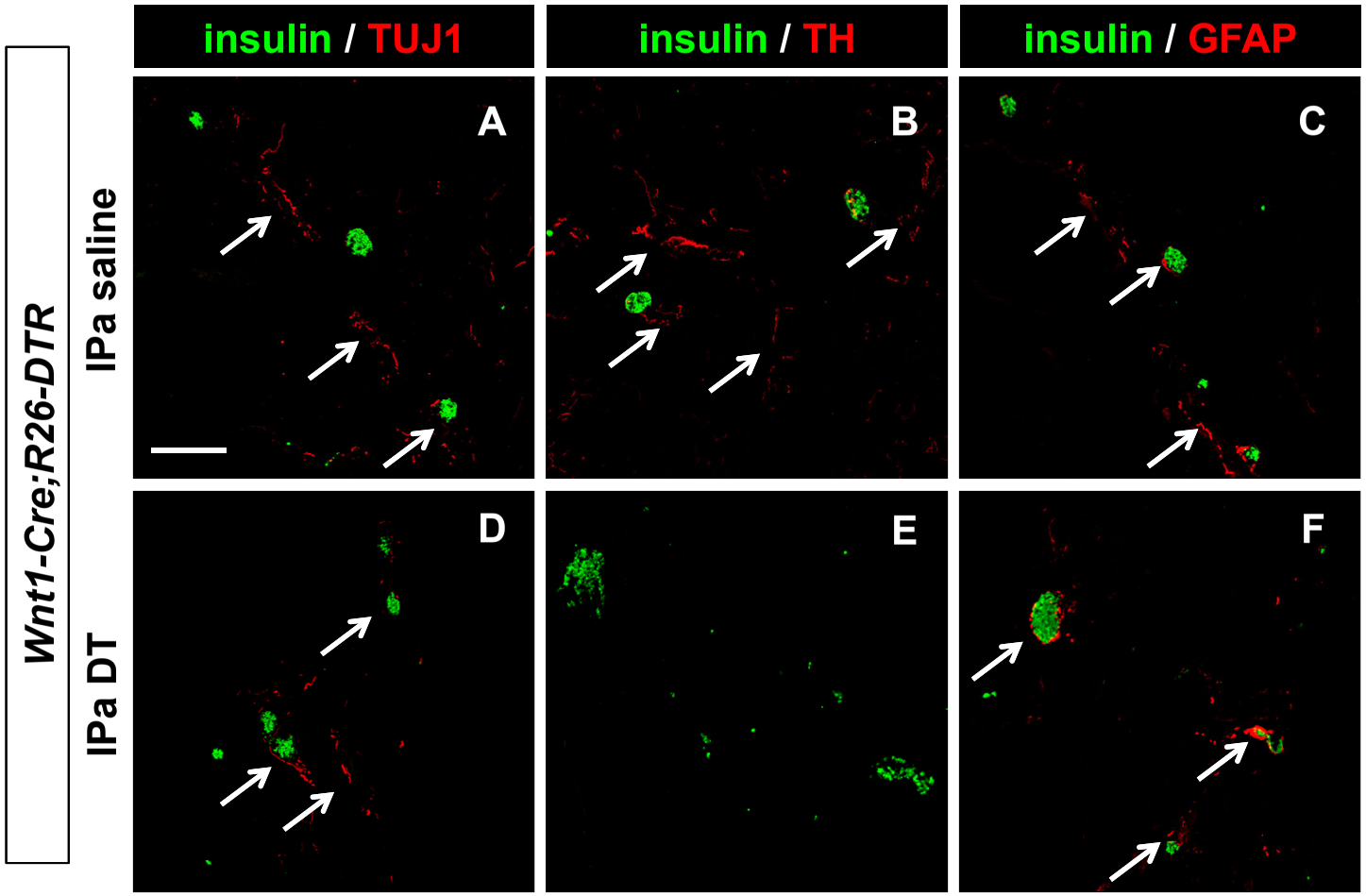

Figure 67. Intrapancreatic (IPa) administration of diphtheria toxin incompletely targets nerves and glia in *Wnt1-Cre;R26-DTR* mice. Compared to saline-treated controls (**A-C**), diphtheria toxin (DT)-treated *Wnt1-Cre;R26-DTR* mice display TUJ1+ nerve fibers (**D**) and GFAP+ glia (**F**), but demonstrate a loss of tyrosine hydroxylase (TH)-expressing neurons (**E**). Neural elements are indicated by arrows. Scale bar in **A** is 200 μm, and applies to all panels.

pancreas of *Wnt1-Cre;R26-DTR* mice; however, a dose that would target pancreatic nerves and glia without disrupting the extrapancreatic nervous system was not found.

Although IPa DT in *Ins2-Cre;R26-DTR* mice resulted in hyperglycemia, it was impossible to determine whether or not the injected DT reached the bloodstream by escaping the pancreas. Indeed, it appears that extrapancreatic effects of DT, i.e., decreased gut motility, killed *Wnt1-Cre;R26-DTR* mice. This phenotype is similar to that observed in a study on the enteric nervous system, which showed that small intestine motility was inhibited following treatment with the gliotoxin fluorocitrate (Nasser et al., 2006).

While IPa DT appeared to damage the enteric nervous system of *Wnt1-Cre;R26-DTR* mice, it did not completely destroy pancreatic nerves and glia. This is somewhat surprising; since *Wnt1-Cre;R26-EYFP* mice were used to genetically label these cells, it was expected that neural crest-derived glia in *Wnt1-Cre;R26-DTR* mice would express the DT receptor and succumb to cell death resulting from an inhibition in protein synthesis. However, it is possible that pancreatic innervation was affected, and that cell death would have occurred if the mice had survived longer. The TUJ1 and GFAP markers label structural elements in the cell, while TH labels an enzyme that presumably has a more rapid turnover. Therefore, decreased TH expression in *Wnt1-Cre;R26-DTR* mice could be a sign of inhibited protein synthesis that precedes cell death.

Because peri-islet Schwann cells could not be specifically targeted in the current experimental design, a mouse model that would more specifically target glial cells in the pancreas is needed. The feasibility of the approach using *Plp1-CreER*^{T2} mice was not completely explored after the DT leakiness was revealed in the *Wnt1-Cre;R26-DTR*

model. It is possible that the *Plp1-CreER*^{T2} model requires higher Tm doses or Tm administration earlier in life to induce CreER translocation and subsequent recombination. However, this model will still show extrapancreatic expression of DTR+ cells, so side effects would likely still be observed, even with IPa DT administration.

Intrapancreatic administration of DT was itself well tolerated by the mice, and no side effects were observed in injected control animals. An alternative approach would be IPa adminstration of the gliotoxin fluorocitrate (Nasser et al., 2006), although its effect on islet endocrine cells is unknown. Alternatively, mice could be infected with an adenovirus encoding DT protein itself under the control of a Schwann cell-specific promoter, such as *Gfap*. Intrapancreatic administration of adenovirus has been used to reprogram pancreatic acinar cells into β-cells (Zhou et al., 2008), so this may currently be the most promising approach to target peri-islet Schwann cells.

CHAPTER VII

CONCLUSION

Significance

The overall goal of this Dissertation was to advance understanding of the interrelationship between islet vascularization, innervation, and function. Specifically, VEGF-A was identified as a major factor coordinating these elements within the pancreatic islet. The roles of VEGF-A in pancreatic islet development and maturity are shown in Figure 68, and summarized below.

VEGF-A is the main factor involved in recruiting endothelial cells during early pancreas development (Brissova et al., 2006; Lammert et al., 2003b; Pierreux et al., 2010). Islet endocrine cell clusters produce angiogenic factors to become vascularized and exposed to blood flow as early as E13.5, the beginning of mature islet formation (Brissova et al., 2006). While neural crest-derived cells, which include nerves and Schwann cells, are present in the pancreas at this time, they begin to interact with endocrine cells of developing islets slightly later, between E13.5 and E15.5 (Plank et al., 2011). However, neural crest-derived cells remain localized to the periphery of developing islets until the postnatal period. In fact, nerve fibers are not consistently found within the islet core until the weaning stage, around three weeks after birth.

The studies described in Chapter III now define a novel role for VEGF-A and the intraislet vasculature in directing islet innervation. Before these studies, very little was known about the mechanisms directing nerve growth to the pancreas and islets. Here, the

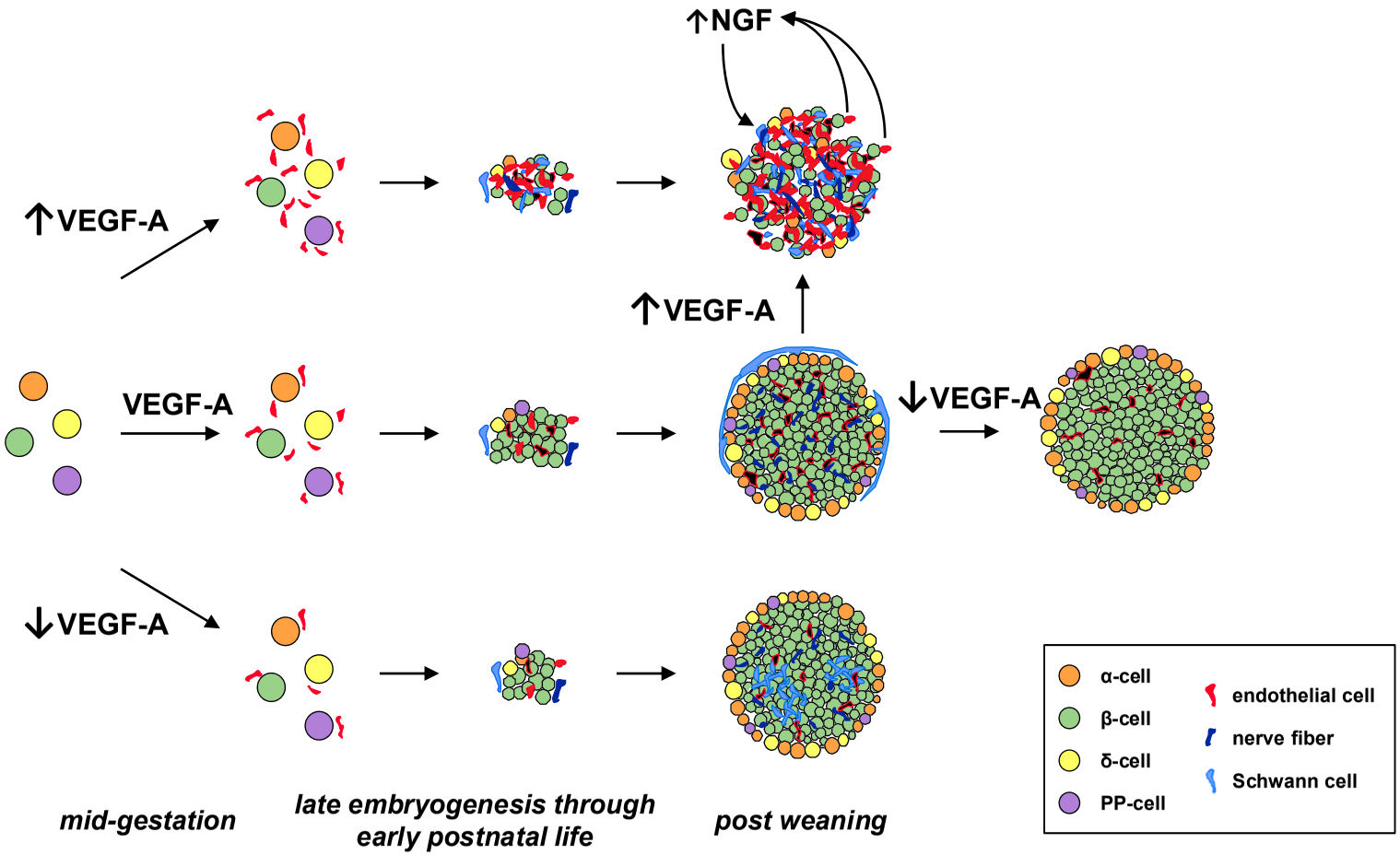

Figure 68. VEGF-A coordinates pancreatic islet vascularization and innervation. VEGF-A deficiency during development impairs islet vascularization and innervation, while VEGF-A excess leads to islet hypervascularization and hyperinnervation. Inactivation of VEGF-A in mature islets reduces islet vascularization, but the effects of VEGF-A inactivation on the innervation of mature islets is unclear (see Appendix).

use of multiple genetic mouse models revealed the requirement for VEGF-A in the formation of islet innervation. VEGF-A is not a direct signal to islet nerves, which do not express the VEGF-A receptors VEGFR2 or NRP1. Instead, VEGF-A is required for patterning of the intraislet vasculature during embryogenesis, and this established capillary network is required for nerve fibers to penetrate the islet core during postnatal islet development. In contrast, experimental induction of hypervascularization by VEGF-A overexpression, either in developing or mature islets, resulted in islet hyperinnervation. Using this model, it was found that endothelial cell-derived factors such as NGF and ECM proteins are likely important signals for neurite growth into the islet. Therefore, the coordinated development of islet vascularization, innervation, and function is dependent on a complex series of interactions between endocrine, endothelial, and neural cells of the pancreatic islet.

Normal pancreatic VEGF-A expression is critical for the recruitment of endothelial cells and the subsequent stimulation of endocrine cell proliferation during islet development. In addition, VEGF-A was also thought to be key in maintaining the function of mature islets, in part through recruiting endothelial cells that provided important signals for β-cells (Eberhard and Lammert, 2009; Olsson and Carlsson, 2006). However, the data presented in Chapter IV showed that intraislet endothelial cells were not as important as once thought. While VEGF-A is required to maintain the high vascular density and fenestrated endothelium of the islet, β-cells demonstrated resilience when faced with a long-term reduction in the intraislet vasculature. In fact, hypovascularized islets maintained β-cell gene expression, β-cell mass, and insulin secretion *in vitro*. These data suggest that while developing β-cells depend on signals that

endothelial cells provide, mature β-cells require less of this interaction for survival and function.

In addition to advancing knowledge of the role of VEGF-A and intraislet endothelial cells in pancreatic islet biology, the studies performed in this Dissertation have provided helpful insight into the use of transgenic mouse models, which has broad implications for biomedical research. Mouse models using Cre-*loxP* recombination are increasingly common in studies of tissue maintenance and organ function, particularly in the pancreas (Kawaguchi et al., 2011). The studies in Chapters IV and V highlighted experimental challenges that must be considered in the use of popular transgenic mouse models. Chapter IV described the surprising discovery that two widely used pancreas-targeted mouse models used in this Dissertation showed ectopic expression of a Cre recombinase transgene in the brain, a caveat that was revealed to be present in multiple current transgenic mouse strains targeting Cre to the pancreas (Wicksteed et al., 2010). Because some of these models have been used for years, the likely ectopic recombination of target genes has been overlooked in several studies, which may have led to erroneous interpretations of data. These findings will influence how investigators plan future studies using gene inactivation approaches within the pancreas.

Furthermore, the data presented indicate that tamoxifen action has a much longer duration than previously thought. Chapter V discussed the development of a bioassay using pancreatic islet transplantation to directly measure Cre-*loxP* recombination at specific times following tamoxifen treatment. Surprisingly, it was found that commonly used doses of tamoxifen could induce Cre-*loxP* recombination for weeks after the last tamoxifen dose. This is dramatically different from the 48 hour-long period of

recombination reported for embryos of tamoxifen-treated dams (Hayashi and McMahon, 2002). This work has considerable implications for all research using tamoxifen-inducible model systems, and particularly for studies using tamoxifen treatment to induce labeling of cells for "pulse-chase" lineage tracing. Because interpretations drawn from such studies are highly dependent on the assumption of a well-defined pulse period, this work provides critical information to investigators designing and interpreting lineage tracing experiments. In all, these results demonstrate important experimental caveats and challenges that must be considered when designing future experiments and when drawing conclusions from such experimental models.

Future Directions

The data presented in this Dissertation expand our knowledge on islet vascularization and islet innervation, two key factors in islet function. Here, some thoughts on intriguing future directions of this work are presented.

Following the inducible overexpression of VEGF-A in islets of adult mice, it was found that expansion of the intraislet endothelial cell population led to enhanced expression of NGF and several endothelial cell-derived proteins that compose the islet basement membrane, resulting in islet hyperinnervation. A pressing issue arising from these studies is the identification of specific endothelial cell-derived factors that control nerve pathfinding during postnatal development. Both endocrine and endothelial cells in the islet express proNGF during development (Cabrera-Vasquez et al., 2009). Therefore, it is likely that signals from both cell types stimulate ingrowth of nerve fibers into the islet, but these fibers require the prior formation of the intraislet capillary plexus and its

basement membrane by endothelial cells. Confirmation of the role of endocrine cell-derived and endothelial cell-derived NGF in this process would require the generation of a mouse model of conditional NGF inactivation. Because a myriad of basement membrane proteins could be important in mediating neurite migration into islets, a more straightforward approach would be to specifically inactivate extracellular membrane receptors in the neural crest before evaluation of islet innervation. For example, β1 integrin is important for migration of neural crest cells during gut development in both chicks and mice (Breau et al., 2009; Nagy et al., 2009), and would be a key candidate for this experiment.

One of the most surprising results of these studies was that hypovascularized islets, which were unable to recruit nerves during development, showed a dramatic increase in the number of islet endocrine cells expressing tyrosine hydroxylase (TH), the rate-limiting enzyme in catecholamine biosynthesis. Data on the potential of islet endocrine cells to synthesize and secrete catecholamines have been conflicting (Cegrell, 1968; Lundquist et al., 1989; Teitelman and Lee, 1987), though more recent studies suggest that islets do have endogenous TH enzymatic activity (Borelli and Gagliardino, 2001; Borelli et al., 2003). Recent data also suggest that islets have the ability to convert L-DOPA (the product of TH) into dopamine, which is released from β-cells as an autocrine signal to regulate hormone secretion (Ustione and Piston, 2012). Therefore, a more detailed investigation of islet expression of other proteins in the catecholamine biosynthetic and secretory pathways would elucidate whether TH expression is selectively upregulated in cells that are truly producing catecholamines. It would also be

interesting to examine whether islets enriched with TH+ endocrine cells show increased catecholamine synthesis and/or secretion, and if this affects hormone secretion.

It was previously suggested that TH+ islet cells represented a population of post-proliferative, senescent endocrine cells (Teitelman et al., 1988). However, the data presented in Chapter III do not support this hypothesis. Hypovascularized islets show a dramatic reduction in β-cell proliferation throughout life (Reinert and Brissova et al., manuscript in preparation), but do not demonstrate increased senescence-associated β-galactosidase staining. Furthermore, an increased number of TH+ endocrine cells was not observed in models of increased β-cell proliferation, as previously reported (Teitelman et al., 1988). The reasons for this discrepancy remain unclear, so a further investigation into the significance of TH+ endocrine cells is needed.

Other studies documented TH expression in early islet cells before and during the primary transition of pancreas development (Alpert et al., 1988; Teitelman and Lee, 1987). From these data, the authors suggested that TH expression marked endocrine precursor cells, though it is now known that those early endocrine cells do not compose a major portion of the mature endocrine pancreas (Gu et al., 2002; Herrera, 2000). TH expression is present in some endocrine cells throughout normal development, as shown in Chapter III and in those prior reports. The significant technological advances in genetic mouse models since these early studies were performed would allow for more precise ways to evaluate TH+ endocrine cells and determine their role in islet function. For example, lineage tracing could now be accomplished using a mouse model that combines a tamoxifen-inducible Cre driven by the TH promoter (Rotolo et al., 2008) with a reporter strain. Additionally, the role of TH in islet endocrine cells could be studied by genetic

inactivation of TH using an islet cell- or β-cell-targeted Cre mouse crossed with a *TH*$^{fl/fl}$ mouse (Hnasko et al., 2006; Tokuoka et al., 2011). Because of the ectopic expression of Cre in the brains of several islet-targeted Cre models, a genetic inactivation experiment would likely require a model with proven islet-specific expression, such as the *MIP-CreER* mouse (Wicksteed et al., 2010).

Both VEGF-A deficiency and VEGF-A overexpression disrupted the typical morphology and localization of peri-islet Schwann cells (pScs). Following VEGF-A inactivation, pScs in hypovascularized, hypoinnervated islets demonstrated reactive gliosis, with upregulation of GFAP expression, while pScs in VEGF-A-overexpressing, hypervascularized islets transformed into more broadly shaped cells. These data suggest that pScs are dynamic players within the islet microenvironment, and may become activated under certain circumstances, such as following hypoinnervation (Chapter III) or β-cell injury (Teitelman et al., 1998). However, the role of either normal pScs or reactive Schwann cells with the islets remains unknown. While genetic and chemical methods to specifically target pScs *in vivo* remain unavailable, the studies performed in Chapter VI, in which pScs were targeted for ablation by diphtheria toxin administration *in vivo*, could be continued *in vitro* to gain even an initial understanding of how pScs may function in islet physiology. It is unknown whether pScs may influence islet hormone secretion or endocrine cell proliferation. To address this, isolated islets with or without diphtheria toxin-mediated ablation of pScs could be studied in an *in vitro* perifusion system to test hormone secretion. Alternatively, the potential supportive role of pScs in islet function could be tested with the addition of purified pScs to cultured islets. One group has demonstrated the ability to isolate and culture pScs in order to define epitopes that may

be targeted by the immune system of NOD mice prior to autoimmune islet destruction (Tsui et al., 2008a). Furthermore, *GFAP-GFP* transgenic mice, which express GFP in glia, would allow for purification of pre-labeled pScs. This technique may enable sufficient numbers of pScs to be obtained for co-culture and co-transplant studies to investigate their capacity to promote β-cell proliferation, survival, and function.

There is great interest in improving our understanding of islet vascularization with an ultimate goal of enhancing islet revascularization during transplantation (summarized in Brissova and Powers, 2008). Because intraislet endothelial cells are important in directing islet innervation during development, they are likely necessary for islet graft reinnervation as well. In that case, optimizing islet revascularization would have the added benefit of promoting islet reinnervation. Supporting this concept, there is some evidence that the combination of VEGF and NGF added to islet grafts transplanted within the pancreas may enhance their functional reinnervation over the addition of NGF alone (Stagner et al., 2008). To test whether endothelial cells enhance reinnervation of islet grafts, transplantation of *RIP-rtTA;TetO-hVegfa* islets could be performed, followed by administration of Dox to the recipient to induce graft hypervascularization. It is hypothesized that the increased endothelial cell population will enhance reinnervation, as in the pancreas. However, because expansion of endothelial cells in this model is quite robust and leads to reduced β-cell mass, reinnervation would need to be studied with a lower level of VEGF-A expression.

As with all studies using model organisms, it is important to consider how faithfully mechanisms will be replicated in humans. While a close relationship between intraislet vessels and nerve fibers has been noted in adult humans (Rodriguez-Diaz et al.,

2011a), the relationship between the two structures has only been briefly explored in human development (Gregg et al., 2012). A detailed analysis of islet innervation during human pancreas and islet development is currently being undertaken by the Powers laboratory.

Two major questions regarding the role of islet vascularization in islet function deserve further attention: (1) do islets have strict temporal requirements for endothelial cells? and (2) do islets require a certain threshold of endothelial cells to maintain β-cell proliferation and function? Pancreas-wide inactivation of VEGF-A leads to a 70% reduction in intraislet vessel density and a lifelong reduction in β-cell proliferation (Reinert and Brissova et al., manuscript in preparation). In contrast, the tamoxifen-induced knockdown of VEGF-A in adult mice reduced islet vascular density by half, which had no apparent effect on β-cell mass maintenance in adult mice. It is possible that the amount of intraislet endothelial cells that persisted in the latter model was sufficient to maintain signaling to islet cells. In this case, the use of additional methods to further reduce the intraislet vasculature, such as inducible inactivation of other angiogenic or angiostatic genes, may reveal a threshold of endothelial cells required for the maintenance of endocrine cell proliferation and gene expression in mature islets. Alternatively, while endocrine cells in adult mice may no longer require endothelial cells, the potential role of intraislet endothelial cells in young mice remains unknown. Therefore, inactivation of VEGF-A in early postnatal life would help define a temporal requirement for VEGF-A in establishment of the intraislet vasculature and maintenance of normal β-cell gene expression, proliferation, and mass.

The tamoxifen-inducible model of VEGF-A inactivation presented in Chapter IV was used to address the question of whether the normal intraislet vasculature was required to maintain glucose tolerance in adult mice. However, this model demonstrated the surprising finding of insulin resistance, as determined by a hyperglycemic clamp study. As discussed in Chapter IV, the etiology of insulin resistance in this model remains unknown. While it is possible that the ectopic expression of Cre in the hypothalamus, and subsequent inactivation of VEGF-A in that tissue, could account for this phenotype, a more detailed analysis of the insulin-sensitive tissues is required to investigate other sites of ectopic recombination. Intriguingly, recent evidence has demonstrated a unique state of insulin resistance in lean subjects with well-controlled type 1 DM. In contrast to whole-body insulin resistance present in individuals with type 2 DM, insulin resistance in these subjects was specific to the liver and skeletal muscle, and not associated with classic predictors like obesity and hyperlipidemia (Bergman et al., 2012). Similar to insulin resistant patients with type 1 DM, mice with islet-targeted VEGF-A inactivation have some disruption in islet function, but do not have the obesity typical of type 2 DM models. Therefore, further analyses are needed to identify the source(s) of insulin resistance in the tamoxifen-inducible model, to determine if the phenotype aligns with the pattern of insulin resistance in type 1 or type 2 DM. It would also be helpful to carefully evaluate glucose metabolism in male mice at earlier time points following islet VEGF-A inactivation, to determine precisely when insulin resistance may arise. Additionally, clamp studies could be performed on female mice, which showed resistance to developing glucose intolerance, even in the setting of a high fat diet.

APPENDIX

STRAIN-DEPENDENT DIFFERENCES IN ISLET INNERVATION

Introduction

As described in Chapter III, VEGF-A and its role in the formation of the intraislet vasculature during development is crucial for the maturation of islet innervation. The data presented in this Appendix describe a preliminary attempt to evaluate islet innervation following the inducible inactivation of VEGF-A in mature islets of adult tamoxifen (Tm)-treated *Pdx1*^{PB}-*CreER*^{Tm};*Vegfa*$^{fl/fl}$ mice. Because the mixed background of *Pdx1*^{PB}-*CreER*^{Tm};*Vegfa*$^{fl/fl}$ mice was thought to result in the altered baseline islet innervation observed in this model, islet innervation was also described in four mouse strains.

Results

Evaluation of islet innervation following VEGF-A inactivation in mature islets

To investigate whether inducible inactivation of VEGF-A in mature islets would alter islet innervation, adult *Pdx1*^{PB}-*CreER*^{Tm};*Vegfa*$^{fl/fl}$ mice were treated with 3 x 1 mg Tm and islet morphology was evaluated by immunohistochemistry one to three months later.

First, the expression of TUJ1+ nerve fibers was examined in VEGF-A-deficient islets in Tm-treated *Pdx1*^{PB}-*CreER*^{Tm};*Vegfa*$^{fl/fl}$ mice. There appeared to be fewer TUJ1+ nerves in VEGF-A-deficient islets compared to controls (Figure A1). However, the density of intraislet nerves was reduced in these *Vegfa*$^{fl/fl}$ controls (on a mixed

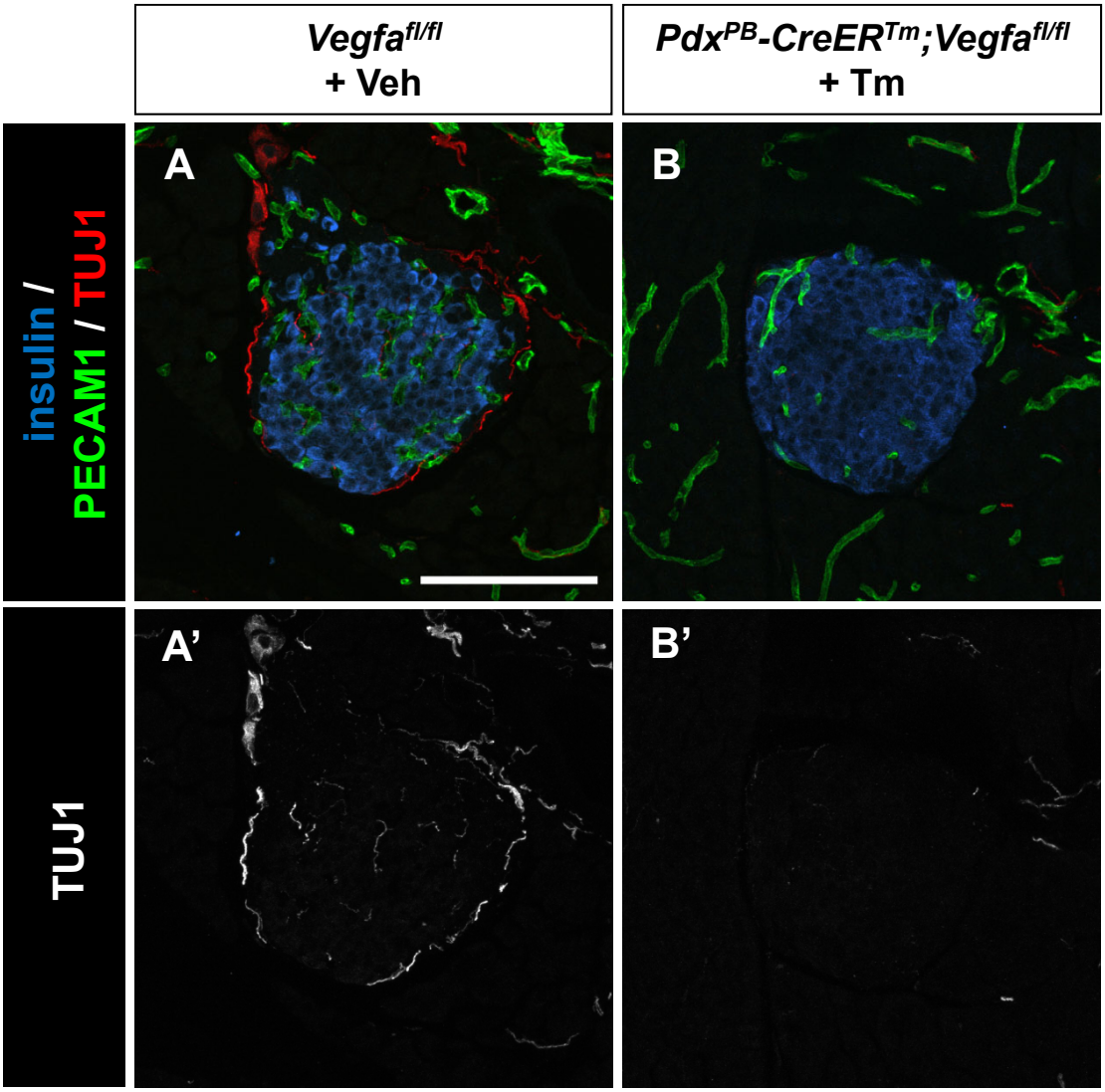

Figure A1. Islet nerve fiber density is reduced following tamoxifen-induced VEGF-A inactivation. Representative islets immunolabeled for insulin (blue), PECAM1 (green), and TUJ1 (red/grayscale). Islets shown were from mice sacrificed one month following Tm or Veh treatment. Scale bar in **A** is 100 μm and applies to all other panels.

background), as compared to the *Vegfa*$^{fl/fl}$ mice (on a C57BL/6J background) described in Chapter III.

The expression of GFAP and TH was also examined in VEGF-A-deficient islets in Tm-treated *Pdx1*^{PB}-*CreER*^{Tm};*Vegfa*$^{fl/fl}$ mice. Surprisingly, these VEGF-A-deficient islets did not display gliosis of GFAP+ Schwann cells (Figure A2). Similarly, the proportion of TH+ β-cells did not appear to be changed in islet from Tm-treated *Pdx1*^{PB}-*CreER*^{Tm};*Vegfa*$^{fl/fl}$ mice (Figure A3).

Evaluation of strain-dependent differences in islet innervation

To address whether there may be strain differences in islet innervation, four eight-week-old mice (two males and two females) of each of four mouse strains were obtained from The Jackson Laboratory: C57BL/6J (stock number 000664), DBA/1J (stock number 000670), FVB/NJ (stock number 001800), and 129S1/SvImJ (stock number 002448). These strains were chosen because they were previously evaluated for differences in whole-body glucose metabolism (Berglund et al., 2008). Pancreata were collected from these mice at ten weeks of age for analysis by immunohistochemistry.

Strain-dependent differences were observed in islet innervation, as islets in C57BL/6J mice showed a dense network of intraislet TUJ1+ fibers (Figure A4A), while islets in 129S1/SvImJ mice appeared to be more sparsely innervated (Figure A4D). Islets in DBA/1J and FVB/NJ mice showed an intermediate density of TUJ1+ nerve fibers (Figure A4B-C). In contrast, all four strains of mice showed a similar peri-islet arrangement of GFAP+ Schwann cells, with few GFAP+ fibers penetrating the islet core (Figure A5).

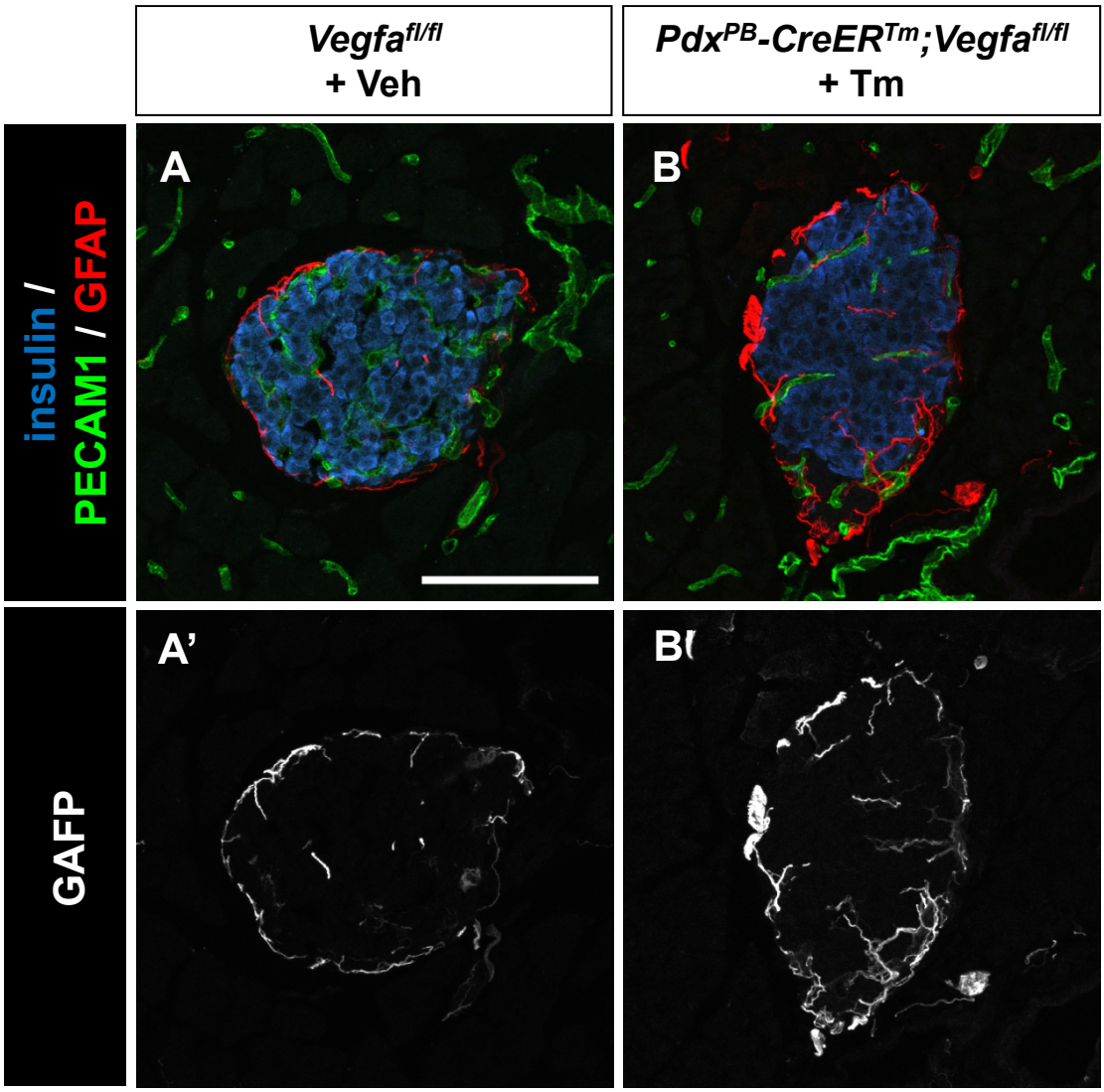

Figure A2. Peri-islet Schwann cells do not show gliosis following tamoxifen-induced VEGF-A inactivation. Representative islets immunolabeled for insulin (blue), PECAM1 (green), and GFAP (red/grayscale). Islets shown were from mice sacrificed one month following Tm or Veh treatment. Scale bar in **A** is 100 μm and applies to all other panels.

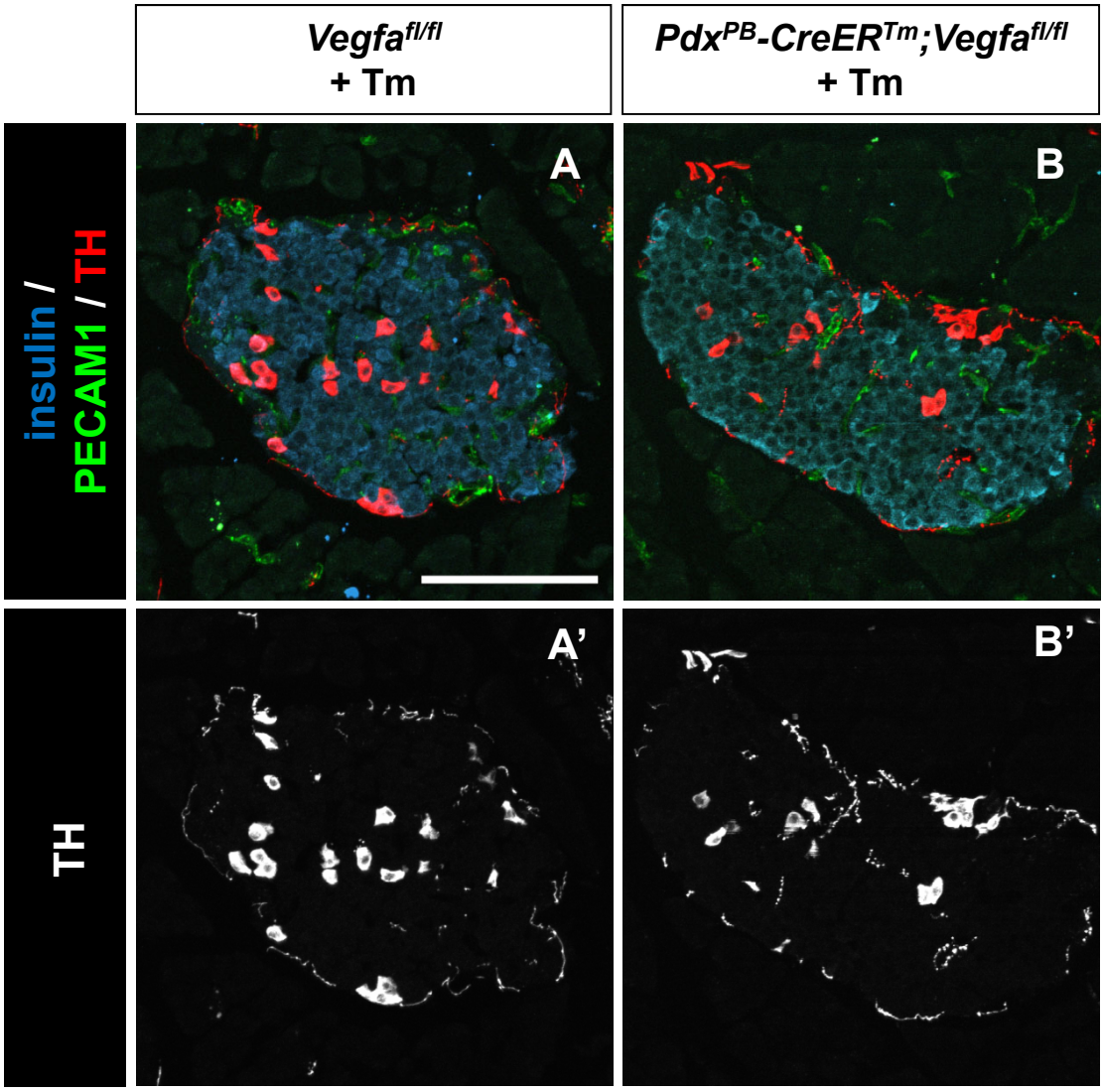

Figure A3. Islet sympathetic innervation is unchanged following tamoxifen-induced VEGF-A inactivation. Representative islets immunolabeled for insulin (blue), PECAM1 (green), and tyrosine hydroxylase (TH, red/grayscale). Islets shown were from mice sacrificed three months following Tm treatment. Scale bar in **A** is 100 μm and applies to all other panels.

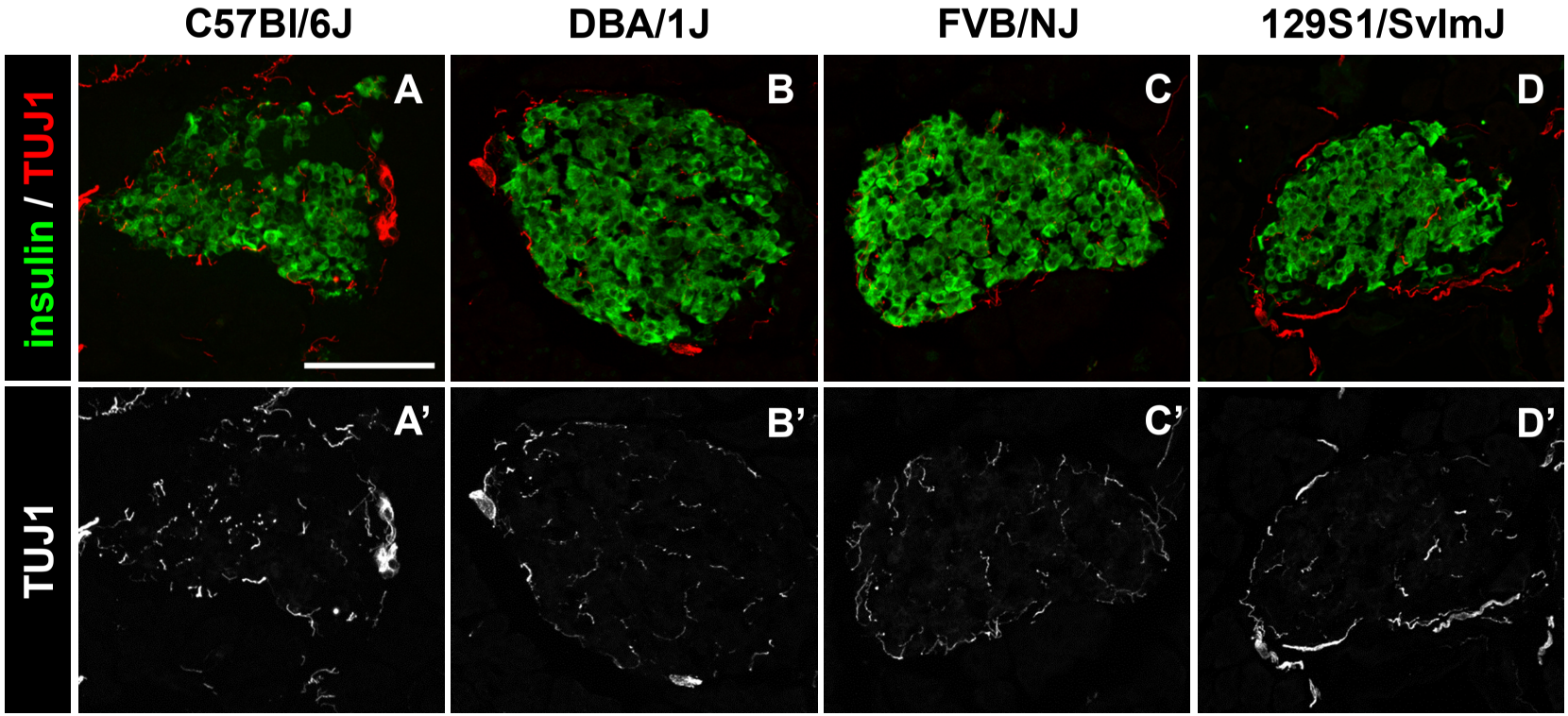

Figure A4. Islet nerve fiber density differs between four mouse strains. Immunohistochemistry was performed on 30 µm-thick pancreatic cryosections, labeling for insulin (green) and TUJ1 (red/grayscale). Scale bar in **A** is 100 µm and applies to all other panels.

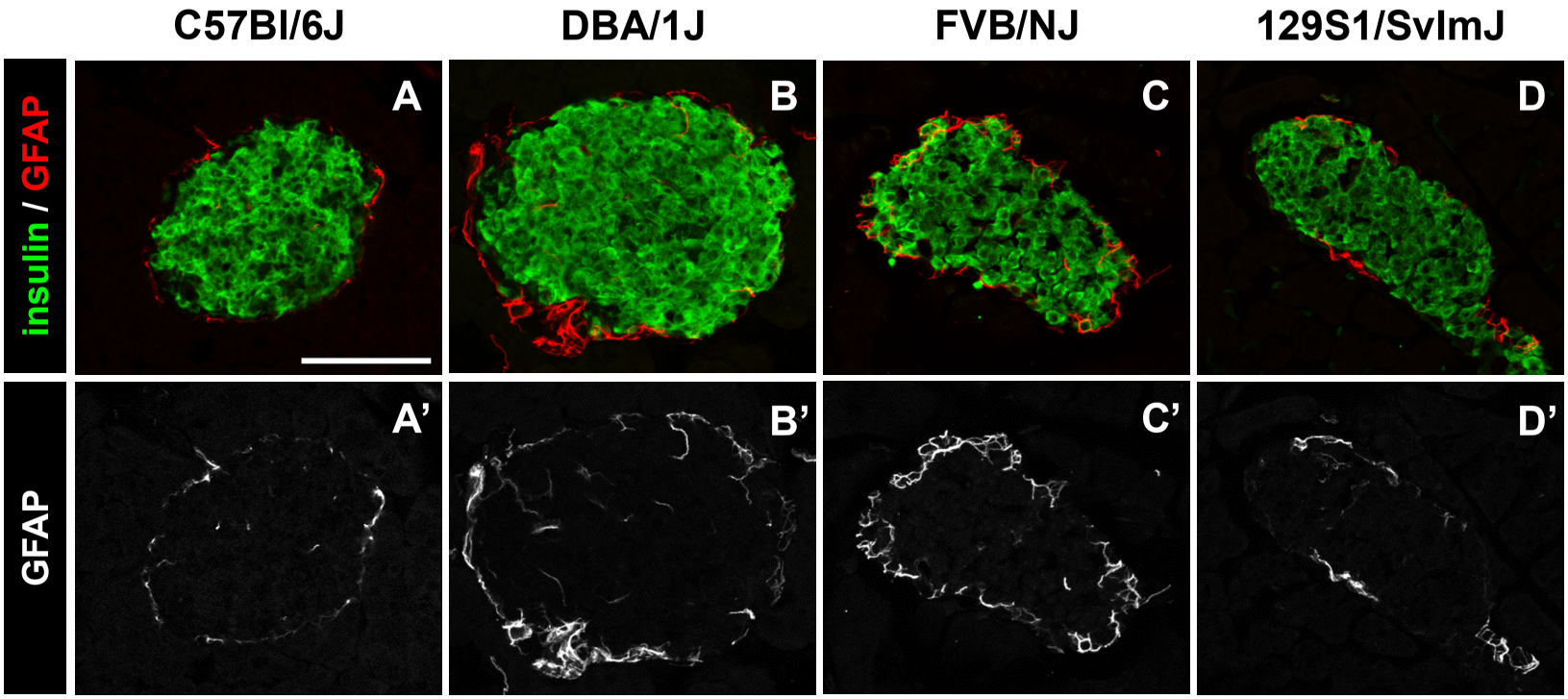

Figure A5. Peri-islet Schwann cells show similar morphology in four mouse strains. Immunohistochemistry was performed on 30 µm-thick pancreatic cryosections, labeling for insulin (green) and GFAP (red/grayscale). Scale bar in **A** is 100 µm and applies to all other panels.

Strain-dependent differences in the proportion of TH+ islet cells were also observed. Islets in C57BL/6J mice had few TH+ β-cells (Figure A6A), while more TH+ cells were present in the other strains (Figure A6B-G). In particular, islets in DBA/1J and 129S1/SvImJ mice showed many TH+ cell bodies (Figure A6B, D, E, G). Most of these TH+ cells were β-cells, but some TH+ cells lacked insulin expression. It is likely that these TH+/insulin- cells were non-β endocrine cells, because they were similar in size and shape to the TH+ β-cells. The proportion of TH+ cells did not change with islet size; both smaller (Figure A6A-D) and larger (Figure A6E-G) islets showed a similar density of intraislet TH+ cells.

Discussion

These studies were initiated to determine if VEGF-A and the islet vasculature provided important signals to nerves in the mature islet, as VEGF-A is important in maintaining autonomic nerves in peripheral resistance arteries (Storkebaum et al., 2010). Because neural crest-derived cells in adult islets did not demonstrate expression of the VEGF-A receptors VEGFR2 or NRP1 (see Chapter III), it is unlikely that VEGF-A plays a direct role in maintaining islet innervation. However, it is possible that islet nerves require the oxygen tension that the dense intraislet vasculature provides. As an example, mice unable to produce VEGF-A in response to hypoxia show a motor neurodegeneration phenotype similar to amyotrophic lateral sclerosis (Oosthuyse et al., 2001).

Using immunohistochemistry, it was found that inactivation of VEGF-A in adult islets resulted in a decrease in the density of intraislet TUJ1+ nerves, compared to controls. However, the fact that controls in this line also showed an obvious decrease in

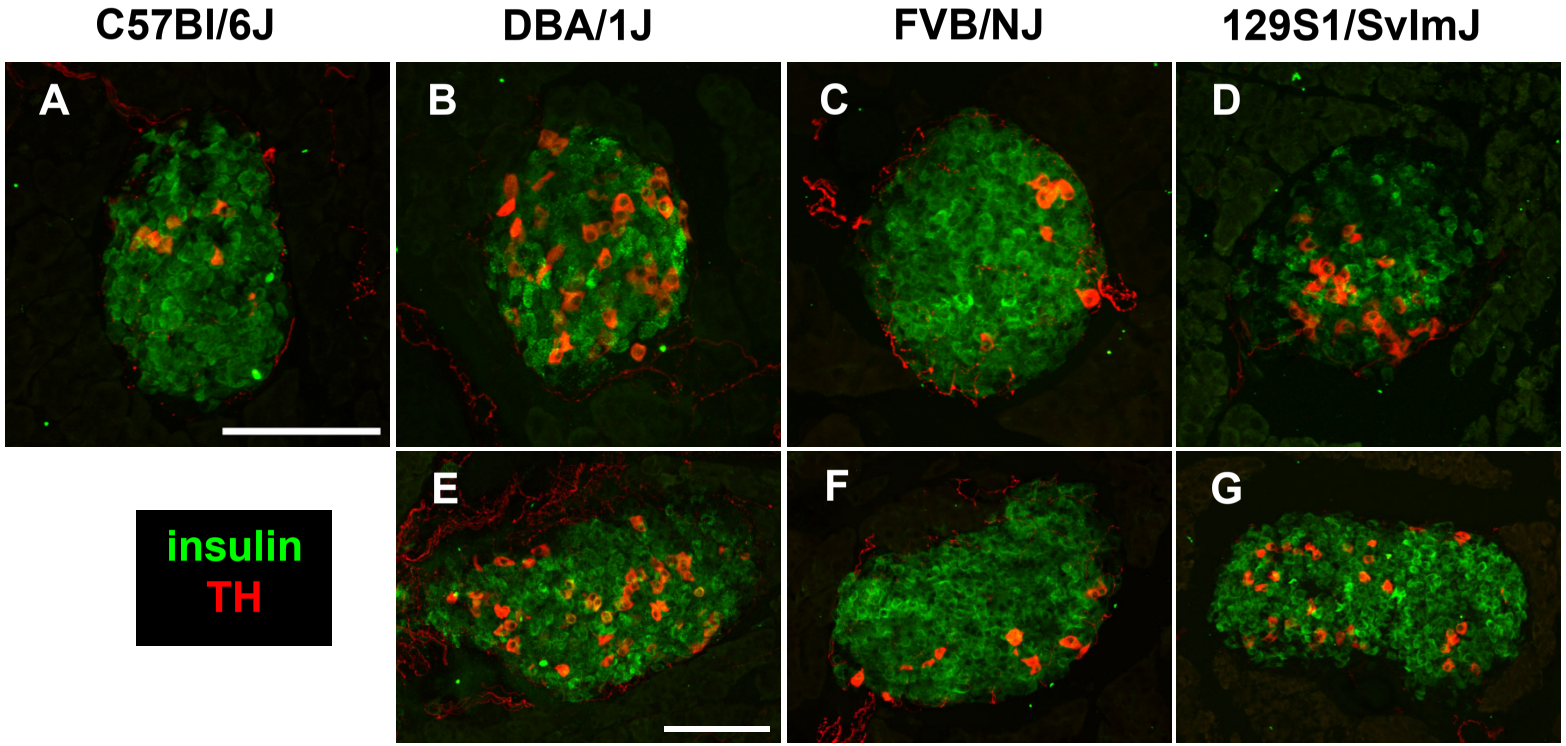

Figure A6. The number of TH+ islet endocrine cells differs between four mouse strains. Immunohistochemistry was performed on 30 μm-thick pancreatic cryosections, labeling for insulin (green) and tyrosine hydroxylase (TH, red). Scale bar in **A** is 100 μm and applies to panels **B-D**. Scale bar in **E** is 100 μm and applies to panels **F-G**.

islet innervation compared to control mice in the *Pdx1-Cre;Vegfa*$^{fl/fl}$ and *RIP-rtTA;TetO-hVegfa* models made the results difficult to interpret. The possibility that a different genetic background accounted for this discrepancy was then considered.

The mice used in this Dissertation were all on mixed backgrounds. *Vegfa*$^{fl/fl}$ mice were generated using 129Sv embryonic stem cells injected into C57BL/6J blastocysts, and the offspring were bred into a C57BL/6J background (Gerber et al., 1999). *Pdx1*^{PB}-*CreER*^{Tm} mice were generated by pronuclear injection of the transgene construct into B6D2 embryos (an F1 hybrid between C57BL/6J and DBA/2J strains; Zhang et al., 2005). *Pdx1-Cre* transgenic mice were generated on a hybrid B6CBAF1 strain (Gu et al., 2002). *RIP-rtTA* transgenic mice were generated by pronuclear injection of B6CBA embryos (an F2 hybrid between C57BL/6J and CBA strains), and the offspring were bred into a C57BL/6J background for three generations (Milo-Landesman et al., 2001). *TetO-hVegfa* mice were generated in an undescribed strain, but founders were bred with C57BL/6J mice (Ohno-Matsui et al., 2002).

In the studies performed in this Dissertation, experimental mice from each colony were compared with age-matched littermate controls to minimize genetic variation within a line. The data presented here suggest that comparing mice with substantial background differences would be difficult, because the controls may have different phenotypes. Mice from the *Pdx1-Cre;Vegfa*$^{fl/fl}$ and *RIP-rtTA;TetO-hVegfa* lines, whose controls demonstrated similar levels of islet innervation, all had black coats, agreeing with their predominant C57BL/6J genetic background. In contrast, almost all of the *Pdx1*^{PB}-*CreER*^{Tm}*;Vegfa*$^{fl/fl}$ mice used in the studies described in Chapter IV had agouti coats, suggesting that their genetic makeup had a considerable contribution from a strain other

than C57BL/6J. While strain differences may be responsible for the discrepancy in basal islet innervation between these mouse lines, the mechanisms underlying these phenotypes remain to be determined.

Strain differences in islet innervation have not been previously investigated. These four strains were chosen because they were shown to have several differences in whole-body glucose metabolism, including dramatically dissimilar glucose-stimulated insulin secretion *in vivo* and varied secretion of counterregulatory hormones in response to hypoglycemia (Berglund et al., 2008). It was found that the strains do differ in the density of intraislet TUJ1+ nerve fibers and in the number of TH+ endocrine cells, but that GFAP+ Schwann cells consistently have a peri-islet morphology. Whether these differences in islet innervation are directly responsible for strain-dependent differences in islet function and glucose metabolism remains to be explored.

REFERENCES

Abouna, S., Old, R. W., Pelengaris, S., Epstein, D., Ifandi, V., Sweeney, I. and Khan, M. (2010). Non-β-cell progenitors of β-cells in pregnant mice. *Organogenesis* 6, 125–133.

Ackermann, A. M. and Gannon, M. (2007). Molecular regulation of pancreatic β-cell mass development, maintenance, and expansion. *J Mol Endocrinol* 38, 193–206.

Adeghate, E. (2002). Pancreatic tissue grafts are reinnervated by neuro-peptidergic and cholinergic nerves within five days of transplantation. *Transpl Immunol* 10, 73–80.

Adeghate, E. and Donáth, T. (1990). Distribution of neuropeptide Y and vasoactive intestinal polypeptide immunoreactive nerves in normal and transplanted pancreatic tissue. *Peptides* 11, 1087–1092.

Aguayo-Mazzucato, C., Koh, A., Khattabi, El, I., Li, W.-C., Toschi, E., Jermendy, A., Juhl, K., Mao, K., Weir, G. C., Sharma, A. and Bonner-Weir, S. (2011). Mafa expression enhances glucose-responsive insulin secretion in neonatal rat β cells. *Diabetologia* 54, 583–593.

Aguayo-Mazzucato, C., Sanchez-Soto, C., Godinez-Puig, V., Gutiérrez-Ospina, G. and Hiriart, M. (2006). Restructuring of pancreatic islets and insulin secretion in a postnatal critical window. *PLoS ONE* 1, e35.

Aguilar-Bryan, L. and Bryan, J. (2008). Neonatal diabetes mellitus. *Endocr Rev* 29, 265–291.

Ahrén, B., Wierup, N. and Sundler, F. (2006). Neuropeptides and the regulation of islet function. *Diabetes* 55 Suppl 2, S98–S107.

Ahrén, B. (2000). Autonomic regulation of islet hormone secretion–implications for health and disease. *Diabetologia* 43, 393–410.

Ahrén, B. (2004). Sensory nerves contribute to insulin secretion by glucagon-like peptide-1 in mice. *Am J Physiol Regul Integr Comp Physiol* 286, R269–R272.

Ahrén, B. (2006). The insulin response to gastric glucose is reduced in PAC1 and GRP receptor gene deleted mice. *Nutr Metab Cardiovasc Dis* 16 Suppl 1, S17–S21.

Ahrén, B. (2008). Role of pituitary adenylate cyclase-activating polypeptide in the pancreatic endocrine system. *Ann N Y Acad Sci* 1144, 28–35.

Ahrén, B. and Holst, J. J. (2001). The cephalic insulin response to meal ingestion in humans is dependent on both cholinergic and noncholinergic mechanisms and is important for postprandial glycemia. *Diabetes* 50, 1030–1038.

Ahrén, B. and Lundquist, I. (1982). Modulation of basal insulin secretion in the obese, hyperglycemic mouse. *Metab Clin Exp* 31, 172–179.

Ahrén, B., Gudbjartsson, T., Al-Amin, A. N., Mårtensson, H., Myrsén-Axcrona, U., Karlsson, S., Mulder, H. and Sundler, F. (1999). Islet perturbations in rats fed a high-fat diet. *Pancreas* 18, 75–83.

Akirav, E. M., Baquero, M.-T., Opare-Addo, L. W., Akirav, M., Galvan, E., Kushner, J. A., Rimm, D. L. and Herold, K. C. (2011). Glucose and inflammation control islet vascular density and β-cell function in NOD mice: control of islet vasculature and vascular endothelial growth factor by glucose. *Diabetes* 60, 876–883.

Alpert, S., Hanahan, D. and Teitelman, G. (1988). Hybrid insulin genes reveal a developmental lineage for pancreatic endocrine cells and imply a relationship with neurons. *Cell* 53, 295–308.

Anastassiadis, K., Glaser, S., Kranz, A., Berhardt, K. and Stewart, A. F. (2010). A practical summary of site-specific recombination, conditional mutagenesis, and tamoxifen induction of CreERT2. *Meth Enzymol* 477, 109–123.

Arntfield, M. E. and van der Kooy, D. (2011). β-Cell evolution: how the pancreas borrowed from the brain: the shared toolbox of genes expressed by neural and pancreatic endocrine cells may reflect their evolutionary relationship. *Bioessays* 33, 582–587.

Ashcroft, F. M. and Rorsman, P. (2012). Diabetes mellitus and the β cell: the last ten years. *Cell* 148, 1160–1171.

Atef, N., Brulé, C., Bihoreau, M. T., Ktorza, A., Picon, L. and Pénicaud, L. (1991). Enhanced insulin secretory response to acetylcholine by perifused pancreas of 5-day-old preobese Zucker rats. *Endocrinology* 129, 2219–2224.

Atef, N., Ktorza, A., Picon, L. and Pénicaud, L. (1992). Increased islet blood flow in obese rats: role of the autonomic nervous system. *Am J Physiol Endocrinol Metab* 262, E736–E740.

Atef, N., Laury, M. C., N'Guyen, J. M., Mokhtar, N., Ktorza, A. and Penicaud, L. (1997). Increased pancreatic islet blood flow in 48-hour glucose-infused rats: involvement of central and autonomic nervous systems. *Endocrinology* 138, 1836–1840.

Atouf, F., Czernichow, P. and Scharfmann, R. (1997). Expression of neuronal traits in pancreatic beta cells. Implication of neuron-restrictive silencing factor/repressor element silencing transcription factor, a neuron-restrictive silencer. *J Biol Chem* 272, 1929–1934.

Badea, T. C., Hua, Z. L., Smallwood, P. M., Williams, J., Rotolo, T., Ye, X. and Nathans, J. (2009). New mouse lines for the analysis of neuronal morphology using CreER(T)/loxP-directed sparse labeling. *PLoS ONE* 4, e7859.

Badea, T. C., Wang, Y. and Nathans, J. (2003). A noninvasive genetic/pharmacologic strategy for visualizing cell morphology and clonal relationships in the mouse. *J Neurosci* 23, 2314–2322.

Baffert, F., Le, T., Sennino, B., Thurston, G., Kuo, C. J., Hu-Lowe, D. and McDonald, D. M. (2006). Cellular changes in normal blood capillaries undergoing regression after inhibition of VEGF signaling. *Am J Physiol Heart Circ Physiol* 290, H547–H559.

Barton, F. B., Rickels, M. R., Alejandro, R., Hering, B. J., Wease, S., Naziruddin, B., Oberholzer, J., Odorico, J. S., Garfinkel, M. R., Levy, M., Pattou, F., Berney, T., Secchi, A., Messinger, S., Senior, P. A., Maffi, P., Posselt, A., Stock, P. G., Kaufman, D. B., Luo, X., Kandeel, F., Cagliero, E., Turgeon, N. A., Witkowski, P., Naji, A., O'Connell, P. J., Greenbaum, C., Kudva, Y. C., Brayman, K. L., Aull, M. J., Larsen, C., Kay, T. W., Fernandez, L. A., Vantyghem, M. C., Bellin, M. and Shapiro, A. M. (2012). Improvement in outcomes of clinical islet transplantation: 1999–2010. *Diabetes Care* 35, 1436–1445.

Bates, D., Taylor, G. I., Minichiello, J., Farlie, P., Cichowitz, A., Watson, N., Klagsbrun, M., Mamluk, R. and Newgreen, D. F. (2003). Neurovascular congruence results from a shared patterning mechanism that utilizes Semaphorin3A and Neuropilin-1. *Dev Biol* 255, 77–98.

Baudoux, S. and Parker, D. (2008). Glial-toxin-mediated disruption of spinal cord locomotor network function and its modulation by 5-HT. *Neuroscience* 153, 1332–1343.

Bautch, V. (2012). VEGF-directed blood vessel patterning: from cells to organism. *Cold Spring Harb Perspect Med* 2, a006452.

Bearden, S. E. and Segal, S. S. (2005). Neurovascular alignment in adult mouse skeletal muscles. *Microcirculation* 12, 161–167.

Bearer, E. L. and Orci, L. (1985). Endothelial fenestral diaphragms: a quick-freeze, deep-etch study. *J Cell Biol* 100, 418–428.

Beattie, G. M., Levine, F., Mally, M. I., Otonkoski, T., O'Brien, J. S., Salomon, D. R. and Hayek, A. (1994). Acid β-galactosidase: a developmentally regulated marker of endocrine cell precursors in the human fetal pancreas. *J Clin Endocrinol Metab* 78, 1232–1240.

Berglund, E. D., Li, C. Y., Poffenberger, G., Ayala, J. E., Fueger, P. T., Willis, S. E., Jewell, M. M., Powers, A. C. and Wasserman, D. H. (2008). Glucose metabolism in vivo in four commonly used inbred mouse strains. *Diabetes* 57, 1790–1799.

Bergman, B. C., Howard, D., Schauer, I. E., Maahs, D. M., Snell-Bergeon, J. K., Eckel, R. H., Perreault, L. and Rewers, M. (2012). Features of hepatic and skeletal muscle insulin resistance unique to type 1 diabetes. *J Clin Endocrinol Metab* 97, 1663–1672.

Berthoud, H. R., Trimble, E. R., Siegel, E. G., Bereiter, D. A. and Jeanrenaud, B. (1980). Cephalic-phase insulin secretion in normal and pancreatic islet-transplanted rats. *Am J Physiol Endocrinol Metab* 238, E336–E340.

Betsholtz, C. and Armulik, A. (2006). Homeostatic functions of vascular endothelial growth factor in adult microvasculature. *Am J Physiol Heart Circ Physiol* 290, H509–H511.

Bhatheja, K. and Field, J. (2006). Schwann cells: origins and role in axonal maintenance and regeneration. *Int J Biochem Cell Biol* 38, 1995–1999.

Biarnés, M., Montolio, M., Nacher, V., Raurell, M., Soler, J. and Montanya, E. (2002). β-cell death and mass in syngeneically transplanted islets exposed to short- and long-term hyperglycemia. *Diabetes* 51, 66–72.

Billemont, B., Medioni, J., Taillade, L., Helley, D., Meric, J. B., Rixe, O. and Oudard, S. (2008). Blood glucose levels in patients with metastatic renal cell carcinoma treated with sunitinib. *Br J Cancer* 99, 1380–1382.

Blaine, S. A., Ray, K. C., Anunobi, R., Gannon, M. A., Washington, M. K. and Means, A. L. (2010). Adult pancreatic acinar cells give rise to ducts but not endocrine cells in response to growth factor signaling. *Development* 137, 2289–2296.

Bockamp, E., Maringer, M., Spangenberg, C., Fees, S., Fraser, S., Eshkind, L., Oesch, F. and Zabel, B. (2002). Of mice and models: improved animal models for biomedical research. *Physiol Genomics* 11, 115–132.

Bonaguidi, M. A., Wheeler, M. A., Shapiro, J. S., Stadel, R. P., Sun, G. J., Ming, G.-L. and Song, H. (2011). In vivo clonal analysis reveals self-renewing and multipotent adult neural stem cell characteristics. *Cell* 145, 1142–1155.

Bonner-Weir, S. (1991). Anatomy of the islet of Langerhans. *The Endocrine Pancreas*. Ed. E. Samols. New York, Raven Press. 15–27.

Bonner-Weir, S. and Orci, L. (1982). New perspectives on the microvasculature of the islets of Langerhans in the rat. *Diabetes* 31, 883–889.

Bonnevie-Nielsen, V. (1982). Different effects of high glucose and high fat diet on pancreatic insulin and glucagon in female and male mice. *Diabete Metab* 8, 271–277.

Borelli, M. I. and Gagliardino, J. J. (2001). Possible modulatory effect of endogenous islet catecholamines on insulin secretion. *BMC Endocr Disord* 1, 1.

Borelli, M. I., Rubio, M., García, M. E., Flores, L. E. and Gagliardino, J. J. (2003). Tyrosine hydroxylase activity in the endocrine pancreas: changes induced by short-term dietary manipulation. *BMC Endocr Disord* 3, 2.

Bosco, D., Armanet, M., Morel, P., Niclauss, N., Sgroi, A., Muller, Y. D., Giovannoni, L.,

Parnaud, G. and Berney, T. (2010). Unique arrangement of α- and β-cells in human islets of Langerhans. *Diabetes* 59, 1202–1210.

Brake, R. L., Simmons, P. J. and Begley, C. G. (2004). Cross-contamination with tamoxifen induces transgene expression in non-exposed inducible transgenic mice. *Genet Mol Res* 3, 456–462.

Breau, M. A., Dahmani, A., Broders-Bondon, F., Thiery, J.-P. and Dufour, S. (2009). β1 integrins are required for the invasion of the caecum and proximal hindgut by enteric neural crest cells. *Development* 136, 2791–2801.

Brennand, K., Huangfu, D. and Melton, D. (2007). All β cells contribute equally to islet growth and maintenance. *PLoS Biol* 5, e163.

Brissova, M. and Powers, A. C. (2008). Revascularization of transplanted islets: can it be improved? *Diabetes* 57, 2269–2271.

Brissova, M., Brahmachary, P., Hong, J. Y., Shostak, A., Aamodt, K., Poffenberger, G., Mellati, M. and Powers, A. C. (In preparation). Microenvironment of bone marrow-derived cells and endothelial cells stimulates β islet cell proliferation and regeneration.

Brissova, M., Fowler, M. J., Nicholson, W. E., Chu, A., Hirshberg, B., Harlan, D. M. and Powers, A. C. (2005). Assessment of human pancreatic islet architecture and composition by laser scanning confocal microscopy. *J Histochem Cytochem* 53, 1087–1097.

Brissova, M., Fowler, M., Wiebe, P., Shostak, A., Shiota, M., Radhika, A., Lin, P. C., Gannon, M. and Powers, A. C. (2004). Intraislet endothelial cells contribute to revascularization of transplanted pancreatic islets. *Diabetes* 53, 1318–1325.

Brissova, M., Shiota, M., Nicholson, W. E., Gannon, M., Knobel, S. M., Piston, D. W., Wright, C. V. E. and Powers, A. C. (2002). Reduction in pancreatic transcription factor PDX-1 impairs glucose-stimulated insulin secretion. *J Biol Chem* 277, 11225–11232.

Brissova, M., Shostak, A., Shiota, M., Wiebe, P. O., Poffenberger, G., Kantz, J., Chen, Z., Carr, C., Jerome, W. G., Chen, J., Baldwin, H. S., Nicholson, W., Bader, D. M., Jetton, T., Gannon, M. and Powers, A. C. (2006). Pancreatic islet production of vascular endothelial growth factor-A is essential for islet vascularization, revascularization, and function. *Diabetes* 55, 2974–2985.

Brocard, J., Warot, X., Wendling, O., Messaddeq, N., Vonesch, J. L., Chambon, P. and Metzger, D. (1997). Spatio-temporally controlled site-specific somatic mutagenesis in the mouse. *Proc Natl Acad Sci USA* 94, 14559–14563.

Buch, T., Heppner, F. L., Tertilt, C., Heinen, T. J. A. J., Kremer, M., Wunderlich, F. T., Jung, S. and Waisman, A. (2005). A Cre-inducible diphtheria toxin receptor mediates

cell lineage ablation after toxin administration. *Nat Meth* 2, 419–426.

Buelow, B. and Scharenberg, A. M. (2008). Characterization of parameters required for effective use of tamoxifen-regulated recombination. *PLoS ONE* 3, e3264.

Buffo, A., Rite, I., Tripathi, P., Lepier, A., Colak, D., Horn, A.-P., Mori, T. and Götz, M. (2008). Origin and progeny of reactive gliosis: a source of multipotent cells in the injured brain. *Proc Natl Acad Sci USA* 105, 3581–3586.

Burns, K. A., Ayoub, A. E., Breunig, J. J., Adhami, F., Weng, W.-L., Colbert, M. C., Rakic, P. and Kuan, C.-Y. (2007). Nestin-CreER mice reveal DNA synthesis by nonapoptotic neurons following cerebral ischemia hypoxia. *Cereb Cortex* 17, 2585–2592.

Burris, R. E. and Hebrok, M. (2007). Pancreatic innervation in mouse development and β-cell regeneration. *Neuroscience* 150, 592–602.

Burrows, H. (1934). The occurrence of scrotal hernia in mice under treatment with oestrin. *Brit J Surg* 21, 507–512.

Bustin, S. A., Benes, V., Garson, J. A., Hellemans, J., Huggett, J., Kubista, M., Mueller, R., Nolan, T., Pfaffl, M. W., Shipley, G. L., Vandesompele, J. and Wittwer, C. T. (2009). The MIQE guidelines: minimum information for publication of quantitative real-time PCR experiments. *Clin Chem* 55, 611–622.

Cabrera, O., Berman, D. M., Kenyon, N. S., Ricordi, C., Berggren, P.-O. and Caicedo, A. (2006). The unique cytoarchitecture of human pancreatic islets has implications for islet cell function. *Proc Natl Acad Sci USA* 103, 2334–2339.

Cabrera-Vasquez, S., Navarro-Tableros, V., Sanchez-Soto, C., Gutierrez-Ospina, G. and Hiriart, M. (2009). Remodeling sympathetic innervation in rat pancreatic islets ontogeny. *BMC Dev Biol* 9, 34.

Cai, Q. (2012). Enhanced expression of VEGF-A in β cells increases endothelial cell number but impairs islet morphogenesis and β cell proliferation. Doctoral dissertation, Vanderbilt University, Nashville, TN.

Cai, Q., Brissova, M., Reinert, R. B., Pan, F. C., Brahmachary, P., Jeansson, M., Shostak, A., Radhika, A., Poffenberger, G., Quaggin, S. E., Jerome, W. G., Dumont, D. J. and Powers, A. C. (2012). Enhanced expression of VEGF-A in β cells increases endothelial cell number but impairs islet morphogenesis and β cell proliferation. *Dev Biol* 367, 40–54.

Calderari, S., Chougnet, C., Clemessy, M., Kempf, H., Corvol, P. and Larger, E. (2012). Angiopoietin 2 alters pancreatic vascularization in diabetic conditions. *PLoS ONE* 7, e29438.

Cariboni, A., Davidson, K., Dozio, E., Memi, F., Schwarz, Q., Stossi, F., Parnavelas, J. G.

and Ruhrberg, C. (2011). VEGF signalling controls GnRH neuron survival via NRP1 independently of KDR and blood vessels. *Development* 138, 3723–3733.

Carlsson, P. O., Andersson, A. and Jansson, L. (1996). Pancreatic islet blood flow in normal and obese-hyperglycemic (ob/ob) mice. *Am J Physiol Endocrinol Metab* 271, E990–E995.

Carlsson, P. O., Iwase, M. and Jansson, L. (1999). Stimulation of intestinal glucoreceptors in rats increases pancreatic islet blood flow through vagal mechanisms. *Am J Physiol Regul Integr Comp Physiol* 276, R233–R236.

Carlsson, P. O., Liss, P., Andersson, A. and Jansson, L. (1998). Measurements of oxygen tension in native and transplanted rat pancreatic islets. *Diabetes* 47, 1027–1032.

Carlsson, P. O., Palm, F., Andersson, A. and Liss, P. (2000). Chronically decreased oxygen tension in rat pancreatic islets transplanted under the kidney capsule. *Transplantation* 69, 761–766.

Carlsson, P. O., Palm, F., Andersson, A. and Liss, P. (2001). Markedly decreased oxygen tension in transplanted rat pancreatic islets irrespective of the implantation site. *Diabetes* 50, 489–495.

Carmeliet, P. and Jain, R. K. (2011). Molecular mechanisms and clinical applications of angiogenesis. *Nature* 473, 298–307.

Carmeliet, P. and Tessier-Lavigne, M. (2005). Common mechanisms of nerve and blood vessel wiring. *Nature* 436, 193–200.

Carmeliet, P., Ferreira, V., Breier, G., Pollefeyt, S., Kieckens, L., Gertsenstein, M., Fahrig, M., Vandenhoeck, A., Harpal, K., Eberhardt, C., Declercq, C., Pawling, J., Moons, L., Collen, D., Risau, W. and Nagy, A. (1996). Abnormal blood vessel development and lethality in embryos lacking a single VEGF allele. *Nature* 380, 435–439.

Cegrell, L. (1968). The occurrence of biogenic monoamines in the mammalian endocrine pancreas. *Acta Physiol Scand Suppl* 314, 1–60.

Cébe-Suarez, S., Zehnder-Fjällman, A. and Ballmer-Hofer, K. (2006). The role of VEGF receptors in angiogenesis; complex partnerships. *Cell Mol Life Sci* 63, 601–615.

Centers for Disease Control and Prevention (2011). National Diabetes Fact Sheet, 2011. 1–12.

Chatenoud, L. (2008). Chemical immunosuppression in islet transplantation–friend or foe? *N Engl J Med* 358, 1192–1193.

Chen, H. X. and Cleck, J. N. (2009). Adverse effects of anticancer agents that target the VEGF pathway. *Nat Rev Clin Oncol* 6, 465–477.

Chen, N., Unnikrishnan I, R., Anjana, R. M., Mohan, V. and Pitchumoni, C. S. (2011). The complex exocrine-endocrine relationship and secondary diabetes in exocrine pancreatic disorders. *J Clin Gastroenterol* 45, 850–861.

Cheng, Y., Liu, Y.-F., Zhang, J.-L., Li, T.-M. and Zhao, N. (2007). Elevation of vascular endothelial growth factor production and its effect on revascularization and function of graft islets in diabetic rats. *World J Gastroenterol* 13, 2862–2866.

Christoffersson, G., Henriksnäs, J., Johansson, L., Rolny, C., Ahlström, H., Caballero-Corbalan, J., Segersvärd, R., Permert, J., Korsgren, O., Carlsson, P.-O. and Phillipson, M. (2010). Clinical and experimental pancreatic islet transplantation to striated muscle: establishment of a vascular system similar to that in native islets. *Diabetes* 59, 2569–2578.

Christofori, G., Naik, P. and Hanahan, D. (1995). Vascular endothelial growth factor and its receptors, flt-1 and flk-1, are expressed in normal pancreatic islets and throughout islet cell tumorigenesis. *Mol Endocrinol* 9, 1760–1770.

Coker, G. T., Studelska, D., Harmon, S., Burke, W. and O'Malley, K. L. (1990). Analysis of tyrosine hydroxylase and insulin transcripts in human neuroendocrine tissues. *Brain Res Mol Brain Res* 8, 93–98.

Coleman, D. L. (1978). Obese and diabetes: two mutant genes causing diabetes-obesity syndromes in mice. *Diabetologia* 14, 141–148.

Correa, D. and Segal, S. S. (2012). Neurovascular proximity in the diaphragm muscle of adult mice. *Microcirculation* 19, 306-315.

Crawford, L. A., Guney, M. A., Oh, Y. A., Deyoung, R. A., Valenzuela, D. M., Murphy, A. J., Yancopoulos, G. D., Lyons, K. M., Brigstock, D. R., Economides, A. and Gannon, M. (2009). Connective tissue growth factor (CTGF) inactivation leads to defects in islet cell lineage allocation and β-cell proliferation during embryogenesis. *Mol Endocrinol* 23, 324–336.

Crawford, S. E., Stellmach, V., Murphy-Ullrich, J. E., Ribeiro, S. M., Lawler, J., Hynes, R. O., Boivin, G. P. and Bouck, N. (1998). Thrombospondin-1 is a major activator of TGF-β1 in vivo. *Cell* 93, 1159–1170.

Dai, C., Brissova, M., Hang, Y., Thompson, C., Poffenberger, G., Shostak, A., Chen, Z., Stein, R. and Powers, A. C. (2012). Islet-enriched gene expression and glucose-induced insulin secretion in human and mouse islets. *Diabetologia* 55, 707–718.

Dai, C., Brissova, M. Reinert, R. B., Nyman, L., Liu, E. H., Thompson, C., Shostak, A., Shiota, M.,Takahashi, T. and Powers, A. C. (In preparation). Pancreatic islet adaptation to insulin resistance involves changes to islet vascularity and blood flow.

Damon, D. H., Teriele, J. A. and Marko, S. B. (2007). Vascular-derived artemin: a determinant of vascular sympathetic innervation? *Am J Physiol Heart Circ Physiol*

293, H266–H273.

Danielian, P. S., Muccino, D., Rowitch, D. H., Michael, S. K. and McMahon, A. P. (1998). Modification of gene activity in mouse embryos in utero by a tamoxifen-inducible form of Cre recombinase. *Curr Biol* 8, 1323–1326.

Deanesly, R. and Parkes, A. S. (1933). Note on the subcutaneous absorption of oils by rats and mice, with special reference to the assay of oestrin. *J Physiol* 78, 155–160.

Defronzo, R. A. and Abdul-Ghani, M. A. (2011). Preservation of β-cell function: the key to diabetes prevention. *J Clin Endocrinol Metab* 96, 2354–2366.

Desai, B. M., Oliver-Krasinski, J., De Leon, D. D., Farzad, C., Hong, N., Leach, S. D. and Stoffers, D. A. (2007). Preexisting pancreatic acinar cells contribute to acinar cell, but not islet β cell, regeneration. *J Clin Invest* 117, 971–977.

Devedjian, J. C., Pujol, A., Cayla, C., George, M., Casellas, A., Paris, H. and Bosch, F. (2000). Transgenic mice overexpressing α2A-adrenoceptors in pancreatic beta-cells show altered regulation of glucose homeostasis. *Diabetologia* 43, 899–906.

Di Sebastiano, P., Fink, T., Weihe, E., Friess, H., Innocenti, P., Beger, H. G. and Büchler, M. W. (1997). Immune cell infiltration and growth-associated protein 43 expression correlate with pain in chronic pancreatitis. *Gastroenterology* 112, 1648–1655.

Doerflinger, N. H., Macklin, W. B. and Popko, B. (2003). Inducible site-specific recombination in myelinating cells. *Genesis* 35, 63–72.

Donev, S. R. (1984). Ultrastructural evidence for the presence of a glial sheath investing the islets of Langerhans in the pancreas of mammals. *Cell Tissue Res* 237, 343–348.

Dor, Y., Brown, J., Martinez, O. I. and Melton, D. A. (2004). Adult pancreatic β-cells are formed by self-duplication rather than stem-cell differentiation. *Nature* 429, 41–46.

Dorrell, C., Erker, L., Schug, J., Kopp, J. L., Canaday, P. S., Fox, A. J., Smirnova, O., Duncan, A. W., Finegold, M. J., Sander, M., Kaestner, K. H. and Grompe, M. (2011). Prospective isolation of a bipotential clonogenic liver progenitor cell in adult mice. *Genes Dev* 25, 1193–1203.

Eberhard, D. and Lammert, E. (2009). The pancreatic β-cell in the islet and organ community. *Curr Opin Gen Dev* 19, 469–475.

Echelard, Y., Vassileva, G. and McMahon, A. P. (1994). Cis-acting regulatory sequences governing Wnt-1 expression in the developing mouse CNS. *Development* 120, 2213–2224.

Edsbagge, J., Johansson, J. K., Esni, F., Luo, Y., Radice, G. L. and Semb, H. (2005). Vascular function and sphingosine-1-phosphate regulate development of the dorsal pancreatic mesenchyme. *Development* 132, 1085–1092.

Edvell, A. and Lindström, P. (1998). Vagotomy in young obese hyperglycemic mice: effects on syndrome development and islet proliferation. *Am J Physiol Endocrinol Metab* 274, E1034–E1039.

Edwards, R. H., Rutter, W. J. and Hanahan, D. (1989). Directed expression of NGF to pancreatic β cells in transgenic mice leads to selective hyperinnervation of the islets. *Cell* 58, 161–170.

Efrat, S. and Russ, H. A. (2012). Making β cells from adult tissues. *Trends Endocrinol Metab* 23, 278–285.

Eich, T., Eriksson, O. and Lundgren, T., for the Nordic Network for Clinical Islet Transplantation (2007). Visualization of early engraftment in clinical islet transplantation by positron-emission tomography. *N Engl J Med* 356, 2754–2755.

Esni, F., Johansson, B. R., Radice, G. L. and Semb, H. (2001). Dorsal pancreas agenesis in N-cadherin-deficient mice. *Dev Biol* 238, 202–212.

Feil, R., Brocard, J., Mascrez, B., LeMeur, M., Metzger, D. and Chambon, P. (1996). Ligand-activated site-specific recombination in mice. *Proc Natl Acad Sci USA* 93, 10887–10890.

Fendler, B., Zhang, M., Satin, L. and Bertram, R. (2009). Synchronization of pancreatic islet oscillations by intrapancreatic ganglia: a modeling study. *Biophys J* 97, 722–729.

Ferrara, N. (2004). Vascular endothelial growth factor: basic science and clinical progress. *Endocr Rev* 25, 581–611.

Ferrara, N., Carver-Moore, K., Chen, H., Dowd, M., Lu, L., O'Shea, K. S., Powell-Braxton, L., Hillan, K. J. and Moore, M. W. (1996). Heterozygous embryonic lethality induced by targeted inactivation of the VEGF gene. *Nature* 380, 439–442.

Fong, G. H., Rossant, J., Gertsenstein, M. and Breitman, M. L. (1995). Role of the Flt-1 receptor tyrosine kinase in regulating the assembly of vascular endothelium. *Nature* 376, 66–70.

Fraker, C. A., Ricordi, C., Inverardi, L. and Domínguez-Bendala, J. (2009). Oxygen: a master regulator of pancreatic development? *Biol Cell* 101, 431–440.

Froud, T., Baidal, D. A., Ponte, G., Ferreira, J. V., Ricordi, C. and Alejandro, R. (2006). Resolution of neurotoxicity and beta-cell toxicity in an islet transplant recipient following substitution of tacrolimus with MMF. *Cell Transplant* 15, 613–620.

Fujita, T. (1989). Present status of paraneuron concept. *Arch Histol Cytol* 52 Suppl, 1–8.

Fujita, T. and Kobayashi, S. (1979). Proposal of a a neurosecretory system in the pancreas. An electron microscope study in the dog. *Arch Histol Jpn* 42, 277–295.

Furr, B. J. and Jordan, V. C. (1984). The pharmacology and clinical uses of tamoxifen. *Pharmacol Ther* 25, 127–205.

Furuyama, K., Kawaguchi, Y., Akiyama, H., Horiguchi, M., Kodama, S., Kuhara, T., Hosokawa, S., Elbahrawy, A., Soeda, T., Koizumi, M., Masui, T., Kawaguchi, M., Takaori, K., Doi, R., Nishi, E., Kakinoki, R., Deng, J. M., Behringer, R. R., Nakamura, T. and Uemoto, S. (2011). Continuous cell supply from a Sox9-expressing progenitor zone in adult liver, exocrine pancreas and intestine. *Nat Genet* 43, 34–41.

Gale, N. W. and Yancopoulos, G. D. (1999). Growth factors acting via endothelial cell-specific receptor tyrosine kinases: VEGFs, angiopoietins, and ephrins in vascular development. *Genes Dev* 13, 1055–1066.

Gannon, M., Ables, E. T., Crawford, L., Lowe, D., Offield, M. F., Magnuson, M. A. and Wright, C. V. E. (2008). pdx-1 function is specifically required in embryonic β cells to generate appropriate numbers of endocrine cell types and maintain glucose homeostasis. *Dev Biol* 314, 406–417.

Gannon, M., Gamer, L. W. and Wright, C. V. (2001). Regulatory regions driving developmental and tissue-specific expression of the essential pancreatic gene pdx1. *Dev Biol* 238, 185–201.

Garcia-Segura, L. M. and McCarthy, M. M. (2004). Minireview: role of glia in neuroendocrine function. *Endocrinology* 145, 1082–1086.

Gardner, W. (1936). Sexual dimorphism of the pelvis of the mouse, the effect of estrogenic hormones upon the pelvis and upon the development of scrotal hernias. *Am J Anat* 59, 459–483.

Gelfand, M. V., Hong, S. and Gu, C. (2009). Guidance from above: common cues direct distinct signaling outcomes in vascular and neural patterning. *Trends Cell Biol* 19, 99–110.

Georgia, S. and Bhushan, A. (2004). β cell replication is the primary mechanism for maintaining postnatal β cell mass. *J Clin Invest* 114, 963–968.

Gerber, H. P., Hillan, K. J., Ryan, A. M., Kowalski, J., Keller, G. A., Rangell, L., Wright, B. D., Radtke, F., Aguet, M. and Ferrara, N. (1999). VEGF is required for growth and survival in neonatal mice. *Development* 126, 1149–1159.

Gibran, N. S., Tamura, R., Tsou, R. and Isik, F. F. (2003). Human dermal microvascular endothelial cells produce nerve growth factor: implications for wound repair. *Shock* 19, 127–130.

Giroix, M.-H., Irminger, J.-C., Lacraz, G., Noll, C., Calderari, S., Ehses, J. A., Coulaud, J., Cornut, M., Kassis, N., Schmidlin, F., Paul, J. L., Kergoat, M., Janel, N., Halban, P. A. and Homo-Delarche, F. (2011). Hypercholesterolaemia, signs of islet

microangiopathy and altered angiogenesis precede onset of type 2 diabetes in the Goto-Kakizaki (GK) rat. *Diabetologia* 54, 2451–2462.

Gittes, G. K. (2009). Developmental biology of the pancreas: a comprehensive review. *Dev Biol* 326, 4–35.

Gregg, B. E., Moore, P. C., Demozay, D., Hall, B. A., Li, M., Husain, A., Wright, A. J., Atkinson, M. A. and Rhodes, C. J. (2012). Formation of a human β-Cell population within pancreatic islets is set early in life. *J Clin Endocrinol Metab* 97, 3197–3206.

Gromada, J., Franklin, I. and Wollheim, C. B. (2007). α-cells of the endocrine pancreas: 35 years of research but the enigma remains. *Endocr Rev* 28, 84–116.

Gu, C., Rodriguez, E. R., Reimert, D. V., Shu, T., Fritzsch, B., Richards, L. J., Kolodkin, A. L. and Ginty, D. D. (2003). Neuropilin-1 conveys semaphorin and VEGF signaling during neural and cardiovascular development. *Dev Cell* 5, 45–57.

Gu, G., Dubauskaite, J. and Melton, D. A. (2002). Direct evidence for the pancreatic lineage: NGN3+ cells are islet progenitors and are distinct from duct progenitors. *Development* 129, 2447–2457.

Guney, M. A., Petersen, C. P., Boustani, A., Duncan, M. R., Gunasekaran, U., Menon, R., Warfield, C., Grotendorst, G. R., Means, A. L., Economides, A. N. and Gannon, M. (2011). Connective tissue growth factor acts within both endothelial cells and β cells to promote proliferation of developing β cells. *Proc Natl Acad Sci USA* 108, 15242–15247.

Guo, C., Yang, W. and Lobe, C. G. (2002). A Cre recombinase transgene with mosaic, widespread tamoxifen-inducible action. *Genesis* 32, 8–18.

Guz, Y., Montminy, M. R., Stein, R., Leonard, J., Gamer, L. W., Wright, C. V. and Teitelman, G. (1995). Expression of murine STF-1, a putative insulin gene transcription factor, in β cells of pancreas, duodenal epithelium and pancreatic exocrine and endocrine progenitors during ontogeny. *Development* 121, 11–18.

Hall, M. E., Smith, G., Hall, J. E. and Stec, D. E. (2011). Systolic dysfunction in cardiac-specific ligand-inducible MerCreMer transgenic mice. *Am J Physiol Heart Circ Physiol* 301, H253–H260.

Ham, J. N., Crutchlow, M. F., Desai, B. M., Simmons, R. A. and Stoffers, D. A. (2009). Exendin-4 normalizes islet vascularity in intrauterine growth restricted rats: potential role of VEGF. *Pediatr Res.* 66, 42–46.

Hamilton, N. B., Attwell, D. and Hall, C. N. (2010). Pericyte-mediated regulation of capillary diameter: a component of neurovascular coupling in health and disease. *Front Neuroenerg* 2, 1–14.

Harlan, D. M., Kenyon, N. S., Korsgren, O. and Roep, B. O., for the Immunology of

Diabetes Society (2009). Current advances and travails in islet transplantation. *Diabetes* 58, 2175–2184.

Hayashi, S. and McMahon, A. P. (2002). Efficient recombination in diverse tissues by a tamoxifen-inducible form of Cre: a tool for temporally regulated gene activation/inactivation in the mouse. *Dev Biol* 244, 305–318.

Hazary, S. and Gardner, W. U. (1960). Influence of sex hormones on abdominal musculature and the formation of inguinal and scrotal hernias in mice. *Anat Rec* 136, 437–443.

Henderson, J. R. and Moss, M. C. (1985). A morphometric study of the endocrine and exocrine capillaries of the pancreas. *Q J Exp Physiol* 70, 347–356.

Herrera, P. L. (2000). Adult insulin- and glucagon-producing cells differentiate from two independent cell lineages. *Development* 127, 2317–2322.

Hnasko, T. S., Perez, F. A., Scouras, A. D., Stoll, E. A., Gale, S. D., Luquet, S., Phillips, P. E. M., Kremer, E. J. and Palmiter, R. D. (2006). Cre recombinase-mediated restoration of nigrostriatal dopamine in dopamine-deficient mice reverses hypophagia and bradykinesia. *Proc Natl Acad Sci USA* 103, 8858–8863.

Holland, A. M., Hale, M. A., Kagami, H., Hammer, R. E. and MacDonald, R. J. (2002). Experimental control of pancreatic development and maintenance. *Proc Natl Acad Sci USA* 99, 12236–12241.

Homo-Delarche, F., Calderari, S., Irminger, J.-C., Gangnerau, M.-N., Coulaud, J., Rickenbach, K., Dolz, M., Halban, P., Portha, B. and Serradas, P. (2006). Islet inflammation and fibrosis in a spontaneous model of type 2 diabetes, the GK rat. *Diabetes* 55, 1625–1633.

Honjin, R. (1956). The innervation of the pancreas of the mouse, with special reference to the structure of the peripheral extension of the vegetative nervous system. *J Comp Neurol* 104, 331–371.

Honma, Y., Araki, T., Gianino, S., Bruce, A., Heuckeroth, R., Johnson, E. and Milbrandt, J. (2002). Artemin is a vascular-derived neurotropic factor for developing sympathetic neurons. *Neuron* 35, 267–282.

Hsieh, P. C. H., Segers, V. F. M., Davis, M. E., Macgillivray, C., Gannon, J., Molkentin, J. D., Robbins, J. and Lee, R. T. (2007). Evidence from a genetic fate-mapping study that stem cells refresh adult mammalian cardiomyocytes after injury. *Nat Med* 13, 970–974.

Imai, J., Katagiri, H., Yamada, T., Ishigaki, Y., Suzuki, T., Kudo, H., Uno, K., Hasegawa, Y., Gao, J., Kaneko, K., Ishihara, H., Niijima, A., Nakazato, M., Asano, T., Minokoshi, Y. and Oka, Y. (2008). Regulation of pancreatic β cell mass by neuronal signals from the liver. *Science* 322, 1250–1254.

Imai, Y., Patel, H. R., Hawkins, E. J., Doliba, N. M., Matschinsky, F. M. and Ahima, R. S. (2007). Insulin secretion is increased in pancreatic islets of neuropeptide Y-deficient mice. *Endocrinology* 148, 5716–5723.

In't Veld, P. and Marichal, M. (2010). Microscopic anatomy of the human islet of Langerhans. *Adv Exp Med Biol* 654, 1–19.

Inada, A., Nienaber, C., Katsuta, H., Fujitani, Y., Levine, J., Morita, R., Sharma, A. and Bonner-Weir, S. (2008). Carbonic anhydrase II-positive pancreatic cells are progenitors for both endocrine and exocrine pancreas after birth. *Proc Natl Acad Sci USA* 105, 19915–19919.

Inai, T., Mancuso, M., Hashizume, H., Baffert, F., Haskell, A., Baluk, P., Hu-Lowe, D. D., Shalinsky, D. R., Thurston, G., Yancopoulos, G. D. and McDonald D. M. (2004). Inhibition of vascular endothelial growth factor (VEGF) signaling in cancer causes loss of endothelial fenestrations, regression of tumor vessels, and appearance of basement membrane ghosts. *Am J Pathol* 165, 35–52.

Indra, A. K., Warot, X., Brocard, J., Bornert, J. M., Xiao, J. H., Chambon, P. and Metzger, D. (1999). Temporally-controlled site-specific mutagenesis in the basal layer of the epidermis: comparison of the recombinase activity of the tamoxifen-inducible Cre-ER(T) and Cre-ER(T2) recombinases. *Nucleic Acids Res* 27, 4324–4327.

Inoue, M., Hager, J. H., Ferrara, N., Gerber, H.-P. and Hanahan, D. (2002). VEGF-A has a critical, nonredundant role in angiogenic switching and pancreatic β cell carcinogenesis. *Cancer Cell* 1, 193–202.

Iturriza, F. C. and Thibault, J. (1993). Immunohistochemical investigation of tyrosine-hydroxylase in the islets of Langerhans of adult mice, rats and guinea pigs. *Neuroendocrinology* 57, 476–480.

Iwashita, N., Uchida, T., Choi, J. B., Azuma, K., Ogihara, T., Ferrara, N., Gerber, H., Kawamori, R., Inoue, M. and Watada, H. (2007). Impaired insulin secretion in vivo but enhanced insulin secretion from isolated islets in pancreatic beta cell-specific vascular endothelial growth factor-A knock-out mice. *Diabetologia* 50, 380–389.

Jabs, N., Franklin, I., Brenner, M. B., Gromada, J., Ferrara, N., Wollheim, C. B. and Lammert, E. (2008). Reduced insulin secretion and content in VEGF-A deficient mouse pancreatic islets. *Exp Clin Endocrinol Diabetes* 116 Suppl 1, S46–S49.

James, J. M. and Mukouyama, Y.-S. (2011). Neuronal action on the developing blood vessel pattern. *Semin Cell Dev Biol* 22, 1019–1027.

Jansson, L. (1984). The blood flow to the pancreas and the islets of Langerhans during an intraperitoneal glucose load in the rat. *Diabetes Res* 1, 111–114.

Jansson, L. and Hellerström, C. (1983). Stimulation by glucose of the blood flow to the pancreatic islets of the rat. *Diabetologia* 25, 45–50.

Jansson, L. and Hellerström, C. (1986). Glucose-induced changes in pancreatic islet blood flow mediated by central nervous system. *Am J Physiol Endocrinol Metab* 251, E644–E647.

Jansson, L., Grapengiesser, E. and Hellman, B. (2010). Purinergic signalling in pancreatic islet endothelial cells. *Extracellular ATP and Adenosine as Regulators of Endothelial Cell Function*. Eds. E. Gerasimovskaya and E. Kaczmarek. New York, Springer Science+Business Media. 215–231.

Jeon, J., Correa-Medina, M., Ricordi, C., Edlund, H. and Diez, J. A. (2009). Endocrine cell clustering during human pancreas development. *J Histochem Cytochem* 57, 811–824.

Jermendy, A., Toschi, E., Aye, T., Koh, A., Aguayo-Mazzucato, C., Sharma, A., Weir, G. C., Sgroi, D. and Bonner-Weir, S. (2011). Rat neonatal beta cells lack the specialised metabolic phenotype of mature beta cells. *Diabetologia* 54, 594–604.

Jiang, X., Rowitch, D. H., Soriano, P., McMahon, A. P. and Sucov, H. M. (2000). Fate of the mammalian cardiac neural crest. *Development* 127, 1607–1616.

Jiang, Y., Liu, M.-T. and Gershon, M. D. (2003). Netrins and DCC in the guidance of migrating neural crest-derived cells in the developing bowel and pancreas. *Dev Biol* 258, 364–384.

Jo, J., Kilimnik, G., Kim, A., Guo, C., Periwal, V. and Hara, M. (2011). Formation of pancreatic islets involves coordinated expansion of small islets and fission of large interconnected islet-like structures. *Biophys J* 101, 565–574.

Johansson, A., Lau, J., Sandberg, M., Borg, L. A. H., Magnusson, P. U. and Carlsson, P.-O. (2009). Endothelial cell signalling supports pancreatic beta cell function in the rat. *Diabetologia* 52, 2385–2394.

Johansson, K. A., Dursun, U., Jordan, N., Gu, G., Beermann, F., Gradwohl, G. and Grapin-Botton, A. (2007). Temporal control of neurogenin3 activity in pancreas progenitors reveals competence windows for the generation of different endocrine cell types. *Dev Cell* 12, 457–465.

Johansson, M., Andersson, A., Carlsson, P.-O. and Jansson, L. (2006a). Perinatal development of the pancreatic islet microvasculature in rats. *J Anat* 208, 191–196.

Johansson, M., Mattsson, G., Andersson, A., Jansson, L. and Carlsson, P.-O. (2006b). Islet endothelial cells and pancreatic β-cell proliferation: studies in vitro and during pregnancy in adult rats. *Endocrinology* 147, 2315–2324.

Jonsson, J., Carlsson, L., Edlund, T. and Edlund, H. (1994). Insulin-promoter-factor 1 is required for pancreas development in mice. *Nature* 371, 606–609.

Kamba, T., Tam, B. Y. Y., Hashizume, H., Haskell, A., Sennino, B., Mancuso, M. R.,

Norberg, S. M., O'Brien, S. M., Davis, R. B., Gowen, L. C., Anderson, K. D., Thurston, G., Joho, S., Springer, M. L., Kuo, C. J. and McDonald DM. (2006). VEGF-dependent plasticity of fenestrated capillaries in the normal adult microvasculature. *Am J Physiol Heart Circ Physiol* 290, H560–H576.

Kapa, S., Gleeson, F. C. and Vege, S. S. (2007). Dorsal pancreas agenesis and polysplenia/heterotaxy syndrome: a novel association with aortic coarctation and a review of the literature. *JOP* 8, 433–437.

Karlsson, S., Myrsén, U., Nieuwenhuizen, A., Sundler, F. and Ahrén, B. (1997). Presynaptic sympathetic mechanism in the insulinostatic effect of epinephrine in mouse pancreatic islets. *Am J Physiol Regul Integr Comp Physiol* 272, R1371–R1378.

Kawaguchi, Y., Takaori, K. and Uemoto, S. (2011). Genetic lineage tracing, a powerful tool to investigate the embryonic organogenesis and adult organ maintenance of the pancreas. *J Hepatobiliary Pancreat Sci* 18, 1–5.

Kawasaki, T., Kitsukawa, T., Bekku, Y., Matsuda, Y., Sanbo, M., Yagi, T. and Fujisawa, H. (1999). A requirement for neuropilin-1 in embryonic vessel formation. *Development* 126, 4895–4902.

Khan, M. H. and Harlan, D. M. (2009). Counterpoint: clinical islet transplantation: not ready for prime time. *Diabetes Care* 32, 1570–1574.

Kiba, T. (2004). Relationships between the autonomic nervous system and the pancreas including regulation of regeneration and apoptosis: recent developments. *Pancreas* 29, e51–e58.

Kim, H., Toyofuku, Y., Lynn, F. C., Chak, E., Uchida, T., Mizukami, H., Fujitani, Y., Kawamori, R., Miyatsuka, T., Kosaka, Y., Yang, K., Honig, G., van der Hart, M., Kishimoto, N., Wang, J., Yagihashi, S., Tecott, L. H., Watada, H. and German, M. S. (2010). Serotonin regulates pancreatic beta cell mass during pregnancy. *Nat Med* 16, 804–808.

Kim, W. and Egan, J. M. (2008). The role of incretins in glucose homeostasis and diabetes treatment. *Pharmacol. Rev.* 60, 470–512.

Kirchgessner, A. L. and Gershon, M. D. (1990). Innervation of the pancreas by neurons in the gut. *J Neurosci* 10, 1626–1642.

Kirchgessner, A. L., Adlersberg, M. A. and Gershon, M. D. (1992). Colonization of the developing pancreas by neural precursors from the bowel. *Dev Dyn* 194, 142–154.

Kobayashi, S. and Fujita, T. (1969). Fine structure of mammalian and avian pancreatic islets with special reference to D cells and nervous elements. *Z Zellforch Microsk Anat* 100, 340–363.

Koch, S. and Claesson-Welsh, L. (2012). Signal transduction by vascular endothelial

growth factor receptors. *Cold Spring Harb Perspect Med* 2, a006502.

Koma, Y.-I., Furuno, T., Hagiyama, M., Hamaguchi, K., Nakanishi, M., Masuda, M., Hirota, S., Yokozaki, H. and Ito, A. (2008). Cell adhesion molecule 1 is a novel pancreatic-islet cell adhesion molecule that mediates nerve-islet cell interactions. *Gastroenterology* 134, 1544–1554.

Konturek, S. J., Zabielski, R., Konturek, J. W. and Czarnecki, J. (2003). Neuroendocrinology of the pancreas; role of brain-gut axis in pancreatic secretion. *Eur J Pharmacol* 481, 1–14.

Koopmans, S. J., Leighton, B. and DeFronzo, R. A. (1998). Neonatal de-afferentation of capsaicin-sensitive sensory nerves increases in vivo insulin sensitivity in conscious adult rats. *Diabetologia* 41, 813–820.

Kopinke, D. and Murtaugh, L. C. (2010). Exocrine-to-endocrine differentiation is detectable only prior to birth in the uninjured mouse pancreas. *BMC Dev Biol* 10, 38.

Kopinke, D., Brailsford, M., Shea, J. E., Leavitt, R., Scaife, C. L. and Murtaugh, L. C. (2011). Lineage tracing reveals the dynamic contribution of Hes1+ cells to the developing and adult pancreas. *Development* 138, 431–441.

Kopp, J. L., Dubois, C. L., Hao, E., Thorel, F., Herrera, P. L. and Sander, M. (2011a). Progenitor cell domains in the developing and adult pancreas. *Cell Cycle* 10, 1921–1927.

Kopp, J. L., Dubois, C. L., Schaffer, A. E., Hao, E., Shih, H. P., Seymour, P. A., Ma, J. and Sander, M. (2011b). Sox9+ ductal cells are multipotent progenitors throughout development but do not produce new endocrine cells in the normal or injured adult pancreas. *Development* 138, 653–665.

Korsgren, O., Andersson, A., Jansson, L. and Sundler, F. (1992). Reinnervation of syngeneic mouse pancreatic islets transplanted into renal subcapsular space. *Diabetes* 41, 130–135.

Korsgren, O., Jansson, L. and Sundler, F. (1996). Reinnervation of transplanted fetal porcine endocrine pancreas. Evidence for initial growth and subsequent degeneration of nerve fibers in the islet grafts. *Transplantation* 62, 352–357.

Korsgren, O., Lundgren, T., Felldin, M., Foss, A., Isaksson, B., Permert, J., Persson, N. H., Rafael, E., Rydén, M., Salmela, K., Tibell, A., Tufveson, G. and Nilsson, B. (2008). Optimising islet engraftment is critical for successful clinical islet transplantation. *Diabetologia* 51, 227–232.

Krapp, A., Knöfler, M., Ledermann, B., Bürki, K., Berney, C., Zoerkler, N., Hagenbüchle, O. and Wellauer, P. K. (1998). The bHLH protein PTF1-p48 is essential for the formation of the exocrine and the correct spatial organization of the endocrine pancreas. *Genes Dev* 12, 3752–3763.

Kuruvilla, R., Zweifel, L. S., Glebova, N. O., Lonze, B. E., Valdez, G., Ye, H. and Ginty, D. D. (2004). A neurotrophin signaling cascade coordinates sympathetic neuron development through differential control of TrkA trafficking and retrograde signaling. *Cell* 118, 243–255.

Kushner, J. A., Weir, G. C. and Bonner-Weir, S. (2010). Ductal origin hypothesis of pancreatic regeneration under attack. *Cell Metab* 11, 2–3.

Lai, Y., Schneider, D., Kidszun, A., Hauck-Schmalenberger, I., Breier, G., Brandhorst, D., Brandhorst, H., Iken, M., Brendel, M. D., Bretzel, R. G. and Linn, T. (2005). Vascular endothelial growth factor increases functional β-cell mass by improvement of angiogenesis of isolated human and murine pancreatic islets. *Transplantation* 79, 1530–1536.

Lain, K. Y. and Catalano, P. M. (2007). Metabolic changes in pregnancy. *Clin Obstet Gynecol* 50, 938–948.

Lammert, E. (2008). The vascular trigger of type II diabetes mellitus. *Exp Clin Endocrinol Diabetes* 116 Suppl 1, S21–S25.

Lammert, E., Cleaver, O. and Melton, D. (2001). Induction of pancreatic differentiation by signals from blood vessels. *Science* 294, 564–567.

Lammert, E., Cleaver, O. and Melton, D. (2003a). Role of endothelial cells in early pancreas and liver development. *Mech Dev* 120, 59–64.

Lammert, E., Gu, G., McLaughlin, M., Brown, D., Brekken, R., Murtaugh, L. C., Gerber, H. P., Ferrara, N. and Melton, D. A. (2003b). Role of VEGF-A in vascularization of pancreatic islets. *Curr Biol* 13, 1070–1074.

Lau, J., Kampf, C., Mattsson, G., Nyqvist, D., Köhler, M., Berggren, P.-O. and Carlsson, P.-O. (2009). Beneficial role of pancreatic microenvironment for angiogenesis in transplanted pancreatic islets. *Cell Transplant* 18, 23–30.

Lausier, J., Diaz, W. C., Roskens, V., LaRock, K., Herzer, K., Fong, C. G., Latour, M. G., Peshavaria, M. and Jetton, T. L. (2010). Vagal control of pancreatic β-cell proliferation. *Am J Physiol Endocrinol Metab* 299, E786–E793.

Lavine, R. L., Chick, W. L., Like, A. A. and Makdisi, T. W. (1971). Glucose tolerance and insulin secretion in neonatal and adult mice. *Diabetes* 20, 134–139.

Le Marchand, S. J. and Piston, D. W. (2010). Glucose suppression of glucagon secretion: metabolic and calcium responses from α-cells in intact mouse pancreatic islets. *J Biol Chem* 285, 14389–14398.

LeCouter, J., Moritz, D. R., Li, B., Phillips, G. L., Liang, X. H., Gerber, H.-P., Hillan, K. J. and Ferrara, N. (2003). Angiogenesis-independent endothelial protection of liver: role of VEGFR-1. *Science* 299, 890–893.

Lenzen, S. (2008). The mechanisms of alloxan- and streptozotocin-induced diabetes. *Diabetologia* 51, 216–226.

Lepper, C., Conway, S. and Fan, C. (2009). Adult satellite cells and embryonic muscle progenitors have distinct genetic requirements. *Nature* 460, 627–631.

Li, X., Zhang, L., Meshinchi, S., Dias-Leme, C., Raffin, D., Johnson, J. D., Treutelaar, M. K. and Burant, C. F. (2006). Islet microvasculature in islet hyperplasia and failure in a model of type 2 diabetes. *Diabetes* 55, 2965–2973.

Lieberman, S. M. and DiLorenzo, T. P. (2003). A comprehensive guide to antibody and T-cell responses in type 1 diabetes. *Tissue Antigens* 62, 359–377.

Lien, E. A., Solheim, E. and Ueland, P. M. (1991). Distribution of tamoxifen and its metabolites in rat and human tissues during steady-state treatment. *Cancer Res* 51, 4837–4844.

Lifson, N., Kramlinger, K. G., Mayrand, R. R. and Lender, E. J. (1980). Blood flow to the rabbit pancreas with special reference to the islets of Langerhans. *Gastroenterology* 79, 466–473.

Lifson, N., Lassa, C. V. and Dixit, P. K. (1985). Relation between blood flow and morphology in islet organ of rat pancreas. *Am J Physiol Endocrinol Metab* 249, E43–E48.

Lindeberg, J., Usoskin, D., Bengtsson, H., Gustafsson, A., Kylberg, A., Söderström, S. and Ebendal, T. (2004). Transgenic expression of Cre recombinase from the tyrosine hydroxylase locus. *Genesis* 40, 67–73.

Lindsay, T. H., Halvorson, K. G., Peters, C. M., Ghilardi, J. R., Kuskowski, M. A., Wong, G. Y. and Mantyh, P. W. (2006). A quantitative analysis of the sensory and sympathetic innervation of the mouse pancreas. *Neuroscience* 137, 1417–1426.

Lioubinski, O., Müller, M., Wegner, M. and Sander, M. (2003). Expression of Sox transcription factors in the developing mouse pancreas. *Dev Dyn* 227, 402–408.

Liu, H., Guz, Y., Kedees, M. H., Winkler, J. and Teitelman, G. (2010a). Precursor cells in mouse islets generate new β-cells in vivo during aging and after islet injury. *Endocrinology* 151, 520–528.

Liu, Y., Suckale, J., Masjkur, J., Magro, M. G., Steffen, A., Anastassiadis, K. and Solimena, M. (2010b). Tamoxifen-independent recombination in the RIP-CreER mouse. *PLoS ONE* 5, e13533.

Livak, K. J. and Schmittgen, T. D. (2001). Analysis of relative gene expression data using real-time quantitative PCR and the $2^{-\Delta\Delta Ct}$ Method. *Methods* 25, 402–408.

Long, J. B., Jay, S. M., Segal, S. S. and Madri, J. A. (2009). VEGF-A and

Semaphorin3A: modulators of vascular sympathetic innervation. *Dev Biol* 334, 119–132.

Long, M. A. and Rossi, F. M. V. (2009). Silencing inhibits Cre-mediated recombination of the Z/AP and Z/EG reporters in adult cells. *PLoS ONE* 4, e5435.

Love, J. A., Yi, E. and Smith, T. G. (2007). Autonomic pathways regulating pancreatic exocrine secretion. *Auton Neurosci* 133, 19–34.

Lundquist, I., Ahrén, B., Hansson, C. and Håkanson, R. (1989). Monoamines in pancreatic islets of guinea pig, hamster, rat, and mouse determined by high performance liquid chromatography. *Pancreas* 4, 662–667.

Lustig, R. H. (2003). Autonomic dysfunction of the β-cell and the pathogenesis of obesity. *Rev Endocr Metab Disord* 4, 23–32.

Mackenzie, F. and Ruhrberg, C. (2012). Diverse roles for VEGF-A in the nervous system. *Development* 139, 1371–1380.

Maechler, P. and Wollheim, C. B. (1999). Mitochondrial glutamate acts as a messenger in glucose-induced insulin exocytosis. *Nature* 402, 685–689.

Magenheim, J., Ilovich, O., Lazarus, A., Klochendler, A., Ziv, O., Werman, R., Hija, A., Cleaver, O., Mishani, E., Keshet, E. and Dor, Y. (2011). Blood vessels restrain pancreas branching, differentiation and growth. *Development* 138, 4743–4752.

Mao, J., Ligon, K. L., Rakhlin, E. Y., Thayer, S. P., Bronson, R. T., Rowitch, D. and McMahon, A. P. (2006). A novel somatic mouse model to survey tumorigenic potential applied to the Hedgehog pathway. *Cancer Res* 66, 10171–10178.

Marino, J. S., Xu, Y. and Hill, J. W. (2011). Central insulin and leptin-mediated autonomic control of glucose homeostasis. *Trends Endocrinol Metab* 22, 275–285.

Marko, S. B. and Damon, D. H. (2008). VEGF promotes vascular sympathetic innervation. *Am J Physiol Heart Circ Physiol* 294, H2646–H2652.

Mathe, Z., Dupraz, P., Rinsch, C., Thorens, B., Bosco, D., Zbinden, M., Morel, P., Berney, T. and Pepper, M. S. (2006). Tetracycline-regulated expression of VEGF-A in beta cells induces angiogenesis: improvement of engraftment following transplantation. *Cell Transplant* 15, 621–636.

Matsumoto, T. and Claesson-Welsh, L. (2001). VEGF receptor signal transduction. *Sci STKE* 112, re21.

Matthews, D. R. and Clark, A. (1987). Neural control of the endocrine pancreas. *The Proc Nutr Soc* 46, 89–95.

Mattsson, G., Jansson, L. and Carlsson, P.-O. (2002). Decreased vascular density in

mouse pancreatic islets after transplantation. *Diabetes* 51, 1362–1366.

McCall, M. and James Shapiro, A. M. (2012). Update on islet transplantation. *Cold Spring Harb Perspect Med* 2, a007823.

McLennan, R., Teddy, J. M., Kasemeier-Kulesa, J. C., Romine, M. H. and Kulesa, P. M. (2010). Vascular endothelial growth factor (VEGF) regulates cranial neural crest migration in vivo. *Dev Biol* 339, 114–125.

Mei, Q., Mundinger, T. O., Lernmark, A. and Taborsky, G. J. (2002). Early, selective, and marked loss of sympathetic nerves from the islets of BioBreeder diabetic rats. *Diabetes* 51, 2997–3002.

Metzger, D. and Chambon, P. (2001). Site- and time-specific gene targeting in the mouse. *Methods* 24, 71–80.

Miller, K., Kim, A., Kilimnik, G., Jo, J., Moka, U., Periwal, V. and Hara, M. (2009). Islet formation during the neonatal development in mice. *PLoS ONE* 4, e7739.

Milo-Landesman, D., Surana, M., Berkovich, I., Compagni, A., Christofori, G., Fleischer, N. and Efrat, S. (2001). Correction of hyperglycemia in diabetic mice transplanted with reversibly immortalized pancreatic β cells controlled by the tet-on regulatory system. *Cell Transplant* 10, 645–650.

Moesgaard, S. G., Brand, C. L., Sturis, J., Ahrén, B., Wilken, M., Fleckner, J., Carr, R. D., Svendsen, O., Hansen, A. J. and Gram, D. X. (2005). Sensory nerve inactivation by resiniferatoxin improves insulin sensitivity in male obese Zucker rats. *Am J Physiol Endocrinol Metab* 288, E1137–E1145.

Mortazavi, A., Williams, B. A., McCue, K., Schaeffer, L. and Wold, B. (2008). Mapping and quantifying mammalian transcriptomes by RNA-Seq. *Nat Meth* 5, 621–628.

Mukouyama, Y.-S., Gerber, H.-P., Ferrara, N., Gu, C. and Anderson, D. J. (2005). Peripheral nerve-derived VEGF promotes arterial differentiation via neuropilin 1-mediated positive feedback. *Development* 132, 941–952.

Mukouyama, Y.-S., Shin, D., Britsch, S., Taniguchi, M. and Anderson, D. J. (2002). Sensory nerves determine the pattern of arterial differentiation and blood vessel branching in the skin. *Cell* 109, 693–705.

Mundinger, T. O., Mei, Q., Figlewicz, D. P., Lernmark, A. and Taborsky, G. J. (2003). Impaired glucagon response to sympathetic nerve stimulation in the BB diabetic rat: effect of early sympathetic islet neuropathy. *Am J Physiol Endocrinol Metab* 285, E1047–E1054.

Muoio, D. M. and Newgard, C. B. (2008). Mechanisms of disease: molecular and metabolic mechanisms of insulin resistance and β-cell failure in type 2 diabetes. *Nat Rev Mol Cell Biol* 9, 193–205.

Murakami, T., Fujita, T., Miyake, T., Ohtsuka, A., Taguchi, T. and Kikuta, A. (1993). The insulo-acinar portal and insulo-venous drainage systems in the pancreas of the mouse, dog, monkey and certain other animals: a scanning electron microscopic study of corrosion casts. *Arch Histol Cytol* 56, 127–147.

Murtaugh, L. C. (2011). Stem cells and β cells: the same, but different? *Cell Stem Cell* 8, 244–245.

Mwangi, S. M., Usta, Y., Raja, S. M., Anitha, M., Chandrasekharan, B., Parsadanian, A., Sitaraman, S. V. and Srinivasan, S. (2010). Glial cell line-derived neurotrophic factor enhances neurogenin3 gene expression and β-cell proliferation in the developing mouse pancreas. *Am J Physiol Gastrointest Liver Physiol* 299, G283–G292.

Mwangi, S., Anitha, M., Mallikarjun, C., Ding, X., Hara, M., Parsadanian, A., Larsen, C. P., Thule, P., Sitaraman, S. V., Anania, F. and Srinivasan, S. (2008). Glial cell line-derived neurotrophic factor increases β-cell mass and improves glucose tolerance. *Gastroenterology* 134, 727–737.

Myrsén, U., Keymeulen, B., Pipeleers, D. G. and Sundler, F. (1996). Beta cells are important for islet innervation: evidence from purified rat islet-cell grafts. *Diabetologia* 39, 54–59.

Nagy, J. A., Dvorak, A. M. and Dvorak, H. F. (2007). VEGF-A and the induction of pathological angiogenesis. *Annu Rev Pathol* 2, 251–275.

Nagy, N., Mwizerwa, O., Yaniv, K., Carmel, L., Pieretti-Vanmarcke, R., Weinstein, B. M. and Goldstein, A. M. (2009). Endothelial cells promote migration and proliferation of enteric neural crest cells via β1 integrin signaling. *Dev Biol* 330, 263–272.

Nakamura, E., Nguyen, M.-T. and Mackem, S. (2006). Kinetics of tamoxifen-regulated Cre activity in mice using a cartilage-specific CreER(T) to assay temporal activity windows along the proximodistal limb skeleton. *Dev Dyn* 235, 2603–2612.

Nakamura, K., Minami, K., Tamura, K., Iemoto, K., Miki, T. and Seino, S. (2011). Pancreatic β-cells are generated by neogenesis from non-β-cells after birth. *Biomed Res* 32, 167–174.

Nakamura, M., Kitamura, H., Konishi, S., Nishimura, M., Ono, J., Ina, K., Shimada, T. and Takaki, R. (1995). The endocrine pancreas of spontaneously diabetic db/db mice: microangiopathy as revealed by transmission electron microscopy. *Diabetes Res Clin Pract* 30, 89–100.

Nasser, Y., Fernandez, E., Keenan, C. M., Ho, W., Oland, L. D., Tibbles, L. A., Schemann, M., MacNaughton, W. K., Rühl, A. and Sharkey, K. A. (2006). Role of enteric glia in intestinal physiology: effects of the gliotoxin fluorocitrate on motor and secretory function. *Am J Physiol Gastrointest Liver Physiol* 291, G912–G927.

Nekrep, N., Wang, J., Miyatsuka, T. and German, M. S. (2008). Signals from the neural

crest regulate beta-cell mass in the pancreas. *Development* 135, 2151–2160.

Nikolova, G., Jabs, N., Konstantinova, I., Domogatskaya, A., Tryggvason, K., Sorokin, L., Fässler, R., Gu, G., Gerber, H.-P., Ferrara, N., Melton, D. A. and Lammert, E. (2006). The vascular basement membrane: a niche for insulin gene expression and β cell proliferation. *Dev Cell* 10, 397–405.

Ninkovic, J., Mori, T. and Götz, M. (2007). Distinct modes of neuron addition in adult mouse neurogenesis. *J Neurosci* 27, 10906–10911.

Nir, T., Melton, D. A. and Dor, Y. (2007). Recovery from diabetes in mice by β cell regeneration. *J Clin Invest* 117, 2553–2561.

Niswender, K. D., Shiota, M., Postic, C., Cherrington, A. D. and Magnuson, M. A. (1997). Effects of increased glucokinase gene copy number on glucose homeostasis and hepatic glucose metabolism. *J Biol Chem* 272, 22570–22575.

Nolan, C. J. and Prentki, M. (2008). The islet β-cell: fuel responsive and vulnerable. *Trends Endocrinol Metab* 19, 285–291.

Nyman, L. R., Ford, E., Powers, A. C. and Piston, D. W. (2010). Glucose-dependent blood flow dynamics in murine pancreatic islets in vivo. *Am J Physiol Endocrinol Metab* 298, E807–E814.

Nyman, L. R., Wells, K. S., Head, W. S., McCaughey, M., Ford, E., Brissova, M., Piston, D. W. and Powers, A. C. (2008). Real-time, multidimensional in vivo imaging used to investigate blood flow in mouse pancreatic islets. *J Clin Invest* 118, 3790–3797.

Nyqvist, D., Speier, S., Rodriguez-Diaz, R., Molano, R. D., Lipovsek, S., Rupnik, M., Dicker, A., Ilegems, E., Zahr-Akrawi, E., Molina, J., Lopez-Cabeza, M., Villate, S., Abdulreda, M. H., Ricordi, C., Caicedo, A., Pileggi, A., Berggren, P.-O. (2011). Donor islet endothelial cells in pancreatic islet revascularization. *Diabetes* 60, 2571–2577.

Offield, M. F., Jetton, T. L., Labosky, P. A., Ray, M., Stein, R. W., Magnuson, M. A., Hogan, B. L. and Wright, C. V. (1996). PDX-1 is required for pancreatic outgrowth and differentiation of the rostral duodenum. *Development* 122, 983–995.

Ohno-Matsui, K., Hirose, A., Yamamoto, S., Saikia, J., Okamoto, N., Gehlbach, P., Duh, E. J., Hackett, S., Chang, M., Bok, D., Zack, D. J. and Campochiaro, P. A. (2002). Inducible expression of vascular endothelial growth factor in adult mice causes severe proliferative retinopathy and retinal detachment. *Am J Pathol* 160, 711–719.

Ohta, Y., Kosaka, Y., Kishimoto, N., Wang, J., Smith, S. B., Honig, G., Kim, H., Gasa, R. M., Neubauer, N., Liou, A., Tecott, L. H., Deneris, E. S. and German, M. S. (2011). Convergence of the insulin and serotonin programs in the pancreatic β-cell. *Diabetes* 60, 3208–3216.

Olerud, J., Johansson, M., Lawler, J., Welsh, N. and Carlsson, P.-O. (2008). Improved vascular engraftment and graft function after inhibition of the angiostatic factor thrombospondin-1 in mouse pancreatic islets. *Diabetes* 57, 1870–1877.

Olerud, J., Mokhtari, D., Johansson, M., Christoffersson, G., Lawler, J., Welsh, N. and Carlsson, P.-O. (2011). Thrombospondin-1: an islet endothelial cell signal of importance for β-cell function. *Diabetes* 60, 1946–1954.

Olsson, R. and Carlsson, P.-O. (2006). The pancreatic islet endothelial cell: emerging roles in islet function and disease. *Int J Biochem Cell Biol* 38, 492–497.

Olsson, R. and Carlsson, P.-O. (2011). A low-oxygenated subpopulation of pancreatic islets constitutes a functional reserve of endocrine cells. *Diabetes* 60, 2068–2075.

Oosthuyse, B., Moons, L., Storkebaum, E., Beck, H., Nuyens, D., Brusselmans, K., Van Dorpe, J., Hellings, P., Gorselink, M., Heymans, S., Theilmeier, G., Dewerchin, M., Laudenbach, V., Vermylen, P., Raat, H., Acker, T., Vleminckx, V., Van Den Bosch, L., Cashman, N., Fujisawa, H., Drost, M. R., Sciot, R., Bruyninckx, F., Hicklin, D. J., Ince, C., Gressens, P., Lupu, F., Plate, K. H., Robberecht, W., Herbert, J. M., Collen, D. and Carmeliet, P. (2001). Deletion of the hypoxia-response element in the vascular endothelial growth factor promoter causes motor neuron degeneration. *Nat Genet* 28, 131–138.

Pan, F. C. and Wright, C. (2011). Pancreas organogenesis: From bud to plexus to gland. *Dev Dyn* 240, 530–565.

Paulmann, N., Grohmann, M., Voigt, J.-P., Bert, B., Vowinckel, J., Bader, M., Skelin, M., Jevsek, M., Fink, H., Rupnik, M. and Walther, D. J. (2009). Intracellular serotonin modulates insulin secretion from pancreatic β-cells by protein serotonylation. *PLoS Biol* 7, e1000229.

Paulsen, R. E., Contestabile, A., Villani, L. and Fonnum, F. (1987). An in vivo model for studying function of brain tissue temporarily devoid of glial cell metabolism: the use of fluorocitrate. *J Neurochem* 48, 1377–1385.

Pekny, M. and Nilsson, M. (2005). Astrocyte activation and reactive gliosis. *Glia* 50, 427–434.

Pelengaris, S., Khan, M. and Evan, G. I. (2002). Suppression of Myc-induced apoptosis in β cells exposes multiple oncogenic properties of Myc and triggers carcinogenic progression. *Cell* 109, 321–334.

Pellegrinet, L., Rodilla, V., Liu, Z., Chen, S., Koch, U., Espinosa, L., Kaestner, K. H., Kopan, R., Lewis, J. and Radtke, F. (2011). Dll1- and dll4-mediated notch signaling are required for homeostasis of intestinal stem cells. *Gastroenterology* 140, 1230–1240.

Peppiatt, C. M., Howarth, C., Mobbs, P. and Attwell, D. (2006). Bidirectional control of

CNS capillary diameter by pericytes. *Nature* 443, 700–704.

Persson-Sjögren, S., Forsgren, S. and Täljedal, I. B. (1998). Expression of tyrosine hydroxylase, calcitonin gene-related peptide, substance P and protein gene product 9.5 in mouse islets transplanted under the kidney capsule. *Neuropeptides* 32, 307–318.

Persson-Sjögren, S., Forsgren, S. and Täljedal, I. B. (2002). Tyrosine hydroxylase in mouse pancreatic islet cells, in situ and after syngeneic transplantation to kidney. *Histol Histopathol* 17, 113–121.

Persson-Sjögren, S., Forsgren, S., Shi, C. L. and Täljedal, I. B. (2001a). Mouse islets cultured with vasoactive intestinal polypeptide: effects on insulin release and immunoreactivity for tyrosine hydroxylase. *Pancreas* 22, 84–90.

Persson-Sjögren, S., Holmberg, D. and Forsgren, S. (2005). Remodeling of the innervation of pancreatic islets accompanies insulitis preceding onset of diabetes in the NOD mouse. *J Neuroimmunol* 158, 128–137.

Persson-Sjögren, S., Zashihin, A. and Forsgren, S. (2001b). Nerve cells associated with the endocrine pancreas in young mice: an ultrastructural analysis of the neuroinsular complex type I. *Histochem J* 33, 373–378.

Pictet, R. L., Clark, W. R., Williams, R. H. and Rutter, W. J. (1972). An ultrastructural analysis of the developing embryonic pancreas. *Dev Biol* 29, 436–467.

Pierreux, C. E., Cordi, S., Hick, A.-C., Achouri, Y., Ruiz de Almodovar, C., Prévot, P.-P., Courtoy, P. J., Carmeliet, P. and Lemaigre, F. P. (2010). Epithelial: endothelial cross-talk regulates exocrine differentiation in developing pancreas. *Dev Biol* 347, 216–227.

Plank, J. L., Mundell, N. A., Frist, A. Y., Legrone, A. W., Kim, T., Musser, M. A., Walter, T. J. and Labosky, P. A. (2011). Influence and timing of arrival of murine neural crest on pancreatic beta cell development and maturation. *Dev Biol* 349, 321–330.

Porat, S., Weinberg-Corem, N., Tornovsky-Babaey, S., Schyr-Ben-Haroush, R., Hija, A., Stolovich-Rain, M., Dadon, D., Granot, Z., Ben-Hur, V., White, P., Girard, C. A., Karni, R., Kaestner, K. H., Ashcroft, F. M., Magnuson, M. A., Saada, A., Grimsby, J., Glaser, B. and Dor, Y. (2011). Control of pancreatic β cell regeneration by glucose metabolism. *Cell Metab* 13, 440–449.

Quaegebeur, A., Lange, C. and Carmeliet, P. (2011). The neurovascular link in health and disease: molecular mechanisms and therapeutic implications. *Neuron* 71, 406–424.

Radziuk, J., Barron, P., Najm, H. and Davies, J. (1993). The effect of systemic venous drainage of the pancreas on insulin sensitivity in dogs. *J Clin Invest* 92, 1713–1721.

Rawlins, E. L., Okubo, T., Xue, Y., Brass, D. M., Auten, R. L., Hasegawa, H., Wang, F.

and Hogan, B. L. M. (2009). The role of Scgb1a1+ Clara cells in the long-term maintenance and repair of lung airway, but not alveolar, epithelium. *Cell Stem Cell* 4, 525–534.

Razavi, R., Chan, Y., Afifiyan, F. N., Liu, X. J., Wan, X., Yantha, J., Tsui, H., Tang, L., Tsai, S., Santamaria, P., Driver, J. P., Serreze, D., Salter, M. W. and Dosch, H. M. (2006). TRPV1+ sensory neurons control β cell stress and islet inflammation in autoimmune diabetes. *Cell* 127, 1123–1135.

Reetz, A., Solimena, M., Matteoli, M., Folli, F., Takei, K. and De Camilli, P. (1991). GABA and pancreatic β-cells: colocalization of glutamic acid decarboxylase (GAD) and GABA with synaptic-like microvesicles suggests their role in GABA storage and secretion. *EMBO J* 10, 1275–1284.

Reinert, R. B., Brissova, M., Shostak, A., Pan, F. C., Kantz, J., Thompson, C. S., Dai, C. and Powers, A. C. (In preparation). Differential roles for vascular endothelial growth factor A in the developing pancreas versus the mature pancreatic islet.

Reinert, R. B., Cai, Q., Hong, J. Y., Plank, J. L., Shostak, A., Dai, C., Labosky, P. A., Brissova, M. and Powers, A. C. (Submitted). Vascular Endothelial Growth Factor Coordinates Neurovascular Development of the Pancreatic Islet via an Intercellular Signaling Network.

Reinert, R. B., Kantz, J., Ackermann Misfeldt, A., Poffenberger, G., Gannon, M., Brissova, M. and Powers, A. C. (2012). Tamoxifen-induced Cre-loxP recombination is prolonged in pancreatic islets of adult mice. *PLoS ONE* 7, e33529.

Remedi, M. S., Kurata, H. T., Scott, A., Wunderlich, F. T., Rother, E., Kleinridders, A., Tong, A., Brüning, J. C., Koster, J. C. and Nichols, C. G. (2009). Secondary consequences of β cell inexcitability: identification and prevention in a murine model of K_{ATP}-induced neonatal diabetes mellitus. *Cell Metab* 9, 140–151.

Richards, O. C., Raines, S. M. and Attie, A. D. (2010). The role of blood vessels, endothelial cells, and vascular pericytes in insulin secretion and peripheral insulin action. *Endocr Rev* 31, 343–363.

Richins, C. A. (1945). The innervation of the pancreas. *J Comp Neurol* 83, 223–236.

Riedel, M. J., Asadi, A., Wang, R., Ao, Z., Warnock, G. L. and Kieffer, T. J. (2011). Immunohistochemical characterisation of cells co-producing insulin and glucagon in the developing human pancreas. *Diabetologia* 55, 372–381.

Robertson, R. P. (2004). Islet transplantation as a treatment for diabetes – a work in progress. *N Engl J Med* 350, 694–705.

Robinson, S. W., Dinulescu, D. M. and Cone, R. D. (2000). Genetic models of obesity and energy balance in the mouse. *Annu Rev Genet* 34, 687–745.

Rock, J. R., Onaitis, M. W., Rawlins, E. L., Lu, Y., Clark, C. P., Xue, Y., Randell, S. H. and Hogan, B. L. M. (2009). Basal cells as stem cells of the mouse trachea and human airway epithelium. *Proc Natl Acad Sci USA* 106, 12771–12775.

Rodriguez-Diaz, R., Abdulreda, M. H., Formoso, A. L., Gans, I., Ricordi, C., Berggren, P.-O. and Caicedo, A. (2011a). Innervation patterns of autonomic axons in the human endocrine pancreas. *Cell Metab* 14, 45–54.

Rodriguez-Diaz, R., Dando, R., Jacques-Silva, M. C., Fachado, A., Molina, J., Abdulreda, M. H., Ricordi, C., Roper, S. D., Berggren, P.-O. and Caicedo, A. (2011b). Alpha cells secrete acetylcholine as a non-neuronal paracrine signal priming beta cell function in humans. *Nat Med* 17, 888–892.

Rosengren, A. H., Jokubka, R., Tojjar, D., Granhall, C., Hansson, O., Li, D.-Q., Nagaraj, V., Reinbothe, T. M., Tuncel, J., Eliasson, L., Groop, L., Rorsman, P., Salehi, A., Lyssenko, V., Luthman, H. and Renström, E. (2010). Overexpression of alpha2A-adrenergic receptors contributes to type 2 diabetes. *Science* 327, 217–220.

Rossi, J., Santamäki, P., Airaksinen, M. S. and Herzig, K.-H. (2005). Parasympathetic innervation and function of endocrine pancreas requires the glial cell line-derived factor family receptor α2 (GFRα2). *Diabetes* 54, 1324–1330.

Rotolo, T., Smallwood, P. M., Williams, J. and Nathans, J. (2008). Genetically-directed, cell type-specific sparse labeling for the analysis of neuronal morphology. *PLoS ONE* 3, e4099.

Ruiz de Almodovar, C., Fabre, P. J., Knevels, E., Coulon, C., Segura, I., Haddick, P. C. G., Aerts, L., Delattin, N., Strasser, G., Oh, W.-J., Lange, C., Vinckier, S., Haigh, J., Fouquet, C., Gu, C., Alitalo, K., Castellani, V., Tessier-Lavigne, M., Chedotal, A., Charron, F. and Carmeliet, P. (2011). VEGF mediates commissural axon chemoattraction through its receptor Flk1. *Neuron* 70, 966–978.

Ruiz de Almodovar, C., Lambrechts, D., Mazzone, M. and Carmeliet, P. (2009). Role and therapeutic potential of VEGF in the nervous system. *Physiol Rev* 89, 607–648.

Salpeter, S. J., Klein, A. M., Huangfu, D., Grimsby, J. and Dor, Y. (2010). Glucose and aging control the quiescence period that follows pancreatic beta cell replication. *Development* 137, 3205–3213.

Salpeter, S. J., Klochendler, A., Weinberg-Corem, N., Porat, S., Granot, Z., Shapiro, A. M. J., Magnuson, M. A., Eden, A., Grimsby, J., Glaser, B. and Dor, Y. (2011). Glucose regulates cyclin D2 expression in quiescent and replicating pancreatic β-cells through glycolysis and calcium channels. *Endocrinology* 152, 2589–2598.

Samuel, V. T. and Shulman, G. I. (2012). Mechanisms for insulin resistance: common threads and missing links. *Cell* 148, 852–871.

Sangiorgi, E. and Capecchi, M. R. (2008). Bmi1 is expressed in vivo in intestinal stem

cells. *Nat Genet* 40, 915–920.

Sangiorgi, E. and Capecchi, M. R. (2009). Bmi1 lineage tracing identifies a self-renewing pancreatic acinar cell subpopulation capable of maintaining pancreatic organ homeostasis. *Proc Natl Acad Sci USA* 106, 7101–7106.

Sarkar, S. A., Kobberup, S., Wong, R., Lopez, A. D., Quayum, N., Still, T., Kutchma, A., Jensen, J. N., Gianani, R., Beattie, G. M., Jensen, J., Hayek, A. and Hutton, J. C. (2007). Global gene expression profiling and histochemical analysis of the developing human fetal pancreas. *Diabetologia* 51, 285–297.

Sauka-Spengler, T. and Bronner-Fraser, M. (2008). A gene regulatory network orchestrates neural crest formation. *Nat Rev Mol Cell Biol* 9, 557–568.

Schaeffer, M., Hodson, D. J., Lafont, C. and Mollard, P. (2011). Endocrine cells and blood vessels work in tandem to generate hormone pulses. *J Mol Endocrinol* 47, R59–R66.

Scharfmann, R. (1997). Neurotrophin and neurotrophin receptors in islet cells. *Horm Metab Res* 29, 294–296.

Scholten, D., Osterreicher, C. H., Scholten, A., Iwaisako, K., Gu, G., Brenner, D. A. and Kisseleva, T. (2010). Genetic labeling does not detect epithelial-to-mesenchymal transition of cholangiocytes in liver fibrosis in mice. *Gastroenterology* 139, 987–998.

Schwarz, Q., Maden, C. H., Vieira, J. M. and Ruhrberg, C. (2009). Neuropilin 1 signaling guides neural crest cells to coordinate pathway choice with cell specification. *Proc Natl Acad Sci USA* 106, 6164–6169.

Segura, I., De Smet, F., Hohensinner, P. J., Ruiz de Almodovar, C. and Carmeliet, P. (2009). The neurovascular link in health and disease: an update. *Trends Mol Med* 15, 439–451.

Serizawa, Y., Kobayashi, S. and Fujita, T. (1979). Neuro-insular complex type I in the mouse. Re-evaluation of the pancreatic islet as a modified ganglion. *Arch Histol Jpn* 42, 389–394.

Shah, S. R., Esni, F., Jakub, A., Paredes, J., Lath, N., Malek, M., Potoka, D. A., Prasadan, K., Mastroberardino, P. G., Shiota, C., Guo, P., Miller, K. A., Hackam, D. J., Burns, R. C., Tulachan, S. S. and Gittes, G. K. (2011). Embryonic mouse blood flow and oxygen correlate with early pancreatic differentiation. *Dev Biol* 349, 342–349.

Shalaby, F., Rossant, J., Yamaguchi, T. P., Gertsenstein, M., Wu, X. F., Breitman, M. L. and Schuh, A. C. (1995). Failure of blood-island formation and vasculogenesis in Flk-1-deficient mice. *Nature* 376, 62–66.

Shapiro, A. M., Lakey, J. R., Ryan, E. A., Korbutt, G. S., Toth, E., Warnock, G. L., Kneteman, N. M. and Rajotte, R. V. (2000). Islet transplantation in seven patients

with type 1 diabetes mellitus using a glucocorticoid-free immunosuppressive regimen. *N Engl J Med* 343, 230–238.

Shimada, K., Tachibana, T., Fujimoto, K., Sasaki, T. and Okabe, M. (2012). Temporal and spatial cellular distribution of neural crest derivatives and alpha cells during islet development. *Acta Histochem Cytochem* 45, 65–75.

Slack, J. M. (1995). Developmental biology of the pancreas. *Development* 121, 1569–1580.

Smith, P. H. (1975). Structural modification of Schwann cells in the pancreatic islets of the dog. *Am J Anat* 144, 513–517.

Smukler, S. R., Arntfield, M. E., Razavi, R., Bikopoulos, G., Karpowicz, P., Seaberg, R., Dai, F., Lee, S., Ahrens, R., Fraser, P. E., Wheeler, M. B. and van der Kooy, D. (2011). The adult mouse and human pancreas contain rare multipotent stem cells that express insulin. *Cell Stem Cell* 8, 281–293.

Solar, M., Cardalda, C., Houbracken, I., Martín, M., Maestro, M. A., De Medts, N., Xu, X., Grau, V., Heimberg, H., Bouwens, L. and Ferrer, J. (2009). Pancreatic exocrine duct cells give rise to insulin-producing beta cells during embryogenesis but not after birth. *Dev Cell* 17, 849–860.

Sondell, M., Lundborg, G. and Kanje, M. (1999). Vascular endothelial growth factor stimulates Schwann cell invasion and neovascularization of acellular nerve grafts. *Brain Res* 846, 219–228.

Sondell, M., Sundler, F. and Kanje, M. (2000). Vascular endothelial growth factor is a neurotrophic factor which stimulates axonal outgrowth through the flk-1 receptor. *Eur J Neurosci* 12, 4243–4254.

Song, J., Xu, Y., Hu, X., Choi, B. and Tong, Q. (2010). Brain expression of Cre recombinase driven by pancreas-specific promoters. *Genesis* 48, 628–634.

Soriano, P. (1999). Generalized lacZ expression with the ROSA26 Cre reporter strain. *Nat Genet* 21, 70–71.

Srinivas, S., Watanabe, T., Lin, C. S., William, C. M., Tanabe, Y., Jessell, T. M. and Costantini, F. (2001). Cre reporter strains produced by targeted insertion of EYFP and ECFP into the ROSA26 locus. *BMC Dev Biol* 1, 4.

Stagner, J., Ahrén, B., Sundler, F. and White, K. (2008). Reconstructing the pancreas: restoration of normoglycemia, exocrine function, and islet innervation by islet transplantation to the pancreas. *Transplant Proc* 40, 452–454.

Stapor, P. C. and Murfee, W. L. (2012). Spatiotemporal distribution of neurovascular alignment in remodeling adult rat mesentery microvascular networks. *J Vasc Res* 49, 299–308.

Steiner, D. J., Kim, A., Miller, K. and Hara, M. (2010). Pancreatic islet plasticity: interspecies comparison of islet architecture and composition. *Islets* 2, 135–145.

Stendahl, J. C., Kaufman, D. B. and Stupp, S. I. (2009). Extracellular matrix in pancreatic islets: relevance to scaffold design and transplantation. *Cell Transplant* 18, 1–12.

Stoffers, D. A., Desai, B. M., DeLeon, D. D. and Simmons, R. A. (2003). Neonatal exendin-4 prevents the development of diabetes in the intrauterine growth retarded rat. *Diabetes* 52, 734–740.

Storkebaum, E. and Carmeliet, P. (2011). Paracrine control of vascular innervation in health and disease. *Acta Physiol (Oxf)* 203, 61–86.

Storkebaum, E., Lambrechts, D. and Carmeliet, P. (2004). VEGF: once regarded as a specific angiogenic factor, now implicated in neuroprotection. *Bioessays* 26, 943–954.

Storkebaum, E., Ruiz de Almodovar, C., Meens, M., Zacchigna, S., Mazzone, M., Vanhoutte, G., Vinckier, S., Miskiewicz, K., Poesen, K., Lambrechts, D., Janssen, G. M., Fazzi, G. E., Verstreken, P., Haigh, J., Schiffers, P. M., Rohrer, H., Van der Linden, A., De Mey, J. G. and Carmeliet, P. (2010). Impaired autonomic regulation of resistance arteries in mice with low vascular endothelial growth factor or upon vascular endothelial growth factor trap delivery. *Circulation* 122, 273–281.

Strobel, O., Dor, Y., Alsina, J., Stirman, A., Lauwers, G., Trainor, A., Fernández-del Castillo, C., Warshaw, A. L. and Thayer, S. P. (2007a). In vivo lineage tracing defines the role of acinar-to-ductal transdifferentiation in inflammatory ductal metaplasia. *Gastroenterology* 133, 1999–2009.

Strobel, O., Dor, Y., Stirman, A., Trainor, A., Fernández-del Castillo, C., Warshaw, A. L. and Thayer, S. P. (2007b). β cell transdifferentiation does not contribute to preneoplastic/metaplastic ductal lesions of the pancreas by genetic lineage tracing in vivo. *Proc Natl Acad Sci USA* 104, 4419–4424.

Stubbs, D., DeProto, J., Nie, K., Englund, C., Mahmud, I., Hevner, R. and Molnár, Z. (2009). Neurovascular congruence during cerebral cortical development. *Cereb Cortex* 19 Suppl 1, i32–i41.

Suda, K., Nobukawa, B., Takase, M. and Hayashi, T. (2006). Pancreatic segmentation on an embryological and anatomical basis. *J Hepatobiliary Pancreat Surg* 13, 146–148.

Sun, K., Wernstedt Asterholm, I., Kusminski, C. M., Bueno, A. C., Wang, Z. V., Pollard, J. W., Brekken, R. A. and Scherer, P. E. (2012). Dichotomous effects of VEGF-A on adipose tissue dysfunction. *Proc Natl Acad Sci USA* 109, 5874–5879.

Sunami, E., Kanazawa, H., Hashizume, H., Takeda, M., Hatakeyama, K. and Ushiki, T. (2001). Morphological characteristics of Schwann cells in the islets of Langerhans of the murine pancreas. *Arch Histol Cytol* 64, 191–201.

Sundler, F. and Bottcher, G. (1991). Islet innervation, with special reference to neuropeptides. *The Endocrine Pancreas*. Ed. Ellis Samols. New York, Raven Press. 29–52.

Suri, A. and Szallasi, A. (2008). The emerging role of TRPV1 in diabetes and obesity. *Trends Pharmacol Sci* 29, 29–36.

Taborsky, G. J. (2011). Islets have a lot of nerve! Or do they? *Cell Metab* 14, 5–6.

Taborsky, G. J. and Mundinger, T. O. (2012). Minireview: the role of the autonomic nervous system in mediating the glucagon response to hypoglycemia. *Endocrinology* 153, 1055–1062.

Taborsky, G. J., Mei, Q., Hackney, D. J., Figlewicz, D. P., Leboeuf, R. and Mundinger, T. O. (2009). Loss of islet sympathetic nerves and impairment of glucagon secretion in the NOD mouse: relationship to invasive insulitis. *Diabetologia* 52, 2602–2611.

Takahashi, H. and Shibuya, M. (2005). The vascular endothelial growth factor (VEGF)/VEGF receptor system and its role under physiological and pathological conditions. *Clin Sci* 109, 227–241.

Takahashi, N., Kishimoto, T., Nemoto, T., Kadowaki, T. and Kasai, H. (2002). Fusion pore dynamics and insulin granule exocytosis in the pancreatic islet. *Science* 297, 1349–1352.

Tam, B. Y. Y., Wei, K., Rudge, J. S., Hoffman, J., Holash, J., Park, S.-K., Yuan, J., Hefner, C., Chartier, C., Lee, J.-S., Jiang, S., Nayak, N. R., Kuypers, F. A., Ma, L., Sundram, U., Wu, G., Garcia, J. A., Schrier, S. L., Maher, J. J., Johnson, R. S., Yancopoulos, G. D., Mulligan, R. C. and Kuo, C. J. (2006). VEGF modulates erythropoiesis through regulation of adult hepatic erythropoietin synthesis. *Nat Med* 12, 793–800.

Tang, K., Breen, E. C., Gerber, H.-P., Ferrara, N. M. A. and Wagner, P. D. (2004). Capillary regression in vascular endothelial growth factor-deficient skeletal muscle. *Physiol Genomics* 18, 63–69.

Teitelman, G. and Lee, J. K. (1987). Cell lineage analysis of pancreatic islet development: glucagon and insulin cells arise from catecholaminergic precursors present in the pancreatic duct. *Dev Biol* 121, 454–466.

Teitelman, G., Alpert, S. and Hanahan, D. (1988). Proliferation, senescence, and neoplastic progression of β cells in hyperplasic pancreatic islets. *Cell* 52, 97–105.

Teitelman, G., Alpert, S., Polak, J. M., Martinez, A. and Hanahan, D. (1993). Precursor cells of mouse endocrine pancreas coexpress insulin, glucagon and the neuronal proteins tyrosine hydroxylase and neuropeptide Y, but not pancreatic polypeptide. *Development* 118, 1031–1039.

Teitelman, G., Guz, Y., Ivkovic, S. and Ehrlich, M. (1998). Islet injury induces neurotrophin expression in pancreatic cells and reactive gliosis of peri-islet Schwann cells. *J Neurobiol* 34, 304–318.

Teng, L., Mundell, N. A., Frist, A. Y., Wang, Q. and Labosky, P. A. (2008). Requirement for Foxd3 in the maintenance of neural crest progenitors. *Development* 135, 1615–1624.

Teta, M., Long, S. Y., Wartschow, L. M., Rankin, M. M. and Kushner, J. A. (2005). Very slow turnover of β-cells in aged adult mice. *Diabetes* 54, 2557–2567.

Thorel, F., Népote, V., Avril, I., Kohno, K., Desgraz, R., Chera, S. and Herrera, P. L. (2010). Conversion of adult pancreatic α-cells to β-cells after extreme β-cell loss. *Nature* 464, 1149–1154.

Thorens, B. (2011). Brain glucose sensing and neural regulation of insulin and glucagon secretion. *Diab Obes Metab* 13 Suppl 1, 82–88.

Tischer, E., Mitchell, R., Hartman, T., Silva, M., Gospodarowicz, D., Fiddes, J. C. and Abraham, J. A. (1991). The human gene for vascular endothelial growth factor. Multiple protein forms are encoded through alternative exon splicing. *J Biol Chem* 266, 11947–11954.

Tokuoka, H., Muramatsu, S.-I., Sumi-Ichinose, C., Sakane, H., Kojima, M., Aso, Y., Nomura, T., Metzger, D. and Ichinose, H. (2011). Compensatory regulation of dopamine after ablation of the tyrosine hydroxylase gene in the nigrostriatal projection. *J Biol Chem* 286, 43549–43558.

Toyofuku, Y., Uchida, T., Nakayama, S., Hirose, T., Kawamori, R., Fujitani, Y., Inoue, M. and Watada, H. (2009). Normal islet vascularization is dispensable for expansion of beta-cell mass in response to high-fat diet induced insulin resistance. *Biochem Biophys Res Commun* 383, 303–307.

Tsui, H., Chan, Y., Tang, L., Winer, S., Cheung, R. K., Paltser, G., Selvanantham, T., Elford, A. R., Ellis, J. R., Becker, D. J., Ohashi, P. S. and Dosch, H. M. (2008a). Targeting of pancreatic glia in type 1 diabetes. *Diabetes* 57, 918–928.

Tsui, H., Paltser, G., Chan, Y., Dorfman, R. and Dosch, H. M. (2011). "Sensing" the link between type 1 and type 2 diabetes. *Diabetes Metab Res Rev* 27, 913–918.

Tsui, H., Razavi, R., Chan, Y., Yantha, J. and Dosch, H.-M. (2007). "Sensing" autoimmunity in type 1 diabetes. *Trends Mol Med* 13, 405–413.

Tsui, H., Winer, S., Chan, Y., Truong, D., Tang, L., Yantha, J., Paltser, G. and Dosch, H.-M. (2008b). Islet glia, neurons, and β cells. *Ann N Y Acad Sci* 1150, 32–42.

Unger, R. H. and Cherrington, A. D. (2012). Glucagonocentric restructuring of diabetes: a pathophysiologic and therapeutic makeover. *J Clin Invest* 122, 4–12.

Ushiki, T. and Watanabe, S. (1997). Distribution and ultrastructure of the autonomic nerves in the mouse pancreas. *Microsc Res Tech* 37, 399–406.

Ustione, A. and Piston, D. W. (2012). Dopamine synthesis and D3 receptor activation in pancreatic β-Cells regulates insulin secretion and intracellular [Ca2+] oscillations. *Mol Endocrinol* 26, doi:10.1210/me.2012-1226.

van Belle, T. L., Coppieters, K. T. and Herrath, von, M. G. (2011). Type 1 diabetes: etiology, immunology, and therapeutic strategies. *Physiol Rev* 91, 79–118.

Vasioukhin, V., Degenstein, L., Wise, B. and Fuchs, E. (1999). The magical touch: genome targeting in epidermal stem cells induced by tamoxifen application to mouse skin. *Proc Natl Acad Sci USA* 96, 8551–8556.

Vaxillaire, M. and Froguel, P. (2008). Monogenic diabetes in the young, pharmacogenetics and relevance to multifactorial forms of type 2 diabetes. *Endocr Rev* 29, 254–264.

Vetterlein, F., Pethö, A. and Schmidt, G. (1987). Morphometric investigation of the microvascular system of pancreatic exocrine and endocrine tissue in the rat. *Microvasc Res* 34, 231–238.

Virtanen, I., Banerjee, M., Palgi, J., Korsgren, O., Lukinius, A., Thornell, L.-E., Kikkawa, Y., Sekiguchi, K., Hukkanen, M., Konttinen, Y. T. and Otonkoski, T. (2008). Blood vessels of human islets of Langerhans are surrounded by a double basement membrane. *Diabetologia* 51, 1181–1191.

Wang, S., Jensen, J. N., Seymour, P. A., Hsu, W., Dor, Y., Sander, M., Magnuson, M. A., Serup, P. and Gu, G. (2009). Sustained Neurog3 expression in hormone-expressing islet cells is required for endocrine maturation and function. *Proc Natl Acad Sci USA* 106, 9715–9720.

Wang, T., Lacík, I., Brissová, M., Anilkumar, A. V., Prokop, A., Hunkeler, D., Green, R., Shahrokhi, K. and Powers, A. C. (1997). An encapsulation system for the immunoisolation of pancreatic islets. *Nat Biotechnol* 15, 358–362.

Wang, Z. V., Mu, J., Schraw, T. D., Gautron, L., Elmquist, J. K., Zhang, B. B., Brownlee, M. and Scherer, P. E. (2008). PANIC-ATTAC: a mouse model for inducible and reversible β-cell ablation. *Diabetes* 57, 2137–2148.

Wei, K. S. (2011). Inhibition of vascular endothelial growth factor signaling stimulates erythropoiesis and sensitizes hepatic insulin signaling through activation of hepatic hypoxia-inducible factor-2α. Doctoral dissertation, Stanford University, Stanford, CA. Retrieved June 12, 2012, from http://purl.stanford.edu/yn218dm8390.

Wentworth, J. M., Fourlanos, S. and Harrison, L. C. (2009). Reappraising the stereotypes of diabetes in the modern diabetogenic environment. *Nat Rev Endocrinol* 5, 483–489.

Wharton, G. (1932). The blood supply of the pancreas, with special reference to that of the islands of Langerhans. *Anat Rec* 53, 55–81.

Wicksteed, B., Brissova, M., Yan, W., Opland, D. M., Plank, J. L., Reinert, R. B., Dickson, L. M., Tamarina, N. A., Philipson, L. H., Shostak, A., Bernal-Mizrachi, E., Elghazi, L., Roe, M. W., Labosky, P. A., Myers, M. G. Jr., Gannon, M., Powers, A. C. and Dempsey, P. J. (2010). Conditional gene targeting in mouse pancreatic β-Cells: analysis of ectopic Cre transgene expression in the brain. *Diabetes* 59, 3090–3098.

Wierup, N. and Sundler, F. (2006). CART is a novel islet regulatory peptide. *Peptides* 27, 2031–2036.

Winer, S., Tsui, H., Lau, A., Song, A., Li, X., Cheung, R. K., Sampson, A., Afifiyan, F., Elford, A., Jackowski, G., Becker, D. J., Santamaria, P., Ohashi, P., Dosch, H.-M. (2003). Autoimmune islet destruction in spontaneous type 1 diabetes is not β-cell exclusive. *Nat Med* 9, 198–205.

Winzell, M. S. and Ahrén, B. (2007). Role of VIP and PACAP in islet function. *Peptides* 28, 1805–1813.

Woods, S. C. and Porte, D. (1974). Neural control of the endocrine pancreas. *Physiol Rev* 54, 596–619.

Xiao, H., Hirata, Y., Isobe, K.-I. and Kiuchi, K. (2002). Glial cell line-derived neurotrophic factor up-regulates the expression of tyrosine hydroxylase gene in human neuroblastoma cell lines. *J Neurochem* 82, 801–808.

Yang, Y., Gurung, B., Wu, T., Wang, H., Stoffers, D. A. and Hua, X. (2010). Reversal of preexisting hyperglycemia in diabetic mice by acute deletion of the Men1 gene. *Proc Natl Acad Sci USA* 107, 20358–20363.

Yoshitomi, H. and Zaret, K. S. (2004). Endothelial cell interactions initiate dorsal pancreas development by selectively inducing the transcription factor Ptf1a. *Development* 131, 807–817.

Youssef, K. K., Van Keymeulen, A., Lapouge, G., Beck, B., Michaux, C., Achouri, Y., Sotiropoulou, P. A. and Blanpain, C. (2010). Identification of the cell lineage at the origin of basal cell carcinoma. *Nat Cell Biol* 12, 299–305.

Yuan, L., Moyon, D., Pardanaud, L., Bréant, C., Karkkainen, M. J., Alitalo, K. and Eichmann, A. (2002). Abnormal lymphatic vessel development in neuropilin 2 mutant mice. *Development* 129, 4797–4806.

Zhang, H., Ackermann, A. M., Gusarova, G. A., Lowe, D., Feng, X., Kopsombut, U. G., Costa, R. H. and Gannon, M. (2006). The FoxM1 transcription factor is required to maintain pancreatic β-cell mass. *Mol Endocrinol* 20, 1853–1866.

Zhang, H., Fujitani, Y., Wright, C. V. E. and Gannon, M. (2005). Efficient recombination in pancreatic islets by a tamoxifen-inducible Cre-recombinase. *Genesis* 42, 210–217.

Zhang, N., Richter, A., Suriawinata, J., Harbaran, S., Altomonte, J., Cong, L., Zhang, H., Song, K., Meseck, M., Bromberg, J. and Dong, H. (2004). Elevated vascular endothelial growth factor production in islets improves islet graft vascularization. *Diabetes* 53, 963–970.

Zhou, Q., Brown, J., Kanarek, A., Rajagopal, J. and Melton, D. A. (2008). In vivo reprogramming of adult pancreatic exocrine cells to β-cells. *Nature* 455, 627–632.

Zhu, X., Hill, R. A., Dietrich, D., Komitova, M., Suzuki, R. and Nishiyama, A. (2011). Age-dependent fate and lineage restriction of single NG2 cells. *Development* 138, 745–753.

Zhuo, L., Theis, M., Alvarez-Maya, I., Brenner, M., Willecke, K. and Messing, A. (2001). hGFAP-cre transgenic mice for manipulation of glial and neuronal function in vivo. *Genesis* 31, 85–94.